CHANGES IN THE MICROSTRUCTURE OF THIN FILM SILVER CATALYSTS UNDER REACTIVE CONDITIONS

A Thesis submitted for the degree of

DOCTOR OF PHILOSOPHY

of the

UNIVERSITY OF LONDON

by

GEOFFREY LAURENCE PRICE M.A.

Department of Chemical Engineering
and Chemical Technology,
Imperial College,
London, S.W.7.

October, 1970.

CONTENTS.

		Page
	Abstract.	3
	Acknowledgements.	5
I	INTRODUCTION.	6
II	EXPERIMENTAL	78
III	RESULTS	136
IV	DISCUSSION	191
	References.	241

Abstract.

Thin evaporated silver films on silica have been used as a model catalyst system for the study of factors affecting the microstructure of supported metal catalysts under reactive conditions.

The formation of discrete islands on heating the catalyst in oxygen-bearing atmospheres has been observed by electron microscopy to occur in well defined stages. The importance of differential thermal expansion between support and metal is shown by a study of hillock growth in the early stages of agglomeration, where mass transfer by surface diffusion allows relief of the compressive stresses set up. Surface energy driving forces are shown to govern the kinetics of later stages, where island formation occurs by surface diffusion withdrawal of material from the substrate. Quantitative models of hillock growth and hole enlargement have been developed, which account for the observed kinetics. The island structure finally remaining is shown to be related to the mode of growth of the parent evaporated film.

The changes in catalyst surface area caused by the island formation process have been followed by krypton adsorption; they follow closely the area observed by microscopy. Changes in the catalytic activity of the films for ethylene and hydrogen oxidation reactions, caused by agglomeration, follow these surface area changes quite

closely. Abnormally high activity has been detected for a second type of silver deposit partly composed of small discrete islands; large changes in activity are observed during use of this type of deposit as a catalyst.

Acknowledgements.

The author would like to express his thanks to Dr.A.E.B.Presland and Dr.D.L.Trimm for their constant encouragement and valuable advice during the course of this study. For the period of the work, the author has been seconded to Imperial College from the Petrochemical and Polymer Laboratory of Imperial Chemical Industries Ltd., who have also made a generous grant for research expenses. The author has been most grateful for the opportunity thus given by the Company for this study; he would like to thank in particular Dr.J.Dewing of the Laboratory, for his advice and help. Sincere thanks are due to Mr.P.Marlow for construction in electron microscopy techniques, and for his constant help. The author would like to thank Dr.M.Muir and Mrs.M.Culphan for scanning microscopy facilities, Prof.J.C.Anderson for use of the Å-scope, Dr.I.Kerr for the use of the micro-densitometer, Mr.M.P.Jones for use of the "Quantimet", Mr.A.Jones and staff for glassblowing instruction and assistance, Mr.B.Sellick for advice with counting equipment, Mr.M.D.Scothern for assistance with gas chromatography, and Mr.L.Cripps for his expert typing. Most of all, thanks must go to the author's wife, Mavis, for her love and continual support.

CHAPTER 1.

INTRODUCTION.

1.1. Microstructure and reactivity of metal heterogeneous catalysts.

1.1.1. Outline of heterogeneous catalysis 8

1.1.2. Theoretical accounts of the catalytic activity of metals. 11

1.1.3. Microstructure and activity. 16

1.1.3.1. Free metal surfaces. 16

1.1.3.2. Dispersed metals. 21

1.1.4. Changes in the activity of metal surfaces. 24

1.2. Microstructure and properties of evaporated metal films.

1.2.1. Nucleation and growth of metal films on amorphous substrates. 28

1.2.2. Properties of evaporated metal films. 31

1.2.2.1. Microstructure of polycrystalline films. 31

1.2.2.2. Adsorption surface area. 32

1.2.2.3. Adsorption characteristics. 35

1.3. Structure and energetics of metal surfaces.

1.3.1. T.L.K. model of surface structure. 37

1.3.2. Interfacial energy of metals. 39

1.3.2.1. Theory of solid interfacial energies. 39

1.3.2.2. Equilibrium shape of small crystalline particles. 43

1.3.2.3. Surface energy of metal-vacuum/gas surfaces. 45

1.3.2.4. Surface energy of metal-ceramic interfaces. 47

1.3.3. Surface diffusion in metals. 48

1.3.3.1. Clean surfaces. 48

1.3.3.2. Diffusion in the presence of adsorbed layers. 54

1.4. Thermal reorganization effects in metal surfaces.

1.4.1. Free metal surfaces: analysis of Mullins. 59

1.4.2. Continuous single crystal surfaces- analysis of Brandon and Bradshaw. 62

1.4.3. Polycrystalline thin film surfaces. 66

1.4.3.1. Continuous films. 66

1.4.3.2. Discontinuous deposits. 71

1.5. Catalytic activity in relation to microstructural changes in metals.

1.5.1. Interrelation of factors affecting activity and microstructure. 75

1.5.2. Present work. 76

1.1. Microstructure and reactivity of metal heterogeneous catalysts.

1.1.1. Outline of heterogeneous catalysis.

Heterogeneous catalysis is an interfacial phenomenon, frequently involving solid-gas surfaces, affecting the rate of attaining equilibrium in a chemical reaction in contact with the surface. Such effects imply the residence of reactant species at the interface for times sufficient for interaction to be possible, and show that the surface has an influence on the energetics and kinetics of the reaction in such a way as to alter the rate of equilibration.

Preferential concentration of reactant species at solid interfaces, known as adsorption, is inseparable from catalysis by solids. Adsorption occurs at interfaces broadly because of surface forces, ranging from dipole/quadrupole interactions, which give rise to weak reversible 'physical' adsorption, to interactions involving electron rearrangement, giving rise to strong irreversible chemical adsorption. Physical adsorption is only important near the boiling point of the adsorbent, and does not itself occur during catalysis at higher temperatures, although as a precursor to chemisorption physical interactions continue to affect the energetics. Chemisorption, which is possible at high temperatures, and is frequently thermally activated, is an essential preliminary to catalytic reaction at a surface.

The chemistry of subsequent reaction possibilities is closely related to the mode of adsorption, and particularly to the possible electronic configuration of the adsorbent on the surface, in relation to the electronic structure of the catalyst (Dowden, 1967). The strength of adsorption is of equal importance: if a reactant or product is very strongly adsorbed, then the occupied surface is blocked from further part in the reaction (poisoned). Too weak an adsorption, by contrast, may prevent reaction occurring at all, by reducing the residence time. The situation is rendered more complex because the strength of adsorption may vary with the amount of surface covered. If the surface is energetically heterogeneous, which is almost invariably the case, the energy of adsorption will vary according to the type of surface site; it will also vary because of repulsion from neighbouring pre-adsorbed molecules, and in some cases by the effect of adsorbent on the bonding properties of the surface. As a result, catalysis may occur only on a fraction of the total available interface. For detailed accounts of the energetics and kinetics of adsorption and desorption in relation to catalysis, reference may be made to recent reviews by Bond (1962, Chs.4-6), Thomas and Thomas (1967, Ch.3), and for chemisorption, to Hayward and Trapnell (1964), Gregg and Sing (1967, Ch.6).

Chemisorption of the reactant, the subsequent possibility of its migration over the surface, the stability of transition states with neighbouring reactant species, chemical reaction, and desorption of reactants or products, are all steps in which electronic rearrangements - bond forming and breaking - between the surface and the adsorbate are important. As a result, many attempts have been made to relate the electronic properties of solid catalysts, both in the bulk and at surfaces, to catalytic activity. One approach is in terms of the bulk electronic properties of the adsorbent; the band theory of the electronic structure of solids is used as a context for evaluating the energetics of electron transfer and pairing at the surface in relation to the strength of adsorption. Alternatively, the problem has been approached from the standpoint of surface crystallography: broadly, the activation energies associated with adsorption and the formation of intermediates, involving neighbouring surface lattice sites, are affected by the 'match' of separation distances in surface and adsorbate. This, the basis for the so-called "geometric" factor in catalysis, has been extended in more recent discussion in terms of the specific bonding possibilities available to adsorbents at particular crystal faces of the catalyst. Bond (1966) shows that it is possible to give a theoretical framework to explain the geometrical effects of individual

crystal faces by relating the bonding possibilities of a particular metal centre to the coordination vacancies which will be exposed by cleavage along a given crystal plane. This new approach draws on both of the partially successful "geometric" and "electronic" approaches to catalysis, and focusses attention less on the possibility of very general correlations between structure and reactivity, than on the energetics of adsorbent coordination in specific catalytic interactions.

An examination of theories of metal catalysis further illustrates this trend in recent attempts to give a theoretical basis for activity.

1.1.2. Theoretical accounts of the catalytic activity of metals.

Attempts were early made to relate the catalytic activity of metals to the geometry of the interaction of adsorbates with particular catalyst surfaces. Initial support for this "geometric" approach came from the well-known correlations observed by Beeck (1940, 1950) between reactivity and the density of certain crystallographic planes, and between the ethylene hydrogenation activity of transition metals, and their lattice spacing. Balandin also had earlier (1929) suggested relationships between surface lattice spacings and the stability of multiply adsorbed species (Balandin, 1929, 1958). This approach is however insufficient

in itself. Geometric effects cannot be considered an independent factor giving a basis for wide generalization. For example, lattice separation distances are interrelated with the electronic properties of the solid (Pauling, 1949); moreover, attempts to relate catalytic activity with surface lattice features, and larger scale microstructural features, must be treated with some caution, since these, more recently, have themselves been observed to alter in the presence of adsorbents. Rather, arguments from lattice structure effects should probably now be used as one particular approach to questions of surface adsorption or reaction energetics.

Lawson's (1968) work is a good example : results of a radiotracer technique for measuring reactant (formic acid) coverage on specific crystal faces of a silver film, were discussed in terms of the geometry of adsorption on these surfaces: the result is an approach to known specific face effects (e.g. Sosnovsky, 1959) in the catalytic decomposition of formic acid. Again, Boudart et al (1968) find geometrical evaluations of the stability of adsorbed species particularly important for certain reactions which are stereochemically "demanding". Limited use of surface streochemical arguments in this way is probably the best use of the "geometric factor".

No overarching theory has emerged, despite widespread interest and activity, from attempts to unify theories of heterogeneous catalysis with the electronic

properties of solids. The band theory of solids, applied to metals, considers the delocalisation of atomic electrons throughout the crystals through the creation of energy bands, related to the original s,p and d levels, but possibly separated by an energy gap. Electrons fill the bands from the lowest levels, but the occupancy of the bands may not be identical to the electron energy levels in the corresponding free atom. In his valence theory of metals, Pauling tended to treat metal centres more individually. The cohesive forces were discussed in terms of covalent bonding between adjacent metal atoms. In transition metals, some d-orbitals overlap to give electrons which participate in this bonding, and the "percentage d-character" is the extent to which this occurs. Other d-orbitals are associated with electrical conduction, and others are vacant: the number of electrons that can be placed in these vacant d-orbitals from adsorbent species at the surface, decreases as the percentage d-character increases.

Although both these electronic approaches are known to have serious defects, some success has been obtained by their application. Thus, attractive correlations have been pointed out between the percentage d-character of transition metals, and hydrogenation activity (Boudart, 1949; Beeck, 1950). The electronic theory is particularly valuable in explaining the catalytic activity of alloys of transition

metals with completely filled d-bands: for example, the sharp breaks observed in the activity of Pd-Au (Firth, 1966) and Pd-Ag (Moss and Thomas, 1967) alloys at ca. 60% Ag/Au, can be attributed to the filling of incomplete d-bands (although these arguments depend on complete miscibility of the alloy components at the temperature used). Theoretical explanations of this type are, however, mainly based on the behaviour of solids in the bulk. They take no account of possible modifications of electronic properties at the surface of the catalyst, and they can deal only with the overall activity of polycrystalline specimens. As soon as specific face effects are considered, "geometric" considerations of the configuration of adsorbate bonds in relation to the surface must also be considered.

More recent developments of the "electronic" approach to catalyis have used extensions of molecular orbital theory, analogous to that of the bonding and stability of complex metal ions. Just as the stability of transition metal complexes is known to depend on the effect of ligands on the d-electron energy levels, as interpreted by crystal field theory (Orgel, 1966), so Dowden et al (1956, 1961) have shown that variations in activity noted for transition-metal oxides, can be accounted for in terms of the effect of adsorbate on the orbital energies of the lattice metal ions. This approach, although not satisfying every requirement, is perhaps the most satisfactory one currently available. The

geometry of adsorbate coordination can be related to crystal field splitting effects to interpret the energetics of adsorption, although the arguments strictly derive from perfect crystal surface models.

The theory of heterogeneous catalysis on ideal metal surfaces is thus still in a tentative state; when turning to consider actual catalyst surfaces, the difficulties are not lessened, because the effects of surface microtopography and defect structures must then be considered also. Thus Allpress and Sanders (1964a), discussing work on evaporated metal films, point out that though they have been widely used in catalytic studies, their surface topography has largely been ignored, and in some cases their surfaces have been assumed to consist predominantly of close-packed planes. In the following section on microstructure and reactivity, we must therefore consider not only the overall orientation of the surface, but surface defects, and the particular microtopography characteristics of such catalyst surfaces as evaporated films, and metals dispersed on refractory supports.

This gives a background for understanding what is known of microstructure in relation to reactivity (section 1.1.3) and thus brings us directly to the interests of the present work. Here, attention has been directed to the factors affecting the frequently observed decay of catalytic activity under reaction conditions. Although these are

frequently poisoning effects, where activity is lost by the blocking of active surface by strongly adsorbed material or by deposition of solids, changes in microstructure are also known to occur concurrently with loss of activity. Factors affecting changes in reactivity of metals through changes in their microstructure are therefore described subsequently (section 1.1.4).

1.1.3. Microstructure and activity.

1.1.3.1. Free metal surfaces.

a) Crystal face effects.

The most basic microstructure of a metal surface is the lattice configuration of the crystal faces exposed. Theoretical accounts of orientation effects on catalytic activity were discussed earlier, and here reference is made to some of the experimental reports.

Striking differences have been observed between activation energy E_A and pre-exponential factor A for different crystal faces. In Beeck's (1940) early work on hydrogenation on nickel films, (110) films were much more active. In Crocker and Robertson's (1958) work on formic acid decomposition on nickel, E_A varied from 19.0 kcals/mole on the (111) face, to 16.0 and 8.5 kcals/mole on the (110) and (100) faces respectively. The pre-exponential factor also varied, so that rates 'compensated' to fairly equal values on different surfaces. Sosnovsky (1955) had

also found large variations for formic acid, in this case on silver, though here the order was found to be E_A (111) < (100) < (110). In experiments of this kind it is not entirely clear whether the effects of lattice orientation of the pure surface alone are observed. Contamination effects from poor vacua (Beeck) and electropolishing (formic acid reaction) could differ selectively with orientation. The orientation itself is assumed from gross measurements (bulk single crystal, or electron diffraction), ignoring such factors as faceting during electropolishing. Nevertheless, orientation effects have been observed (Jaeger, 1967) on evaporated films deposited under reasonable vacuum conditions, and selective adsorption effects on different faces of the films used have been observed (Lawson, 1968 a,b) which help to explain the results in the absence of such effects. Given sufficient caution against other interfering effects, crystal orientation must be counted an important microstructural feature, at least for certain reactions.

b) Lattice defect effects.

Lattice defects in metals can be classified as i) dislocations, (edge and screw), ii) point defects (Schottky: vacancies, Frenkel: vacancy-interstitial pairs). Accounts of the crystallography of these defects will be found in e.g. Birchenall (1959), Thomas and Thomas (1967).

Measurements associating high defect

concentrations with high activity have been known for some years (e.g. Eckell, 1933, who found rate increases for formic acid decomposition on nickel after cold-rolling). The main difficulties in characterising the importance of the effect are to ensure surface purity, and to isolate the contributions of different types of defects. Cold rolling experiments carry the suspicion of surface contamination; to some extent this can be overcome by annealing the specimen slowly and comparing dislocation density changes with reactivity changes (e.g. Kishimoto, 1963; Bhakta and Taylor, 1966). A better method of introducing dislocations is the argon ion bombardment method used by Sosnovsky (1959), which was shown in supporting work to increase the dislocation concentration in silver used for formic acid decomposition. Ion bombardment energies up to 3 kev produced large increases in the pre-exponential factor and the activation energy for decomposition, with an overall compensation effect. Point defects were considered to be absent after annealing, and the large activity rises were attributed to production of active centres at the intersection of dislocations with the surface: this explanation is valid providing that no concurrent effects of argon embedding, or even complete surface re-ordering, occurred. The work of Bagg et al (1963) reported in the next section, used dislocations already present in evaporated metal films: this is a step towards a system for studying dislocation effects in the absence of interfering factors.

c) Microstructure and reactivity in evaporated metal films.

The ease with which metal surfaces of high purity may be produced by evaporation of metals onto a cold substrate in vacuum, has given rise over a long period to work on the catalytic activity of vacuum deposited films. The topographical complexity of such surfaces has only been realized when observed with the high resolution attainable in electron microscopy. Nevertheless, they have yielded results which are still of value, even though today single crystal surfaces of exceptional cleanliness are used if the complicating effects of the structure peculiar to evaporated films are to be eliminated.

When Beeck et al (1940) began work on catalysis on evaporated films, they were only able to report on the structure by means of electron diffraction, used to determine the overall orientation of the surface.

The complexity of evaporated film surface structure has now been emphasised in a series of papers from Sanders and his co-workers. In addition to assumed point defects, e.m. reveals grain and twin boundaries, isolated dislocations, and stacking faults. An adaptation of Bassett's (1958) gold decoration technique reveals kink sites on complex planes (see below, section 1.3.1), and gives an indication of the extent of close-packed planes on the

surface. Surface irregularity due to the underlying crystallite structure is clearly visible in replicas (Sanders, 1964; Allpress and Sanders, 1964 a,b). Marked effects of substrate, substrate temperature and annealing are observed on all these features, illustrating the problems encountered in comparing different results from various laboratories. These observations are the raw material of that surface inhomogeneity which is detectable in adsorption (Baker and Fox, 1965), and which affect the energetics and kinetics of adsorption and reaction in catalysis.

In this series of studies, observations were subsequently made to compare the activity of silver films for formic acid decomposition, with the densities of all observed defects (Bagg et al, 1963; Jaeger, 1967). It was concluded that defect densities did not affect reactivity, and that observed changes in A and E were caused by variations in the proportion of flat (111) oriented surface. This result is not typical of other studies of defect effects mentioned earlier, and is quite surprising. It is possible that defects are only important for certain reactions. It must be remembered, however, that comparison of results can only be valid after the most stringent characterisation of the surface: In this respect, the work of Jaeger and Sanders has much to commend itself. The detail of adsorption and catalytic studies is difficult to relate to the detail of metallurgical and other surface microstructural studies, but it is

potentially very revealing. The work of Moss et al (1963), closely correlating carbon monoxide oxidation activity to the nucleation and growth process for silver films, is a move in this direction.

1.1.3.2. Dispersed metals.

To increase and stabilize the surface area available for reaction, metal catalysts are generally dispersed on a porous refractory support. All the microstructural features affecting the activity of free metal surfaces apply in principle to supported metals, but investigation is hampered because of the inaccessibility of the detailed surface topography and structure. Most attention has been given to further features which are specific to supported metals - effects of support, metal concentration, crystallite size, - and these are discussed below.

A number of reports has appeared of decreases in the specific activity of supported metals after reaction, associated with increases in mean crystallite size. These are greater than would be caused by the consequent loss of surface area (e.g. Selwood et al (1955) (benzene hydrogenation : Ni); Carter et al (1966) (ethane hydrogenolysis: Ni). In these and other reports, 'crystallite sizes' are measured indirectly from X-ray line broadening and/or chemisorption studies. The inherent assumption that crystallite size

equals size of particles does not seem to have been discussed, although this is not unreasonable for small particles after annealing, as is supported by comparisons between e.m., X-ray and chemisorption crystallite size measurements (Adams, 1962; Brooks, 1968), who considers atomically dispersed metal). Only Dorling and Moss (1966) overcame the difficulties of direct observations of catalyst microstructure by perfecting an ultramicrotome sectioning technique. Where genuine, reported changes in specific activity with crystallite size invite explanation in terms of properties specific to small metal crystallites (e.g. high concentration of 'edge' atoms: see Dorling and Moss (1967), Cormack and Moss (1969)).

However, there is not a general relation between crystallite size and reactivity. Some systems do show loss of overall activity, but nearly constant specific activity during crystallite growth (e.g. Slin'ko and Cheslova (1956) (SO_2/H_2 oxidation, Pt); Boudart et al (1966) (cyclopropane hydrogenation on Pt); Yates et al (1964) (ethane hydrogenolysis on Ni); Echigoya et al (1968) (benzene hydrogenation on Pd). Reviewing results of this type, Boudart et al conclude that the constant specific activity of Pt observed for a large variety of reactions, depends on their being insensitive to the presence of surface structural variations (facile); only in the case of neopentane hydrogenolysis over Pt did they find a "demanding" reaction, sensitive to surface stereochemical environment (proportion of surface atoms). Any relation

between crystallite size and specific activity does not necessarily therefore exist for all reactions.

It is possible to focus so much attention on crystallite size measurements that the possibility of other parameters varying simultaneously in neglected. This is apparent from the recent results of Dorling et al (1969). Thus, the effect earlier (1967) reported of a crystallite size effect for ethylene hydrogenation over Pt which was only apparent in low Pt content samples, or catalysts fired at high temperatures has been found to arise from poisoning or self-poisoning of the Pt areas. Variations in the reduction temperature of the H_2PtCl_6 impregnated support, altered not only the crystallite size, but reduced the residual chlorine content, which was shown to promote the reaction if replaced. Allowing for these factors, the specific activity was found to be independent of crystallite size. This work illustrates the difficulty of isolating parameters affecting catalyst activity.

Effects of the support on the activity of metals have been noted by some authors. The possibility of charge transfer effects between metal and support was considered by Szabo and Solymosi (1960) who progressively doped semi-conductor supports for nickel, and showed a relation between support conductivity and activation energies for formic acid decomposition (changes in nickel oxidation state were not considered). Effects of change of support on activity have

been noted e.g. by Taylor et al (1964) and Yates et al (1965) for Ni, Co on silica-alumina. Support effects seem to be strongest at the lowest metal levels - as observed for Ni on SiO_2/SiO_2-Al_2O_3 for benzene/ethane hydrogenation by e.g. Taylor and Staffin (1967) and by Taylor et al (1965). This suggests that the first increments of a metal deposited on a support could selectively interact with the most energetic sites of a surface, resulting in a heterogeneity of metal sites.

Reviews, with further references, of the factors affecting supported metal activity will be found in Taylor (n.d.) and Sinfelt (1967). It is plain that no unified account of the activity of supported catalysts is yet possible, though probably the main factors have been recognised in crystallite size, substrate, metal concentration, facile/demanding reaction, and residual contaminants.

1.1.4. Changes in the activity of metal surfaces.

In-service changes in the activity of metal catalysts may occur, in the present context, as a result of changes in any of the properties mentioned in the preceding section. For example, 'poisoning' of reaction sites and/or of faces favourable for reaction, may occur through selective strong adsorption of products or impurities, or by deposition of solids such as carbon. Annealing out of defects may cause loss of reactivity - e.g. the work of Kishimoto (1963),

Bhakhta and Taylor (1966) referred to in section 1.1.3.1. Surface topography changes may also occur on annealing, affecting the proportion of reactive planes, inhomogeneity of adsorption etc. For example, Meelheim et al (1960) observed progressive changes in the surface structure of copper single crystals during catalysis of the hydrogen-oxygen reaction at 400°C; all faces except (111) rearranged to give (111) facets, and a number of special growths occurred; no correlation was made with reactivity. In a later paper (Swank and Lawless, 1965) morphology changes in thin film copper single crystals were observed under similar conditions, including growth of holes (see further section 1.4.2). Nielsen et al (1967) correlated identical observations of reorganization, with catalytic activity measurements for the H_2-O_2 reaction. A lattice work of (111) planes developed, and an initial rise in catalytic activity seemed to be associated with this step, indicating preferential reaction on (111). Changes in the experimentally observed values of the pre-exponential factor and the activation energy following annealing of silver films, were also noted by Bagg et al (1963), and correlated with changes in the proportion of (111) plane exposed.

Factors specific to activity changes in supported metals have been mainly thought of in terms of activity loss following growth in crystallites (section 1.1.3.2). The mechanism of particle size increase has received little

attention. Brownlie et al (1969), who observed particle growth during changes in the activity of Pd-graphite sintered catalysts, suggested that mobility of complete particles across the substrate was responsible for the growth, as observed by Sears and Hudson (1963; see further section 1.4.3.2.). By contrast, Furuoya et al (1969 a,b and refs) investigated the sintering mechanism of a Pd/silica-alumina catalyst by X-ray diffraction and electron microscopy. Two mechanisms of activity loss were distinguished. Air annealing caused particle growth, by transport of metal over the support. This transport, and the consequent loss of activity, was considered to be due to the migration of Pd^{2+} ions over the surface; oxygen adsorption increased $[Pd^{2+}]$ and so accelerated particle growth. The process could be inhibited by doping with 3- or 4-valent ions while 1- or 2-valent ions were ineffective. Particle growth did not occur in hydrogen (where Pd^{2+} would be absent); activity losses nevertheless occurred, and were ascribed to defect annealing.

Two mechanisms of particle growth (gross mobility, and ionic surface diffusion) clearly emerge from these suggestions; further investigation of their validity in some or all cases of activity loss in supported catalysts should prove valuable.

From the reports just reviewed of changes in the

activity of supported catalysts, the importance for catalytic activity changes of e.g. surface area and orientation changes, and of metal migration between crystallites, is apparent. The present work has been intended to throw some light on the factors governing morphological changes of this type, when metals held on refractory supports are annealed in reactive atmospheres. To facilitate the use of microscopy to quantify changes in metal distribution, it was decided (section 1.5) to work with thin metal films on flat non-porous supports as a model metal catalyst-support system. This meant that the factors affecting the annealing behaviour of such catalysts could be considered in the light of existing work on the structure and stability of metal surfaces, and particularly of thin metal films. For these reasons, an introduction is now given to relevant topics in the growth and properties of thin evaporated metal films; this is followed by a discussion of the energetic and diffusion properties of metal surfaces, as a basis for a review of thermal reorganization effects observed in metal surfaces and dispersed metals. The relevance of such work to supported catalyst studies is considered, and this allows the reasons for the approach adopted in the present work, to be discussed in more detail.

1.2. Microstructure and Properties of Evaporated Metal Films.

1.2.1. Nucleation and growth of metal films on amorphous substrates.

Recent work on the nucleation, growth and properties of thin solid films has been very extensive; the interest has been generated not only from the technical importance of thin film devices in the electronics and optical fields, but from the areas of overlap with theoretical interest in atomic sticking coefficients, adsorption, nucleation theory, physical metallurgy and electron optics. See, for example, the conference reports of (ed.) Neugebauer et al, 1959; (ed.) Niedermayer and Mayer (1966). The present review is not intended to be comprehensive, but rather to serve as an introduction to the formation of thin metal films, which will then lead to consideration of particular properties which have come to be of interest in the present work. Only vacuum deposited metal films are considered.

The condensation of evaporated metal vapour onto a solid substrate is a phase change, and the nucleation problem is concerned with the initiation of particles of the new (solid) phase. While the average deposit thickness is less than 1 Å, the existence of discrete three-dimensional nuclei has been demonstrated in several cases (Cu on Ag: Newman and Pashley, 1955). This nucleation is to be expected in the absence of any special surface sites, due to

the extremely high supersaturation of a vapour at ca. 3000°K meeting a substrate at ca. 300°K. However, preferential nucleation at surface steps is well established; the effect of other surface imperfections (dislocations, vacancies, adsorption layers) was reviewed by Bethge (1969). As is general in nucleation, there is a critical cluster size below which the probability of atoms being lost is greater than the arrival rate. The nucleation density is higher the smaller this critical cluster; the experimentally observed nucleation rates are such as to suggest that the critical clusters contain only a few atoms.

Earlier theoretical discussions of the nucleation process were extensions of the classical treatment of the vapour-liquid phase change e.g. Volmer and Weber (1925). They used bulk thermodynamic concepts to discuss the energetics of formation of the nucleus, assumed to be a small spherical cap: see for example Hirth and Pound (1963). The difficulties of assuming that bulk thermodynamic treatments are appropriate to very small adatom clusters have led to a statistical-mechanical approach to nucleation, e.g. Rhodin and Walton (1963), Zinsmeister (1966, 1968), Lewis and Campbell (1967). The newer theory is in good agreement with observed nucleation rates, and should probably be regarded as more appropriate for this particular type of nucleation.

Eventually, the nucleation density is so high,

that all arriving atoms on the surface are captured without renucleation. The subsequent growth of the nuclei leads to coalescence, with a marked steady decrease in their number. The growth sequence has been illustrated frequently (e.g. Pashley et al, 1964 for gold on carbon and molybdenite) for these and subsequent stages. Surface-diffusion migration effects over the islands are very important at the island coalescence stage,and striking liquid-like rearrangement phenomena are observed (ibid). At this stage, crystallite reorientation can occur, and on ordered substrates, the final film may contain large areas with the same orientation. Considerable recrystallization may also occur, so that a single grain in the completed film contains a large number of the initial nuclei, and thus the grain size of the final film is not completely controlled by the initial nucleation density.

Further growth of coalesced nuclei leads to a network, and soon a channel structure. Filling in of the final holes is slow, and leaves the upper surface of the film, even when continuous, marked by the grain structure (e.g. Allpress and Sanders (1964), fig.2). It is during the coalescence of larger islands, and during the filling-in of channels, that permanent dislocations become incorporated in the film (Pashley et al, 1964). The lattice geometry of the regions around many of the holes in the final stages before continuity is such that dislocations are inevitably formed

when they fill in.

1.2.2. Properties of evaporated metal films.

1.2.2.1. Microstructure of polycrystalline films.

The microstructure of polycrystalline films on amorphous substrates may be understood in relation to their growth sequence. High critical supersaturation of the condensing vapour leads to high nucleation densities, and, despite recrystallization effects during growth, a very small final crystallite size results which is inversely related to the melting point of the metal for a given substrate, For example, Umanskii and Krylov (in Pinsker, 1953, p.205) quote film crystallite sizes varying from Cd ≈ 100 Å, through Ag - 50 Å to W - 10 Å. The defect density is high, particularly because of the defect trapping effect at the final stages of film growth. From direct measurements on micrographs of ca. 1000 Å silver films deposited at ca. 10^{-5} torr, Bagg et al (1963) have estimated the following defect concentrations:

300°K	Grain boundary length (cm/cm^2)	Stacking fault and coherent twin boundary length (cm/cm^2)	Isolated dislocations (cm^{-2})
Glass	ca. 6.5×10^4	ca. 7×10^4	ca. 10^9
Mica	ca. 7.7×10^4	ca. 4×10^4	ca. 10^9

The surface topography can readily be observed

from carbon replicas (e.g. Bagg et al, 1963, p.456); it follows closely the underlying grain structure of the film. The same authors have used this as a method of following the recrystallization of such films during their use in catalysis. The density of residual holes in the films is well known to decrease steadily with thickness, but so far as can be determined, no quantitative measurements of hole density have yet appeared.

1.2.2.2. Adsorption surface area.

The account given of the growth from the vapour of thin films would tend to suggest that the area exposed to gas environments was the upper, nearly plane, surface alone. In fact, gas adsorption may also occur at internal pores, grain boundaries, dislocations, and stacking faults, at least. Two main methods are available for determining whether such sites contribute an effective "internal surface" in such films. These are direct gas adsorption, and the accurate determination of film densities (mainly by X-ray absorption) compared with the bulk (any negative deviation indicates unfilled internal volume, suggesting but not proving internal area accessible to adsorption).

Among reports of porous films based on gas adsorption measurements are those of Beeck et al (1940) for nickel on glass deposited in "high vacuum". Hydrogen and

carbon monoxide chemisorption showed amounts adsorbed/unit area to be proportional to film thickness. By depositing copper at 78°K on glass at ca. 10^{-6} torr, similar results were obtained by Allen and Mitchell (1950) and by Allen et al (1959). The oxygen adsorbed in both cases was close to 1.5×10^{20} mols/gram of metal. The results of Allen and Mitchell indicated that the adsorption surface area of a 2000 Å copper film was 15x the substrate area. Porter and Tompkins (1953) working on iron films evaporated on glass at ca. 10^{-5} torr also found surface adsorption proportional to film thickness.

From X-ray density determinations, the recent work of Weinstein et al (1968) reporting copper densities of ca. 91% d_{bulk} in films deposited at ca. 10^{-6} torr, is a contribution against the majority of reports which indicate no such effect. Supporting evidence is given by Blois and Reiser (1954), who observed deviations from d_{bulk} for rapidly evaporated Ag and Cu (500 Å/second). Other X-ray observations of $d \approx d_{bulk}$ are from highly reactive metals. Hartmann (1965) found a 3% deviation for Al at 10^{-6} torr using a piezoelectric quartz balance for mass determination (but see Edgecumbe, 1965, below), and Wolter (1965) by the same technique found d for chromium differing considerably from d_{bulk}, depending on the rate of evaporation, and the residual oxygen pressure.

In vacua of ca. 10^{-6} torr, the following workers have reported non-porous films: Hartmann (1965): Ag, Au, vacuum microbalance; Edgecumbe (1966): Al and Au; Wainfain (1959) for Cu above ca. 200 Å; Wolter (1965) for Al, Au, Ag, Cu above ca. 200 Å, quartz microbalance; Lovell (1968) for Al, Cu, Ag, Au, direct weighing. In addition, Allen and Mitchell (1950) and Allen et al (1959) found that copper films deposited at or above room temperature, otherwise identically to those found porous, were non-porous, and had areas equal to the geometric area. Trapnell (1953) pointed out that all low melting point metal films (Cu, Al, K, Zn, Cd, In, Sn, Pb, Ag and Au), sintered to roughness factors of about one at or below room temperature.

It seems then that porous films may be formed when (i) the gas pressure is high (above 10^{-2} torr) or (ii) the metal is highly reactive or (iii) the substrate temperature is low or (iv) the evaporation temperature of the metal is high. These conditions would lead to either (a) low mobility of the deposit on the substrate and/or (b) discrete particle condensation before reaching the substrate. (a) could lead to porosity by encouraging unfilled channel formation between nuclei - for discussion see Waterbeemd and Oosterhout (1967). (b) would be equivalent to aerosol formation with subsequent packing of the particles on the substrate, easily giving a porous structure - e.g. Harvey et

al (1960): three dimensional networks from Ag, Au in air above 3 torr: extended to Ni also by Kimoto et al (1963).

1.2.2.3. Adsorption characteristics.

Xenon and krypton have been found to be the most suitable gases for physical adsorption measurements on evaporated metal films. When specimens are generally of low area (below 1000 cm^2), a gas with a low saturation vapour pressure ($p_{Kr}^{78^\circ K} \simeq 2$ mm) leaves only a small proportion of unadsorbed gas over the sample, thus minimising errors due to the dead-volume in the measurement of the small amount adsorbed.

The adsorption of these gases on evaporated metal films has been reviewed by Gregg and Sing (1967). The isotherms observed are of the general type II (concave to the pressure axis). On nickel films, the c-parameter in the well-known B.E.T. equation describing physical adsorption is large, giving rise to a long flat or nearly flat 'plateau' region in the isotherm (e.g. Klemperer and Stone (1957); Roberts (1960); Anderson and Baker (1962). The large value of c corresponds to a high heat of adsorption, and indicates the adsorption may be in some intermediate region between chemical and physical adsorption.

Krypton has been used in the experimental work. Some uncertainty exists with krypton, as to the relative pressure at which "point B" (the "knee-point") occurs on

evaporated films at ca.0.01 (Brennan et al, 1963), or at the more usual ca. 0.1 (Klemperer and Stone; Roberts). In addition, the specific surface area A_m of krypton on these films is also uncertain. On quartz, carbon black, glass and metal oxides, values in the range 17.7 - 23.6 $\mathring{A}^2$ are observed, and the value 19.5 $\mathring{A}$ gives quite fair agreement in those few cases where direct calibration by comparison with microscopy has been attempted (see Gregg and Sing, p87). However, reports exist of much lower values of A_m on metal films - 14.6 $\mathring{A}^2$ from Beeck and Ritchie (1950), and from Campbell and Duthie (1965) who noted a reduction in A_m from 19.5 - 14.5 $\mathring{A}^2$ on nickel following admission and chemisorption of oxygen. Anderson and Baker (1962) argue however for a value of 17.9 $\mathring{A}^2$ for krypton on nickel, on the basis that a "lattice-packed" monolayer will be formed in which krypton will localize at the closest possible low energy sites on the nickel lattice, as its migration over the surface is energetically unfavourable at these temperatures (Ehrlich and Hudda, 1959). The nature of the adsorbent surface is undoubtedly important: high values of the heat of adsorption will imply strong localization of the krypton-metal bond, and in extreme cases, the dimensions of the adsorbate lattice will determine A_m.

1.3. Structure and Energetics of Metal Surfaces.

1.3.1. Terrace-ledge-kink (T.L.K.) model of surface structure.

Direct observation of the structural details of metal surfaces on an atomic scale is possible by field-ion microscopy (e.g. Moore, 1963). Patterns obtained from the tips of refractory b.c.c. and f.c.c. metals show that close packed planes consist of atomically flat "terraces", while exposed planes of slightly differing orientation (vicinal planes) consist of segments of terraces intersected by monatomic "ledges". Many of these ledges are not straight, but show monatomic jogs or "kinks". This situation is that proposed by Kossel in 1927, and used extensively since (e.g. Burton, Cabrera and Frank, 1951) in discussions of crystal growth and solution.

The T.L.K. model of a surface at $0^{o}K$ is simple since the equilibrium concentration of defects in a surface is zero (configurational entropy = 0). Fig. 1.1a) shows a vicinal [100] surface consisting of [100] terraces separated by monatomic steps. When the zone axis of the surface does not coincide with any close-packed direction of the crystal, the steps are kinked (fig.1.1b). At finite temperatures, a variety of adsorbate and/or defect and/or adatom concentration can also occur at the surface, as illustrated in fig. 1.1b). Below the melting point,

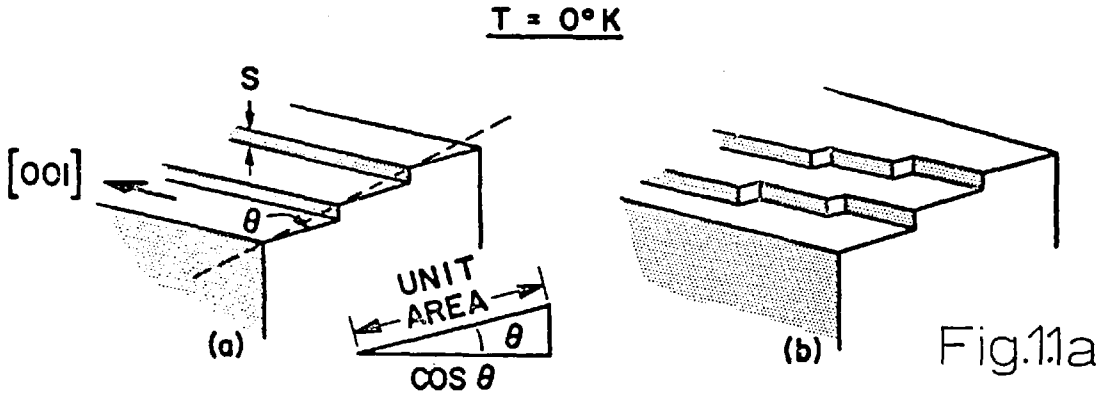


Fig.11a

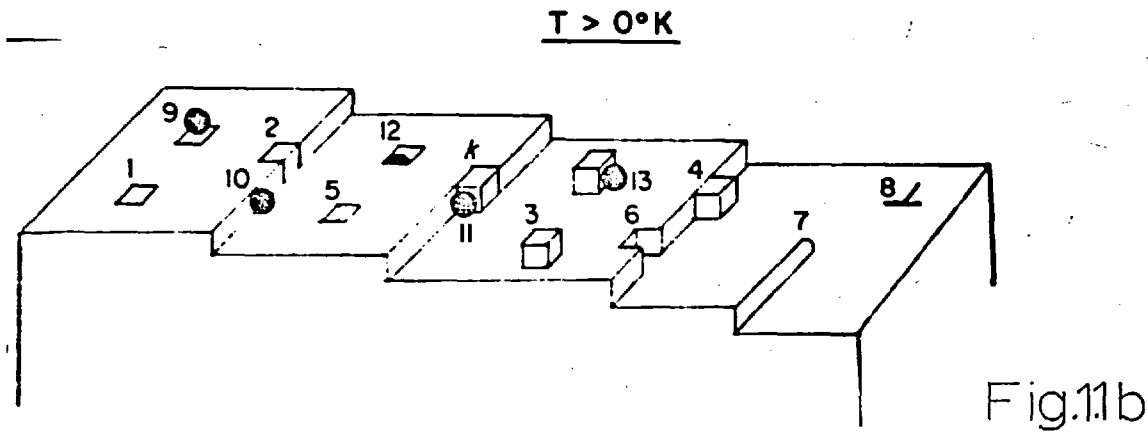


Fig.11b

T.L.K. model of a surface above 0°K in the presence of adsorbent (after Dunning, 1967)

1 terrace site
2 ledge site
3 self-adsorbed on ledge
4 self-adsorbed at step
5 terrace vacancy
6 step vacancy
7 screw dislocation
8 edge dislocation
9 adsorbate at terrace
10 adsorbate at ledge
11 adsorbate at kink
12 adsorbate in terrace
13 adatom-adsorbate pair

vacancy-adatom pair formation is energetically more favourable at ledges than on terraces, (Gjostein and Winterbottom, 1967) and at temperatures above $T_m/2$ causes complete roughening of the ledges; the terraces on the other hand remain almost atomically smooth to the melting point.

In the following discussion of surface energies and diffusivities, reference at the atomic level will be made to the T.L.K. model. Extensive reviews of the thermodynamics of the model and its application to these properties will be found in Burton et al (1951), Gjostein (1963a) and (1967) (surface diffusion), Dunning (1967) and Hirth (1965), where references to the original papers of Kossel, Stranski, Frenkel and others on the structure of surfaces will be found.

1.3.2. Interfacial energy of metals.

1.3.2.1. Theory of solid interfacial energies.

In general, an interface is a bounding surface between two adjacent phases. Microscopic examination soon reveals that a line passing through the surface goes through a region of discontinuity. Gibbs (1928) formalized the interface by constructing it as a geometrical surface, coincident with the interface within observational limits, but defined precisely as passing through the set of "all points which are similarly situated with respect to the adjacent matter". The definition was completed for solid-

solid interfaces by the convention that the excess surface concentration Γ of the principal constituent at the interface, should be zero.

Atoms at the interface region have a higher energy than the same atom in the normal lattice positions. Broadly speaking, this excess energy arises at a solid-ideal vacuum interface from the abnormally low coordination number ("broken bonds") of surface atoms. At solid-solid interfaces, lattice misfit involving abnormal coordination also produces high energy sites. This simple approach is expanded in theoretical treatments of the surface energy of metals. For example, Skapski (1956) analyses the energetics of incomplete coordination of surface atoms to next nearest neighbours; Cyrot-Lackmann (1969) considers the surface energy as the energy of perturbation in the band-structure of metals caused by the intersection of the interface with the lattice. Further discussion of these theoretical approaches can be found in Dunning (1967). Both approaches give fair agreement with the experimental values of the surface energy, γ , which, for Group IB clean metal surfaces, are of the order of 1000 erg/cm^2.

The surface energy γ of a solid interface may be defined as the reversible work required to create unit area of new surface. This is not the work required to deform the surface to produce unit area of new interface. For a

liquid interface the two quantities would be identical, but for a solid, new atoms do not, at least at low temperatures, arrive to restore a stressed interface to equivalence with its original state. The surface stress energy thus differs from the energy to create new interface by adding new atoms. This surface energy γ may be defined as

$$\gamma = f - \sum_{1}^{i} \mu_i \Gamma_i \qquad (1.1)$$

where f is the Helmholtz free energy/unit area, and μ_i is the chemical potential of component i.

Besides lacking diffusive mobility of atoms to interfaces, solids also differ from liquids in having long-range order of the atoms at interfaces. Since the forces giving rise to surface energy are specific to the atomic spacings and symmetry of the surface, γ for crystalline solids is a function of the orientation of the interface in question. This function is represented graphically by a polar diagram (known as a Wulff plot) representing a closed surface for which the length of the radius vector $\underline{r}$ is proportional to the value of γ in a plane normal to $\underline{r}$. A two dimensional illustration is given in fig. 1.2. This surface is characterised by a number of cusps (i.e. orientations of minimum γ) whose origins can be seen by reference to the T.L.K. model of surface structure. The energy γ of a stepped surface exceeds that of a terrace amount $\frac{e.a}{h}$ where e is the ledge energy/unit length, and

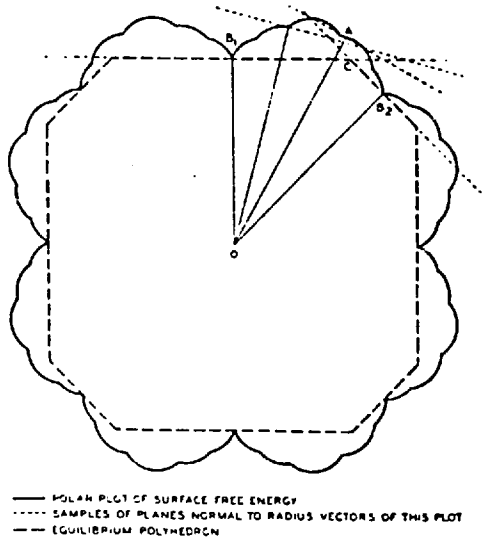


FIG. 1. Typical polar plot of surface free energy for a crystal and the Wulff construction based on it.

From Herring, (1952)

Fig 1.2

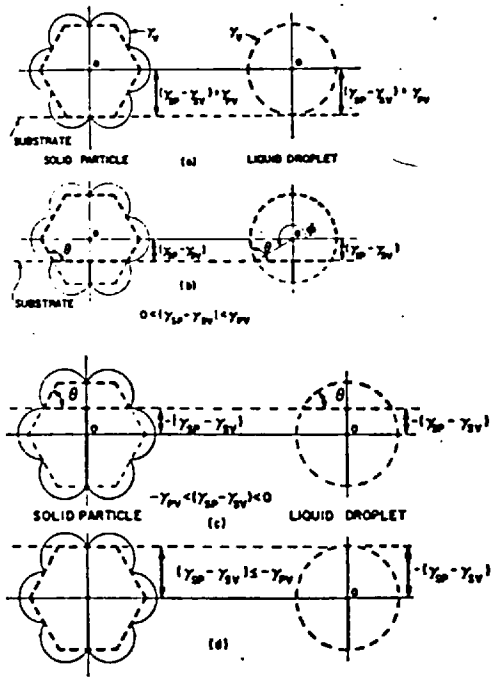


FIG. 3. γ^s-plots and corresponding equilibrium shapes for a two dimensional solid and liquid:
(a) non-wetting
(b) partial wetting, $(\gamma_{SP} - \gamma_{SV}) > 0$
(c) partial wetting, $(\gamma_{SP} - \gamma_{SV}) < 0$
(d) complete wetting.

From Winterbottom, (1968)

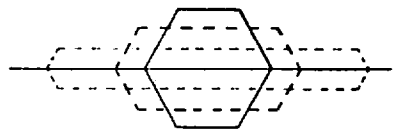


FIG. 6. Schematic illustration of the influence of increased binding between particle and substrate when $(\gamma_{SP} - \gamma_{SV}) < 0$ (dashed figures). The free particle shape is portrayed for reference (solid figure).

Fig 1.3

α is the inclination (small) of the surface to that of an atomically flat plane, h being the ledge height (ledge density = α/h for α small). Hence

$$\gamma = \{\gamma_o + e(\tfrac{\alpha}{h})\} \cos\theta \quad \text{for small } \theta \simeq 0 \qquad (1.2)$$

and γ at the singular orientation is a minimum. In principle this predicts (Herring, 1953) that a cusp will occur at <u>all</u> rational orientations (for $T = 0^oK$); but in practice, working at $T > T_m/2$, step roughening is so considerable that cusps only occur at a few low-index rational orientations.

Adsorption will affect the γ plot according to the sites occupied by adsorbent atoms. For example, preferential adsorption at ledges, lowering the ledge energy e, decreases the amount by which γ for a vicinal orientation differs from γ_o: i.e. the cusp is shallower. Preferred adsorption on a terrace deepens the cusp, leading to formation of facets of that terrace's orientation. The use of the T.L.K. model to discuss the effect of adsorption on the γ-plot, has been reviewed by Gjostein (1963 b,c) and by Robertson and Shewmon (1963), and by Gjostein and Winterbottom (1967).

1.3.2.2. <u>Equilibrium shape of small crystalline particles</u>.

The anisotropy of γ for crystalline solids gives rise to the following problem: what is the shape

which minimizes the total surface energy $\int \gamma \, dA$ of a given particle? Assuming the shape to be a polyhedron, Wulff (1901) found the construction for a relative minimum $\int \gamma \, dA$, by a proof which was later corrected (Herring, 1953, p.25). Dinghas (1944) later showed the solution to give an absolute minimum energy; Herring showed (ibid) that the solution was valid, irrespective of the class of solid body considered.

Wulff's solution is illustrated in fig. 1.2. A set of planes (lines in the illustration) is drawn through the end of, and perpendicular to, each radius vector of the γ -plot. Wulff's theorem is, that the equilibrium shape is the body joined by all points reachable from the origin without crossing any of these planes.

The theory has recently been extended to cover the equilibrium shapes of metal particles in contact with a substrate. Winterbottom (1967) has defined a general surface energy γ^* to deal with this problem, where $\gamma^* = \gamma_{PV}$ for the particle-vapour interface, and $\gamma^* = \gamma_{SP} - \gamma_{SV}$ for the common interface: SP = substrate particle, SV = substrate-vapour. In this way, the problem is simplified by reducing it to that of the equilibrium shape of an <u>equivalent</u> free particle with surface energy γ^*. This is of course amenable to the Wulff solution; fig.1.3 from Winterbottom's paper, illustrates the solutions obtained

for various degrees of substrate-particle bonding, and compares them with the behaviour of liquid droplets.

Recently, analysis of the equilibrium shape of small metal particles has been extended to cover examples with less than 1000 atoms, showing that polyhedra are still obtained (Romanowski, 1969).

1.3.2.3. Surface energy of metal-vacuum/gas surfaces.

Particular attention will be paid to the energy of Group IB metals, in view of the concentration in the present work on catalysis on silver surfaces (section 1.5).

The surface energy of silver in helium has been measured by the weighted wire method (Buttner, Funk and Udin, 1952), giving a mean value of $\gamma = 1140 \pm 90$ ergs/cm^2 for the range 875-932°C. This agrees quite well with the value computed by Pilliar and Nutting (1967) by the method of Skapski (1956) (1.4.2.1):

Metal	$\gamma_{(111)}$ ergs/cm^2	Temp. °C.
Au	1260	1000
Ag	1040	700
Cu	1390	850

Measurement of the anisotropy of γ proved more difficult than prediction of the effect it would have on the equilibrium shape of small particles. The only reliable method (Winterbottom, 1966) was developed by Mykura (1961), and

depends on the influence of γ anisotropy on the dihedral groove angles developed at twin boundary-free surface intersections in f.c.c. metals. Recent developments have been discussed in McLean and Gale (1969). Complete γ plots have only been obtained for nickel, f.c.c. iron, gold and copper (Mykura, 1961; McLean and Mykura, 1964; Winterbottom and Gjostein, 1966; McLean and Gale, 1969).

Sundquist (1964 a,b) has applied the technique of finding the equilibrium shape of small metal particles to the determination of the γ plot of a number of metals including silver. Although Winterbottom (1967) has pointed out that the way in which the particles were formed implies a degree of surface contamination, the results compared well with the theoretical prediction of the T.L.K. model for f.c.c. surfaces. The effect of oxygen in deepening the cusps of the (100) and (111) planes, thus causing the equilibrium shape to become faceted, was confirmed. The effect of small impurity concentrations in removing the anisotropy of γ was also studied: for example, silver + 0.25% lead exhibited spherical final particles.

The effect of adsorbed gases on surface energy has not been widely studied although Buttner, Funk and Udin (1952) measured γ for silver by the weighted wire method for a number of partial pressures p_{O_2} (atmospheres) of oxygen in helium. The results obtained showed a linear decrease in γ with

log p_{O_2}, as expressed in the relation

$$\gamma = 223 - 188 \log_{10} p_{O_2} \quad \text{ergs/cm}^2 \qquad (1.3)$$

By modifying the Gibbs adsorption isotherm the data on γ variation was used to find the degree of oxygen adsorption on the surface. Hirth (1965) has recently substituted into their calculation the more recent oxygen-silver solubility data of Eichenauer and Muller (1962) in an illustration of the concentration profiles at a silver-oxygen interface. A log dependence of surface energy on p_{O_2} has also been found for b.c.c. iron (Hondros, 1968).

1.3.2.4. Surface energy of metal-ceramic interfaces.

Liquid metal-ceramic energies have frequently been measured from the contact angle of a sessile metal drop with a ceramic plaque: e.g. Pask and Fulrath (1962). More recently, a technique has been developed for measuring the energy for a solid-solid interface (Pilliar and Nutting, 1967), which depends on observations of the equilibrium shape of small metal particles on γ-alumina after prolonged annealing, and analysis equivalent to that of Winterbottom (1967) case (b). Values obtained were

Interface	γ ergs/cm^2	Temp. ^{o}C.
Au - Al_2O_3	1725	1000
Ag - Al_2O_3	1630	700
Cu - Al_2O_3	1925	850

The more recent work of Winterbottom (1967) has underlined the need for careful characterisation of ceramic metal interfaces used for γ measurements. Similar experiments for silver on beryllia were carried out; in one case, initial deposition was in an untrapped oil diffusion-pumped system at about 10^{-6} torr, as used by Pilliar and Nutting; in the second case, deposition was in an oil-free U.H.V. system at 10^{-9} torr. The particles obtained by annealing the first deposit behaved as group (b), and as those of Pilliar and Nutting, gave a γ_{SP} of about 1100 ergs/cm^2. Particles from the second deposit by contrast had much stronger wetting (c) and gave γ_{SP} of about 2200 ergs/cm^2. Contamination effects are thus most important in the study of metal-ceramic energies, and await more detailed study.

1.3.3. Surface diffusion in metals.

1.3.3.1. Clean surfaces.

Surface self diffusion in metals has been the subject of a number of recent reviews: Blakley (1963), Gjostein (1963a, 1967), Hirth (1965), Shewmon (1966), Birchenall and Williams (1966), Winterbottom and Gjostein (1967) and Rhead (1969). This extensive coverage reflects the extension of surface diffusion experiments made possible after the analysis by Mullins (1957, 1960) of the kinetics of grain boundary grooving in metal surfaces, which was soon

shown experimentally (Mullins and Shewmon, 1959; Gjostein and Rhines, 1959) to be governed by surface self-diffusion. Generalization of this analysis to the decay of any surface profile on annealing (Mullins, 1963) allows the surface self-diffusion coefficient to be measured from the decay of sinusoidal surface profiles and isolated scratches, and the recession of ledges on field emission tips (references in Gjostein and Winterbottom, 1967). Alternative methods are available: the monitoring of surface diffusion by tracer techniques, the decay of protrusions on field emitter tips (Melmed, 1967), the coalescence of inert gas bubbles in the interior of the metal sample (Nichols, 1967; Bowden and Baluffi, 1969), and the growth of necks at the contact point of spherical particles (Johnson, 1969 and refs.) have all been used.

Early reviews (e.g. Gjostein, 1963a) noted the wide discrepancies between various measurements of D_s, the surface diffusion coefficient. On dividing them into groups according to whether they came from (i) dry hydrogen or good vacua, (ii) medium vacua ($\geq 10^{-6}$ torr), (iii) radiotracer experiments, Gjostein found that the first group yielded consistently high values of D_o ($> 10^3$ cm^2/sec) and Q_s (> 36 kcals/mo). These values were accepted since they fitted well with diffusion constants then estimated for the "rolling ball" diffusion of self-adsorbed atoms in relation

to the T.L.K. surface model. Other results were considered to represent abnormally low values due to impurity adsorption ($D_o = 10^{-3}$ cm^2/sec., Q_s = 15-25 kcal/mole).

Since then however "low" but indisputable values of Q_s and D_o have been obtained (refs. in fig. 1.4) (also Bonzel and Gjostein, 1968). Earlier, Birchenall and Williams (1966) had pointed out deviations in some cases from strict Arrhenius variation of D_s, and had speculated on a succession of mechanisms controlling surface diffusion at different temperatures. In fact, Gjostein (1967) has now shown that tracer results may be neglected for reasons he reviews (see also Birchenall and Williams, 1966, p.138), and that an important rationalization of D_s data can be made by plotting D_s against the relative temperature T/T_m of the measurement, as shown in fig. 1.4. Irrespective of the metal, the data plotted fits on a curve whose slope increases with temperature, suggesting that different mechanisms of diffusion and/or different surface structures are present at different temperatures. The results are expressed by:

$$\frac{T}{T_m} > 0.77, \quad D_s = 740 \exp [-30\ T_m/RT] \qquad (1.4)$$

$$\frac{T}{T_m} < 0.77, \quad D_s = 1.4 \times 10^{-2} \exp [-13\ T_m/RT] \qquad (1.5)$$

Results since reported strengthen this observation. Values for D_o and Q_s obtained on nickel by a new laser diffraction technique for observing sinusoidal decay (Bonzel and

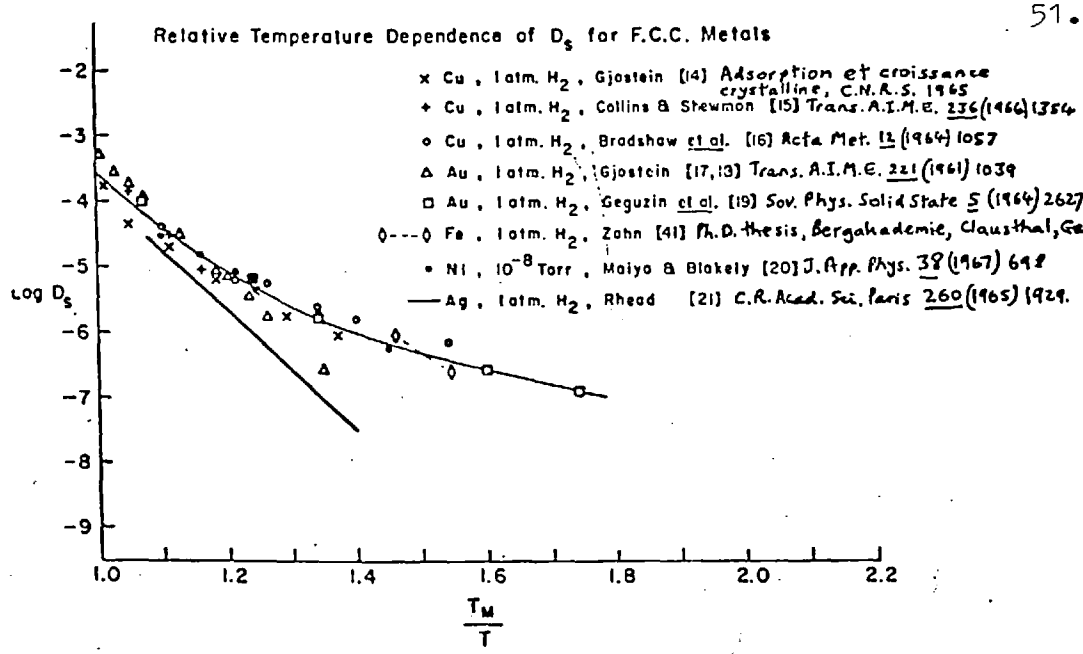


FIGURE 7. Relative temperature dependence of D_s for FCC metals.

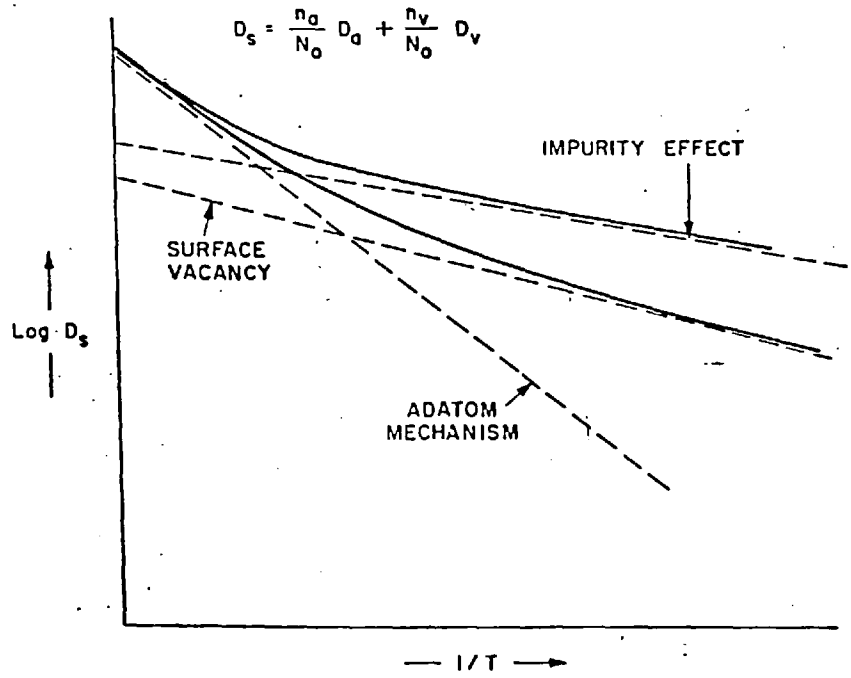


FIGURE 9. Schematic representation of temperature dependence of log D_s when both the adatom and surface vacancy mechanisms are operative. Possible influence of impurities on the surface vacancy mechanism (upper solid curve).

from Gjostein 1967 Fig. 1.4

Gjostein,(1968); see also Blakeley and Olson, 1968) agree well with the predicted values. Again, a sharply curved Arrhenius plot has been shown for (110) vicinal surfaces in nickel and copper, for tungsten and for nickel, by the same technique (Bonzel and Gjostein,(1969), Bowden and Singer, 1969 and Mills et al,(1969), and for a copper field emitter tip by Warner (1967). In addition, Rhead (1969) has shown that very high values for D_s obtained near the melting point in the presence of adsorbed species fit a high-slope extension of the base curve of Gjostein very well.

Discussion of the factors causing the variation in D_s with relative temperature is still proceeding. Gjostein (1967) originally suggested that adatom diffusion dominated at high temperatures while surface vacancy transport was important at low ($T \leq 0.7\ T_m$) temperatures. At the time, theoretical estimates of adatom diffusivity energies agreed well with the observed high temperature Q_s, and the low value of Q_s for vacancies (Q_s^v) was ascribed to greater relaxation in the electronic structure around a vacancy than an adataom; alternative support could be drawn from the calculations of Schwoebel (1967) showing (from simple bond-breaking calculations) that the energy for surface vacancy generation from kinks is less than that required to dissociate an atom from a kink to a self-adsorbed position.

The addition of vacancy D_o^v and adatom D_o^a

diffusivities to the total D_s on this theory is illustrated in fig. 1.4, where n_a, n_v and N_o are the adatom, vacancy and total surface concentrations respectively. Expansion of the equation used gives

$$D_s = \frac{n_a}{N_o} D_o^a \exp\left[-Q_s^a/RT\right] + \frac{n_v}{N_o} D_o^v \exp\left[-Q_s^v/RT\right] \qquad (1.6)$$

In a later paper (Wynblatt and Gjostein, 1968) it was realized that in order for this explanation to hold, it must be true that for all surface orientations, $Q_s^a > Q_s^v$ and $D_o^a >> D_o^v$.

However, detailed calculations of the relaxation and migration energies of adatoms and terrace vacancies on (111), (110) and (100) surfaces yielded results that indicated that these inequalities were not both satisfied in crucial cases. This added strength to the arguments advanced in Bonzel and Gjostein (1969)(supported by Mills et al, 1969) that the adatom-vacancy hypothesis was inadequate to account for the variation in D_s. The hypothesis was then modified to include the contribution of paired defects to the vacancy diffusivity, and thus becomes similar to the suggestions (Seeger et al, 1965 , Nowick and Dienes, 1967, Wynblatt, 1969) of multivacancy contributions to bulk self diffusivities in metals.

An entirely different approach to the problem is made by McLean and Hirth (1968),who present an analysis of the

temperature dependence of Q_s in terms of ledge faceting. In view of the limited experimental data available, one can only speculate as to the actual mechanism of the diffusion predominating at low temperatures.

1.3.3.2. Diffusion in the presence of adsorbed layers.

In a number of cases, values of D_s have been reported which differ widely from those quoted in fig. 1.4: these are plotted in fig. 1.5, from Gjostein's paper. Gjostein suggests that it is reasonable to suspect impurity adsorption in those cases where D_s does not fall on the base curve: for example, the results of Brandon, Bradshaw and Wheeler (1964) show a steady increase in D_s from those obtained in hydrogen (base curve), through those obtained at 10^{-7} torr vacuum, to the high result obtained at 5×10^{-5} torr. Other adsorbents cause decreases in D_s however, and theoretical prediction of the effect of adsorbents gives little help in judging the effect of a particular adsorbent on a metal surface. At low impurity coverages, enhancement of D_s may occur by reduction in the heat of formation for adatom or vacancy formation, thus increasing $\frac{n_a}{N_o}$ or $\frac{n_v}{N_o}$. Alternatively, foreign atom-vacancy complex formation may be possible; if the jump frequency of such complexes is sufficiently high, they will raise the value of D_s. By contrast, reductions in D_s may be ascribed to the formation of foreign adatom-vacancy pairs, with low jump frequencies:

or to the 'pinning' of ledges by the preferential adsorption, at short intervals, of adatoms, preventing mass transport by ledge movements. Until direct experimental evidence of any of these processes affecting measured diffusion coefficients is available, the postulated mechanisms can be little better than speculation.

Self-diffusion in the presence of near-complete adsorbent coverage is shown in fig. 1.5. Diffusion can take place within any of the three layers: by metal vacancy diffusion in level 3, by impurity or metal vacancy diffusion in level 2, or by adatom diffusion in level 1: adatoms could arrive at this level either from level 2, or from level 3 after tunneling through defects in the adsorbate layer. There appears to be no calculations available on the energetics of these various processes, and theoretical prediction of self-diffusion behaviour in the presence of strongly adsorbed species is not yet possible.

Experimental work on self-diffusion in the presence of adsorbed layers is sparse. The work of Collins and Shewmon (1966), and of Brandon, Bradshaw and Wheeler on copper in the presence of adsorbed sulphur and oxygen respectively, showed (fig. 1.5) increases in D_s of up to an order of magnitude, under conditions where monolayer coverage was approached. Mills et al (1969) found, however, that the value of D_s decreased on nickel in the presence of oxygen.

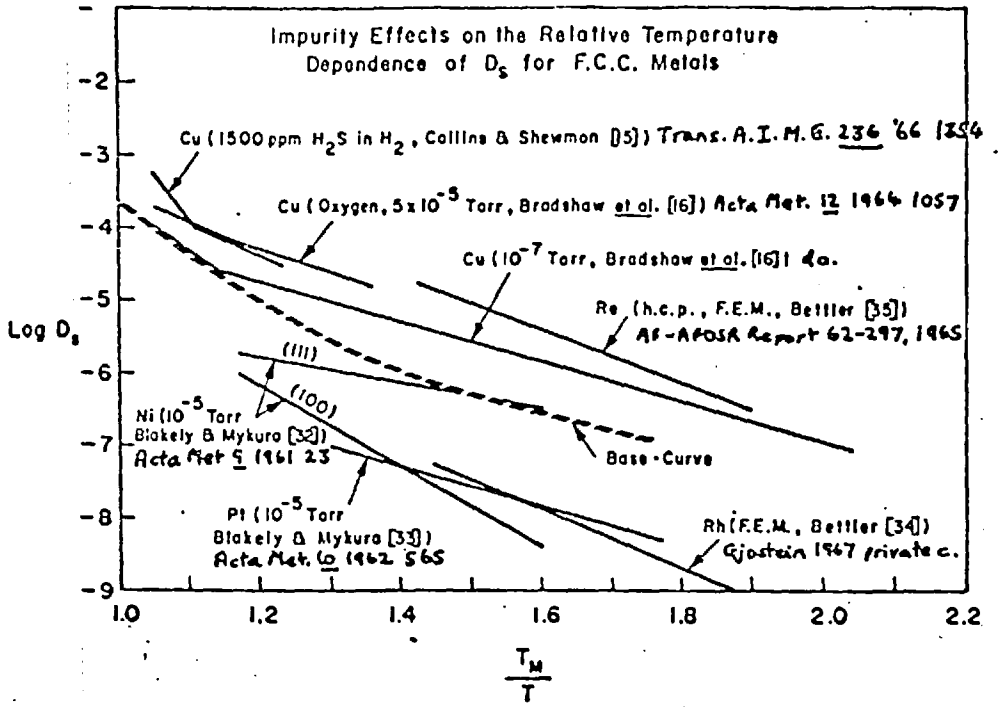


FIGURE 10. Impurity effects on the relative temperature dependence of D_s for FCC metals.

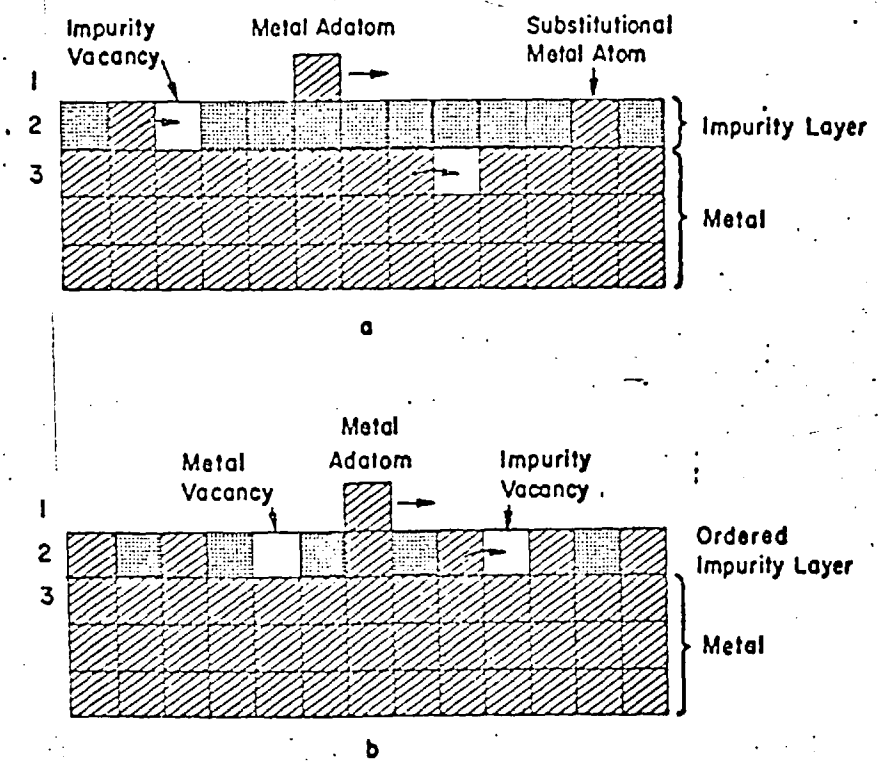


FIGURE 13. (a) Schematic representation of diffusion of metal atoms by adatom mechanism (layer 1), impurity vacancies (layer 2), and metal vacancies (layer 3). (b) Same as 13 (a) for ordered impurity layer.

from Gjostein (1967) Fig 1.5

On silver, sulphur is known to cause large increases in D_s of several orders of magnitude (Perdereau and Rhead, 1967). Oxygen also increases D_s in silver: results from Rhead (1965), and Brandon and Bradshaw (1966), are plotted together in fig. 1.6, together with results from silver in hydrogen (Perdereau and Rhead, 1967). Although there are some discrepancies between $9 < 10^4/T < 10.2$, and the scatter on the low temperature points is wide, there is a general progression for high activation energy (54 kcals/mole) for silver in air at temperatures above $\frac{T}{T_m} = 0.80$, through 28.3 kcals/mole for $0.87 > \frac{T}{T_m} > 0.60$, to 19.4 kcals/mole below $\frac{T}{T_m} = 0.53$. Thus even in the presence of a strongly adsorbed layer, the possibility exists of some kind of dual-mechanism diffusion process as was proposed for clean surface by Gjostein (1967). Secondly, D_s is increased in air by between $10^{0.5}$ - $10^{1.3}$ by comparison with hydrogen at high temperatures. At low temperatures, the only comparison available is that of Brandon and Bradshaw (1966), where an increase of $10^{1.8}$ - $10^{2.2}$ was observed in air compared with a vacuum of 10^{-6} torr.

1.4. Annealing Behaviour of Metal Surfaces.

A variety of changes in the surface topography of metals occurs at temperatures sufficiently elevated to allow diffusion mass transport. In the following section, types of surface change in free metal surfaces are briefly described first, as an introduction to the comparable changes that have

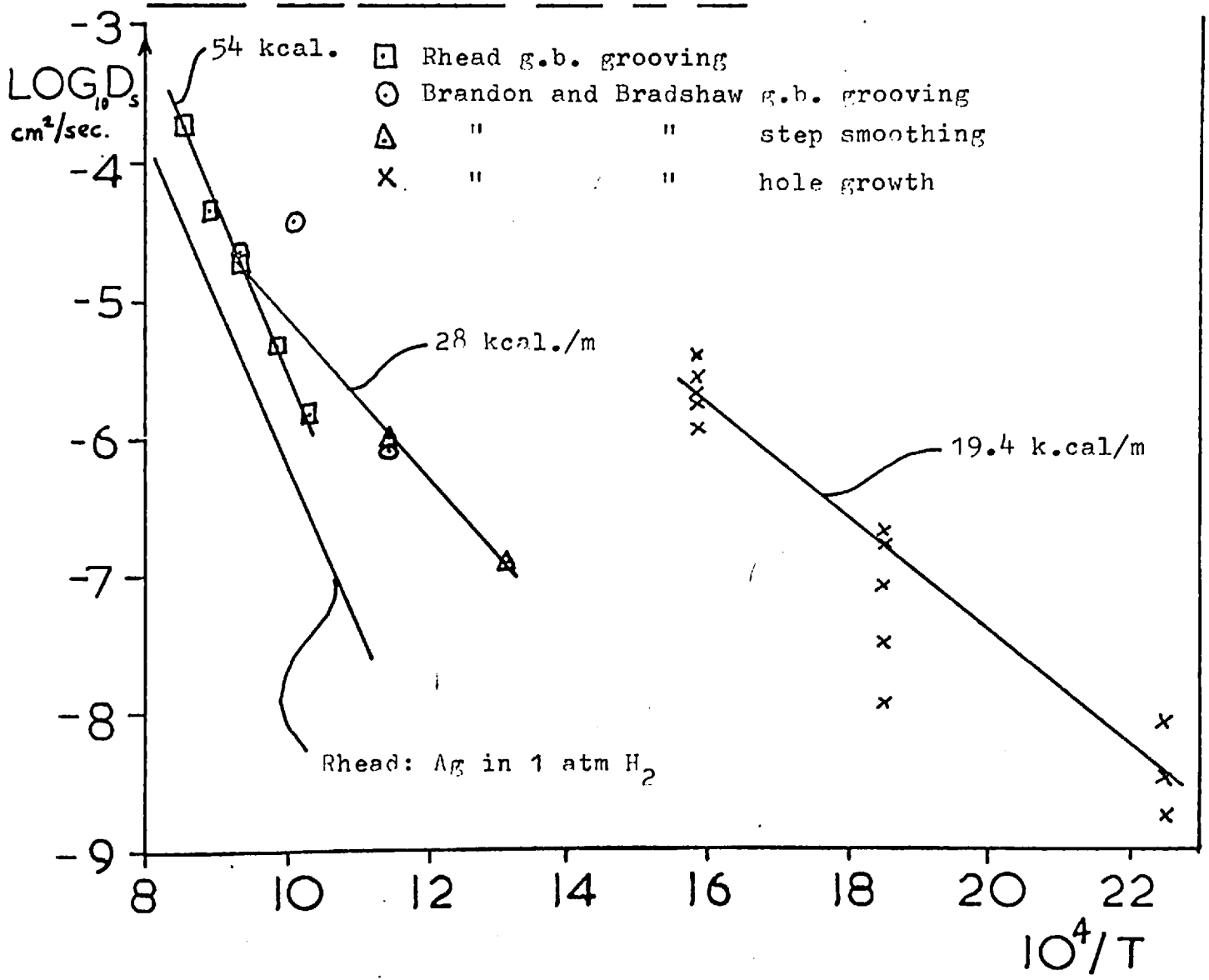

SILVER SELF-DIFFUSION DATA IN AIR
LOG10Ds
cm²/sec.
-3
-4
-5
-6
-7
-8
-9
8
10
12
14
16
18
20
22
10⁴/T
54 kcal.
Rhead g.b. grooving
Brandon and Bradshaw g.b. grooving
" " step smoothing
" " hole growth
28 kcal./m
19.4 k.cal/m
Rhead: Ag in 1 atm H2

Fig 1.6

been observed in thin single crystal or polycrystalline films. Existing analyses of the kinetics of the shape changes are outlined.

1.4.1. Free metal surfaces - analyses of Mullins.

Under the influence of surface energy, grooves develop at the intersection of a grain, or twin, boundary and a free surface, in most metals. A schematic thermal groove is shown in fig. 1.7. The grain boundary (interfacial energy γ_b) will shorten in the y direction until γ_b is balanced by the energy γ_s of the two solid-vapour interfaces; i.e. $\gamma_b = 2\ \gamma_s \sin\theta$, where θ is the equilibrium groove angle. The surface curvature implied in the formation of the groove, gives a higher chemical potential which can be related to the surface curvature K by the Gibbs-Thomson relation,

$$\Delta\mu = \gamma\Omega/r = \gamma\Omega K \qquad (1.7)$$

where $\Delta\mu$ is the change in chemical potential, γ the surface energy, and Ω the atomic volume. A flux of atoms therefore occurs along the chemical potential gradient, resulting in the widening and deepening of the groove.

The theory of the thermal grooving process was given by Mullins (1957, 1960). Several mechanisms for mass transport were considered, including surface and volume diffusion, evaporation-condensation, and mass transport through a passive gaseous phase. Grooves formed by

evaporation-condensation have no maxima at the groove edge, but all others do (fig. 1.7), where the time dependence of groove dimensions are also shown). The analytical solutions for all cases are similar. Surface-diffusion grooves may be used as an example: the groove width w (between maxima) and depth d are shown to depend on time according to the relations

$$d = 0.973\, n\, (Bt)^{1/4} \qquad \text{where } n = \tan\theta$$
$$w = 4.6\, (Bt)^{1/4} \qquad \text{and } B = \frac{D_s \delta \Omega^2 \gamma_s}{kT} \qquad (1.8)$$

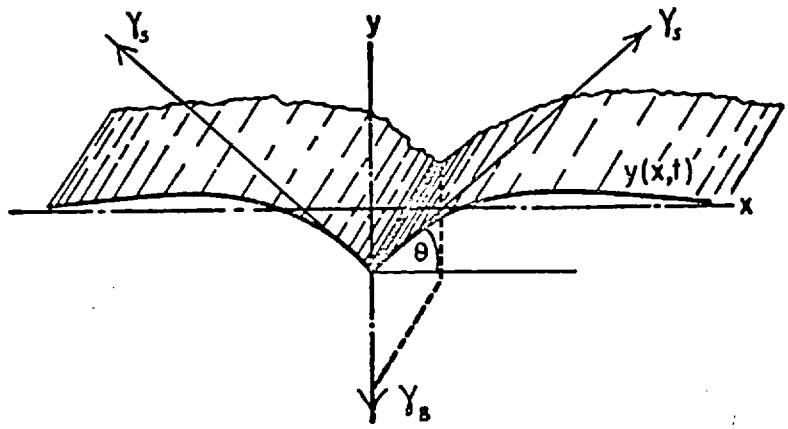
where δ is the effective depth of the high diffusivity surface layer, and Ω is the atomic volume.

A second type of surface profile change results from thermal faceting (reviewed by Moore, 1963). Under certain conditions, (generally at a critical pressure of oxygen or, in some cases, sulphur, in the atmosphere) flat metal surfaces annealed at sufficiently high temperatures break up into a hill and valley structure, consisting of the facet - a simple, low-index plane - and a complex plane. This generally occurs as a result of the lowering by preferential adsorption of the surface energy of the simple plane, and the process appears to rearrange the surface under the new conditions to give minimum free energy. The half-width of the facet x has been shown by Mullins (1961) to vary with time t according to $x = w(Bt)^{1/4}$ where w is a function of the facet-complex plane angle.

Mass-transport topography changes in free metal surfaces

Fig 1.7

i. Grain boundary grooving

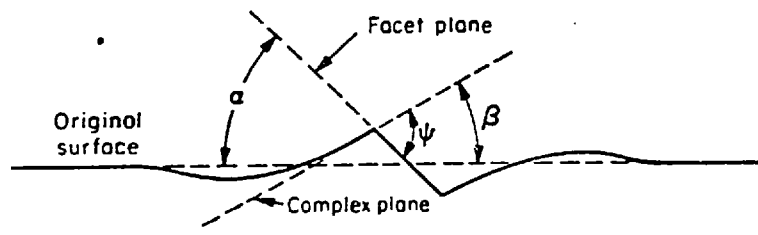


Profile of ideal thermal groove. Vertical exaggeration, about 5×. (8)

Table 1. Time Dependence of Thermal-Groove Dimensions and Shape of Groove Profile for Various Mechanisms of Matter Transport

Transport mechanism	Time dependence	Shape of profile
Evaporation-condensation	$t^{1/2}$	No maximums
Surface diffusion	$t^{1/4}$	Maximums: $w/d = \frac{4.73}{\tan \beta}$
Volume diffusion in solid	$t^{1/3}$	Maximums: $w/d = \frac{4.95}{\tan \beta}$
Volume diffusion in passive gas at 1 atm pressure	$t^{1/3}$	Maximums: $w/d = \frac{4.95}{\tan \beta}$

ii. Faceting



From Gjostein (1963)

The smoothing of artificially produced scratches, and of sinusoidal surfaces, also occurs by surface diffusion; Gjostein (1963) discusses the kinetics of the process, which follows Mullins' general theory (1959) of surface flattening under the influence of surface forces.

1.4.2. Continuous single-crystal thin film surfaces: analysis of Brandon and Bradshaw.

Specialised cases of surface-diffusion controlled shape changes have been studied for thin film evaporated single crystals, mainly of silver, by Brandon and Bradshaw (1966). The decay of two types of step, and the growth of holes, was observed; the last is here reviewed in detail, as the theory developed for the process will later be expanded to account for results obtained in the present work.

1.4.2.1. Decay of a step.

During the evaporation of metal onto mica having cleavage steps in the surface, the upper surface formed replicates the underlying topography. Under conditions where surface diffusion was known to be the dominant mass-transfer mechanism, the theory of Mullins (1959) for surface smoothing was extended to evaluate the profile $s(x,t)$ of a step after time t at distance x from the edge. The driving force for surface diffusion is the high chemical potential of atoms at the small radius of curvature of the step edge. $s(x,t)$ was shown to be given by a converging series involving the initial

height α , and the dimensionless quantity $u = x/(Bt)^{1/4}$.

In experiments carried out on stepped silver surfaces, Brandon and Bradshaw were able (by optical microscopy) to follow profile changes down to 480°C, with D_s values of about 1.5×10^{-7} cm^2/sec. The results obtained are plotted in fig. 1.6.

1.4.2.2. Smoothing of a stepped deposit-substrate boundary.

Surface migration from the edge of a stepped deposit onto the surrounding blank substrate will cause continual smoothing of the step (fig. 1.8a). A series defining the profile change was not obtained, and additional experimental difficulties with copper prevented quantitative comparison of step smoothing with theory.

1.4.2.3. Growth of holes in evaporated films.

The growth of holes in a film reduces the total interfacial energy of the deposit. Such a hole, radius r, is schematized in fig. 1.8b. Brandon and Bradshaw assume that the film-substrate contact angle is constant at 90° (this could be checked by s.e.m., as could the following point), and that the radius of curvature of the 'hump' around the hole is a constant, x. Then the difference in chemical potential between an atom at the hole edge μ_L and at the undisturbed surface μ_∞ (assumed to begin beyond a distance $s = \pi x$ from the hole edge) is given by

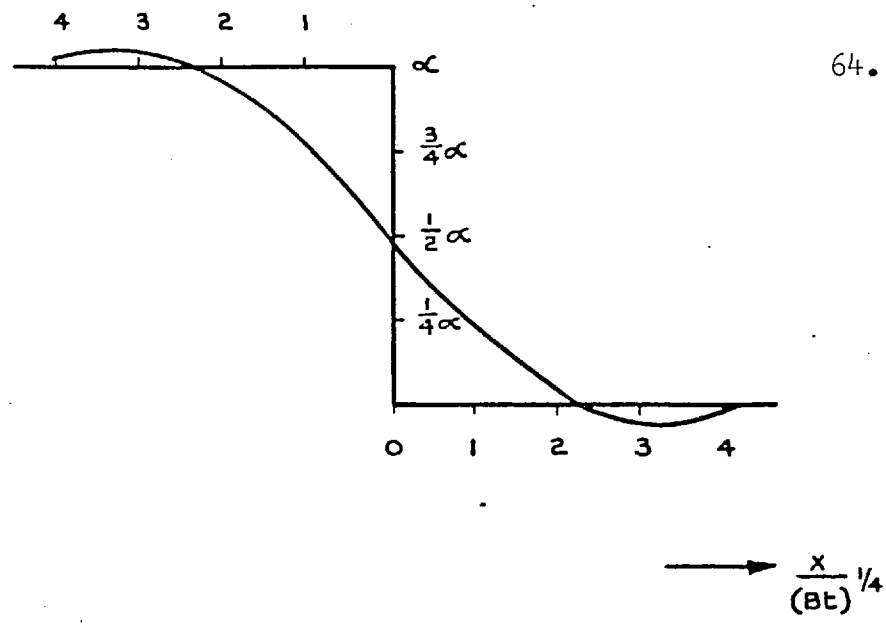
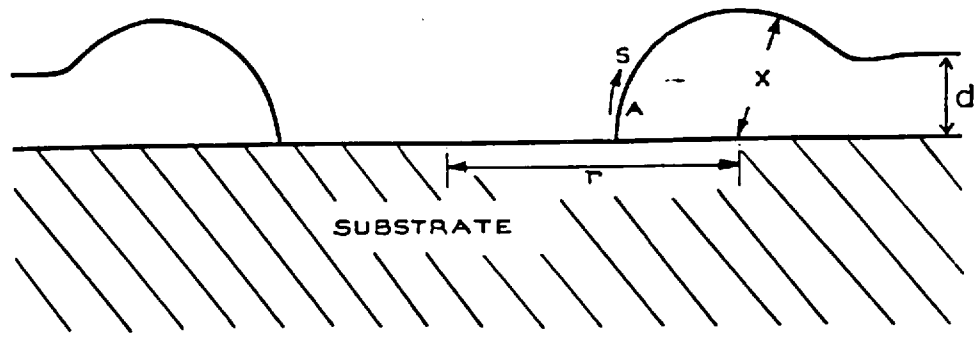


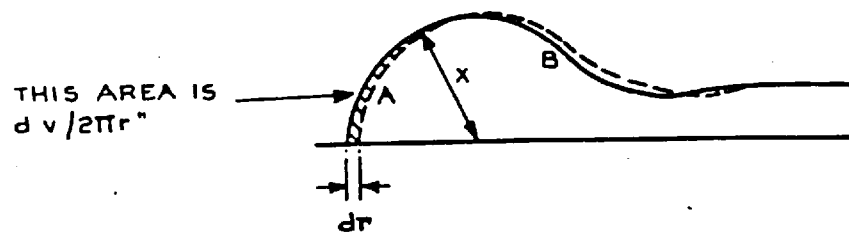
Fig 1.8a THE SMOOTHING OF A STEP OF HEIGHT α, DUE TO SURFACE DIFFUSION

Fig 1.8b HOLE GROWTH

Analysis of Brandon and Bradshaw



a. Hole profile



b. Profile change

$$\mu_L - \mu_\infty = - \Omega \gamma_s \left\{\frac{1}{x} - \frac{1}{r}\right\}$$

$$\simeq - \Omega\gamma_s/x \quad \text{for } r >> x. \qquad (1.9)$$

The net flux j_s along the surface is given by

$$j_s = - \frac{D_s}{kT} \frac{\partial \mu}{\partial s} \nu$$

where ν = surface concentration of atoms (1.10)

Hence $$j_s = \frac{D_s \Omega \gamma_s}{kT \pi x^2} \nu \qquad (1.11)$$

The volume rate of transfer $\frac{dV}{dt}$ across the hole perimeter $2\pi r$ is $j_s 2\pi r \Omega$. Hence

$$\frac{dV}{dt} = \frac{2D_s \Omega^2 \gamma_s r}{kT x^2} \nu \qquad (1.12)$$

From this, r can be eliminated since $\pi x^2 = rd$ (mass balance) and $(\frac{dV}{dt})$ can be eliminated using the fact, seen from fig. 1.8b, that

$$dV = 2\pi r x \, dr \qquad (1.13)$$

Hence $$\frac{dV}{dt} = 2\pi r \frac{rd}{\pi} \frac{dr}{dt} \qquad (1.14)$$

Substituting and integrating gives

$$r^{5/2} = \frac{\pi^{1/2} Bt}{2d^{3/2}} \qquad (1.15)$$

where B has its usual significance.

Hence for a given film thickness d, the variation of $r^{5/2}$ with time t should be linear.

Using single crystal silver films in air, good agreement with this law was obtained by Brandon and Bradshaw for the growth of holes as followed by optical microscopy. D_s values were deduced, and are plotted in fig. 1.6. As a method for determining diffusion coefficients, the method has the advantage that by using sufficiently thin films, optically measurable changes occur in reasonably short times, even for values of B and D_s one or two orders of magnitude less than those producing measurable changes in practicable time intervals by other methods: e.g., using a 1100 Å film, measurements of D_s of ca. $10^{8.5}$ cm^2/sec were made at 175°C.

1.4.3. Polycrystalline thin-film surfaces.

1.4.3.1. Continuous films.

Existing work on surface morphology annealing effects in thin films is not extensive, and although some indication of factors controlling the kinetics may be inferred, the lack of work describing more fully the structure and energetics of such processes will be apparent. Two main classes of effect have been observed: agglomeration into discrete islands, and surface hillock growth.

a) Agglomeration.

The structures formed when thin polycrystalline films agglomerate into islands are barely resolvable by optical microscopy (Brandon and Bradshaw, 1966),

and electron microscopy was in fact used in an early report of agglomeration effects by Borel (1955). Island formation was there found to occur whenever a silver film on collodion supports was heated, whether directly in air or by the electron beam in the microscope. The brief observations of Gimpl et al (1964) indicated similar conclusions for gold and nickel films, of which thin (below 400 Å) films heated in an electron microscope formed, first a hole structure, and then discrete islands (supported by an amorphous layer) at about 700°C, with equilibration to more circular islands above 700°C. Caswell and Budo (1964) observed agglomeration when continuous tin films deposited below 2×10^{-8} torr at 78°K on freshly deposited SiO were allowed to warm to room temperature. In this case, the admission of oxygen at ca. 10^{-4} torr pressure prevented or arrested agglomeration, although the mechanism for this effect was not apparent. The fixation effect was removed when the tin was protected with an evaporated SiO overlayer. Hole formation followed by agglomeration at higher temperatures was also observed for tin, on freshly evaporated SiO at 100°K by Scharnhorst (1969), who found that the temperature for first forming holes increased with the thickness of the film. Hole formation was suggested to be due not to dust contamination (Holland (1956); Jorgenson and Wehner (1963)), but to the tendency of the film to agglomerate. The final number of holes was

always largest in films with the largest residual resistivities, and this suggested that hole formation depends on the defects in the original film.

Annealing studies of a thin-film 'sandwich' structure of gold between CdS layers, were made by Kane et al (1965), who also used exposed gold films on CdS. By varying the thickness of exposed films which were then annealed in vacuo for a constant time, agglomeration was seen to proceed faster and to produce smaller islands when thinner films were used. 'Sandwiching' the films did not greatly affect agglomeration, but in these specimens the islands tended to remain interconnected by narrow bridges of metal. The agglomemeration was followed in conjunction with measurements of resistance versus time; a portion of the latter curve was found to follow the relationship $R = R_o e^{\alpha t}$, where α varied with temperature according to $\alpha = \alpha_o e^{-E/kT}$. Correlation with micrographs suggested that this linear portion corresponded to the hole growth period. E was found to be ca. 1.8 eV (or 41 kcals/mole), and the authors suggested that this figure defines the activation energy for the migration of gold atoms during agglomeration. This value compares well with Q = 41.7 kcals/mole for the volume self-diffusion of gold (Holcomb and Norberg, 1955). The value of Q for surface self-diffusion at these temperatures ($T/T_m < 0.6$) is much lower, ~ 15kcals/mole (Geguzin et al.,1964). It

seems reasonable to suppose that volume diffusion is important in the hole growth stage of the results of Kane et al.

Extensive hole growth effects have also been observed in the work of Swank and Lawless (1965) and of Nielsen et al (1967) on catalysis over thin films of copper at moderate temperatures.

b) Hillock growth.

A few observations exist of an unusual mode of surface reorganization in evaporated films: hillock growth. d'Heurle et al observed the annealing of a 5000 Å aluminium film, deposited at 10^{-7} torr and known to have a tensile stress of 2×10^{-9} dynes/cm^2. On annealing at 560°C in nitrogen for 20 minutes, hillocks were produced on the surface, which did not extend beyond the original grain boundary. Annealing was known to increase the tensile stress by 0.7×10^{-9} dynes/cm^2. Similar observations on lead films were made by Caswell et al (1963). Pennebaker (1968) also reports hillock growth on gold films, finding their height to be proportional to the area occupied.

Two somewhat different accounts have been given for hillock growth, both in terms of stress relief as the driving force. Pennebaker assumes that hillocks form at those grains where the structure allows rapid local stress relief by grain boundary movement. The stress relieved by

Diffusion stress relief in relation to hillock formation

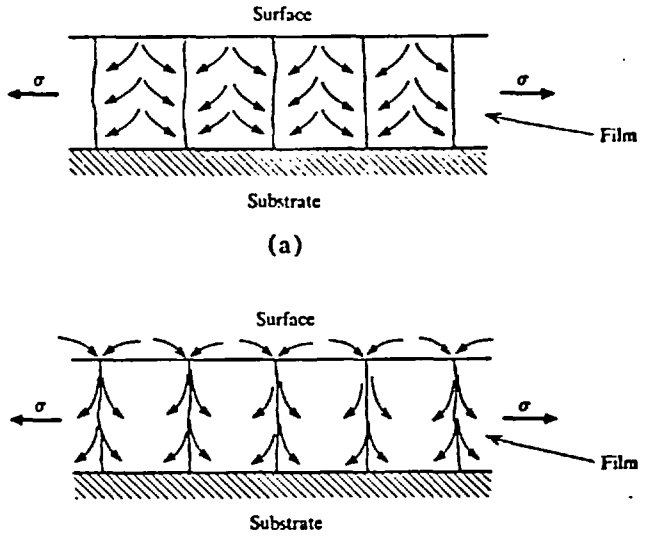


Figure 6 Schematic representation of diffusion currents in a film. (a) Volume diffusion is rate-controlling. (b) Grain boundary diffusion is rate-controlling.

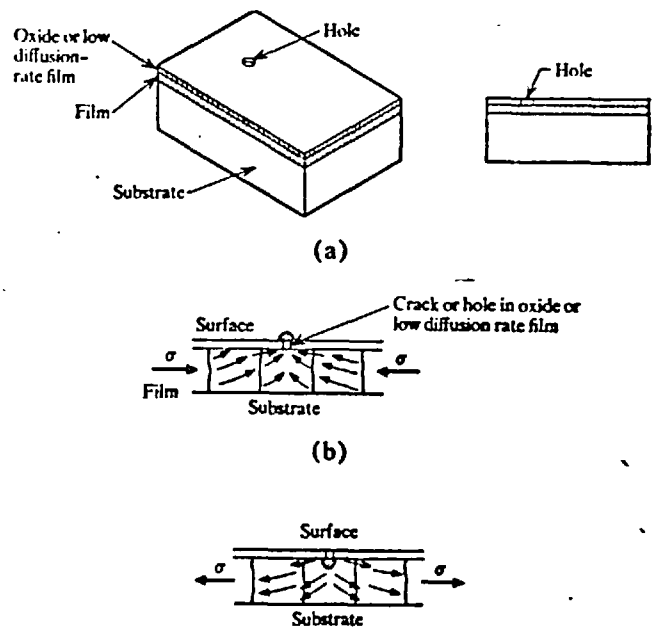


Figure 7 Film on a substrate covered by another film that has lower diffusion rates. (a) Hole or crack in a local spot in the covering film. (b) Mass flows out of the film under a compressive stress and is deposited on the surface of covering film. (c) Mass flows into the film under a tensile stress leaving a crater or depression near the hole or crack.

from Chaudhari (1969) Fig.1.9

this recrystallization is assumed to come from the difference in thermal expansion of film and substrate. Using a theory by Mott for the effect of driving force on grain boundary motion, a model is developed which accounts for the slow rate of stress relief and the hillock growth kinetics. Chaudhari (1969) points out that during stress relief by diffusion creep in the polycrystalline films, material is transferred from the interior of a film under compressive stress, to its surface (and vice versa). If only selected areas of the surface are able to act as mass sinks (e.g. cracks or holes in a low-diffusion rate surface layer), then hillock growth will occur. In this case, no experimental correlation is offered, other than the hillock growth observations quoted; these are unlikely to have been affected by low diffusivity surface layers.

1.4.3.2. Discontinuous films.

The annealing of discontinuous metal films has been observed by a number of authors, e.g. Bachmann et al (1964); Perrin and Fauré (1966); Skofronick and Phillips (1966, 1967); and Phillips, Desloge and Skofronick (1967). Where microstructures were observed, increases in the mean radius and radius dispersion of the particles were noted, together with a decrease in the fraction of substrate area covered by nuclei. Perrin and Fauré observed such effects for 19-37 Å silver films deposited on carbon at ca. 10^{-5} torr

and then simply exposed to air for 28 hours. Bachmann et al report 5-10 x particle size increases using ca. 25 Å thick copper films evaporated at 10^{-9} torr onto carbon substrates and annealed at 500°C in vacuo, but found no agglomeration on SiO substrates. However, Skofronick and Phillips (1967) using gold, did obtain agglomeration on both carbon and SiO substrates. A computer technique was developed for numerical analysis of the particle distribution from micrographs, and the results have been used for an analysis of the statistical behaviour of the islands, which were assumed to move bodily from a 'trapping site' when given sufficient thermal energy. Good agreement was obtained in most cases with a prediction that (mean island radius)$^{7/2}$ α annealing time, and the results were used to give a binding energy of 1.29 eV = 29.7 kcals/mole for gold-carbon, and 1.52 eV = 35 kcals/mole for gold-SiO. Very different results were however obtained at low substrate temperatures in an experiment by Skofronick and Phillips on steady resistance increases in similar thin gold films on mica deposited at 90-297°K, which occurred more rapidly at higher temperatures, and on changes in cold-deposited films allowed to warm to room temperature, where R first decreased and then increased. In a model in which the changes were assumed to be due to coalescence of thermally activated islands, assumed island spacings of ca. 30 Å and an activation energy

for motion of ca. 0.17 eV (3.9 kcals/mole) produced good agreement with the observed resistance-time curves.

Both direct and theoretical support exists for the model of bodily island movement followed by coalescence during annealing. Alternative mechanisms of mass transport are unlikely at the temperatures employed since the energy requirements are too great: e.g. for the removal of an atom from a gold island, which could subsequently migrate over the substrate, Zinsmeister estimates (1966b) an energy of 2.23 eV, showing that atomic break-up of nuclei is negligible below 700°K. Equally, evaporation-condensation would be negligible at these temperatures.

Direct observations of coalescence have been made by Pashley et al (1964) and by Bassett (1961) during electron microscope observations of the growth of gold and silver deposits from the vapour onto graphite and molybdenite. Bassett reported that silver crystallites of 20-100 Å diameter moved randomly over the heated substrate (300°C), while maintaining an orientation relationship (seen by moiré fringes),and could coalesce with other particles on collision. Particle-free 'capture paths' behind large islands were observed in specimens of Phillips et al (1967, figs 1-3). Sears and Hudson (1963), discussing the results of Bassett, proposed that the migration involved Brownian motion of the particles, made possible by the presence of an adsorbed gas layer intervening at the contact with the substrate and

having a very low shear stress (ca. 10^6 dynes/cm^2). Subsequently, Thomas and Walker (1964), discussing Sears and Hudson's explanation, pointed out from experimental results that under identical conditions, some metals might show their mobility (Ag, 630°, Ta, 720° on graphite [0001] surface in Ar, N_2), while others showed none (Fe, Co, Ni, Mn). Secondly, the atmosphere had a profound influence on mobility: in oxygen, cobalt particles, oxide-coated, moved rapidly and rotated. These observations indicated that the simple boundary shearing explanation of Sears and Hudson must then be adjusted to take account of the effects of adsorbed oxide layers, both on themetal and possibly on the graphite surface.

Further work in this field therefore demands careful investigation of the observed adsorption effects on mobility, and the discovery of the origin and mechanism of the thermally activated coalescence process, particularly in view of the widely differing results of Skofronick et al, on gold at low and high temperatures.

1.5. Catalytic Activity in Relation to Microstructural Changes in Metals.

1.5.1. Interrelation of factors affecting activity and microstructure.

Earlier (1.1.4) it was concluded that many catalytic activity changes were related to alteration in microstructure or microdispersion during reaction. It is now possible to see that these microstructural changes are accessible to investigation as problems in metal surface physics: e.g. the energetics and kinetics of topography changes in metal surfaces and films. For example, the growth of metal crystallites under pre-reduction or reaction conditions, which is often connected with a loss in catalytic activity (1.1.3.2), can be related to existing investigations of possible mechanisms of island growth in annealed supported island structures (1.4.4.3 b), even though the pore structure of the substrate in practical catalysts poses practical problems of observation. If surface diffusion over the substrate were shown to be the mechanism of growth, ways of inhibiting the diffusion might then become accessible. Again, the observations of Nielsen et al (1960) (1.4.4.3) were of catalytic activity changes under conditions where surface faceting was operating. However, the link between surface physics problems and those of catalyst rearrangement is not a direct one: for the conditions under which catalysts undergo changes in

microstructure are in general far less well defined, and reproducible, than those under which metal surface studies designed to isolate one particular property, are carried out. Thus in an attempt to overcome the ill-understood effects of hydrocarbon vapour contamination, surface diffusion experiments are now carried out for preference under ultra-high vacuum ion-pumped conditions. The results of diffusion studies under clear conditions can only with caution be extended to interpret metal transport observed under catalytic conditions where a variety of adsorbents, not all necessarily known, may be present. Nevertheless, the attempt is necessary if catalytic studies are to be placed on a rational basis. It was on this basis that the present study of microstructural changes in catalysis, now to be outlined, was carried out under conditions approaching those met in reactive catalytic atmospheres.

1.5.2. Present work.

The present study was devised to investigate the interelation of microstructural changes in supported catalysts, with activity changes; and to determine the effect of reactive atmosphere and of reactive conditions on these microstructural changes. Two alternative approaches were possible, one using metals dispersed on conventional porous pellets of refractory material, (the form in use for technical applications), the other using a comparable metal-

support system, but with simpler support geometry. The advantages of using a plane, non-porous support were that uniform behaviour could be expected over extended areas, without complicating effects from pore geometry, and that microstructural changes could be observed without resort to difficult sectioning techniques. It was decided therefore to use a plane support, using vacuum deposition to avoid non-gaseous contamination and to produce an initial structure which, though complex, was well described in the literature on thin solid films. The behaviour of this model metal-support system under reactive atmosphere could then be studied under typical conditions using both microscopy and catalytic activity measurements to follow the changes that occur; gas adsorption surface area measurement could also be used to monitor changes in the area available for reaction.

Silica was chosen as the support, and silver for the catalyst metal. The use of silver had the great advantage of particularly ready access in other work to data on its microstructure in films, on its surface energy, diffusivity, and adsorption properties. The importance of silver as a catalyst is in oxidation reactions, and the specific activity for the oxidation of ethylene and hydrogen could be used as tools to monitor changes in catalytic activity of the films. The experimental approach required by this overall plan is detailed in the following chapter.

CHAPTER 2.

EXPERIMENTAL.

2.1. Choice of experimental method.

2.1.1. Microstructural examination of catalyst. 80

2.1.2. Interfacial area measurements. 81

2.1.2.1. Metal-substrate areas. 81

2.1.2.2. Metal-gas areas. 82

2.1.3. Catalytic activity and selectivity. 83

2.2. Preparation of catalyst films.

2.2.1. Materials. 83

2.2.2. Film deposition. 84

2.2.2.1. Apparatus. 84

2.2.2.2. Procedure. 84

2.2.3. Film thickness determination. 86

2.2.3.1. Apparatus. 86

2.2.3.2. Procedure. 88

2.3. Controlled atmosphere annealing of catalyst films.

2.3.1. Static atmosphere annealing. 89

2.3.2. Flowing atmosphere annealing. 91

2.3.2.1. Apparatus. 91

2.3.2.2. Procedure. 92

2.3.3. Partial vacuum annealing. 95

2.3.3.1. Apparatus. 95

2.3.3.2. Procedure. 96

2.4. Microstructural examination of catalyst films.

2.4.1. Transmission electron microscopy. 96

2.4.1.1. Apparatus. 96

2.4.1.2. Specimen preparation. 96

2.4.1.3. Specimen examination. 99

2.4.1.4. Hole and island density measurements. 100

2.4.2. Reflection scanning microscopy. 101
2.4.2.1. Apparatus. 101
2.4.2.2. Specimen preparation. 101
2.4.2.3. Specimen examination. 101
2.4.3. Transmission electron diffraction. 101
2.5. Interfacial area determination.
2.5.1. Metal-substrate areas. 102
2.5.1.1. Apparatus. 102
2.5.1.2. Micrograph examination procedure. 105
2.5.2. Metal-gas areas. 107
2.5.2.1. Apparatus. 107
2.5.2.2. Labelling and handling of krypton. 107
2.5.2.3. Pressure determination. 112
2.5.2.4. Apparatus calibration. 117
2.5.2.5. Specimen preparation. 121
2.5.2.6. Adsorption procedure. 121
2.6. Catalytic oxidation.
2.6.1. Static gas system. 125
2.6.1.1. Apparatus. 125
2.6.1.2. Procedure. 127
2.6.2. Flowing gas system. 127
2.6.2.1. Apparatus. 127
2.6.2.2. Procedure. 128
2.7. Gas analysis.
2.7.1. Apparatus. 130
2.7.2. Procedure. 131
2.7.3. Calibration. 134

2.1. Choice of Experimental Method.

2.1.1. Microstructural examination of catalyst.

The use of microscopy in preference to techniques yielding information on the average distribution of metal in a given sample of catalyst (e.g. X-ray diffraction, physical adsorption etc.), followed naturally from the interest in this work in the mechanism of microstructural changes during annealing, and the consequent need to record the morphology of the metal catalyst at different stages.

Structural changes in single-crystal metal deposits during annealing have been followed by optical microscopy (e.g. Brandon and Bradshaw, 1967), but the scale of structures formed by annealing polycrystalline deposits as used in the present work, is at least one order of magnitude smaller, and demands the far greater resolution available from electron microscopy. Transmission electron microscopy was therefore used for the majority of the work. The preparation of specimens in a form appropriate to the method is described in section 2.4.1. The information obtainable by this method was largely concerned with the two-dimensional distribution of the metal in the plane of the support surface; this was supplemented by the use of reflection scanning microscopy (section 2.4.2) to observe the three-dimensional morphology of the catalyst on the support surface.

2.1.2. Interfacial area determination.

2.1.2.1. Metal-substrate areas.

One of the objectives in using electron microscopy to investigate microstructural changes was to quantify as far as possible the information contained in the micrographs obtained. Much of this aim was achieved by direct counting to yield the density of features observed in micrographs (holes and islands: 2.4.1.3). In addition, the progress of changes during film annealing was followed by measuring the changing area of the interface between metal and support seen in the transmission electron micrographs. Until recently, such area measurements have had to be carried out by the manual division and estimation of the appropriate areas from prints of micrographs. A novel technique (Fisher, 1966) is now available for the measurement of the areas of uniform brightness in microscopic and other images, this is the 'Quantimet' image analysing computer. This instrument has allowed the measurement of a large number of metal-substrate areas from micrographs in a much shorter time than that required by manual methods. The principle of the instrument is given in section 2.5.1.1, and the adaptation of micrographs for examination on the instrument in section 2.5.1.2.

2.1.2.2. Metal-gas areas.

Techniques for the measurement of the metal-gas interface were limited by the small geometric area (up to ca. 1000 cm^2) that could reasonably be produced by evaporation methods onto supports of the type chosen. A gas adsorption method was required, both to investigate the possible porosity of the metal films and to allow correlation between the area of the specimen available for catalytic reaction and the geometric area deducible from electron micrographs. The adsorption method chosen had to be sufficiently sensitive to detect 5% of a monolayer at least. Since a monolayer of nitrogen on an area of 1000 cm^2 weighs 28 $\mu g = 2.24 \times 10^{-3}$ ml., at N.T.P., conventional volumetric methods were unsuitable, having a limit of detection of ca. 0.01 ml under good conditions. Vacuum microbalance techniques offer sufficient sensitivity (down to 10^{-8} g), but the attachment of large areas of catalyst film, even on very thin substrates, to such a balance presented problems both of size and of permissible balance load. A modified volumetric technique was finally chosen, that of Aylmore and Jepson (1961), in which the difficulty of very small pressure/volume changes on adsorption is overcome by the use of radioactively labelled adsorbent for pressure measurements. By measuring the time taken to detect a constant number of emitted particles from the adsorbent in a fixed volume cell, the pressure can be measured to a

precision independent of its absolute value, thus allowing very small pressure changes to be recorded. The method is described in section 2.5.2.

2.1.3. Catalytic activity and selectivity.

After investigating the effects of reactive atmospheres on catalyst microstructure, attention was turned to the relation between catalytic activity and microstructure. Apparatus used for oxidation reactions is described in section 2.6. The static apparatus initially used (2.6.1), in which the rate of reaction was followed by the pressure reduction on the formation of products, was found to be unsatisfactory. The availability of a gas chromatograph system allowed a new approach to be made with a flow reactor (2.6.2). This flow system was also used for the study of ethylene oxidation to ethylene oxide. Progress of the reaction was now followed by in-line sampling of roducts (section 2.7).

2.2. Preparation of catalyst films.

2.2.1. Materials.

Silver and gold: 99.99% wire, 0.010 inch diameter (Johnson Matthey Ltd).

Silica: transparent silica tube, lowest water content.

Pyrex: New 19 mm. no. 1 Chance cover-slips.

2.2.2. Film deposition.

2.2.2.1. Apparatus.

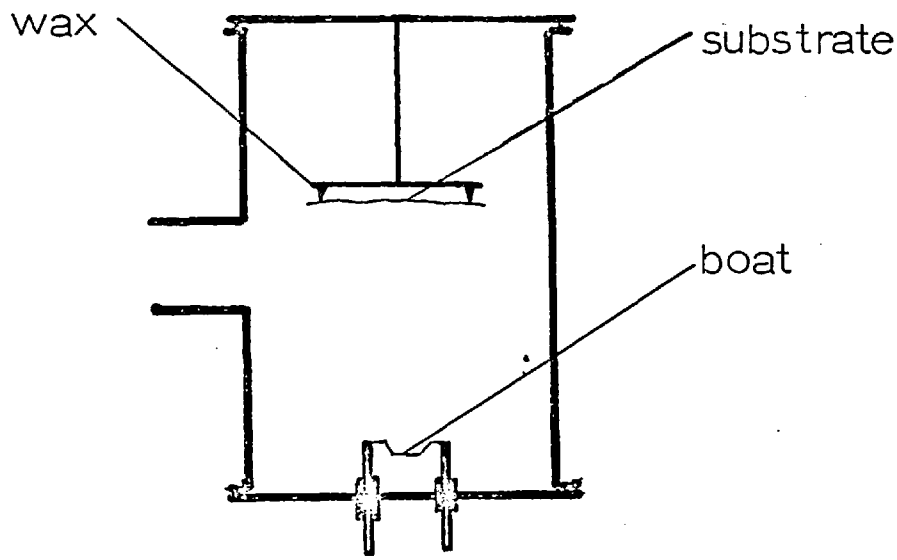
A small high-speed vacuum system was used for most specimen preparation; this was a Balzers Micro BA3 system, in which a rough vacuum is achieved with a two-stage oil-filled rotary pump, and lower pressures with an air-cooled oil diffusion pump. For catalyst film preparation, an N.G.N. 12" bell-jar vacuum system with the rotary and oil diffusion pumping was used. The two systems are illustrated in figs. 2.1 a,b.

2.2.2.2. Procedure.

Silica substrates were produced by blowing a bubble of the molten material in an oxygen-butane flame. Reasonably flat surfaces with a thickness of ca. 0.005 cm could be obtained from large bubbles. Areas of this flame polished surface were mounted in the vacuum system.

Evaporation of the silver was carried out from a molybdenum boat, electrically heated from the power supply of the vacuum unit. The boat was pre-cleaned by heating to ca. 2000°C for ca. 1 minute in a vacuum of 5×10^{-5} torr, in order to remove volatile contaminants. A measured length of silver was degreased in acetone, dried, and placed in the boat. Evaporation was carried out in times of ca. 20-40 secs at ca. 5×10^{-5} torr; the pressure

Balzers system



NGN system

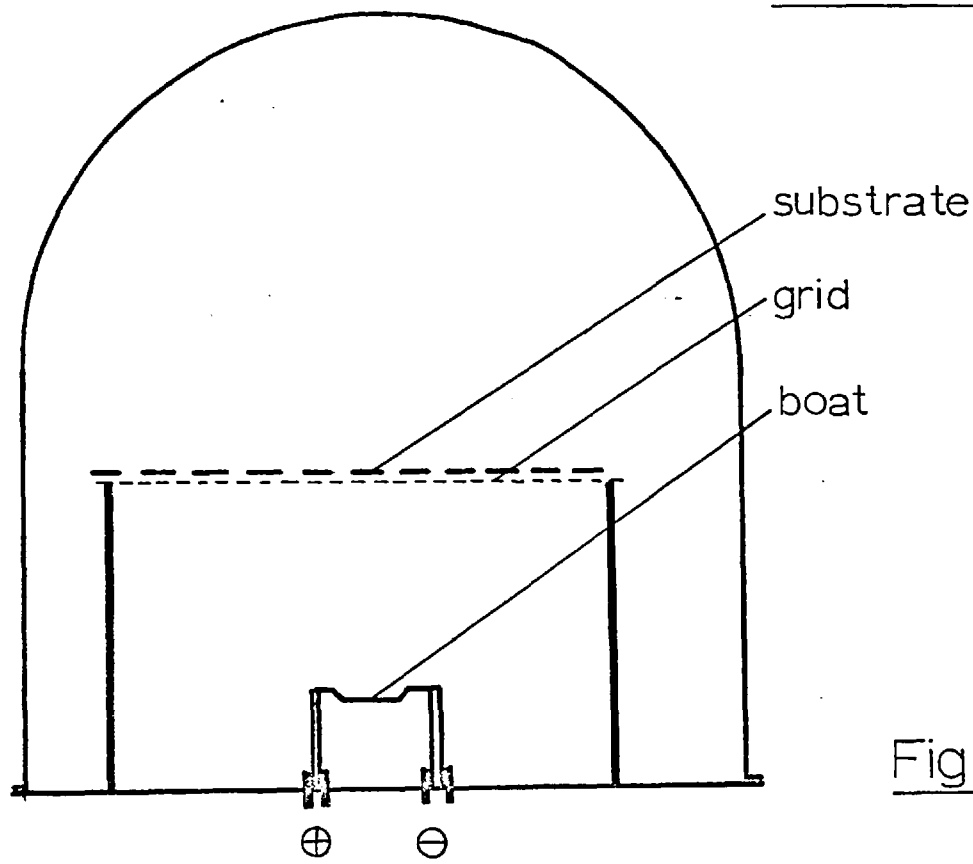


Fig 2.1

was not allowed to rise above 10^{-4} torr. A boat-substrate distance of 15 cm was found to give maximum uniformity in the thickness of the deposit. Care was taken to mount the substrate symmetrically with respect to the evaporation source.

For catalyst film preparation, 19 mm pyrex circular substrates were used, supported by two different methods. Either a copper gauze, 0.21 cm mesh, of .04 cm dia. wire, was used: in this case, the area exposed to the source directly was ca. 65% of the total. Alternatively, an aluminium plate, drilled with 15 mm dia. holes, was used; the area exposed to the source on each pyrex circle above the hole was ca. 60% of its total area.

2.2.3. Film thickness determination.

2.2.3.1. Apparatus.

Although in principle the thickness of evaporated films can readily be calculated from the amount of evaporant and the source distance, uncertainties arise from incomplete evaporation of the material used, and from possible non-uniform dispersion of the material. Thicknesses were therefore measured from equivalent films after the evaporation by multiple beam interferometry, this method depends only on the wavelength of the light used, and is the standard against which other methods are calibrated (Tolansky, 1948; Holland, 1958).

VARIAN MULTIPLE BEAM INTERFEROMETER

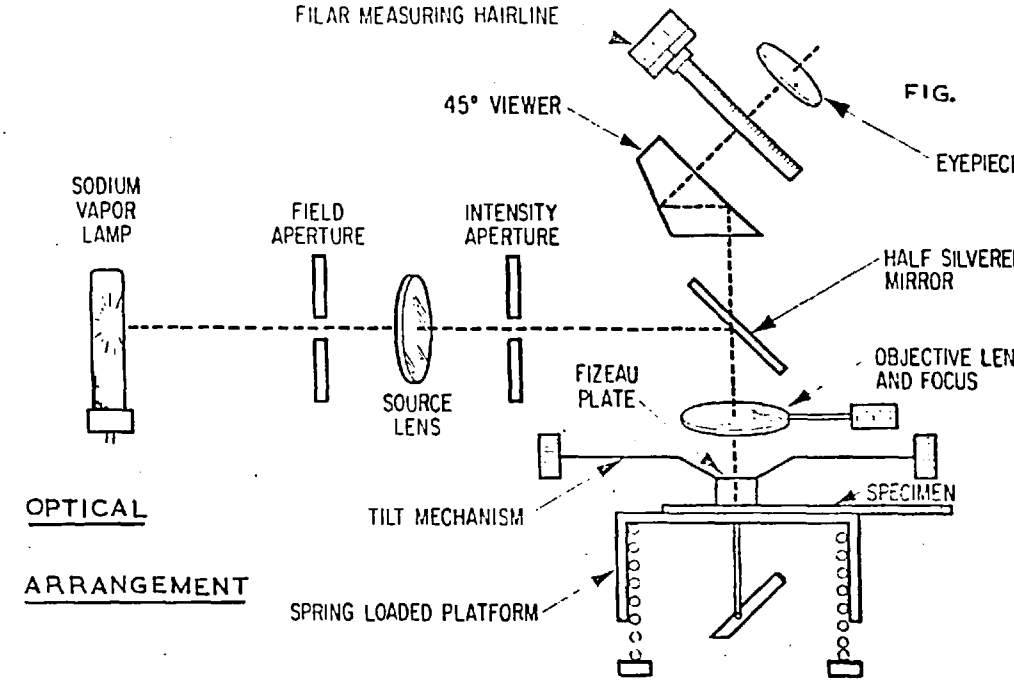


FIG.

OPTICAL ARRANGEMENT

RELATION OF FRINGE STEPS TO FILM THICKNESS STEP

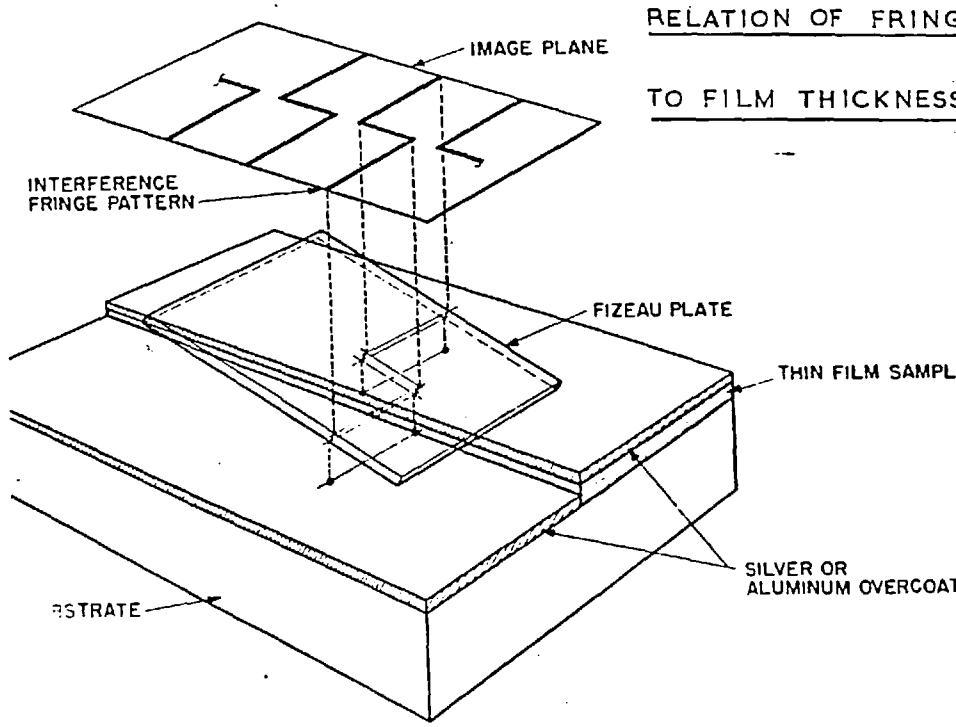


FIG. 2.2

A Varian 'Å-scope' interferometer was used; the principle of the instrument, and the optical path, are illustrated in fig. 2.2. Interference fringes in monochromatic (sodium-D: 2946 Å) light are formed by interaction between rays reflected at the highly reflecting specimen surface and those returning from the half-silvered Fizeau plate in contact with it. The two surfaces are inclined at a very small, adjustable angle so that the path difference required for fringe formation recurs at regular intervals across the field of view. The occurrence of multiple reflections destroys changes in intensity from points very near to the fringe peak, leading to very sharp fringes. Irregularities in the surface observed (in this case the film thickness step) alter the path difference in the interferometer cell, and change the position of the fringes, as illustrated in fig. 2.2.

2.2.3.2. Procedure.

During evaporation, a section of cleaned glass microscope slide was placed next to the silica substrate. The slide was partly obscured by a razor edge in contact with it in order to produce a stepped deposit. The whole of the slide was then made reflective by coating it with ca. 1000 Å aluminium by evaporation. This effectively replicated the step in the upper surface. In the interferometer, the orientation of the slide was adjusted so that the fringes

were perpendicular to the step, with about 15 fringes visible in the field of view. A minimum of ten step heights h and fringe spacings d' were measured. The film thickness is given by:

$$l = 2946 \frac{h}{d'} \quad \text{Å} \qquad (2.1)$$

2.3. Controlled atmosphere annealing of catalyst films.

2.3.1. Static atmosphere annealing.

In initial experiments, specimens were annealed in a static atmosphere. A tubular furnace was fitted with a silica cylindrical chamber, at one end of which was mounted a long silica spoon within a pyrex glass guide. After placing the specimen in the spoon, the apparatus was evacuated to ca. 5×10^{-4} torr by means of a mercury diffusion pump, and the chosen gas was admitted; after re-evacuation, the final atmosphere was admitted to the closed system. The spoon was then moved to the uniform temperature zone of the furnace by the force from an external magnet on an iron slug in the spoon. This apparatus is shown diagrammatically in fig.2.3.

The preliminary experiments in this apparatus were in nitrogen atmospheres, purified over heated copper and in a liquid nitrogen-cooled trap. It was soon found that the microstructural changes observed in the specimens were irreproducible and erratic. The main disadvantages of the

QUARTZ TUBE FURNACE

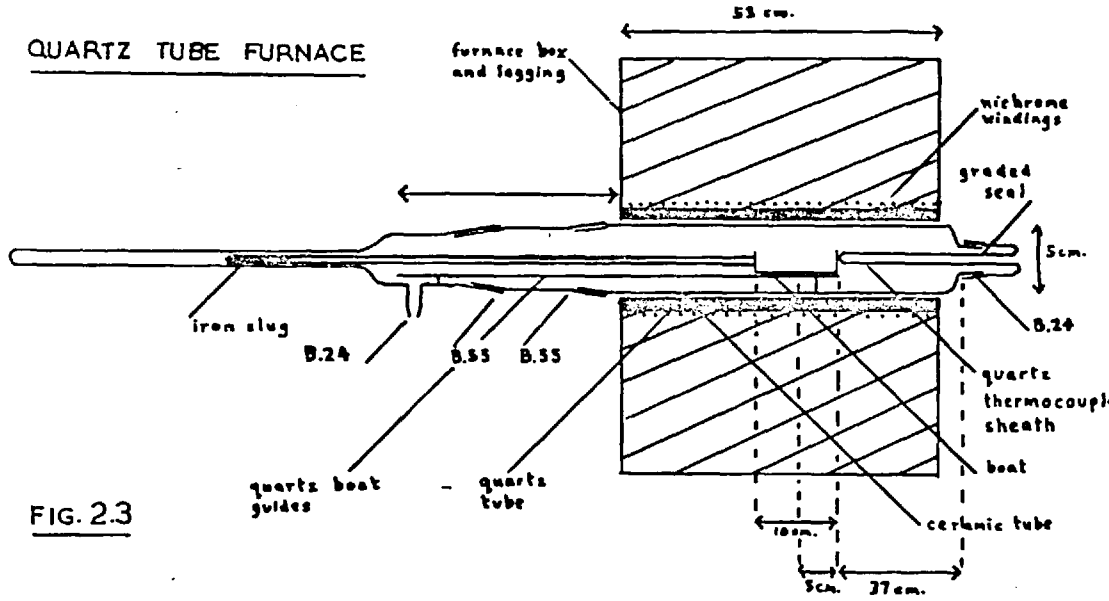


FIG. 2.3

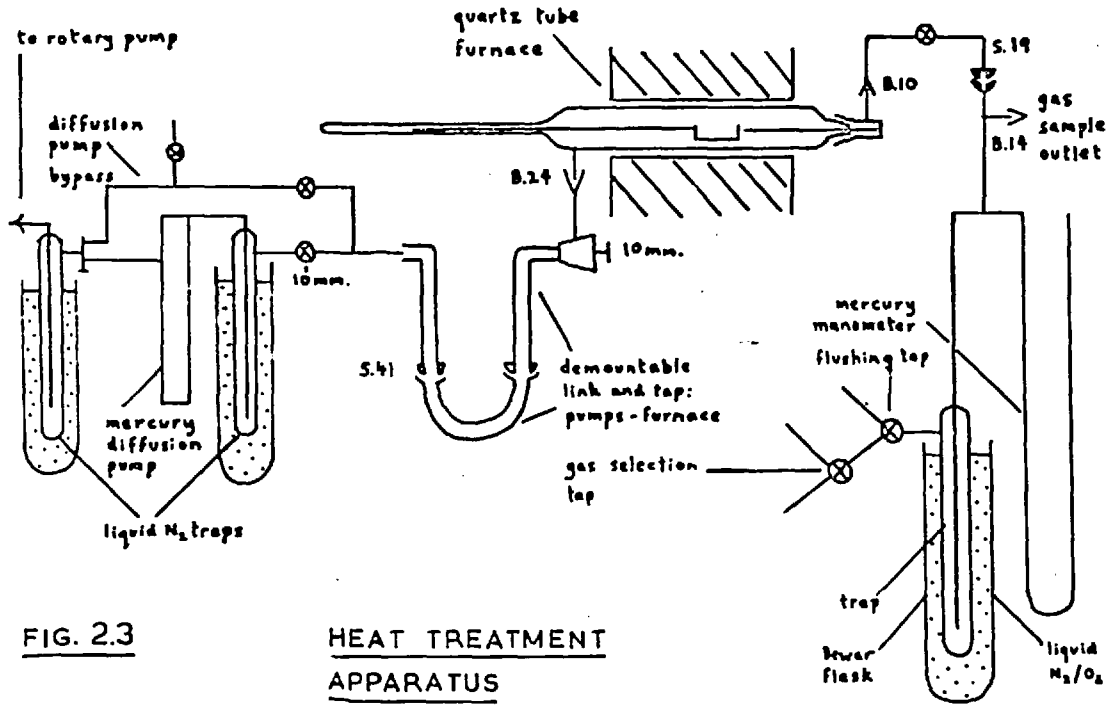


FIG. 2.3 HEAT TREATMENT APPARATUS

system were: the use of greases in cone and socket joints, with the attendant possibility of hydrocarbon contamination of the atmosphere; the possibility of mercury contamination from the manometer used to control the admission of gases; the difficulty of ensuring that no air leaked into the system during a run; the lengthiness of experiments using the apparatus. The static gas system was therefore discarded in favour of a much simpler flowing gas system.

2.3.2. Flowing atmosphere annealing.

2.3.2.1. Apparatus.

A small chamber (volume ca. 20 ml) through which gas could be passed, was constructed in two halves, joined by a B.24 'Clearfit' polished glass cone-and-socket joint (fig.2.4a). The specimen could easily be inserted or removed, and the chamber could be placed in the uniform temperature zone of the tubular furnace for annealing. Irreproducibility of specimen annealing was removed by use of this simple system.

Temperature control in the furnace was achieved with a platinum resistance thermometer linked to an A.E.I. proportional controller RT3/R, giving a signal controlling the power output from an RS4/XVI power regulator. Tests showed that temperature excursions did not exceed $\pm$ 0.5°C over long periods.

Temperature measurement was by means of a chromel-alumel thermocouple (checked against a Pt-Pt 13% Rh standard junction) placed on the axis of the tubular furnace in a silica shield. The thermoelectric e.m.f. was, in earlier experiments, measured on a Pye precision potentiometer, incorporating a Weston cell which had been checked against a digital voltmeter. Later, temperatures were measured with a Croydon Precision Instrument Co. thermocouple potentiometer. Checks showed agreement between the two methods to $\pm$ 1°C.

The (open-ended) furnace temperature gradient was determined (fig.2.5). Annealing was carried out in the uniform temperature zone of ca. 5 cms at the centre.

2.3.2.2. Procedure.

After the insertion of a specimen into the flow chamber, the controlled atmosphere was allowed to pass for at least 15 minutes at room temperature in order to remove atmospheric oxygen. The vessel was then placed in the hot furnace, and after the chosen annealing period, the chamber was quickly cooled by an air blower, and the specimen removed for a small sample of the film to be taken. The flushing process was repeated before continuing the annealing.

Where the gas stream was dried, a liquid nitrogen cooled trap was inserted in the gas flow, containing a layer of molecular sieve which had previously been dried by

Fig 2.4 a) Annealing chamber for flowing atmospheres

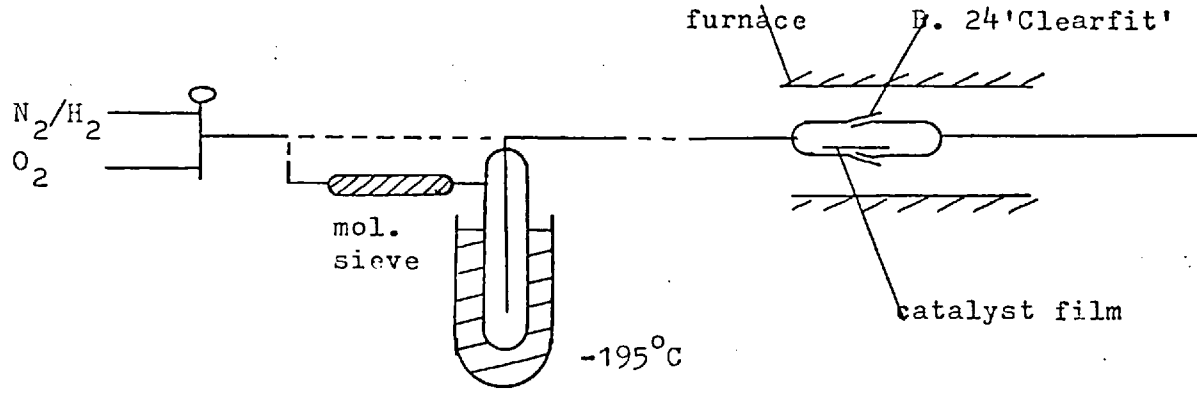
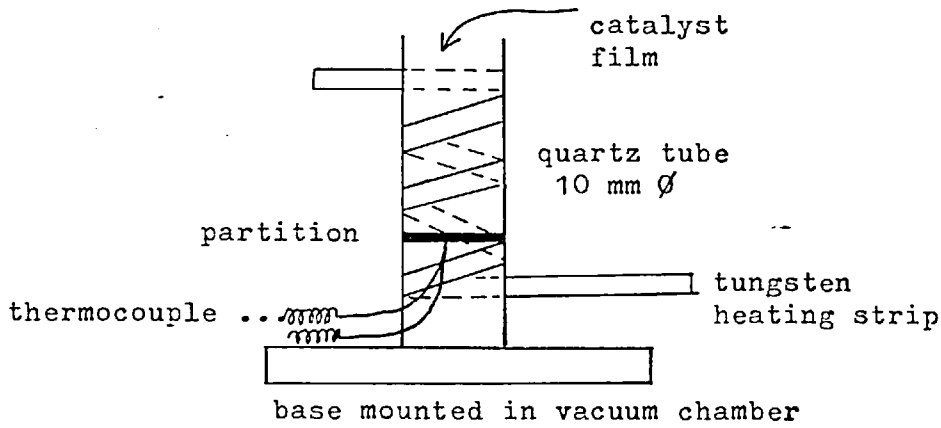
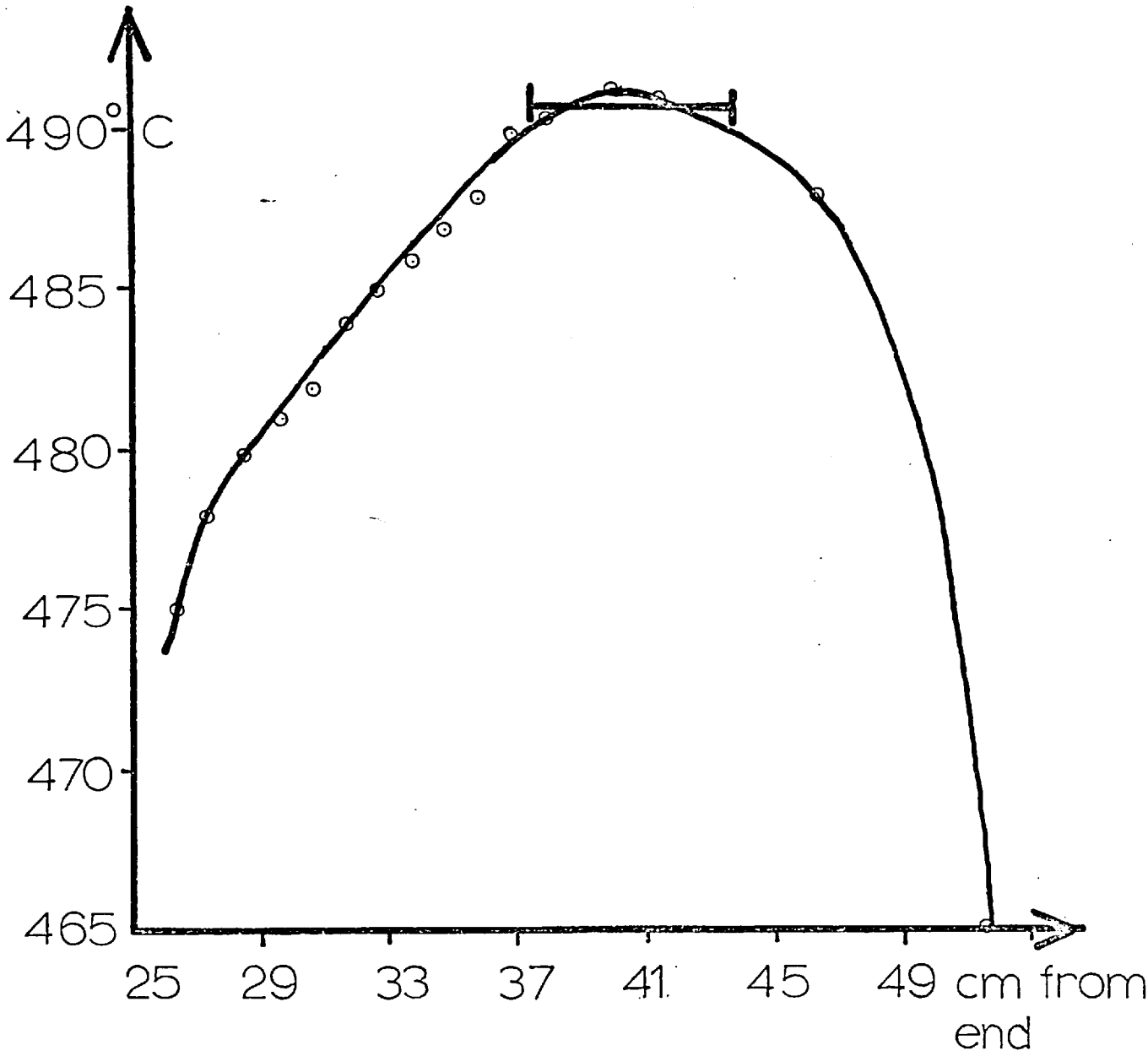


Fig 2.4 b) Annealing chamber below 10^{-2} torr O_2



Furnace temperature gradient

Fig 2.5



heating at 300°C in a nitrogen stream.

On insertion of the annealing chamber into the furnace, a temperature rise time was unavoidable. Experiments with a thermocouple inside an equivalent wall thickness of Pyrex showed the time to attain 0.95 T_{final} °K to be approximately 2 mins. with the furnace at 260°C.

Annealing in oxygen atmospheres from 10^{-1} - 10^{1} torr partial pressure was carried out in the normal specimen chamber, using a mixed flow of nitrogen and oxygen. Conventional bubble flow-meters were used to determine the nitrogen flow, and a small soap bubble flow meter was calibrated to determine the oxygen flow.

2.3.3. Partial vacuum annealing.

2.3.3.1. Apparatus.

Annealing in oxygen atmospheres below 10^{-1} torr partial pressure was carried out in the Balzers vacuum system. A small quartz furnace was used inside the vacuum chamber (fig.2.4b). Temperature measurement was by means of a chromel-alumel thermocouple near the specimen position. Pressure measurement was by means of a Penning gauge incorporated in the pumping system. Pressure adjustment was effected with a needle valve, leaking air into the system at pressures up to 10^{-3} torr, the limit being set by the stability of the oil in the diffusion pump.

2.3.3.2. Procedure.

Specimen annealing in the vacuum chamber was carried out by slowly heating the tubular furnace electrically. The main difficulty experienced was the long response time between the temperature of the thermocouple and sample, and that of the furnace windings.

2.4. Microstructural examination of catalyst films.

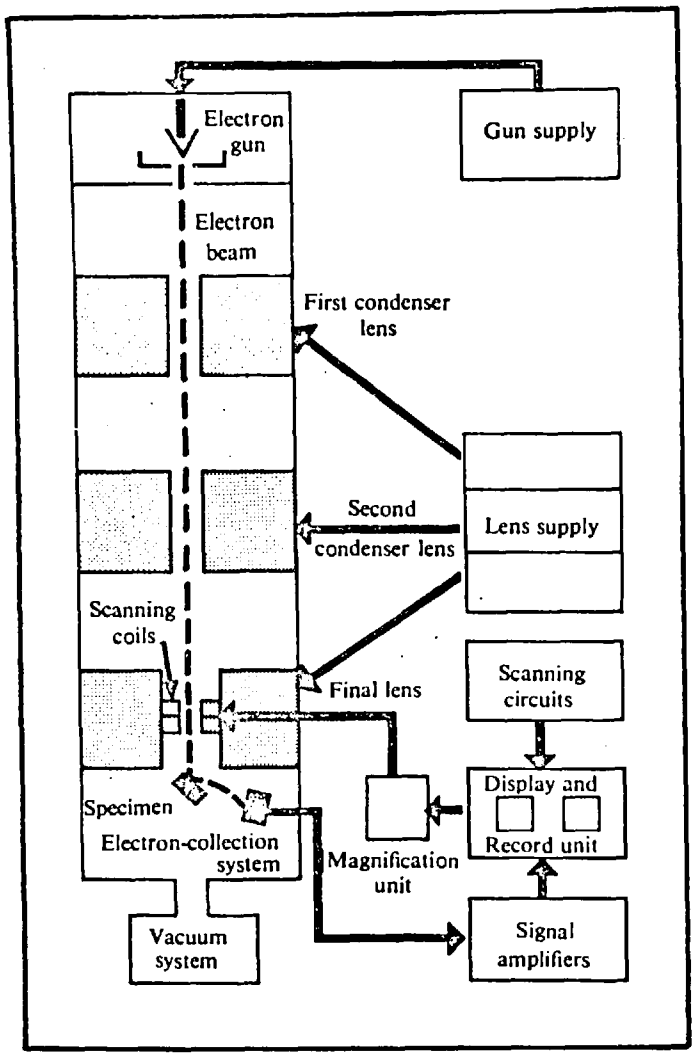
2.4.1. Transmission electron microscopy.

2.4.1.1. Apparatus.

Conventional transmission electron microscopy (t.e.m.) was carried out in two instruments, a Siemens Elmiskop I and a Japan Electron Optical JEM.7. Dark field observations when needed were made in the JEM.7 instrument using electrical beam tilting so that the selected beam passed axially through the objective. Image formation in transmission is shown in fig.2.6a. Bright and dark field microscopy are illustrated in fig.2.7. The electron optics of image formation in transmission are extensively discussed in e.g. Cosslett (1950), Hall (1953), Hirsch et al (1965).

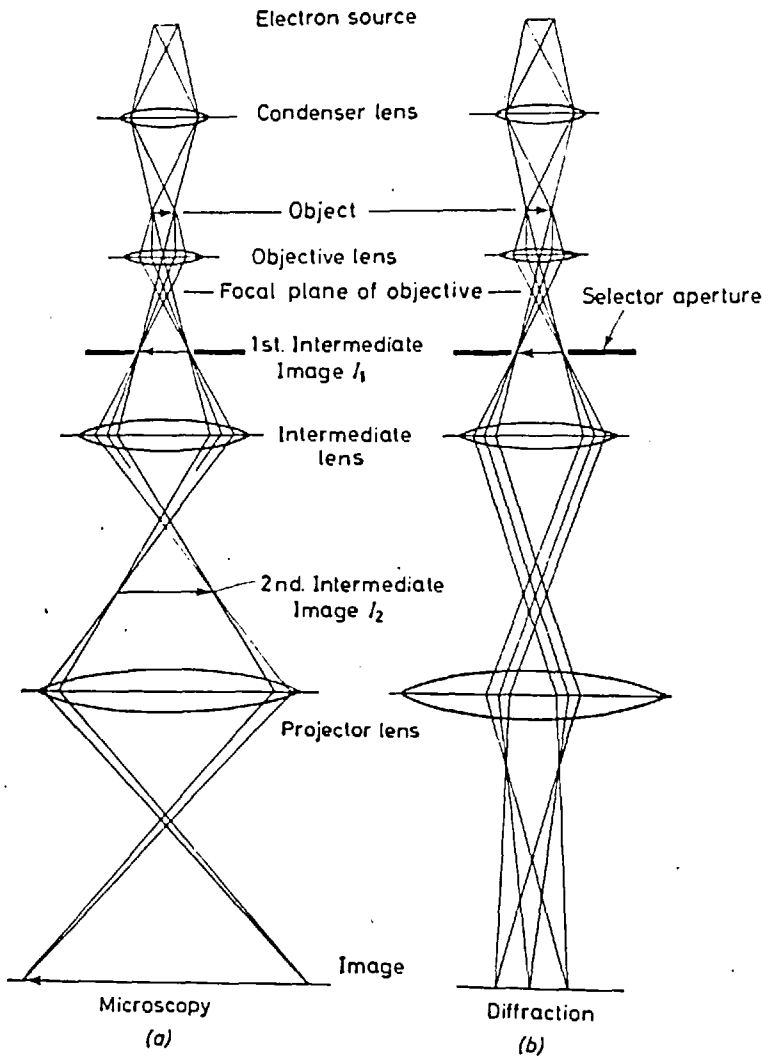
2.4.1.2. Specimen preparation.

For t.e.m. it was necessary to remove the silver film from the silica substrate, which was electron opaque due to its thickness (ca. .005 cm). Since the microstructural changes occurring on annealing led to



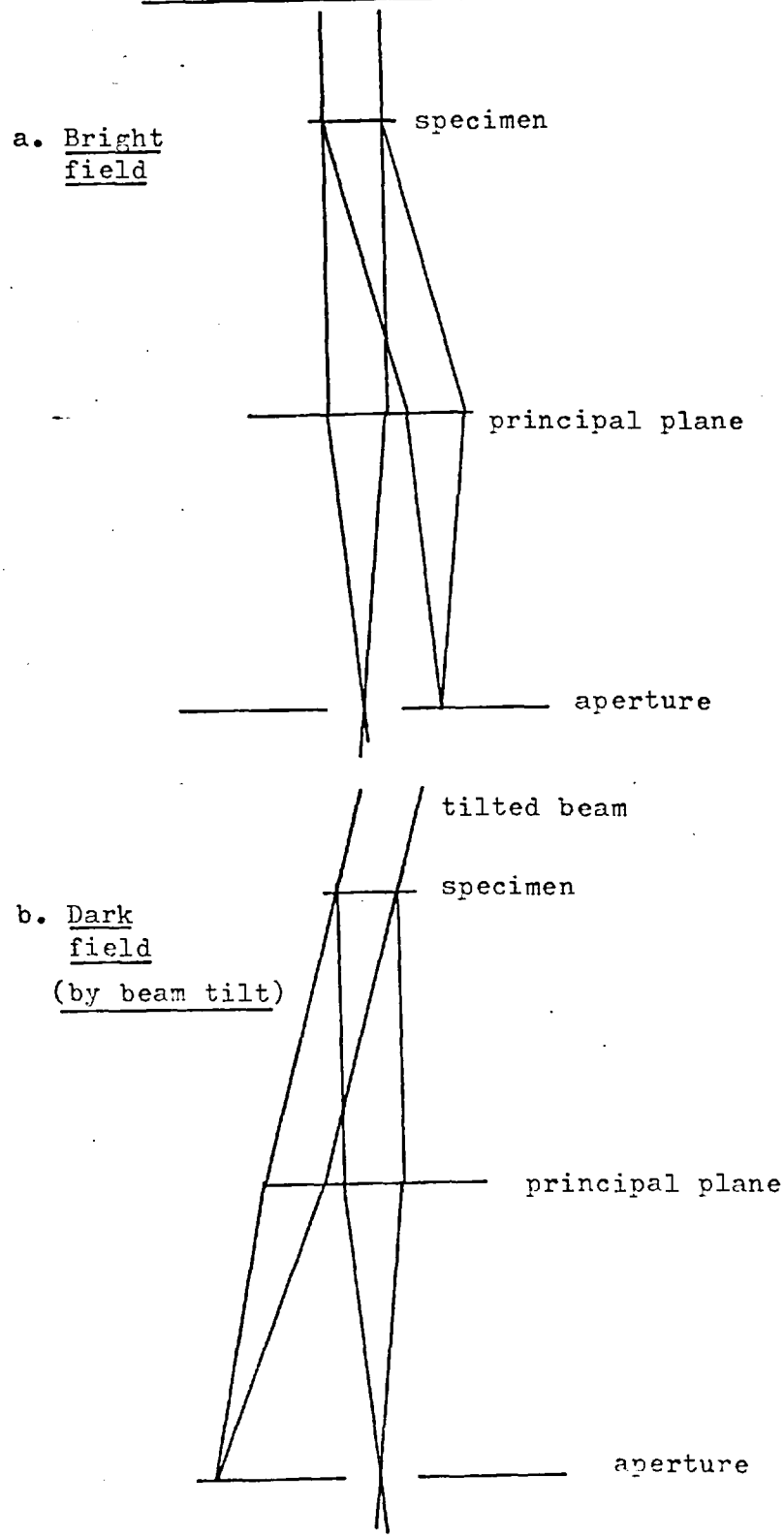
2.6 Stereoscan image formation

from Hirsch Howie et al 1965



2.6 Transmission imaging and diffraction

Fig2.7 Mechanism of diffraction contrast in transmission electron microscopy



discontinuity in the silver film, it was necessary to preserve the silver deposit with a protective coating applied before removing the silica support: this is equivalent to the extraction replica technique of Smith and Nutting (1956) for removal of surface inclusions.

A continuous carbon film was deposited on the specimen by vacuum evaporation to a thickness of ca. 200 Å. The thickness was monitored by the colour change in a thin film of gold on aluminium; when a blue colour developed, the required thickness of ca. 200 Å had been deposited. A number of specimens was coated at one time, being kept separate in numbered depressions on a small metal table constructed to fit in the evaporation unit. By examining the specimens in a stereoscopic optical microscope at x40 magnification it could be checked whether the silver-coated side was uppermost.

In order to remove the silica substrate, the specimens were floated silver-side upward on a solution of ca. 20% hydrofluoric acid for several hours. After the silica had dissolved, the film was removed on a glass spoon and, after washing in two baths of distilled water, was mounted on a copper electron microscope grid.

2.4.1.3. Specimen examination.

Transmission microscopy was carried out at an accelerating voltage of 80 kV, except where the dark field

technique was used, in which case 100 kV was employed. Electron images were recorded on Ilford Special Lantern Contrasty plates, which were developed in Ilford PQ developer (1:19). Where measurement of metal-substrate areas was planned, the exposures were chosen to give dark images of the hole areas, with little density from the continuous metal film areas: the resulting high contrast in the developed image was needed for the 'Quantimet' image analyser. (2.4.1).

2.4.1.4. Island and hole density measurements.

Densities of both islands and holes were determined by direct counting from the whole area of electron micrographs projected at 3x magnification in an enlarger. At the standard plate magnification used of x2400, the area occupied by the whole image was 670 microns^2 using the J.E.M. microscope. In almost all cases, micrographs from the different areas of the same specimen were used. In the case of hole densities, some estimation in judging between holes and multiple grain boundary intersections was inseparable from the measurements; this was particularly difficult in the case of the thinnest films with the greatest hole density, and in this case the micrographs were examined at greater projector magnifications.

2.4.2. Scanning electron microscopy.

2.4.2.1. Apparatus.

Reflection scanning microscopy (s.e.m.) was carried out in a Cambridge Instruments 'Stereoscan' instrument, the optics of which are illustrated in fig.2.6b. The principles of scanning microscopy have been extensively discussed by Thornton (1968).

2.4.2.2. Specimen preparation.

Specimens were prepared for s.e.m. by attaching them with 'Durofix' glue to the standard 1 cm diameter specimen stubs of the instrument. In order to prevent image distortion by charging of the specimen in the electron beam, a conductive coating of ca. 100 Å aluminium was applied by vacuum evaporation at 10^{-4} torr, and a conduction path to the metal stub was provided by painting around the specimen with a colloidal suspension of silver in methyl ethyl ketone ('Silver-Dag').

2.4.2.3. Specimen examination.

Specimens were normally examined with the beam at 30° to the plane of the tilted surface. An accelerating voltage of 30 kV was used. Images from both primary and secondary electrons combined were used.

2.4.3. Transmission electron diffraction.

Crystallite sizes were measured by line

broadening measurements from transmission electron diffraction patterns. Very low illuminating intensities were used, and care was taken to keep within the linear range of the emulsion used. Line widths were measured on a Joyce-Loebel microdensitometer. Crystallite sizes $\bar{d}$ were calculated from the formula

$$\bar{d} = \frac{L\lambda}{B} \qquad (2.2)$$

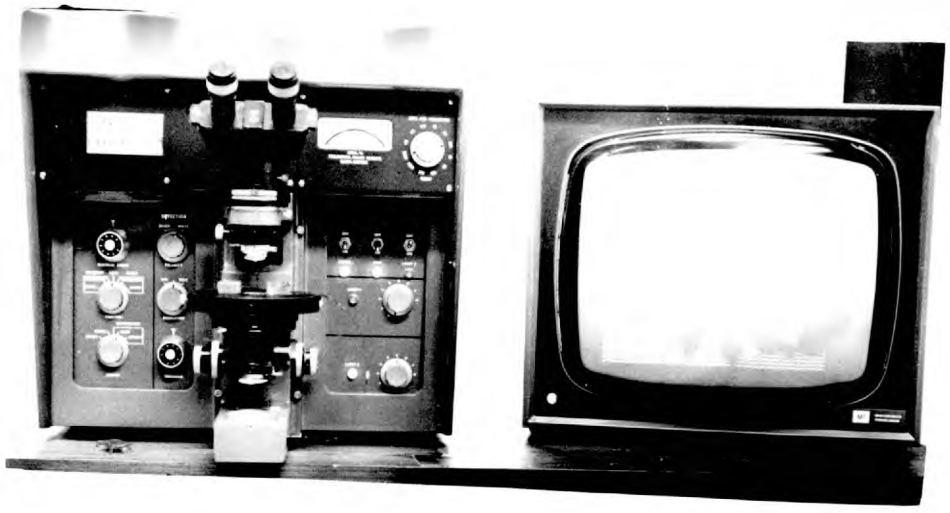
(Pinsker, 1953,p.201) where L is the camera length x wavelength and B is the half-width of the peak.

2.5. Interfacial area determination.

2.5.1. Metal substrate areas.

2.5.1.1. Apparatus.

Area measurements were made on a Metals Research Ltd 'Quantimet' image analysing computer. This instrument will measure, from an image presented to it, the following parameters: the projected area of a phase, or array of particles; the total particle number; total particle length; particle size and chord size distribution. The optical image from a microscope is scanned in a videocamera; the camera scan is then analysed for level, continuity and duration in the detector and computer of the instrument, and the output for the desired parameter indicated on a meter (see fig.2.9). The instrument itself is shown in fig.2.8.



'Quantimet' Fig 2.8

Area hatching Fig 2.10

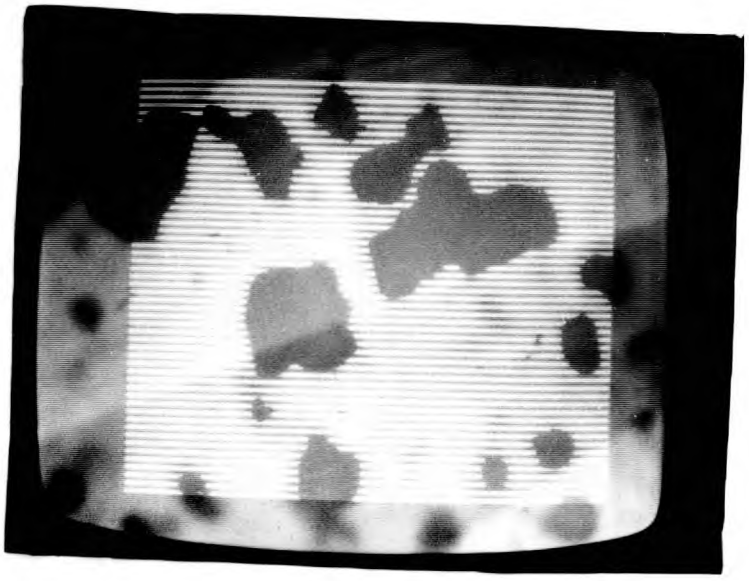
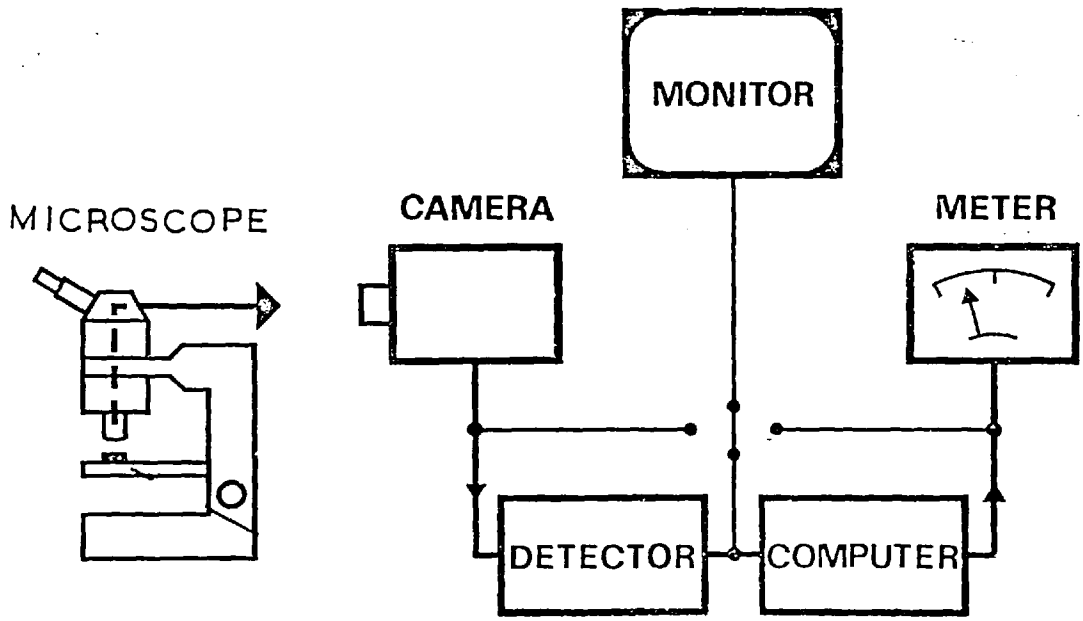


FIG. 29

'QUANTIMET' IMAGE ANALYSING COMPUTER

SIMPLIFIED DIAGRAM



2.5.1.2. Micrograph examination procedure.

The 'Quantimet' was used only for metal-substrate interfacial area measurements; this was because particle sizing is only possible for images of circular, non-touching particles, which condition could not be met with many of the micrographs. Hole and island density measurements were therefore carried out manually (section 2.4.1.4).

The instrument available was designed for use with metallurgical specimens and accepted a magnified image from an optical microscope; with the lowest power objective (x2), the field of view was approximately 2 mm in diameter. The intensity discriminator system was found to work well only when the image was of high contrast. Accordingly, the electron micrographs had to be presented in demagnified form with the maximum contrast. This was achieved by re-photographing them onto 35 mm film at about 8x demagnification, so that the whole micrograph was contained in an area of about 10 x 7 mm. High contrast and the best resolution were obtained by using a very slow fine grain emulsion (Kodak 'Microfile'), underexposed, and overdeveloped in a rapid high contrast developer (Kodak D-11). Transmission illumination was used when the reduced image was viewed in the 'Quantimet' microscope. Ten overlapping areas could be scanned successively from each micrograph.

Areas of black and white in the image were distinguished in the instrument by using a threshold level control. This brought a broad hatching (fig.2.10) to the area chosen. When this hatching coincided with the edge of the metal image area, the hole area could be read off on the meter.

The standard deviation of the measurement was determined from six sets of ten readings, each made from a single micrograph. The results are shown in Table 2.1.

Table 2.1.

Set no.	Mean area A	Standard deviation s
1	67.5	4.02
2	67.6	4.22
3	66.8	2.87
4	68.4	3.35
5	70.1	2.16
6	67.2	3.51
	$\bar{A}$ = 67.9	$\bar{s}$ = 3.3(5)

A standard deviation of ca. 4.9% of the area measured is therefore to be attached to measurements from the 'Quantimet' using sets of ten readings. In view of the irregularities in metal distribution observed in microscopy, this was considered an acceptable accuracy.

2.5.2. Metal-gas interfacial areas.

2.5.2.1. Apparatus.

The apparatus used for adsorption surface area measurements was a slightly modified form of that employed by Aylmore and Jepson (1961). The only change was the use of a mercury burette for varying the system volume, instead of mercury in previously calibrated bulbs. The apparatus is shown in general view in fig.2.11, the storage and dosing system in fig.2.12, and the adsorption system in fig.2.13.

The apparatus is a modification of the normal volumetric adsorption method, and uses radioactively labelled krypton for pressure measurements. In a cell of fixed volume, the count rate after correction for counting losses and background is proportional to pressure, and so pressure can be determined to an accuracy limited only by the number of pulses counted (Taylor, 1951). The count rate thus gives measure of the amount of gas removed from the total present by adsorption at the specimen surface. The amount of gas present before and after adsorption is calculated from the volume of the apparatus, and the respective pressures.

2.5.2.2. Krypton storage and dosing.

a) Materials.

^{85}Kr: 0.188 cc (N.T.P.) activity 10 mC (Radiochemical Centre, Amersham) 99% main contaminant Xe.

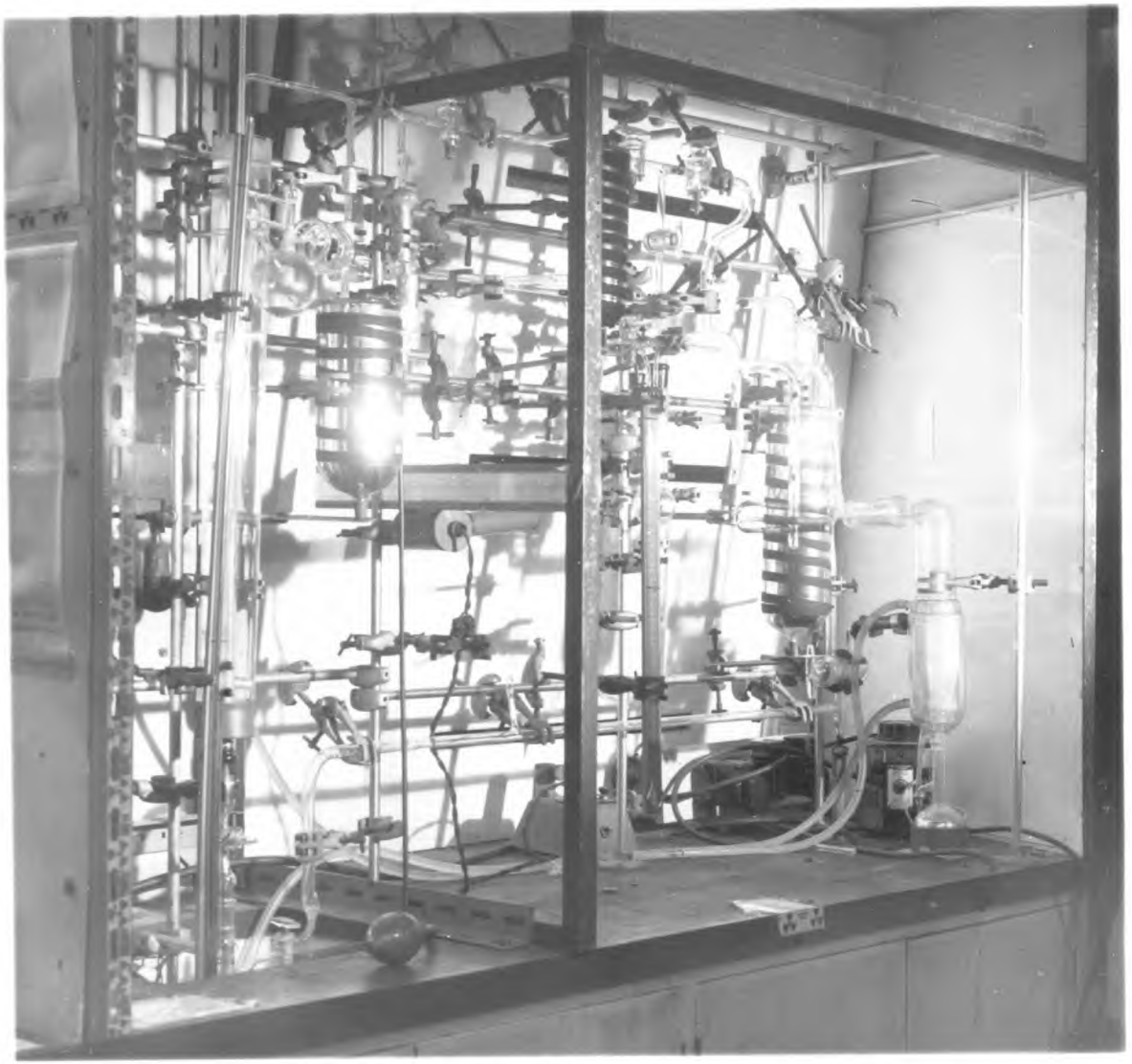


Fig 2.11 Krypton adsorption system

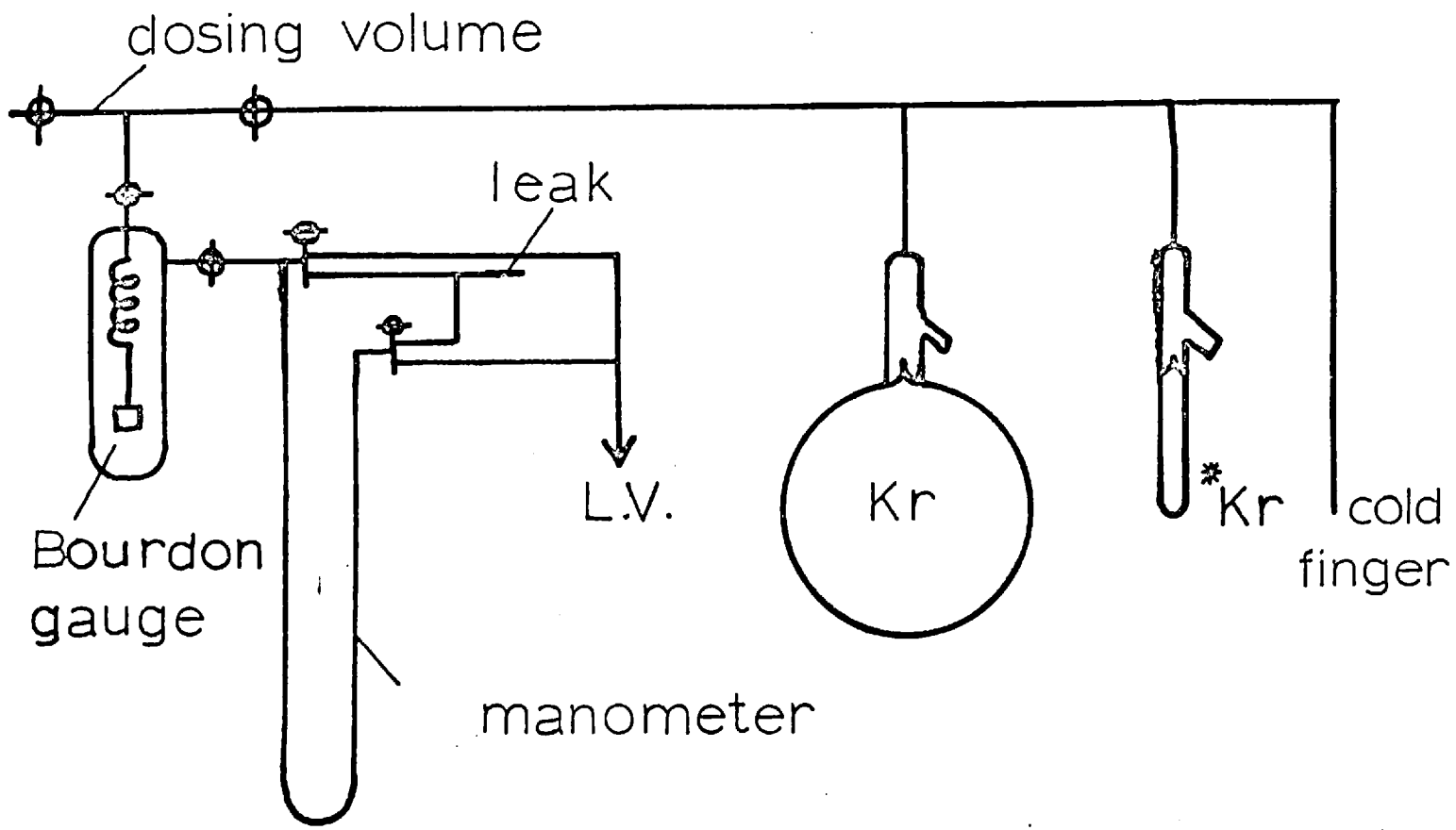


FIG 2.12 KRYPTON DOSAGE & RESERVOIR

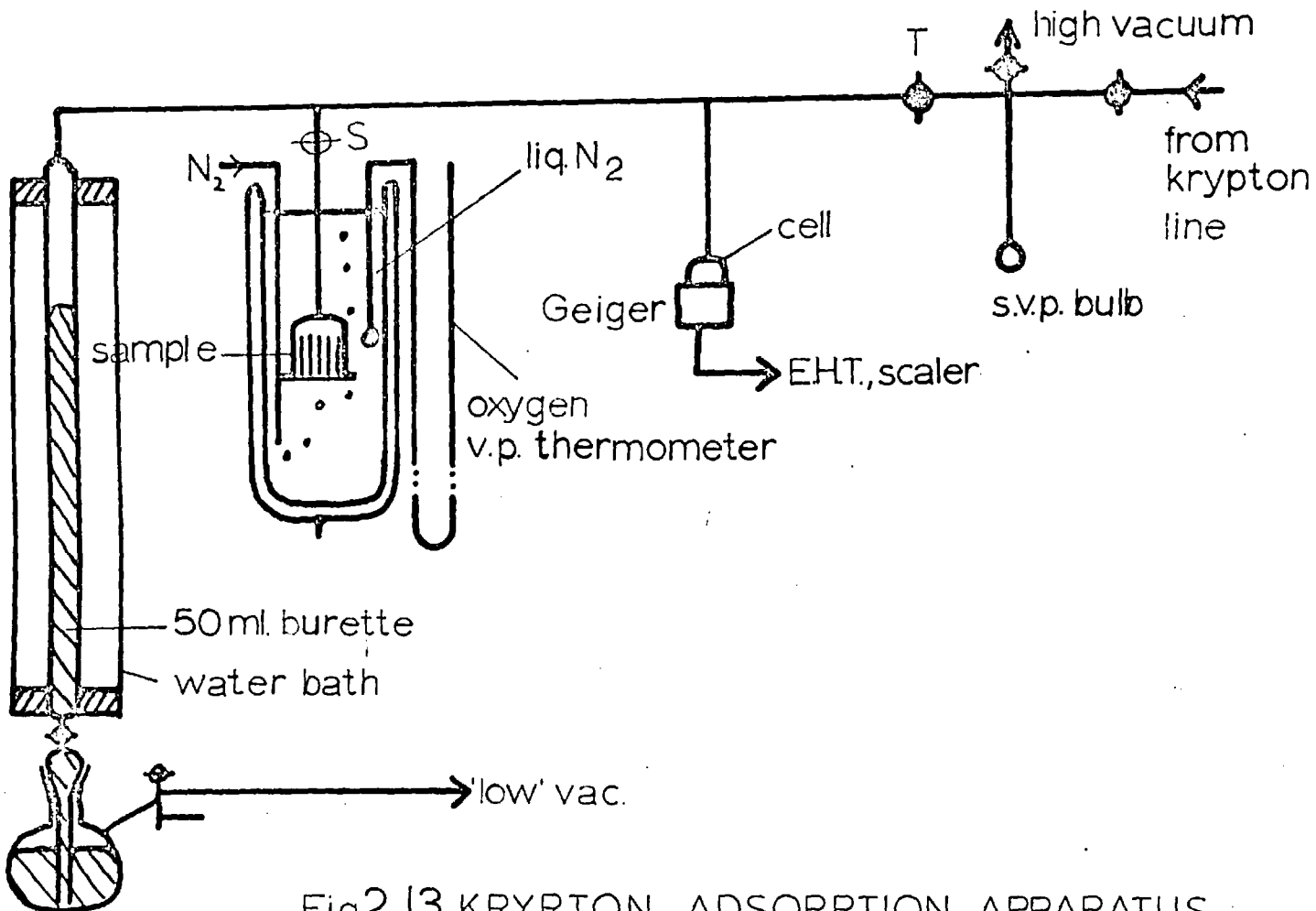


Fig 2.13 KRYPTON ADSORPTION APPARATUS

^{84}Kr: 2.5 l. (N.T.P.) (British Oxygen), 99.9%, contaminants (in p.p.m.): Xe (50), N_2(25), O_2(5), CO_2(5), He(5), H_2(5).

b) Special equipment.

Vacuum gauge: Edwards Penning Head (series 7).

Pressure gauge: Spiral Bourdon (T.W.Wingent Ltd.).

c) Procedure.

Handling of the krypton was carried out in previously evacuated sections of the apparatus; a high vacuum line was connected at the junction of the storage and adsorption systems (fig.2.11) for this purpose. No operation was carried out until a pressure of 3.10^{-5} torr had been reached and maintained without pumping for a few minutes (to ensure degassing of water vapour from the walls of the apparatus).

To label the ^{84}Kr with ^{85}Kr, the cold finger and section connecting the ampoule was evacuated to 10^{-5} torr and closed, before breaking the seals by dropping steel balls with the aid of an external magnet. Thorough mixing of the krypton was ensured by repeated condensation of it into the cold finger at 78°K and re-evaporation.

Dosing of krypton at known pressures was carried out without the gas coming into contact with mercury, by means of the spiral Bourdon pressure gauge; the position of the spiral was followed by a mirror at its end, and a lamp and scale.

The pressure in the body of the gauge could be set at up to 10 cm Hg by means of the mercury manometer and air leak shown in fig. 2.11. This resulted in compression of the spiral; krypton was then admitted to restore the mirror spot to its null position, when the pressure was equal to that set up outside the spiral.

2.5.2.3. Pressure determination.

a) Special equipment.

Geiger counter: EW2b, (20th Century Electronics), organic quenched, aluminium end window, 30 mg/cm^2.

Signal lead: 4.5 feet of 21 pF/foot coaxial cable .23" dia. (total capacity 102.5 pF).

Scaler: Nuclear Enterprises decade scaler, model model 1700 series II.

b) Procedure.

Krypton pressures p (torr) were determined from the corrected count rate N (pulses/second) observed from the fixed volume cell attached to the Geiger, compared with the corrected rate N_o observed from krypton at the known saturation vapour pressure p_o. The relation is

$$p = a \cdot N T \qquad (2.3)$$

where T is the temperature (^oK) of the cell, and a is a constant, derived from p_o and N_o.

The optimum working potential for the counter was

determined by measuring the count rate from a fixed pressure of krypton ($78^{o}K$) at varying potentials. N_o dead time correction was applied, as this varies with the applied potential. The results are shown in fig. 2.14. The expected plateau region was not observed; this may have been due to rising counting efficiency for beta particles, whose low energy (0.67 meV) would have been reduced by passing through the thick geiger window. The counter was used at the point of inflection (1425 volts) to minimise the effect of voltage potentials. The applied potential was carefully checked before all readings.

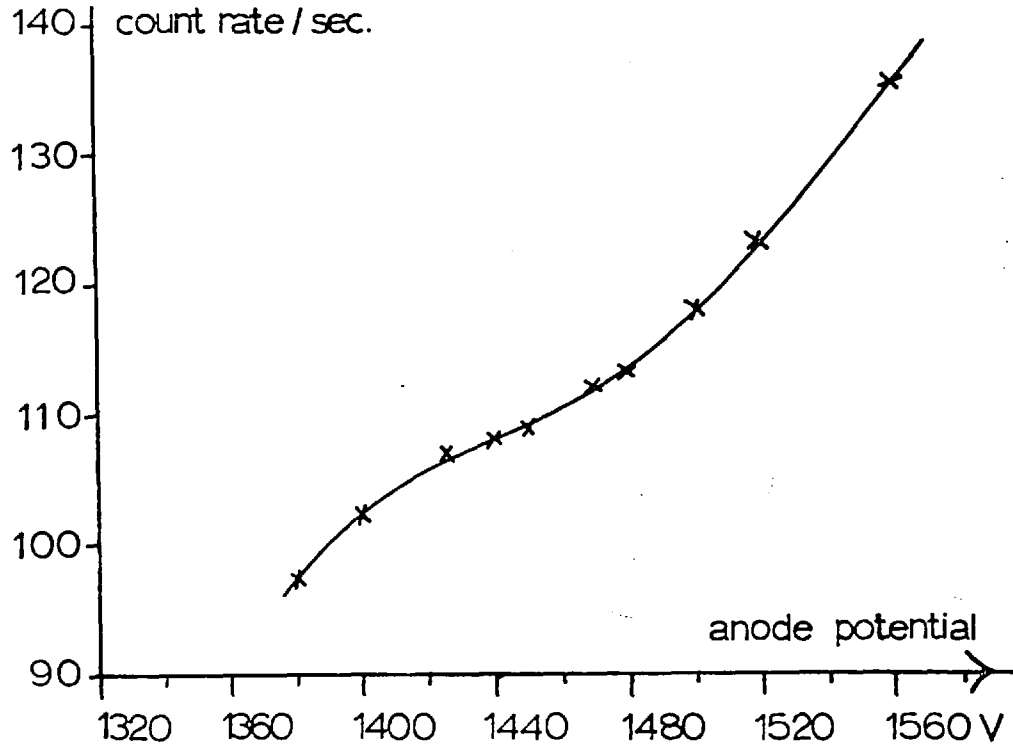
Before using the counter for pressure determinations, the correction for loss of counts was determined and checked. This occurs because of the finite time after the initiation of a pulse during which no further pulse can be produced (the 'dead time'). This interval is followed by a recovery time during which pulses of reduced amplitude are produced. If n_t is the time rate, n_o observed, and t the inoperative time, then

$$n_t - n_o = \frac{n_o^2 t}{1 - n_o t} \qquad (2.4)$$

(Taylor, 1951).

Since the arrival of particles is random, and the recovery period is affected by pulse rate, the number lost is uncertain. Conventionally, a'quench unit' is inserted between counter and scaler, producing a known dead time

Fig 14 EW 2B Geiger characteristic



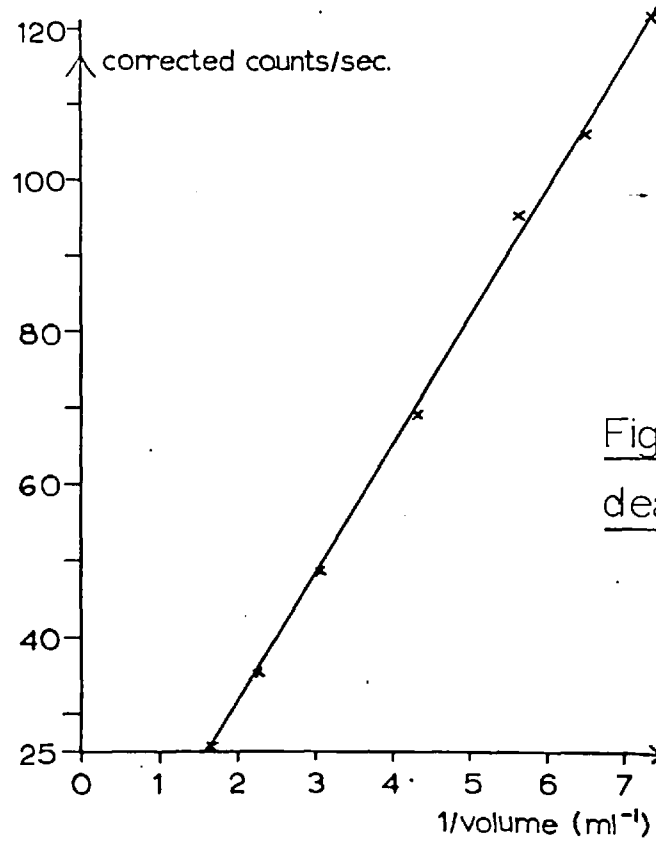
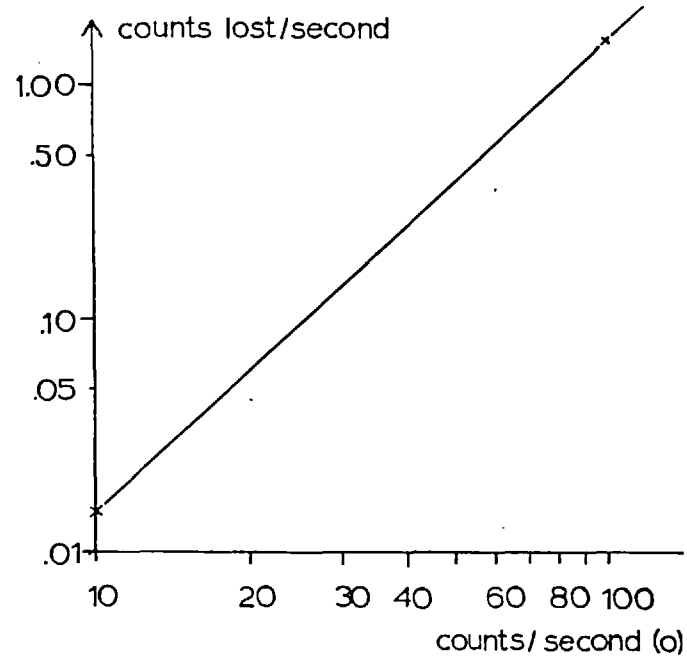


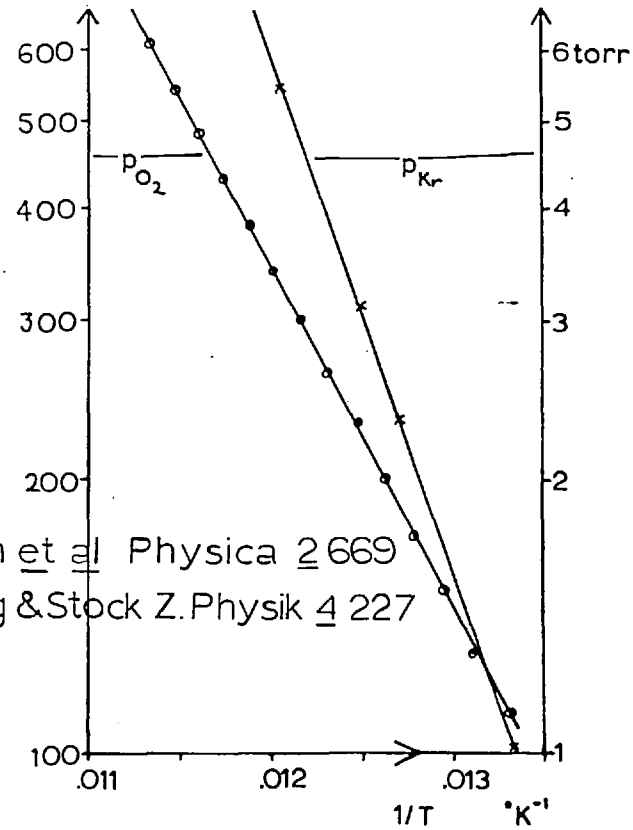
Fig 15 Test of Geiger dead time correction

independent of the rate. In the present work, low count rates (below 120 c/s) were envisaged, and the possibility of using the quoted approximate dead time (150 microsec.) for the EW2b counter was investigated. A known amount of krypton at the s.v.p. was introduced, with the burette full of mercury, and tap T was closed. The volume of the apparatus was varied, and the count rate determined, adding a correction based on a 150 microsec. dead time, and subtracting the background (0.60 c/sec). The proportionality of rate to pressure was checked, assuming Boyle's law, by plotting the rate against volume^{-1} (fig.2.15). Inaccuracies in the count rate correction should result in deviations from linearity of the plot at high rates, this was not observed, and so the need for a quench unit at the count rates to be employed was removed. 150 microsec. was taken as the effective dead time; a plot of the correction vs. count rate is shown in fig. 2.16.

Reliable values of the count rate N could then be used for absolute pressure p determinations. This was done by determining the constant a in equation 2.3. using the s.v.p. of solid krypton as the standard pressure. Tables of this vapour pressure were given by Keesom et al (1935) (fig. 2.17). The solid krypton was condensed in the s.v.p. bulb of the adsorption line, in a liquid nitrogen bath. Its temperature was determined to $\pm$ 0.05°C by means of an oxygen vapour pressure thermometer whose bulb was

Fig 2.16 Count loss in Geiger: 150 μs dead time





Kr Keesom et al Physica 2 669
O_2 Henning & Stock Z. Physik 4 227

Fig 2.17 Calibration of oxygen v.p. thermometer vs. Krypton v.p.

immersed in the nitrogen bath as close as possible to the s.v.p. bulb. The thermometer is shown in fig. 2.18 and was constructed as described in Farkas and Melville (1939). The temperature was measured by comparison of the observed pressure with the oxygen vapour pressure measurements of Henning and Stock (1921). It was found that the temperature of a fresh nitrogen bath dropped appreciably during the first hour, and then remained reasonably constant (fig. 2.19). When the temperature had settled, ten successive count rate determinations were made each using 4×10^4 counts. Radioactive decay of ^{85}Kr (half life 9.6 years) causes a decrease in a of approximately 1% in two months, so the value was redetermined after greater times than this.

2.5.2.4. Calibration of the apparatus.

The 50 ml Grade A burette was used as the standard in determining the volumes of other sections of the apparatus. The dead volume of the adsorption system was first determined. The capillary leading to the specimen chamber was closed at point L. Krypton at the s.v.p. was introduced into the adsorption system through tap T, the s.v.p. bulb (fig. 2.13) being held at $78^{\circ}K$. With tap T closed, the volume of the burette was varied by lowering the mercury from an initial position near the top; from the change in pressure, the dead volume V_d could be determined, checked from repeated measurements of the rate.

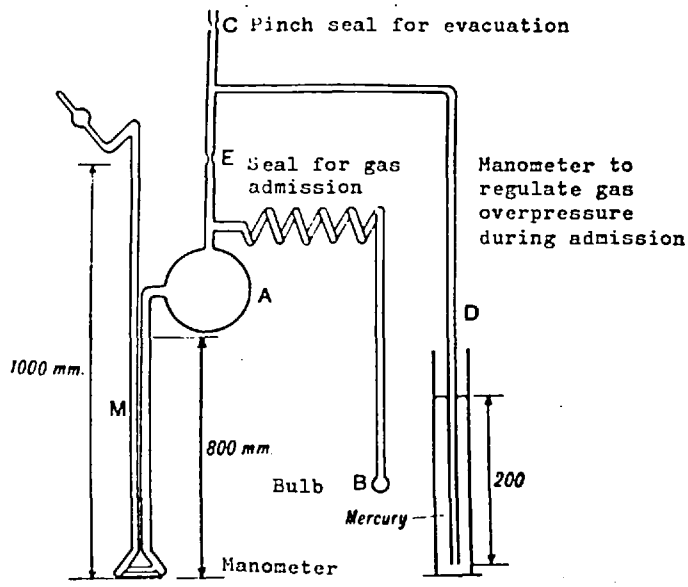


FIG. 75. Vapour pressure thermometer.

2.18

Design and construction of gas vapour pressure thermometer: Farkas and Melville 1939

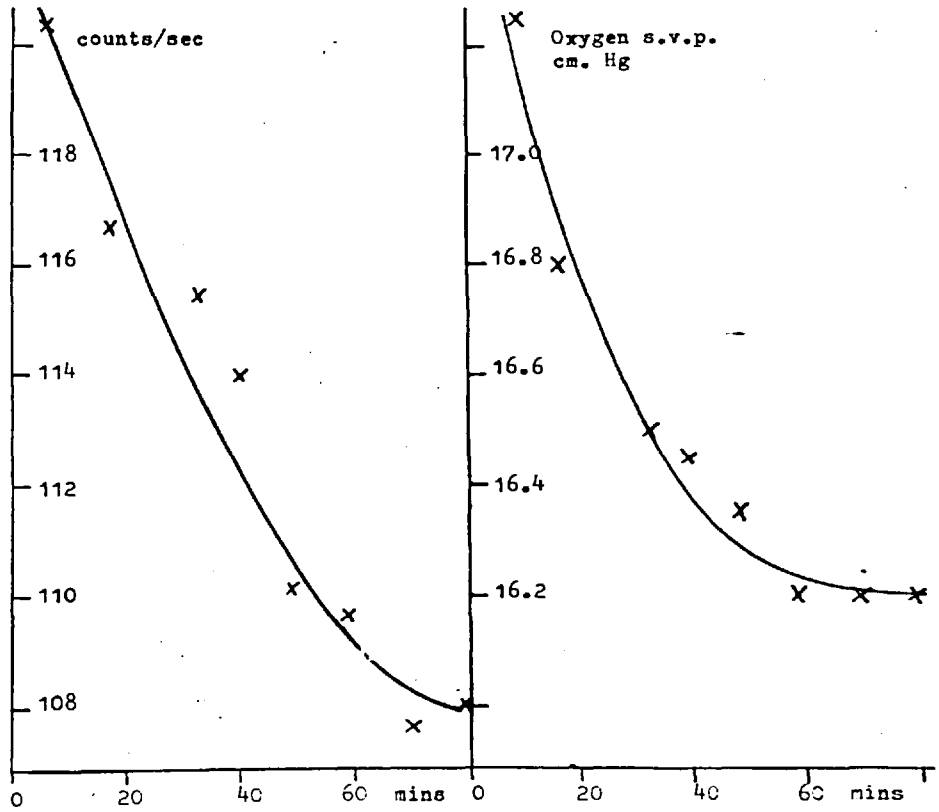


Fig 2.19 Gradual stabilizing of count rate from svp bulb, and of vapour pressure thermometer reading, on immersion in liquid N_2

The value was found to be 6.78 ml.

The volumes of the sample chamber V_s (see section 2.4.2.4) and of the dosing volume, were determined by volume sharing from a dose of krypton admitted from the adsorption system, whose total volume was now known.

A correction was made during adsorption measurements (at liquid nitrogen temperature) for thermal transpiration of krypton in the capillary tube connecting the specimen chamber to the apparatus. This causes the pressure observed at the 'hot' end of the tube to exceed that obtaining near the sample. The pressure p in the counting cell is related to the pressure p' in equilibrium with the adsorbent, by the expression

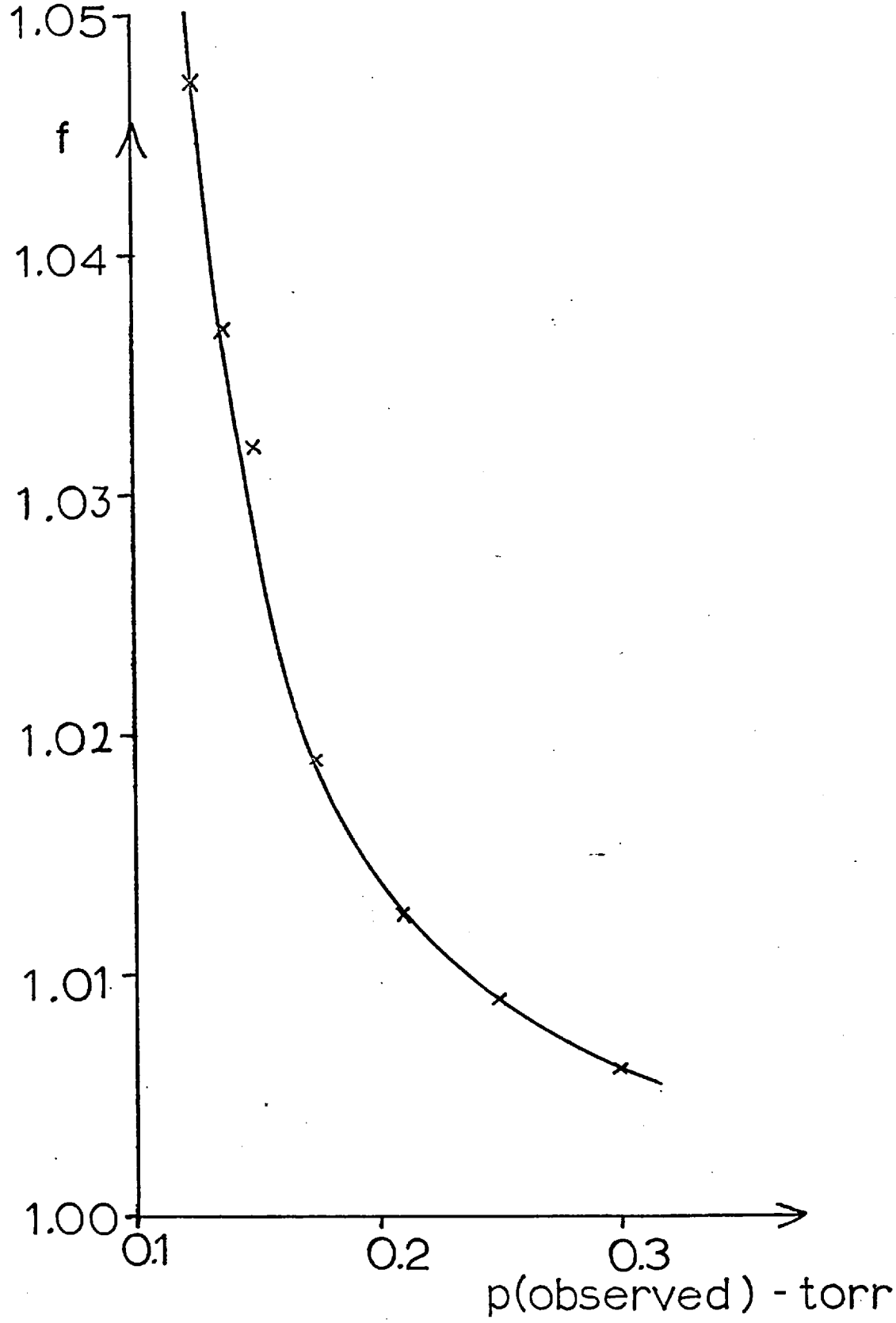
$$p' = f\,p \qquad (2.5)$$

where f is a function of pressure depending on the diameter d of the capillary. In this work, d = 1.81 mm (measured by travelling microscope). Values of f were calculated from the semi-empirical formula of Liang (1953, 1955), verified by Rosenberg (1956):

$$f = \left[1 - \left(\frac{0.490}{37.2d^2\,p^2 + 14.45\,d\,p + 1} \right) \right]^{-1} \qquad (2.6)$$

where d = tube diameter. Fig. 2.20 shows the variation of f with pressure for a 1.81 mm capillary. The factor is not strictly valid for values of d x p less than 0.07 torr-mm.,

Fig. 2.20 Thermomolecular flow correction 1.81 mm tube



(Rosenberg, 1956). However, in determining the low pressure end of adsorption isotherms, the correction was extended below this range without apparent discrepancies (section 3.4.1).

2.5.2.5. Specimen preparation.

The geometric form of the supported silver films did not lend itself easily to containment in an adsorption chamber of low dead volume. It was intended to use silica substrates, but the sections of silica bubble normally used were diffuclt to produce on a large scale (for 100 - 1000 cm^2 area) and to pack in an adsorption cell. Square sections of flame polished silica were available, but these were found to present great problems in the fabrication of a square specimen chamber; the cost of thin circular sections was prohibitive. Pyrex substrates were therefore adopted for this portion of the work; circular coverslips of 19 mm diameter were used, fitting closely into a specimen chamber constructed from a B.24 pyrex socket joint. (fig. 2.21). Evaporation of silver was carried out as usual onto both sides of 155 such slips to a mean thickness of ca. 600 Å. The slips were stacked individually in the specimen chamber, and separated by short sections of 42 S.W.G. copper wire.

2.5.2.6. Adsorption isotherm and surface area determination.

Fig2.21 Specimen chamber for adsorption measurements

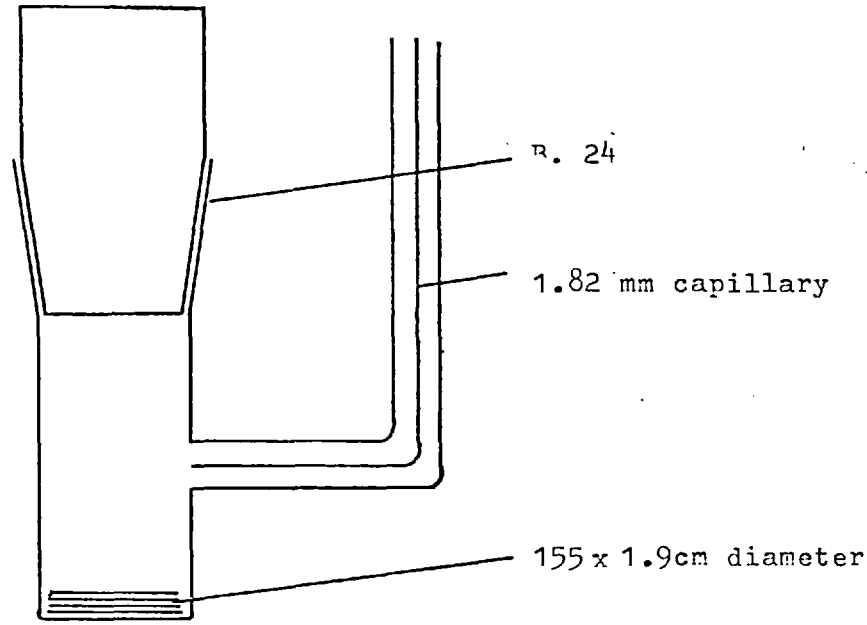
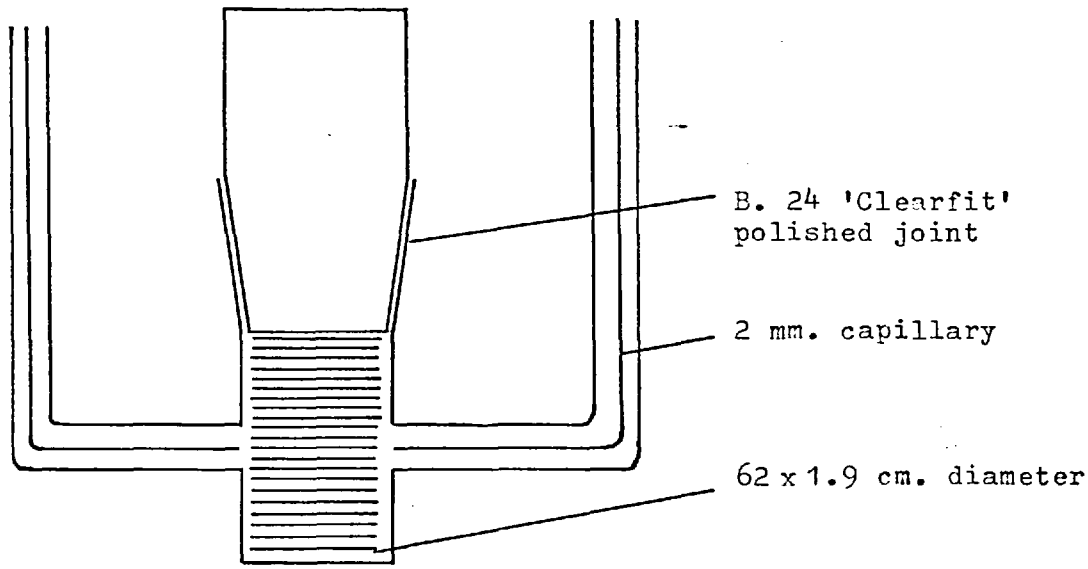


Fig2.23 Reaction chamber for catalytic oxidation



After sealing the specimen chamber capillary to the apparatus at point L, (fig. 2.13) the whole apparatus was evacuated at 10^{-3} torr for at least 12 hours, and at 3×10^{-5} torr for at least 3 hours. Increasing the lowest pressure degassing time was found not to affect the amounts of krypton adsorbed.

A dose of krypton at a pressure of ca. 2 cm Hg in the dosing volume (6.90 ml) was found ample for all measurements. By cooling the s.v.p. bulb to 78°K, the dose could be admitted at ca. 2 torr pressure to the rest of the system. After closing tap T, the initial count rate N_i was determined with burette volume V_i. The specimen chamber was then cooled in liquid nitrogen up to the level of point L, and left for an hour to equilibriate. The new count rate N_j was determined at burette volume V_j. The amount adsorbed was then given by:

$$V = K\left[\frac{N_i}{100} (V_i+V_d+V_s) - \frac{N_j}{100} \left(V_j+V_d+ \frac{T_j}{T_N} V_s\right) \right] \text{ml(NTP)} \quad (2.7)$$

where $K = \frac{27300}{760}$, T_j = room temperature when N_j determined, T_N = liquid nitrogen bath temperature.

It was quickly found that, with the unavoidably large specimen chamber volume (V_s), an insufficient range of partial pressure could be covered by adjusting the burette mercury level. A tap was therefore inserted at S (fig.2.13) and a method of successive reduction of the total dose was

employed. After each determination of N_j, tap S was closed, and the rest of the system evacuated through tap T (removing $K [N_j/100 (V_j + V_d)]$. Tap T was then closed, tap S opened, and after equilibriation (ca. 10 min.), a new reading of N_j made.

In order to check the apparatus against an external standard, a sample weighing 0.1677 gm. of a 7.5 m^2/g large-pore catalyst was taken. Degassing at 250°C for 12 hours was carried out at 2.10^{-5} torr, the standard treatment that had been used in normal volumetric adsorption determination of the sample area (Gabbay, 1969). The adsorption of krypton followed the B.E.T. equation, and the area deduced was as follows (Kr = 19.5 $\AA^2$)

Measured area: 1.08 m^2

Known area of standard: 1.26 m^2.

A calibration factor of 1.17 x was therefore adopted for area determined by krypton adsorption. The error could arise through errors in the thermal transpiration correction, or from very small errors in the dead volume measurement.

2.6. Catalytic studies.

Two methods were used for determining the catalytic activity of the films in hydrogen-oxygen and ethylene-oxygen mixtures. The first was a static system. The catalyst film was placed in a furnace chamber which was quickly evacuated to 10^{-2} torr, and then filled with the

hydrogen-oxygen mixture; the reaction rate was to be followed by the decrease in total pressure as water vapour formed was condensed in a cold finger. No measurable rate of combination was detected with this arrangement, and, to gain greater sensitivity, a flow system was used, where a stream of gas could be passed over the catalyst film, and the products could be sampled and analysed in a gas chromatograph.

2.6.1. Static gas system.

2.6.1.1. Apparatus.

A diagram of the apparatus used in shown in fig. 2.22. The bulb B was used for mixing the gases; evacuation of the bulb and the reactor was by means of a rotary oil pump to ca. 10^{-2} torr. Oil vapour was prevented from reaching the system by a bed of molecular sieve and by a trap cooled in liquid nitrogen. The pressure changes in the furnace were followed by the mercury manometer; mercury vapour was prevented from reaching the catalyst film by an intervening liquid oxygen trap. Condensation of water vapour formed during the reaction could occur at cold finger F again cooled in liquid oxygen (to prevent condensation of the oxygen present in the reaction mixture). The electrical heating of the furnace chamber by an RS4XVI power supply controlled by an RT3/R proportional controller (A.E.I.) was as before (section 2.3.1).

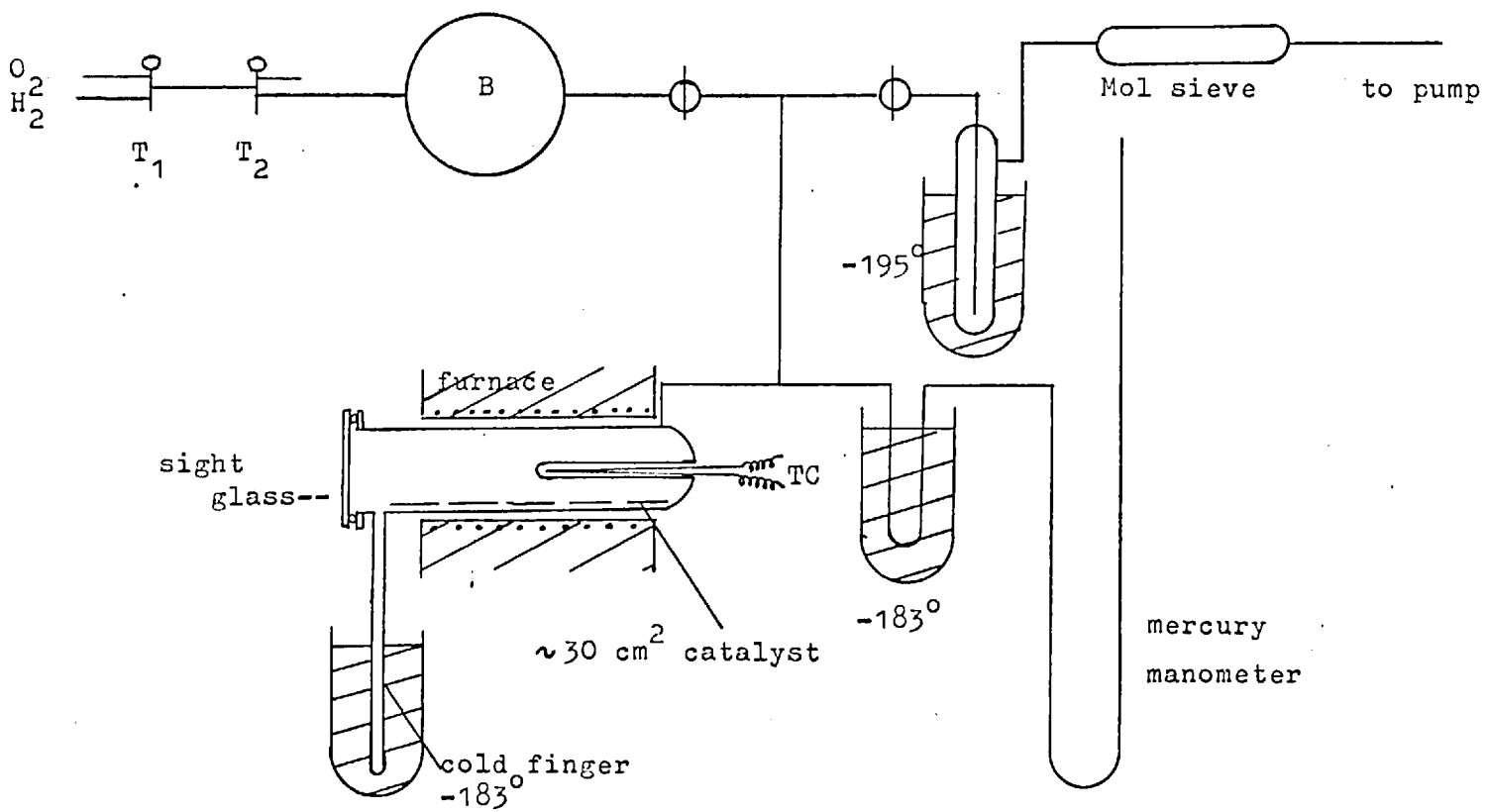


Fig2.22 Static apparatus for hydrogen oxidation reaction

2.6.1.2. Procedure.

The hydrogen-oxygen mixture was made up by first evacuating the bulb B; oxygen was then admitted through the two-way tap system T_1 and T_2 after flushing out through the bubbler. B was isolated while hydrogen was flushed through T_1, T_2 and the bubbler, and then hydrogen was admitted to B through T_2.

A nitrogen stream was led through the opened reactor, and the catalyst film placed inside; the vessel was closed by the sight-glass and O-ring seal and quickly evacuated. The pump was then isolated and the gas mixture admitted; the operation took ca. 1½ mins. in all. Samples were obtained by evacuating the gas mixture from the system and admitting nitrogen before opening the furnace; errors caused by the sample being exposed to uncontrolled atmospheres were minimised by removing samples at similar times whatever gas mixture was used, so that the effects of this quite simple procedure were the same in all cases. During the annealing, pressure changes were followed on the manometer, the leak rate having previously been chcked.

2.6.2. Flowing gas system.

2.6.2.1. Apparatus.

Measurement of the catalytic activity of the films under mixtures of hydrogen or ethylene with oxygen in a flow system, required a reaction vessel similar to the

adsorption chamber eariler used (fig. 2.23). Again, the film was on 19 mm cover slips, but was separated by short sections of .010" dia. silver wire. The chamber was sealed by a polished glass plug ('Clearfit'). For hydrogen oxidation, only one cover slip in five carried catalyst, in order to reduce the water vapour produced to below the s.v.p.

The arrangement for leading the reactant mixture to the catalyst chamber is shown in fig. 2.24. Float flowmeters (Rotameter) of 5-50 ml/minute capacity were used to check the input flow rates; by means of a tap, the inlet flow could be diverted straight to the sample loop of the chromatograph if necessary. The furnace heating the reaction vessel was a stirred air-bath heated by a resistance element, controlled at the desired temperature by a platinum resistance thermometer mounted very near the reaction vessel which was linked to the usual control unit and power regulator.

The water content of the effluent stream was measured in the chromatograph described in section 2.7.

2.6.2.2. Procedure.

The choice of ethylene:oxygen ratio was governed by the results of Twigg (1945), which indicated that, in the flow system, maximum (ethylene oxide:carbon dioxide) selectivity was obtained at 235°C and at 1:10 (ethylene: air) ratio. Here, in fact, conditions of 228°C

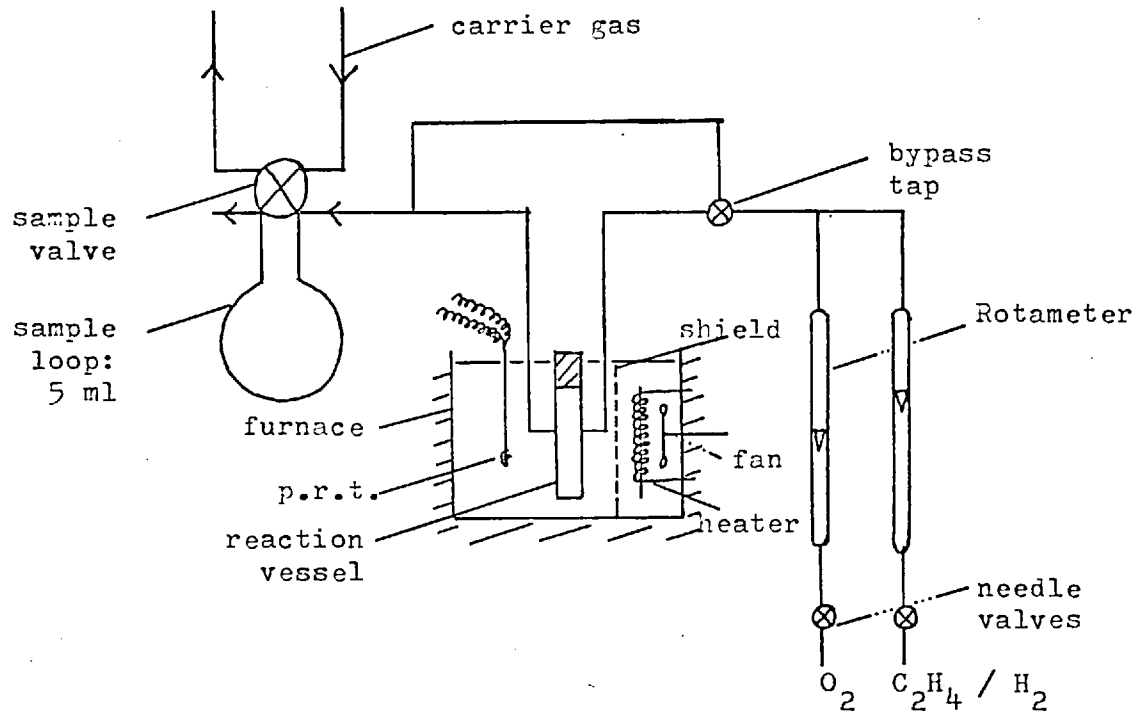
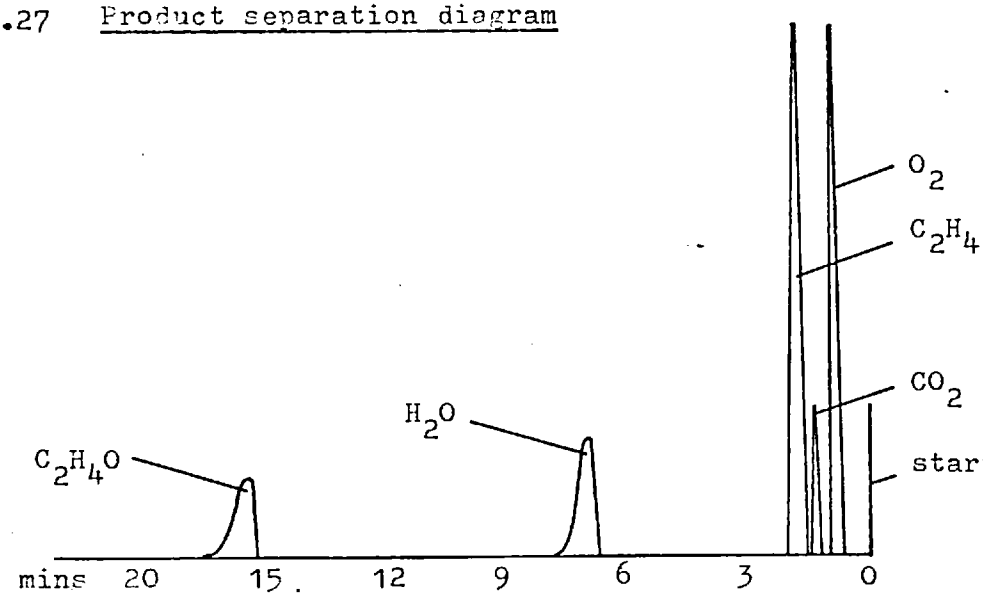


Fig 2.24 Gas-flow paths for catalytic oxidation

Fig 2.27 Product separation diagram



Elution pattern: $4\frac{1}{2}$ ft x 1/4" Porapak Q column
120°C Carrier H_2 79 ml/minute

and 1:2 (ethylene:oxygen) were used. The chosen (hydrogen: oxygen) ratio was the stoichiometric 2:1. and the temperature again 228°C. The reactor was fitted with 62 catalyst film circles (2.2.2), separated by 2 cm lengths of thin silver wire.

Hydrogen, or ethylene, and oxygen in the chosen proportions were allowed to flow through the reactor for ca. 30 mins. to ensure a controlled atmosphere in all parts of the system. The reaction was then started by lowering the reactor into the air-bath furnace, as near as possible to the platinum resistance thermometer. On-line sampling of the product stream at chosen intervals was by means of the sample valve.

2.7. Gas chromatography.

2.7.1. Apparatus.

Despite the advantages of high sensitivity offered by flame ionisation detectors, they are not suitable for the non-combustible products (H_2O, CO_2, O_2). A thermal conductivity detector was therefore used so that all gases could be measured (with suitable choice of carrier).

Choice of columns for separation of products was particularly affected by the need to separate water without 'tailing' for quantitative measurement, and the need to separate oxygen from nitrogen, should a nitrogen diluent for the reactant stream be employed. 'Porapak-Q', a cross-

linked polystyrene giving a good water separation, was chosen for the main column; an alternative column of molecular sieve (80-100 mesh) was used to separate the air peak where necessary. Hydrogen was used as the carrier gas.

A diagram of the chromatograph is shown in fig. 2.25. The equipment used was as follows:

Katharometer:	Servomex Microkatharometer MK 158
Katharometer oven:	Servomex I.O.199.
Oven controller:	Servomex T.C. 201
Katharometer bridge control:	Servomex G.C. 197
Columns:	1.'Porapak Q', 1/4" x 4 ft tube 80-100 mesh 120°C.
	2. Molecular sieve (80-100 mesh), 1/8" x 8 ft.
Sample valve:	Pye Series 104
Recorder:	Leeds & Northrup Speedomax-W, 0-1 mV

A general view of the chromatograph besides the apparatus for catalytic oxidation is given in fig. 2.26.

2.7.2. Procedure.

A carrier-gas flow rate of 89 ml/minute through the Porapak-Q column at a temperature of 120°C was found to be sufficient to elute ethylene oxide, the longest retained component, in 14 mins., without undue crowding of the earlier peaks. The order of elution of the various components is shown in the retention time diagram, fig.2.27.

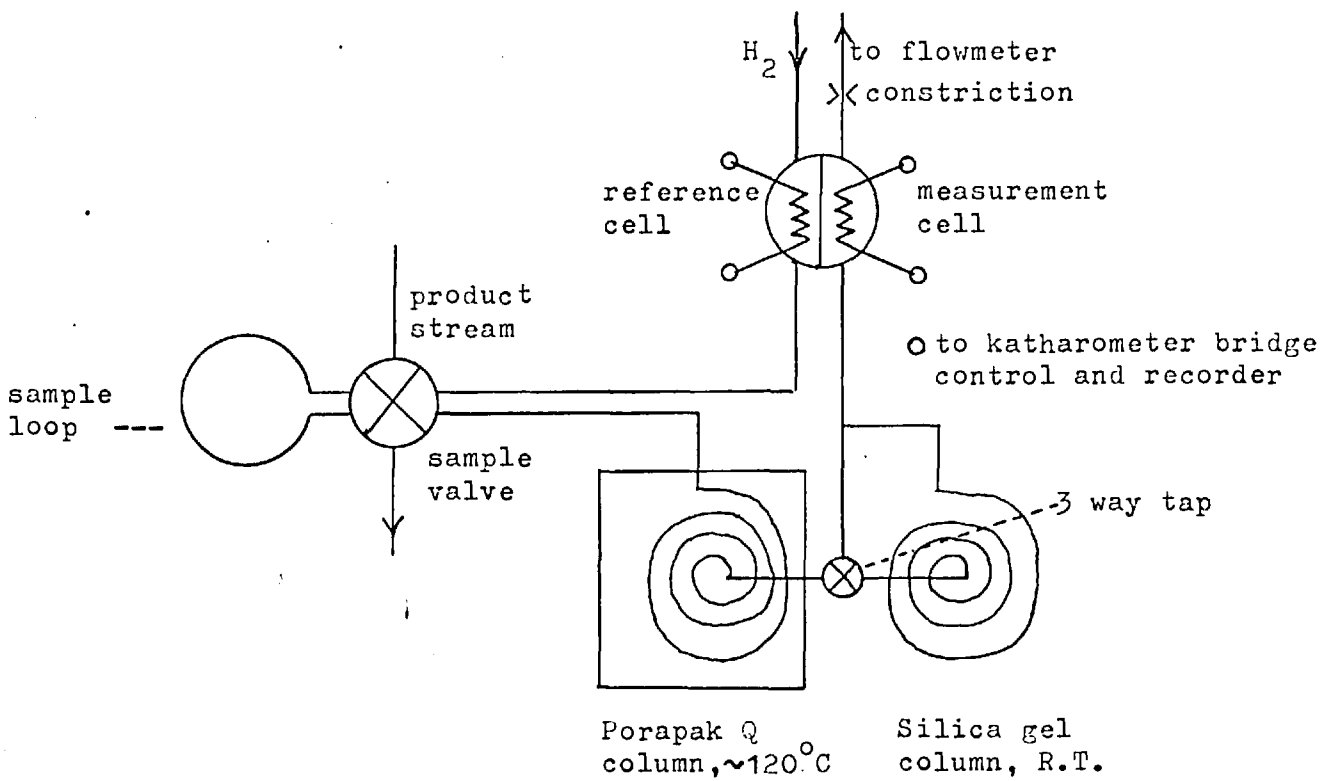
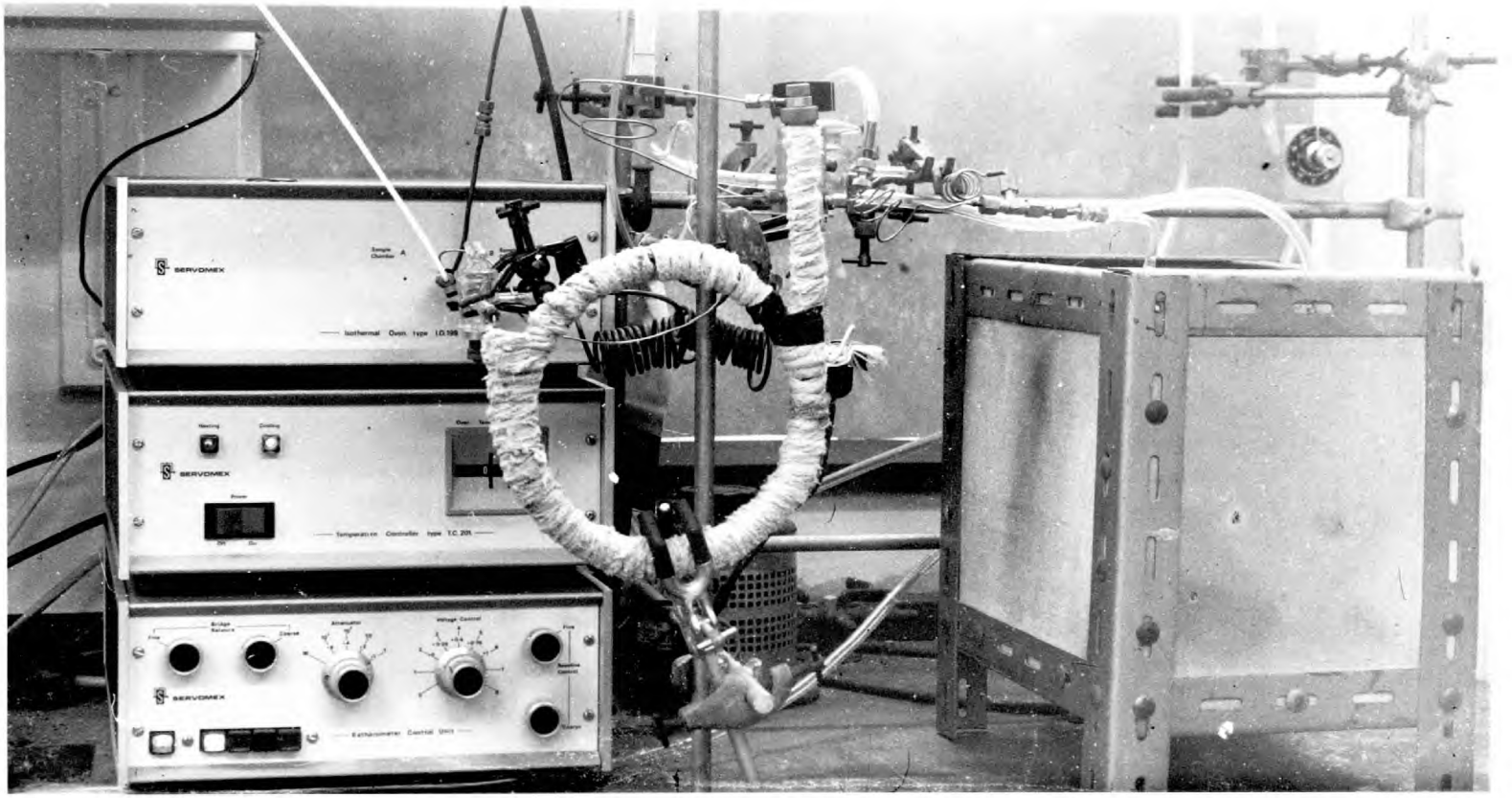


Fig.2.25 Product stream sampling and chromatographic analysis



Catalytic reactor and chromatograph FIG 2.26

In some cases, oxygen was allowed to flow into the molecular sieve column first before switching the main column straight to the detector: this had the advantage of improving the separation of the other, earlier components using a lower initial flow rate (28 ml/minute).

'Tailing' of the water peak was removed when the katharometer temperature was raised to 75°C to reduce adsorption on its metal walls and inlets. At 110°C on Porapak-Q the peak was reasonably sharp on elution, lasting for about 1½ minutes when recorded at low attenuation.

2.7.3. Calibration.

Calibration for sensitivity to gases was carried out with an auxiliary gas reservoir system, with arrangements for evacuating the sample loop, and filling with the gas in question at a measured pressure. Calibration for water sensitivity involved the injection of a 5% water in methanol solution, from a syringe. The peaks recorded were regular, and peak areas were measured assuming triangular shapes. Sensitivities were closely linear within the range measured, and were as follows:

Table 2.2.

	Chart speed	sensitivity
O_2	F	6.28 $x10^{-7}$(moles/cm^2 x 1)
CO_2	F	9.46 "
C_2H_4	F	7.94 "
H_2O	S	4.80 "
C_2H_4O	S	24.50 "

F : 30 mm/min. S: 10 mm/min.

CHAPTER 3.

RESULTS.

3.1. Microstructure of evaporated catalyst films.

3.1.1. Surface structure. 138

3.1.2. Hole density. 138

3.1.3. Crystallite size. 138

3.2. Annealing of catalyst films in reactive atmospheres.

3.2.1. Classification of effects of annealing atmosphere. 140

3.2.2. Sequence of microstructural changes in agglomeration. 140

3.2.3. Induction period. 143

3.2.3.1. Microstructural effects. 143

3.2.3.2. Effect of temperature on induction time. 149

3.2.3.3. Effect of temperature on hole density. 149

3.2.3.4. Effect of film thickness on induction time. 151

3.2.3.5. Effect of oxygen pressure on induction time. 153

3.2.3.6. Effect of water vapour. 153

3.2.4. Hole growth period. 153

3.2.4.1. Changes in microstructure. 153

3.2.4.2. Kinetics of hole growth-effect of temperature. 155

3.2.5. Island withdrawal and equilibration. 162

3.2.5.1. Microstructural changes. 162

3.2.5.2. Effect of film thickness on final island density. 162

3.2.5.3. Effect of temperature on final island density. 166

3.2.5.4. Effect of oxygen partial pressure on final island density. 168

3.2.5.5. Island crystallinity. 168

3.3. Adsorption study of catalyst films.

3.3.1. Adsorption isotherms. 173

3.3.2. Surface area variation during annealing. 173

3.4. Changes in catalytic activity of films in relation to microstructural changes.

3.4.1. Ethylene oxidation. 179

3.4.1.1. Continuous film catalysts. 179

3.4.1.2. "Shadowed" catalyst. 180

3.4.2. Hydrogen oxidation. 187

3.4.2.1. Continuous film catalysts. 187

3.4.2.2. "Shadowed" catalyst. 190

3.1. Microstructure of Evaporated Metal Films.

Three features of the microstructure of fresh films were investigated in detail for comparison purposes, after preliminary study of the effects of film annealing had suggested their importance.

3.1.1. Surface structure.

The topography of the silver films used was examined by s.e.m. as a basis of comparison with the surfaces of annealed films. The upper surface was found to be virtually planar, viewed at magnifications up to 20,000x; a few isolated agglomerates were visible on the surface. Experience suggested that excessive radiation from the boat used in the evaporation of the sample could cause the agglomeration. Fig. 3.2a shows the surface of an 1100 Å film as seen in the s.e.m.

3.1.2. Hole density.

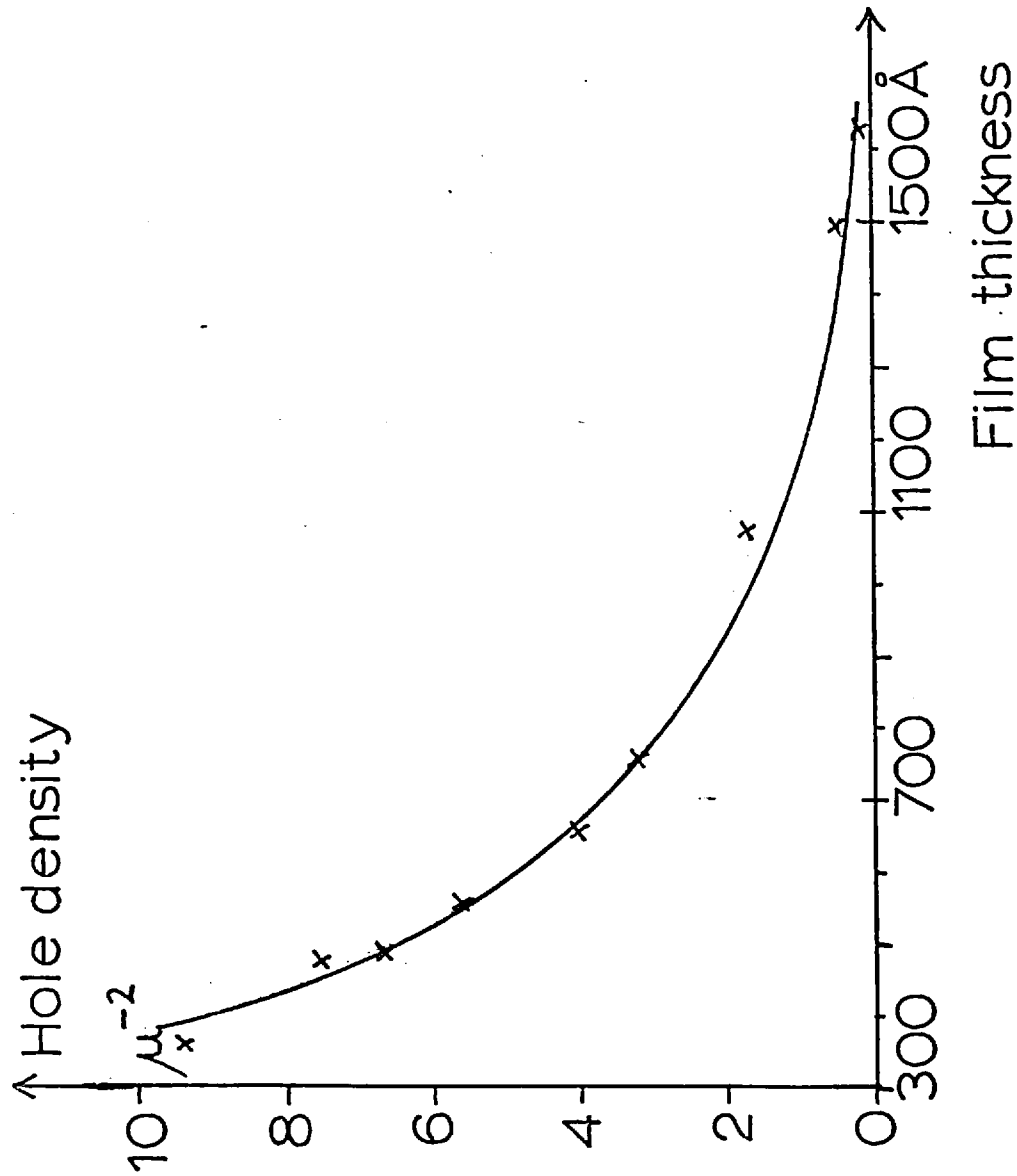
The density of holes in a number of fresh films was measured from transmission micrographs. The density was found to decrease steadily with increasing film thickness over the thickness range 350 - 1650 Å, as shown in fig. 3.1.

3.1.3. Crystallite size.

The initial crystallite size of films of 1180 Å thickness was measured from broadening of the (220)

Relation between initial film thickness l (Å) and hole density n (μ^{-2})

Fig 3.1



reflection in the electron diffraction pattern obtained in transmission using 80 kV electrons. The mean crystallite size was found to be approximately 90 Å.

3.2. Annealing of Catalyst Films in Reactive Atmospheres.

The annealing atmospheres used have been found to fall into two main classes according to their effect on the microstructure of the catalyst film. In hydrogen, oxygen-free nitrogen, and ethylene atmospheres, no gross surface rearrangement of the film takes place, although the expected crystallite size increases, by recrystallization, occur. The effect of atmosphere on recrystallization rate was briefly investigated: no differences were detected. In oxygen or oxygen-containing mixtures, massive changes occur in the distribution of the metal over the support, leading to the formation of discrete islands of metal from a formerly continuous film. In fig. 3.2, typical s.e.m. micrographs of (a) fresh 1180 Å silver film, (b) similar film annealed in hydrogen, 16 hr. 404°C, (c) similar film annealed for only 79 mins in oxygen at 221°C, are shown.

3.2.2. Sequence of microstructural changes leading to agglomeration.

The microstructural changes occurring in oxygen-bearing atmosphere can conveniently be divided for the sake of description into four stages:

Fig 3.2

REACTIVE ATMOSPHERE EFFECTS



6,600x

1100 Å Ag

as deposited



14,000x

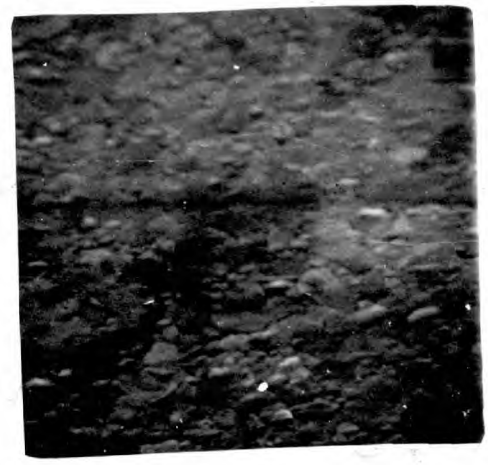
16h. H_2 404°C

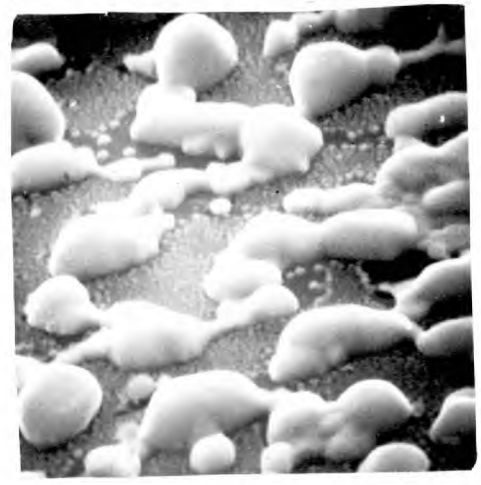


6,000x

79m O_2 221°C







i) No increase in the area of holes in the film is seen during an initial period called the 'induction period'; rearrangement begins on the upper surface.

ii) Growth of holes follows, leading to a network structure.

iii) Separation of agglomerates occurs by 'necking' at narrow regions of the network.

iv) Withdrawal of islands to a final equilibrium shape which is approximately hemispherical.

A check was carried out that the observed changes did not involve any overall loss of material. The estimated volume of an island structure, assumed to be hemispheres, agreed with that of an 1180 Å film from which it had been produced within about 20%.

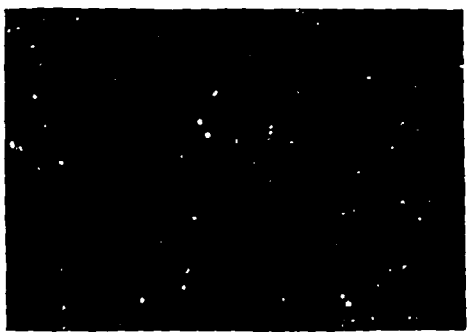
Transmission micrographs illustrating these four stages of agglomeration are shown in fig. 3.3. a-d.

3.2.3. The Induction Period.

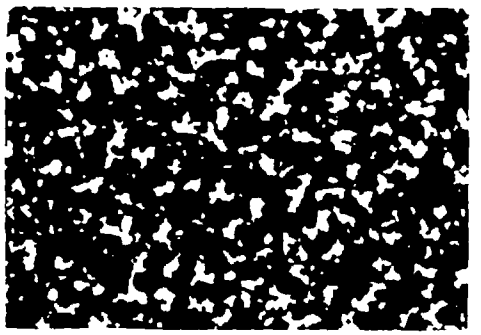
3.2.3.1. Microstructural effects.

When examined by t.e.m., films showed little change during the induction period. The density of holes during the induction period was investigated, to check for possible grain boundary grooving effects. It remained constant (within the limits of scatter observed in between different areas of the same specimen). The hole density

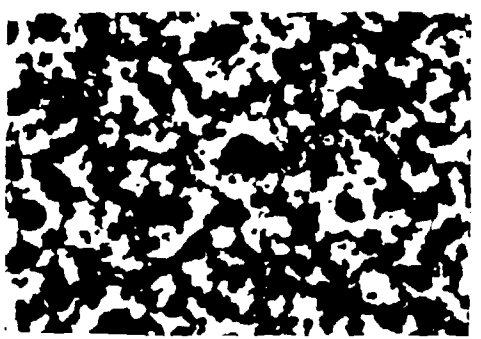
STAGES OF FILM BREAK-UP IN OXYGEN



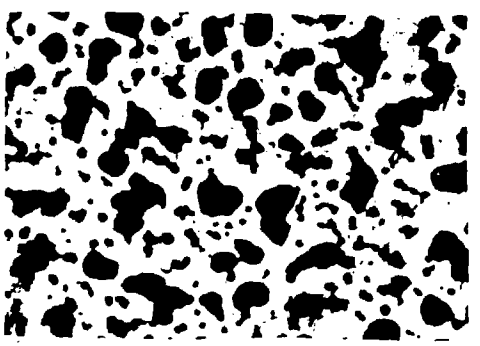
a UNHEATED/INDUCTION PERIOD



b CATALYST REMOVAL FROM HOLES



c SEPARATION



d ISLAND WITHDRAWAL

10μ

FIG 3.3

for a 1180 Å film heated at 221°C in oxygen for various times is shown in table 3.1.

Table 3.1

Hole density during induction period.

1180 Å film, 221°C, annealed in oxygen 760 torr.

Time mins.	Holes/micron^2
0	0.584
5	0.444
22	0.540
29	0.398
34	0.467

Specimens from the induction period were examined by s.e.m. The impression from t.e.m., of little change in this period, was not confirmed: progressive growth of agglomerates on the upper surface was detected, as illustrated in fig. 3.4.

The induction time t_i was defined as the time after which hole growth (= decrease in the metal-substrate area) occurred. This was found by interpolation from a plot of metal-substrate area against time. Such a plot for an 1180 Å film in oxygen at 221°C is shown in fig. 3.5. The value of t_i was subsequently used as a quantitative measure of the rate of agglomeration in the induction period.

GROWTH OF SURFACE AGGLOMERATES

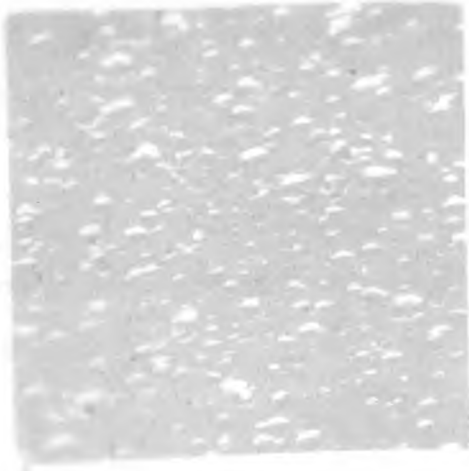
6,600x

221°C O_2

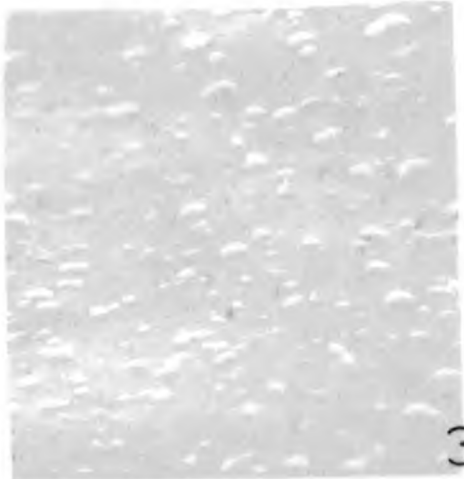


FIG 3.4

5'

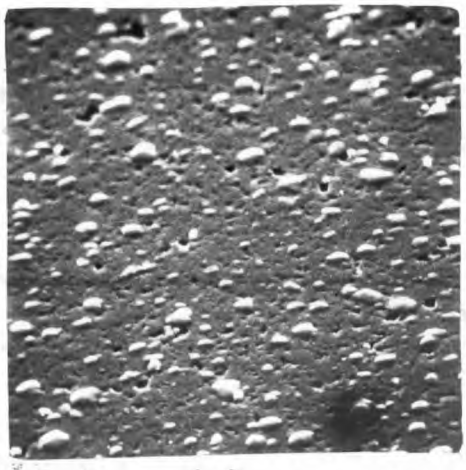


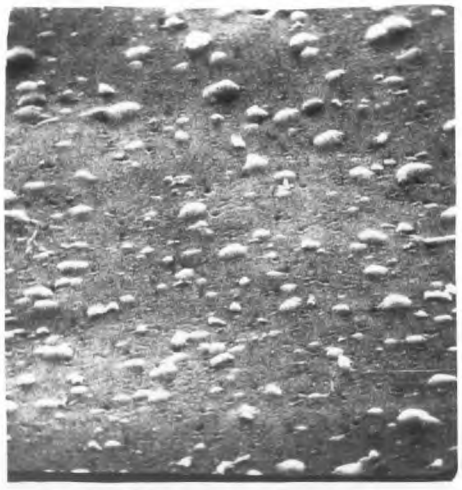
27'



34'



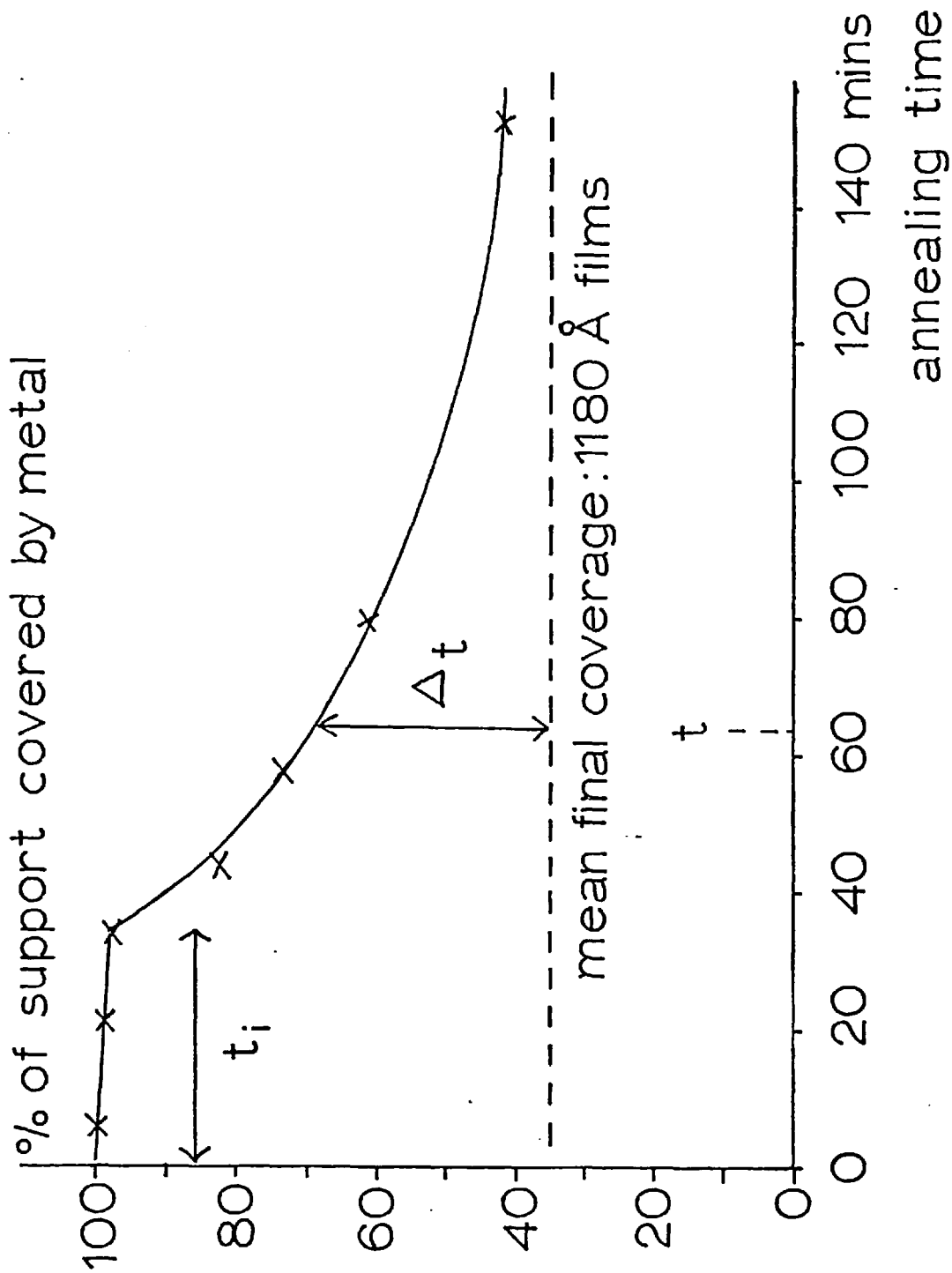




Variation of metal-support interfacial area with annealing time:

1180 Å film in oxygen, 760 torr

Fig 3.5



3.2.3.2. Effect of temperature on induction time.

Using films of a constant thickness (1180 Å ± 50Å) in oxygen at 760 torr pressure, the induction time was measured at a range of temperature from 210°C to 345°C. The results are plotted as an Arrhenius graph in fig. 3.6, where it can be seen that t_i decreased steadily with increasing temperature, at a rate equivalent to an activation energy of 14.9 kcals/mole.

3.2.3.3. Effect of temperature on hole density during induction period.

In the course of examining different mechanisms for island formation, it became necessary to know whether the density of holes in the induction period, thought to influence the final island density, depended on temperature. The mean hole density during the induction period of a series of 1180 Å films heated in oxygen at temperatures between 221°C and 324°C was measured. The results are shown in table 3.2. They show that there is no systematic trend in hole density with changing temperature.

Dependence of induction time t_i (mins) on annealing temperature T°C : 1180 Å film in oxygen, 760 torr

Fig 3.6

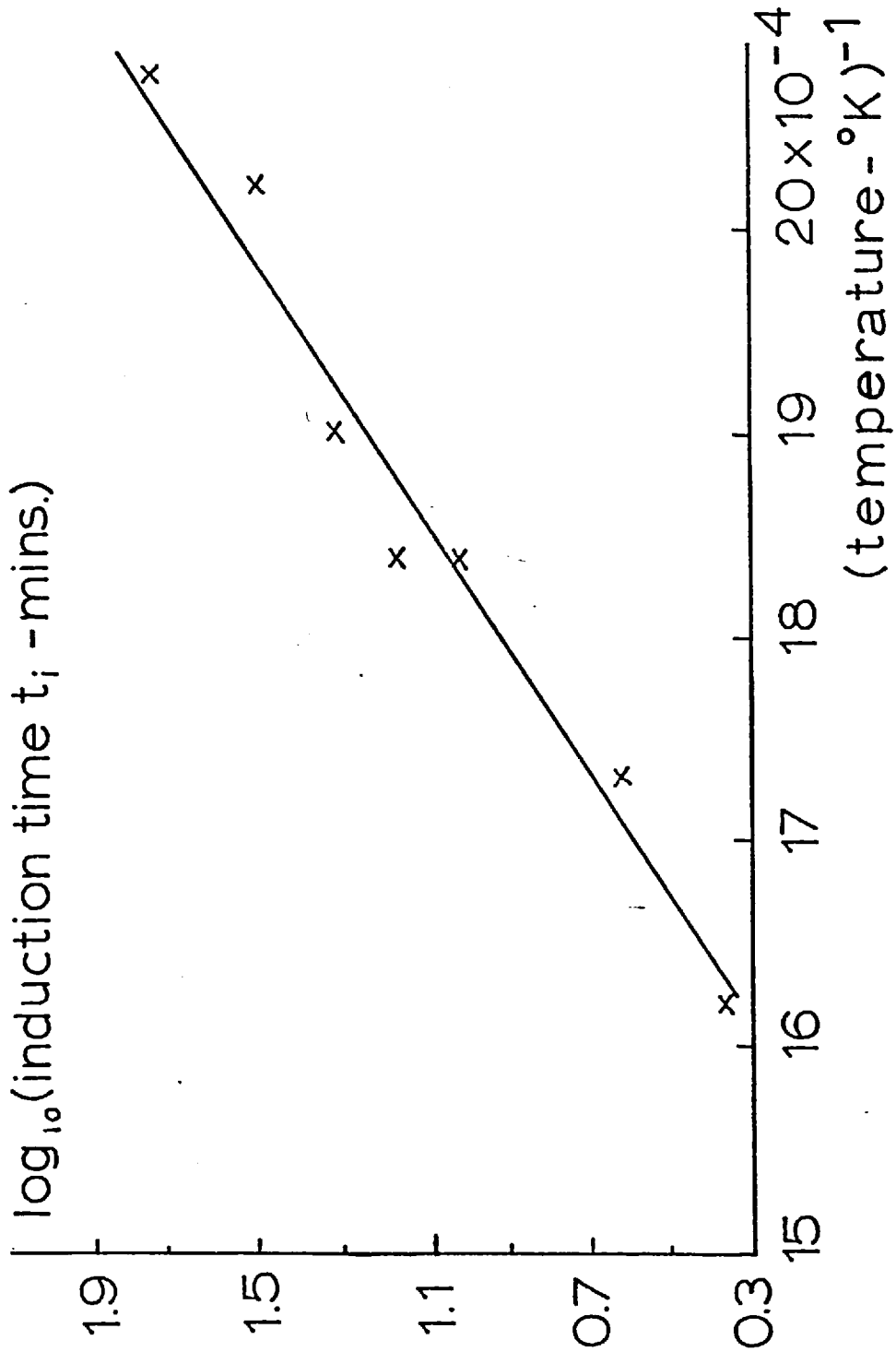


Table 3.2.

Effect of temperature on mean hole density observed during induction period.

1180 Å films annealed in oxygen, 760 torr.

Temperature °C.	Holes/micron^2
221	0.465
237.5	0.381
266	0.346
287	0.364
305	0.380
324	0.290

Weighted standard deviation for 19 hole density observations ±0.070 holes/micron^2.

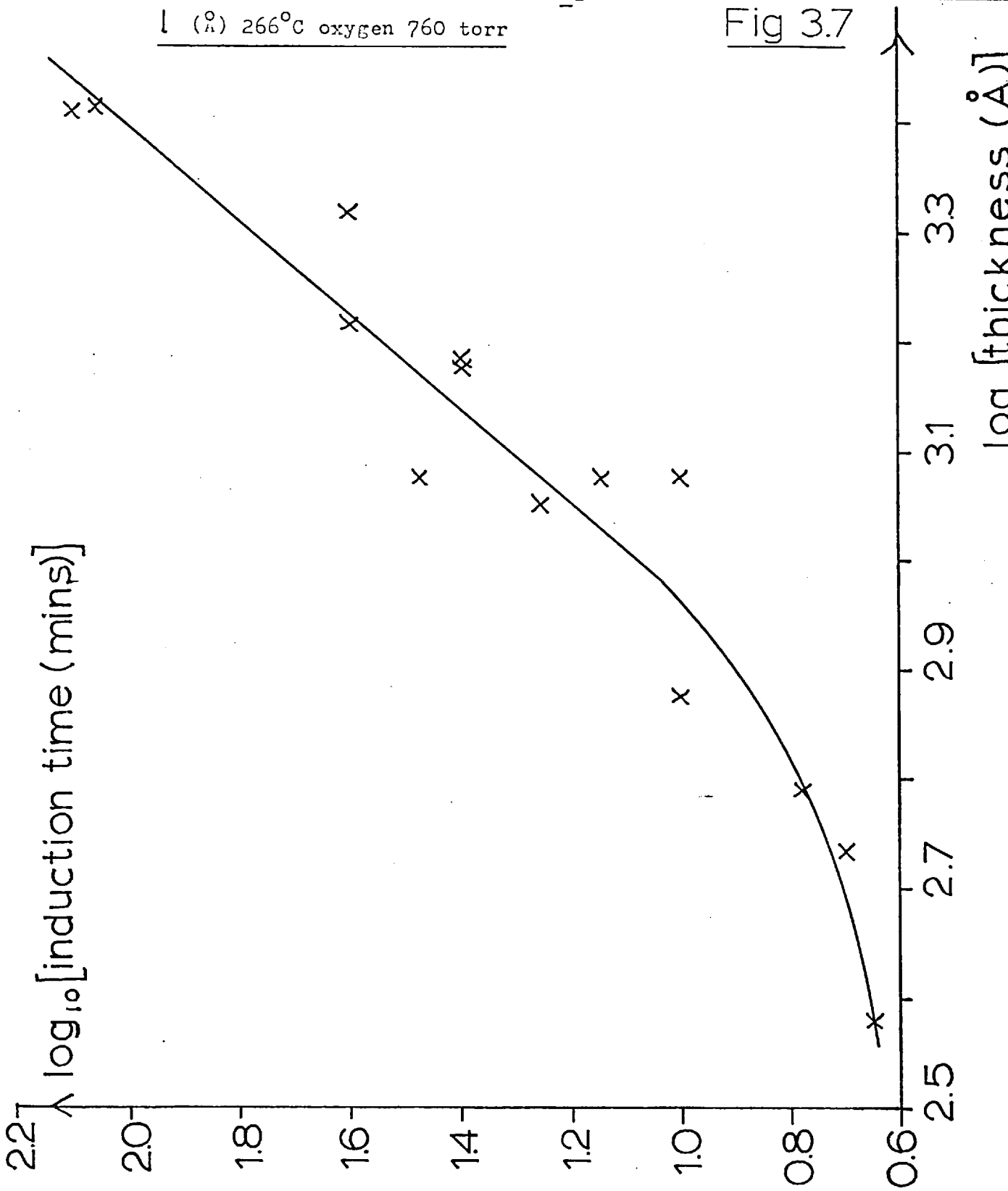
3.2.3.4. Effect of film thickness on induction time.

The kinetics of the induction period in relation to film thickness were investigated, to assess a hypothesis that the induction period time was governed by the rate of the thermal grooving of grain boundaries. At 266°C, at a pressure of 760 torr, a series of films of thicknesses varying between 380 and 2600 Å was annealed in oxygen, and the induction period determined from transmission micrographs of samples. The induction time increased sharply with film thickness: the results are plotted in log-log form in fig. 3.7. Points from films greater than ca. 800 Å lay about a straight line, indicating the

Relation between induction time t_i (mins) and initial film thickness

l (Å) 266°C oxygen 760 torr

Fig 3.7



relationship

$$t_i = a\, l^3 \qquad (3.1)$$

where l = film thickness, $a = 3.8 \times 10^{-9}$ mins/Å^3.

3.2.3.5. Effect of oxygen pressure on induction time.

Using films of 380 Å thickness, again at 266°C, the induction period was measured from specimens heated in varying partial pressures of oxygen p_{O_2} between 10^{-6} torr and 760 torr. Reducing p_{O_2} had the effect of increasing the induction time considerably; the results are plotted in fig. 3.8. This shows a linear relationship between t_i (mins.) and log p_{O_2} (torr) expressed by

$$t_i = 11.5 - 3.8 \log p_{O_2} \qquad (3.2)$$

3.2.3.6. Effect of water vapour.

Measurements of t_i using 1180 Å films at 266°C were made using both oxygen saturated with water vapour, and oxygen dried over a liquid nitrogen trap containing dried molecular sieve: no deviation from the value of t_i (12 ± 2 mins.) found for normal oxygen streams was observed.

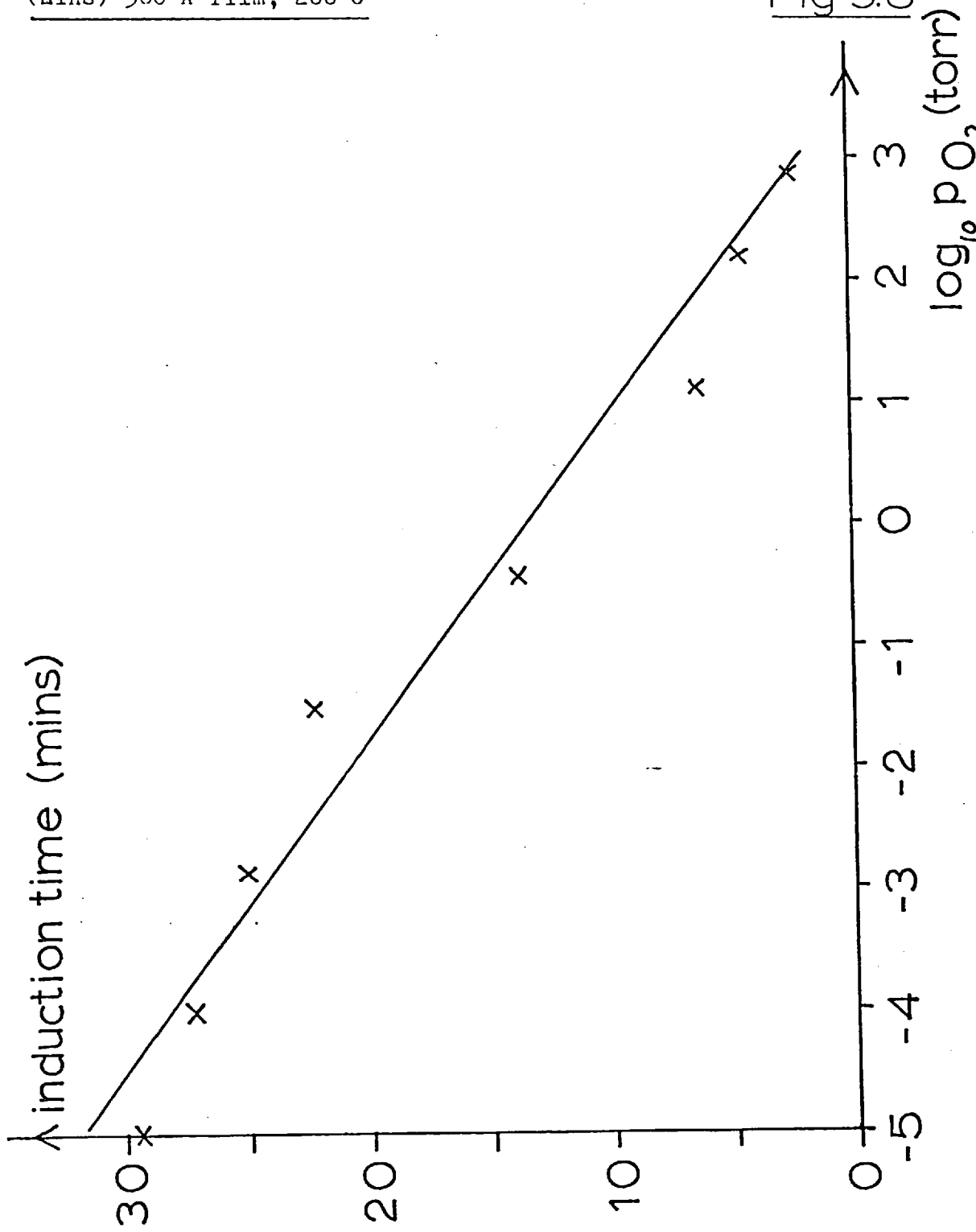
3.2.4. Hole growth period.

3.2.4.1. Microstructural changes.

The growth of holes in the film by withdrawal of material from the substrate, results in structures seen in

Effect of oxygen partial pressure p_{O_2}(torr) on induction time t_i (mins) 380 Å film, 266°C

Fig 3.8



transmission as fig. 3.3b. Using s.e.m., the upper surface is now seen to have larger agglomerates, many but not all of which are located at the edge of a growing hole (fig. 3.9). The holes themselves have multiple cusps, pointing outwards; transmission microscopy shows that these cusps are located at grain boundaries (e.g. fig. 3.10).

The density of holes during this period was measured for two series of specimens annealed at 266°C in oxygen at 760 torr. The results are plotted in fig. 3.11, which shows that the hole density does not decrease greatly by coalescence during the growth period.

An attempt was made to follow the size distribution of the holes during the growth period for the same two sets of specimens; the estimation involved in judging the mean diameter of the very irregular holes was considerable. The results are plotted in fig. 3.12, and show that the relative size distribution is reasonably constant during the growth.

3.2.4.2. Kinetics of hole growth: effect of temperature.

Mean metal-substrate areas were measured during the hole-growth stage for a series of 1180 Å specimens heated in oxygen at 760 torr at a range of temperatures between 221°C and 324°C. The rate of hole growth was found to increase with temperature. A selection of the results

Fig 39

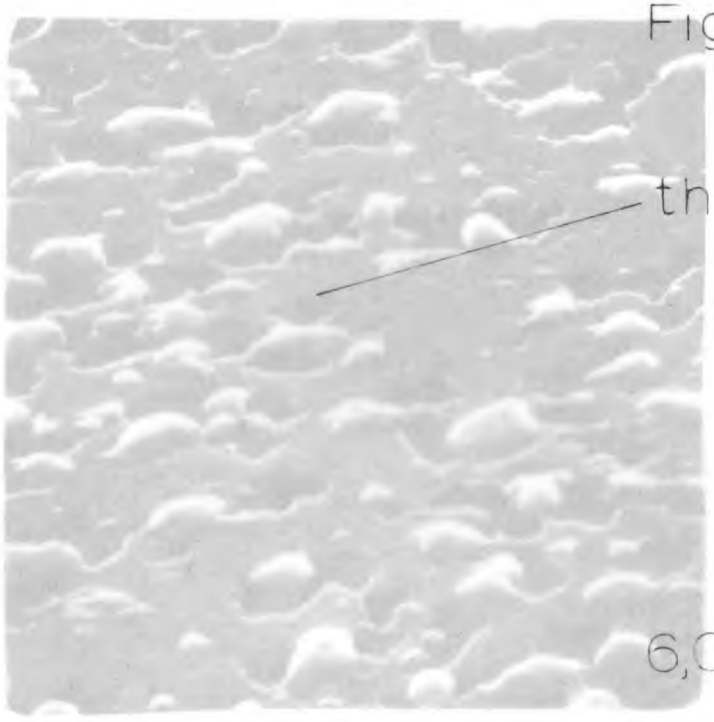


6,000 x 60°

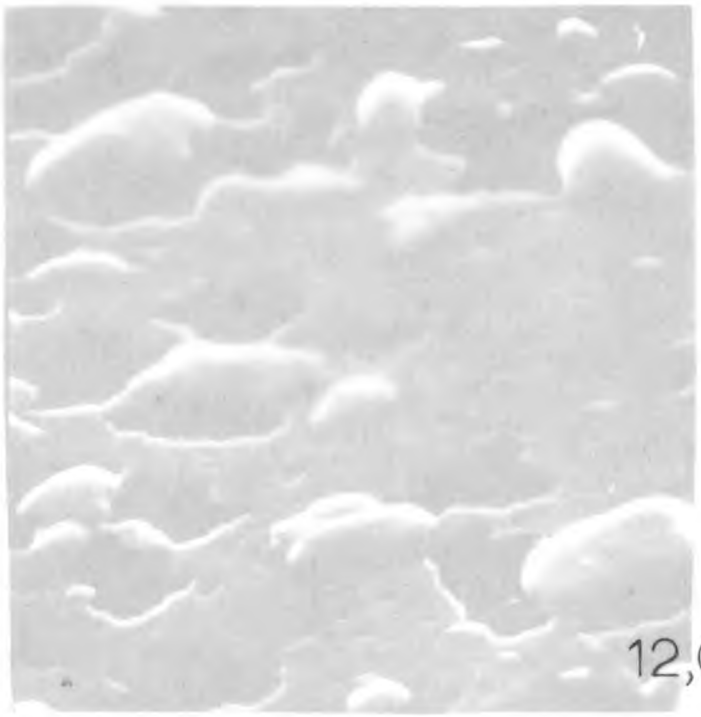
HOLE GROWTH

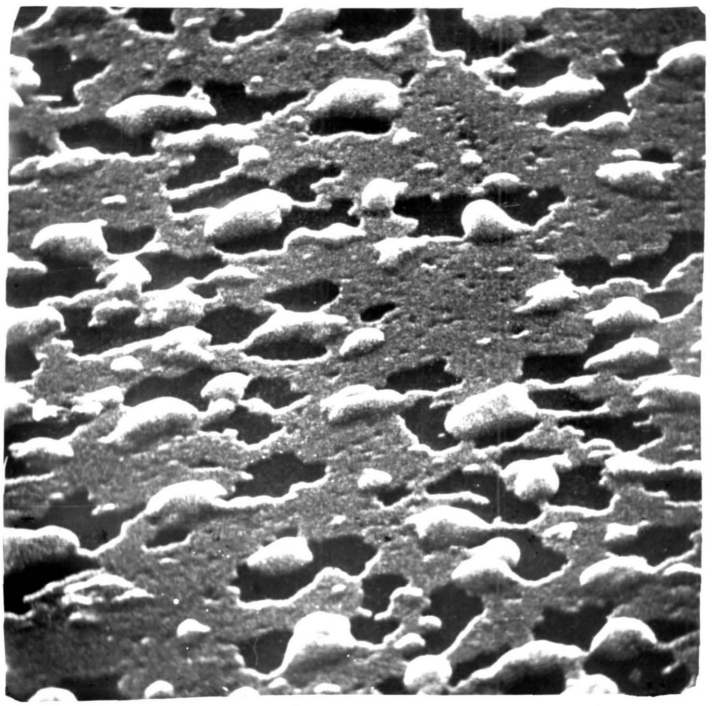
12,000 x 60°

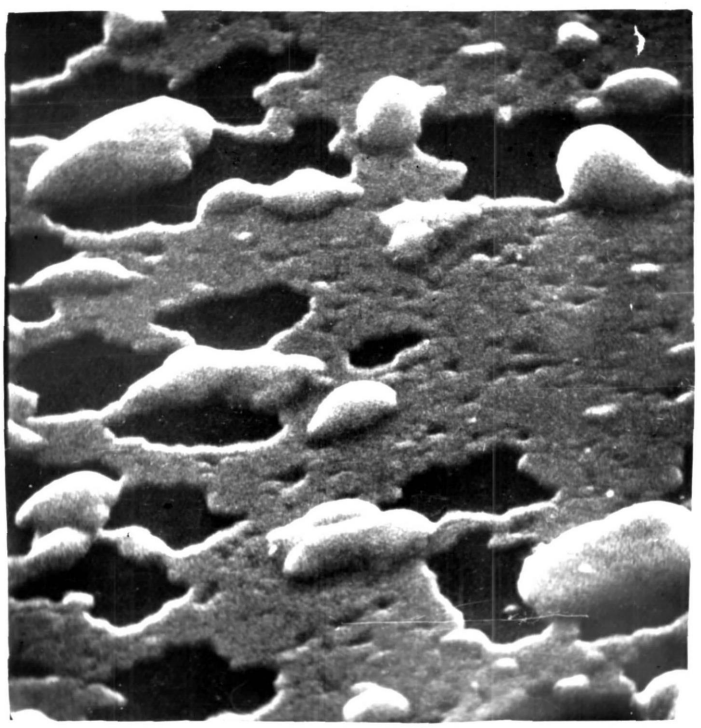
Fig 39



HOLE GROWTH



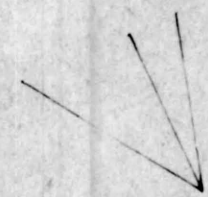




BIMODAL DISTRIBUTION FIG 315

7200 x

ISLAND SEPARATION FIG 310

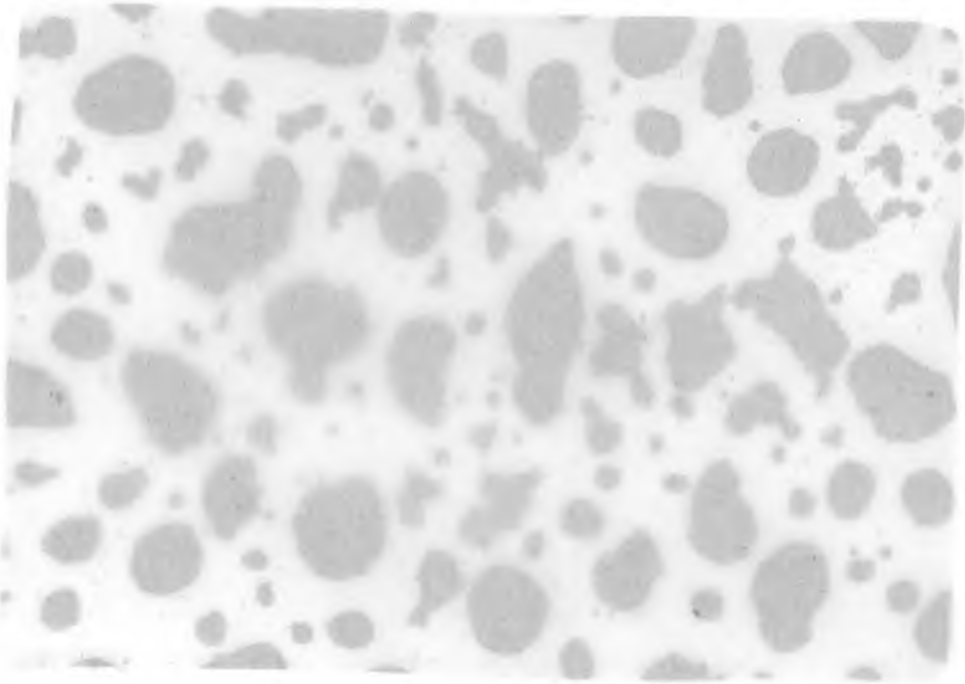


separation
at grain
boundaries

55,000 x

159

BIMODAL DISTRIBUTION FIG 315

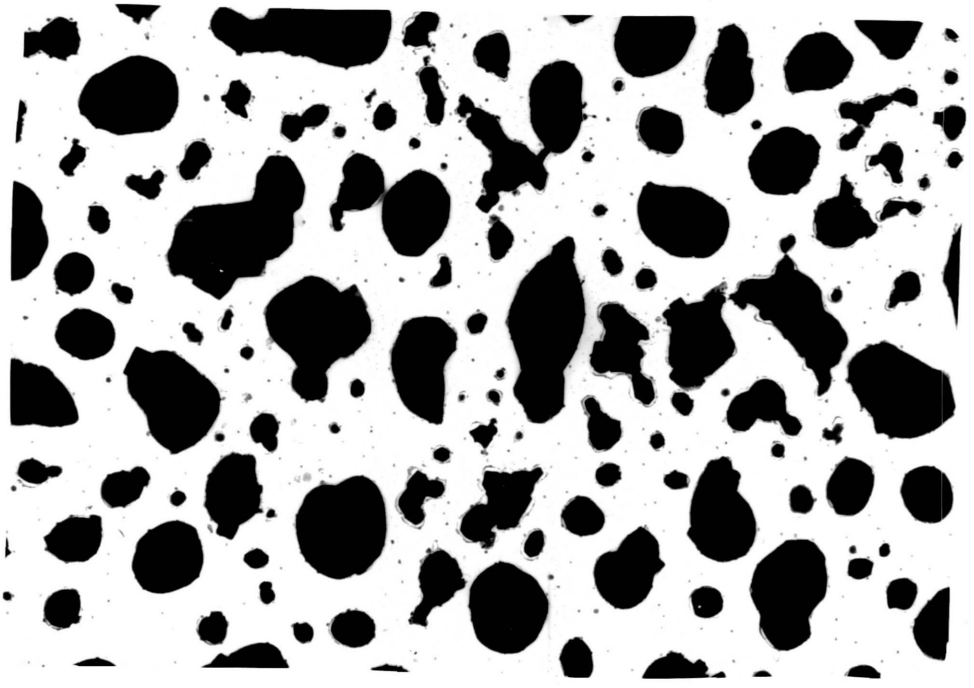


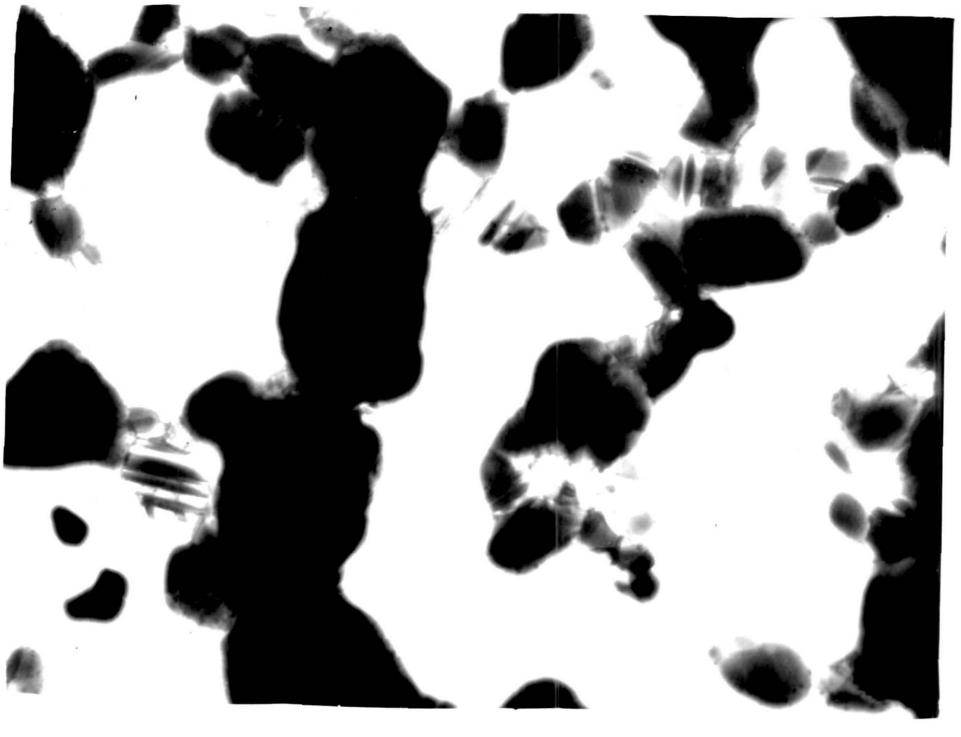
7200 ×

ISLAND SEPARATION FIG 310



55,000 ×





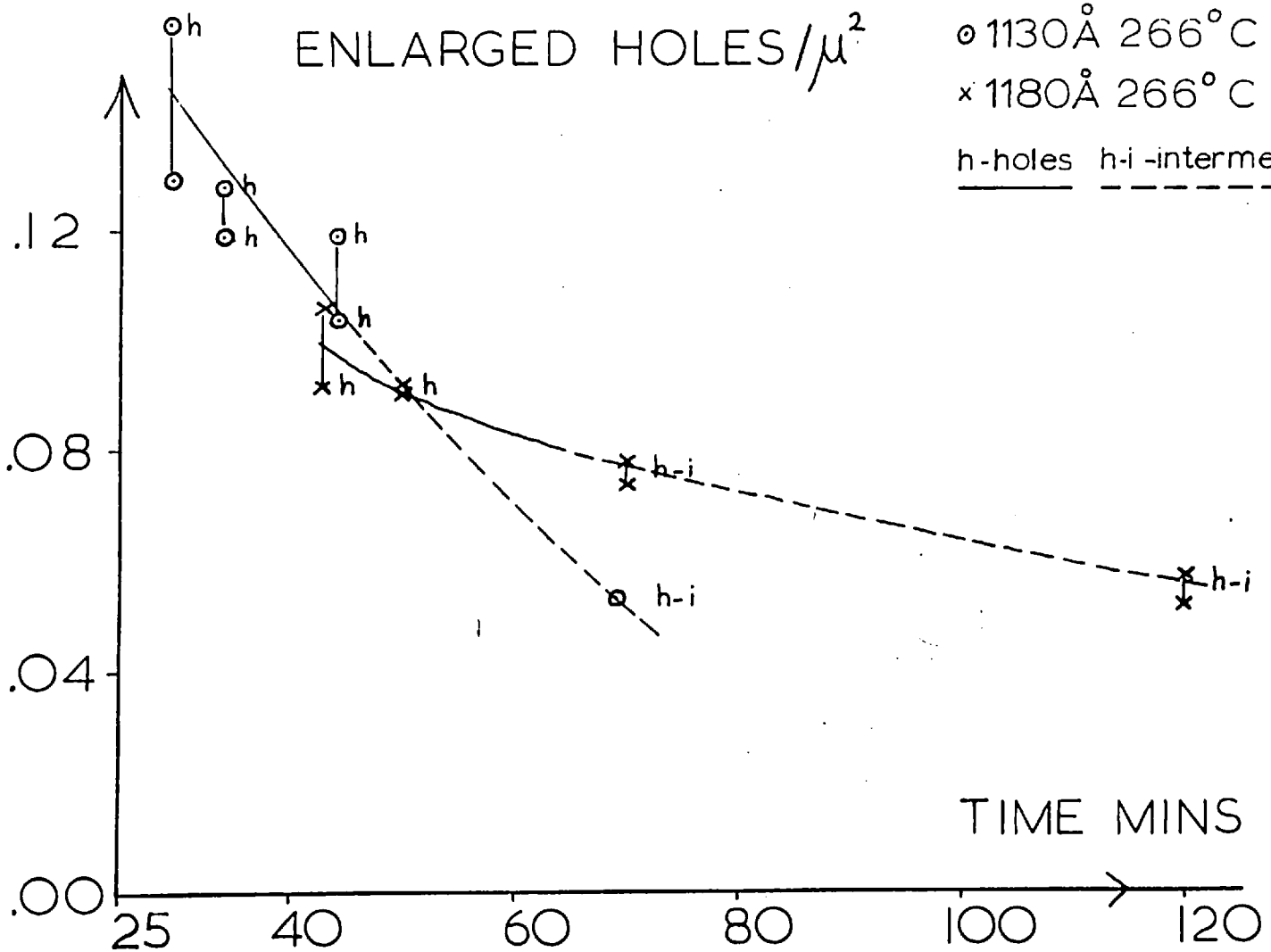
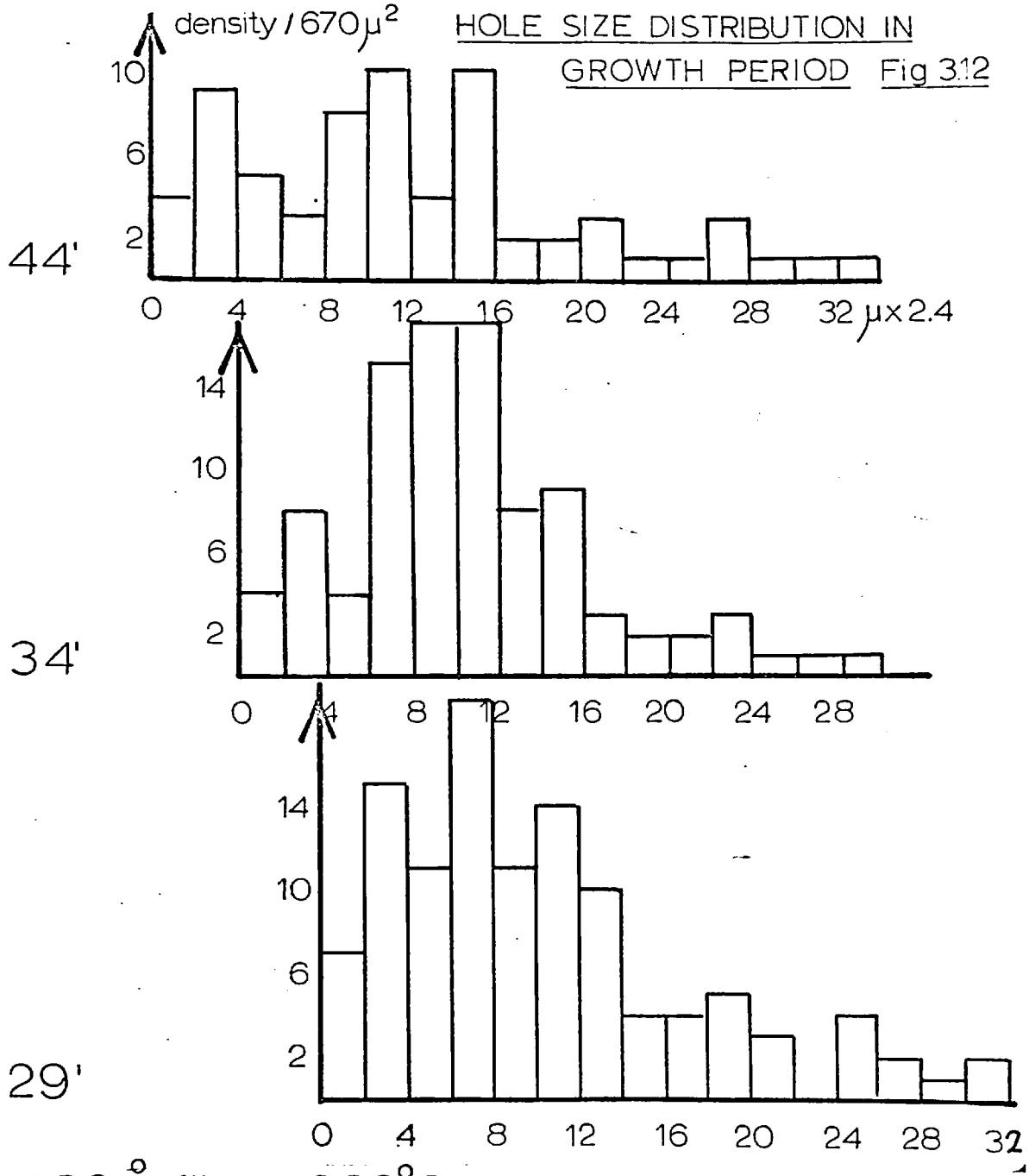

ENLARGED HOLES/μ^2
⊙ 1130Å 266°C
× 1180Å 266°C
h-holes h-i -intermediate
.12
.08
.04
.00
25
40
60
80
100
120
TIME MINS
h
h-i

Fig 3.11

HOLE SIZE DISTRIBUTION IN GROWTH PERIOD Fig 3.12



1180 Å film 266°C

(omitting repeat runs at the same temperature) is shown in fig. 3.13.

3.2.5. Island withdrawal and equilibration.

3.2.5.1. Microstructural changes.

Progressive growth of holes leaves narrow regions which tend to separate, particularly by the joining together of hole cusps (fig. 3.4c). The result is to leave discrete but irregular areas of metal, generally including a large agglomerate, surrounded by a section of the thin 'land' left behind from the remainder of the film after transfer of material to the agglomerates. This situation after 'necking-off', observed by s.e.m., is shown in fig. 3.14. By this stage, in some specimens, a population of very much smaller islands could be observed between the main masses, probably left by adhesion of metal to small areas of the intervening substrate (fig. 3.15). The effect of film thickness, temperature, and oxygen pressure, on the main final island population, was then studied; the island density was used as a measure of the structure.

3.2.5.2. Effect of film thickness on final island density.

Measurements of final island density were made for a series of films with thicknesses of 350 - 1490 Å heated in oxygen at 266°C for several hours. The island density decreased rapidly with increasing film thickness. Only

Hole growth rate : temperature variation, 1180Å films

Fig 3.13

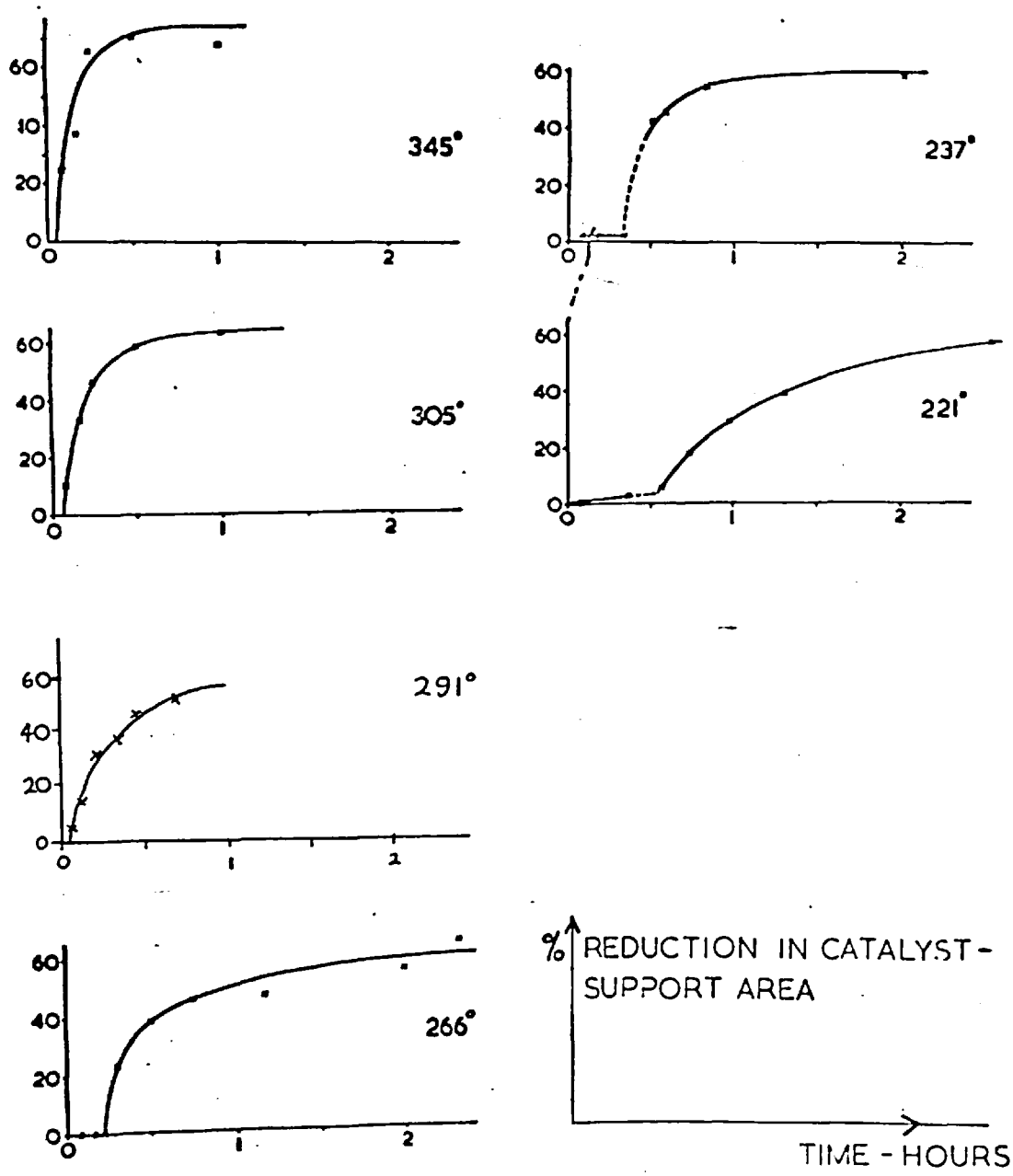
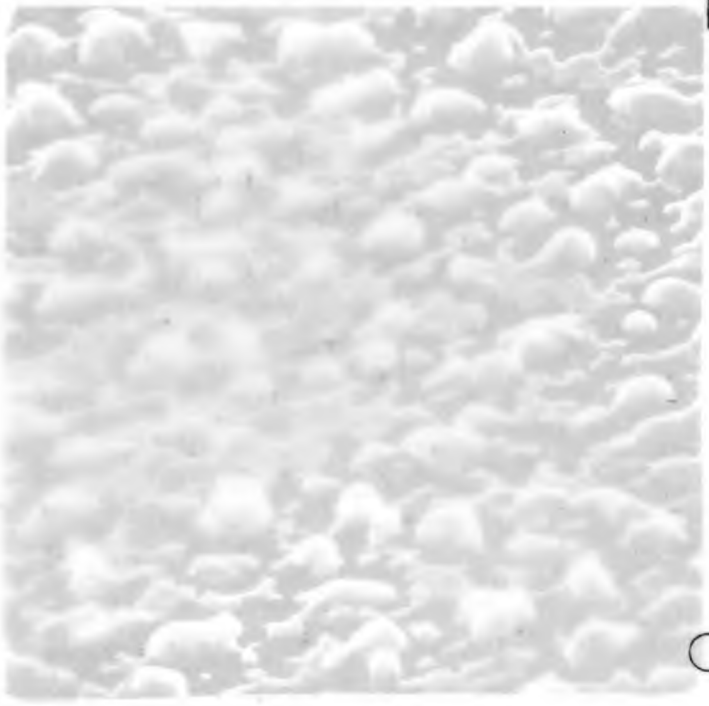
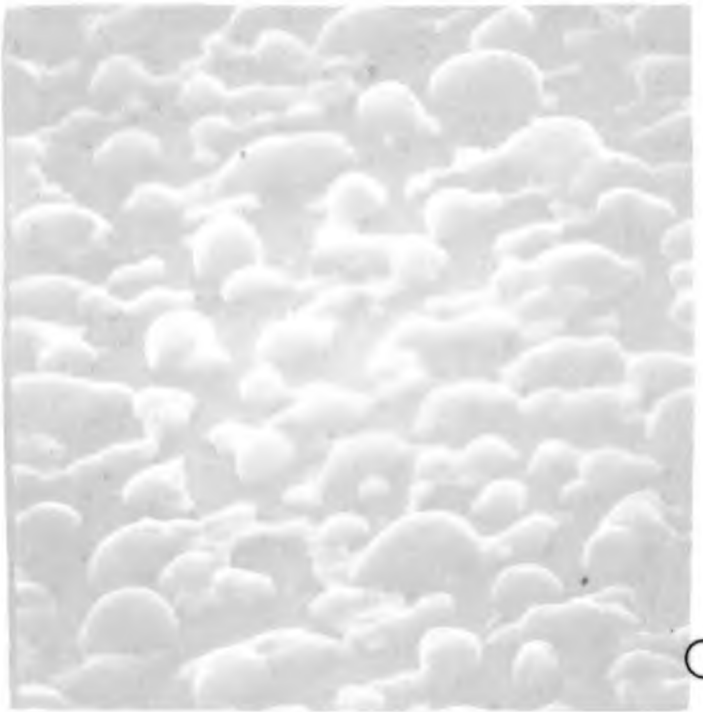


Fig. 3.14



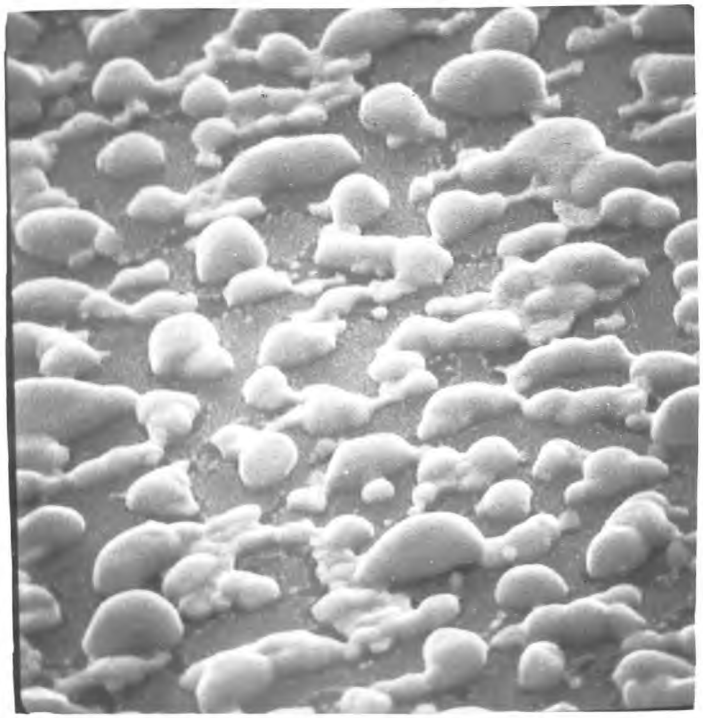
59′ O_2 221°C

ISLAND WITHDRAWAL



79′ O_2 221°C





the main population of large islands (ca. 0.3 - 1.0 x maximum diameter) was included; those left on the substrate by adhesion (3.2.5.1) were omitted. The results are presented in fig. 3.16 in terms of a catchment area, A_c, which is defined as the mean area (in microns^2) from which the islands of the final structure have withdrawn material for growth. Thus, if the island population/square micron is I, then

$$A_c = 1/I \qquad (3.3)$$

Log A_c is seen to vary linearly with log l ($\mathring{A}$), according to the relation

$$\log_{10} A_c = 2.1 \log_{10} l - 5.34 \qquad (3.4)$$

or,

$$A_c = 4.57 \times 10^{-6} l^2 \qquad (3.5)$$

3.2.5.3. Effect of temperature on final island density.

Final island densities I were measured as before from the structures obtained on heating the series of 1180 $\mathring{A}$ films in oxygen at 760 torr for several hours at temperatures in the range 210°C to 324°C. Results were not obtained from those specimens that had not been heated sufficiently long to produce discrete islands, but sufficient data was available to indicate (Table 3.3) that any effect of temperature on I was small.

Relation between catchment area $A_c(\mu^2)$ and initial film thickness l (Å): 266°C, oxygen 760 torr.

Fig 3.16

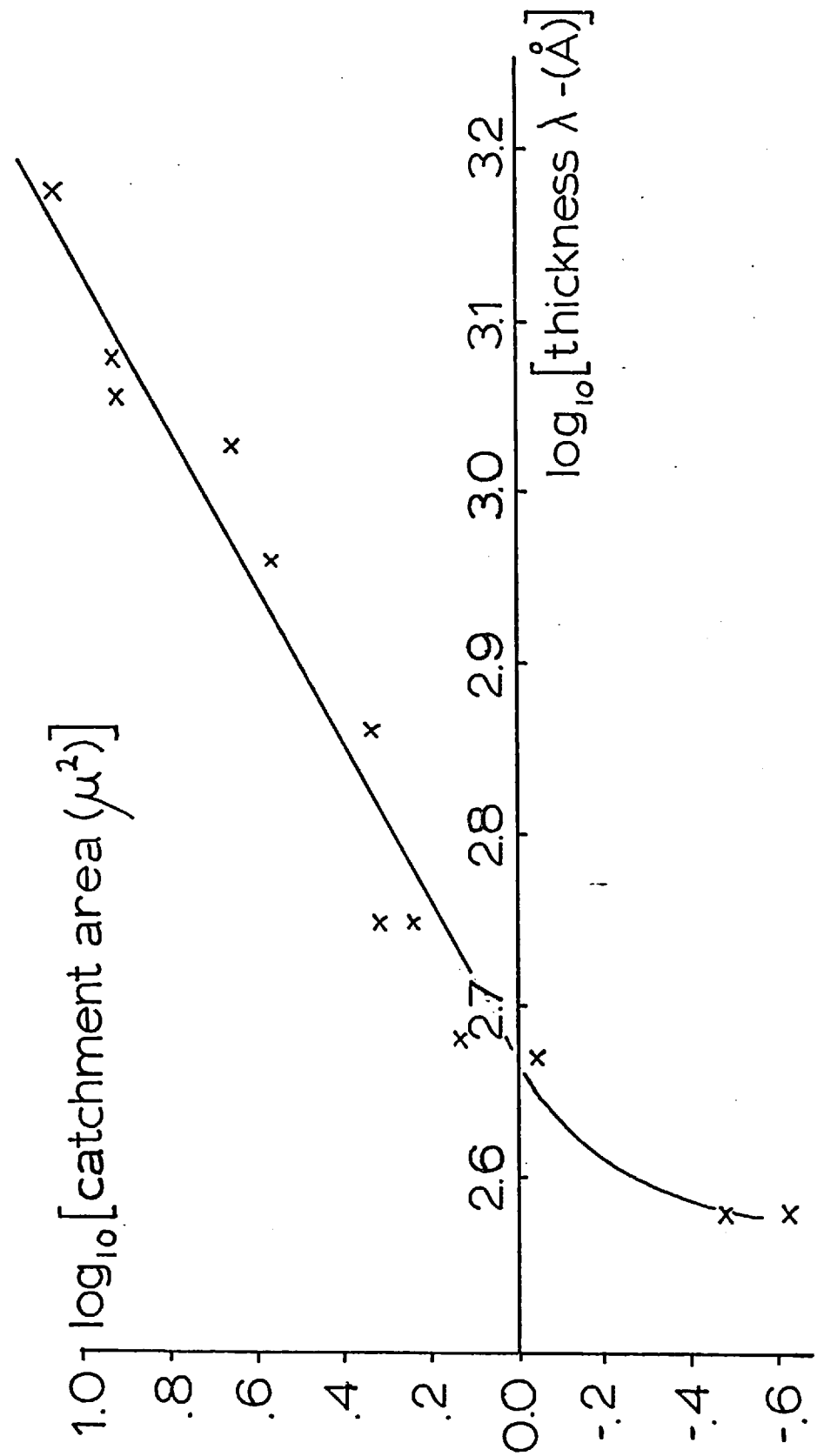


Table 3.3.

Effect of temperature on final island density I.

Temperature °C	I/micron^2
210	0.154
221	0.181
266	0.112
324	0.117

1180 Å films annealed in oxygen, 760 torr.

3.2.5.4. Effect of oxygen partial pressure on final island density.

I was measured as before from the final island structures produced by long annealing of the series of 380 Å films heated in varying partial pressures of oxygen. The results are shown in fig. 3.17, indicating a fairly well defined linear trend towards larger values of A_c as log p_{O_2} decreases. The line drawn corresponds to the expression

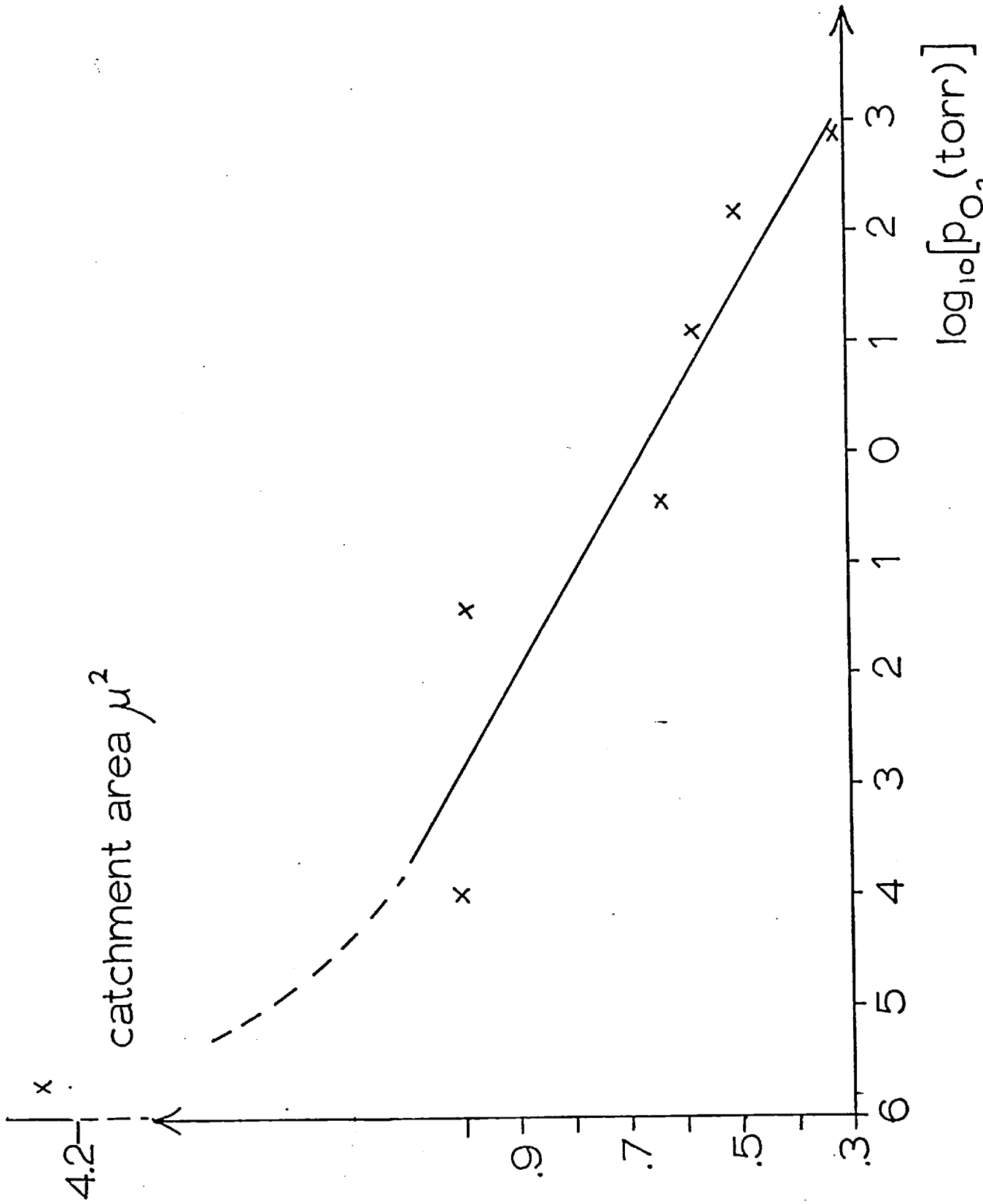
$$A_c = 0.67 - 0.16 \log_{10} p_{O_2} \qquad (3.6)$$

3.2.5.5. Island crystallinity.

A study was made of the crystallinity of the final island structure from a film of 380 Å heated in oxygen at 404°C for 16 hrs. The islands produced had a size distribution ranging up to ca. 4000 Å diameter, as shown in the frequency histogram (fig. 3.18). Dark field

Relation between catchment area A_c (μ^2) and oxygen partial pressure p_{O_2} (torr): 380 Å film, 266°C

Fig 3.17



transmission microscopy using (111) or (200) reflections was used to examine individual islands of the structure. The results showed that the final islands were single crystals, as follows: for any one setting of the illumination with the condenser lens, a few islands at a time became visible by transmission in a narrow band around their complete perimeter, without interruption by grain boundaries; an example is shown in fig. 3.19. The effect of island thickness on electron absorption was briefly studied. A number of images of islands was recorded, and the density variation across each measured with a micro-densitometer. The slit height used was not more than 1/3 of the image diameter. Traces from islands of increasing size are shown in fig. 3.20. In Table 3.4, the widths of the peaks observed at the edge of the particle image are shown. Where a second peak was observed within the first, its width is also recorded.

Table 3.4.

Width of electron transmission intensity peaks in Å: dark field (111) and (200) images of silver islands at 100 kV.

Particle diameter Å	First peak width Å	Second peak Å
680	88	-
1320	116	-
1600	126	38

ISLAND SIZE DISTRIBUTION 380 Å FILM

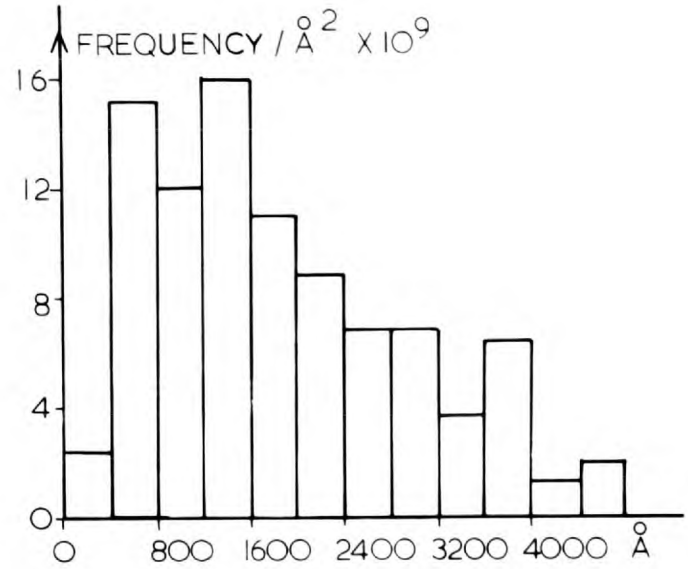


Fig 3.18

DARK FIELD IMAGE : 1400 Å
ISLAND
X 375,000

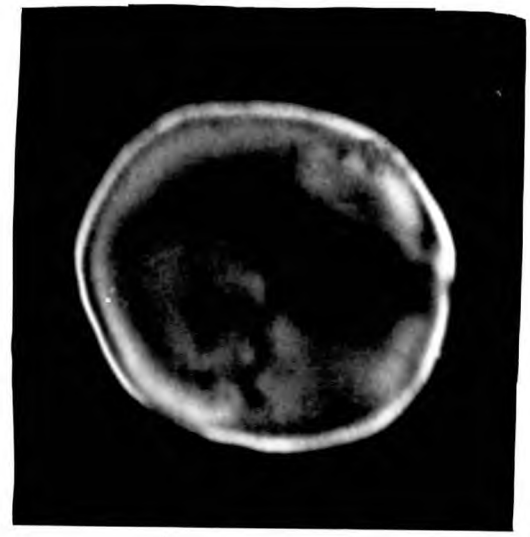
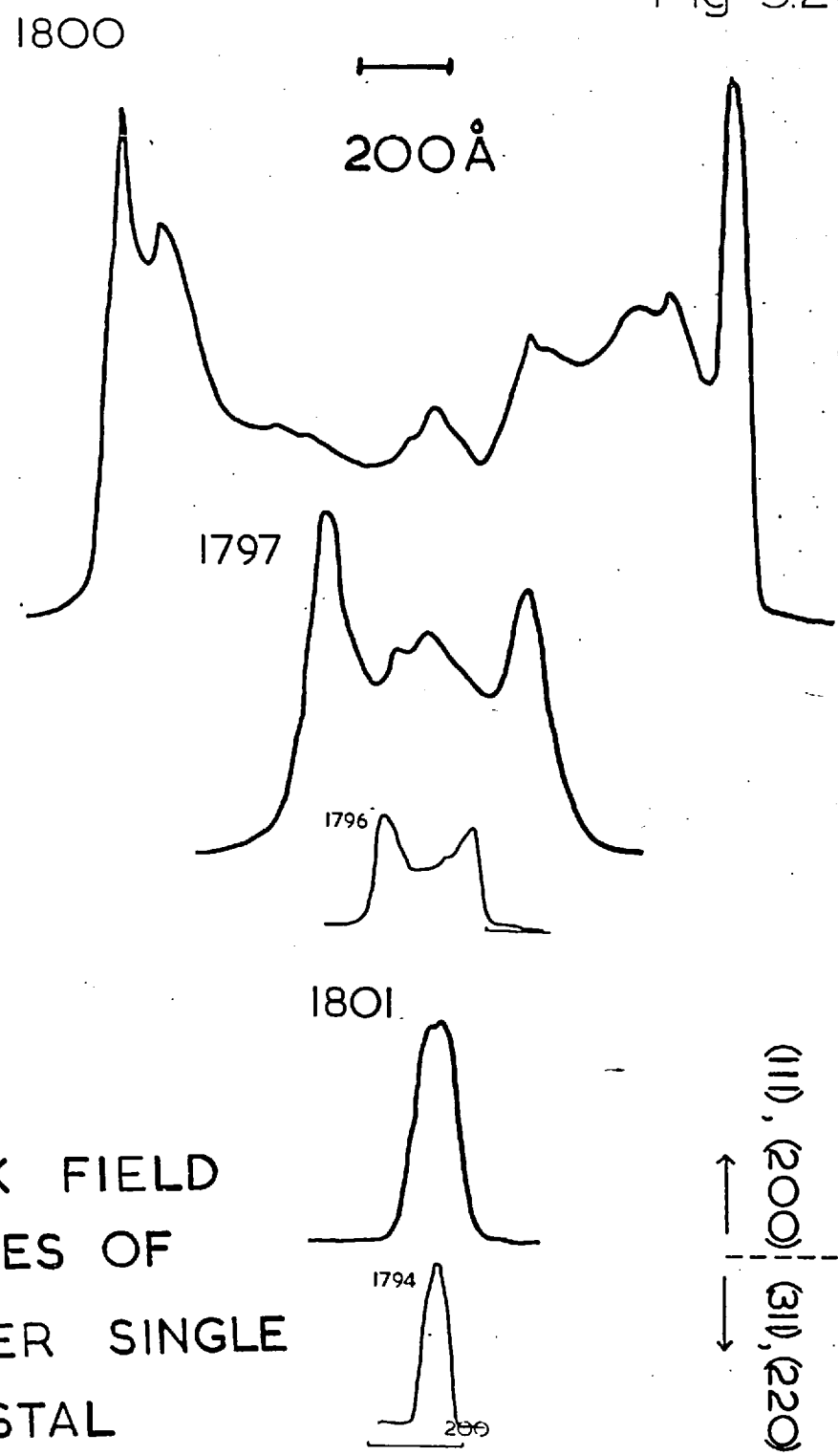


Fig 3.19

Fig 3.20



DARK FIELD IMAGES OF SILVER SINGLE CRYSTAL HEMISPHERES

100 kV

VERTICAL SCALE NOT UNIFORM

3.3. Adsorption Study of Catalyst Films.

3.3.1. General shape of adsorption isotherms.

The adsorption behaviour of krypton on unannealed silver films was studied over the full range of partial pressure at 78°K. The isotherm (fig. 3.21) had a very long plateau region, falling only below $p/p_o = 0.05$, and rising steeply only just below the saturation vapour pressure p_o.

It was found that the isotherm obeyed the B.E.T. equation even at pressures below 0.1 torr, where the thermal transpiration correction (section 2.5.2.3) was not expected to apply exactly. The B.E.T. plot for the unannealed film is shown in fig. 3.22. Subsequent adsorption measurements were therefore extended down to $p/p_o = 0.02$ in order to check the shape of the isotherms.

3.3.2. Film surface area variation during annealing.

Adsorption isotherms were obtained from a 380 Å silver film deposited on 155 pyrex slides, (a) when the film was unannealed, (b) after 6 mins. and (c) after 60 mins. annealing in oxygen at 266°C. S.e.m. micrographs of a sample of the same film after annealing are shown in fig. 3.23. The adsorption isotherm and B.E.T. plot for the unannealed film has already been referred to (fig. 3.22); the results after the successive stages of annealing are shown in figs. 3.24 and 3.25.

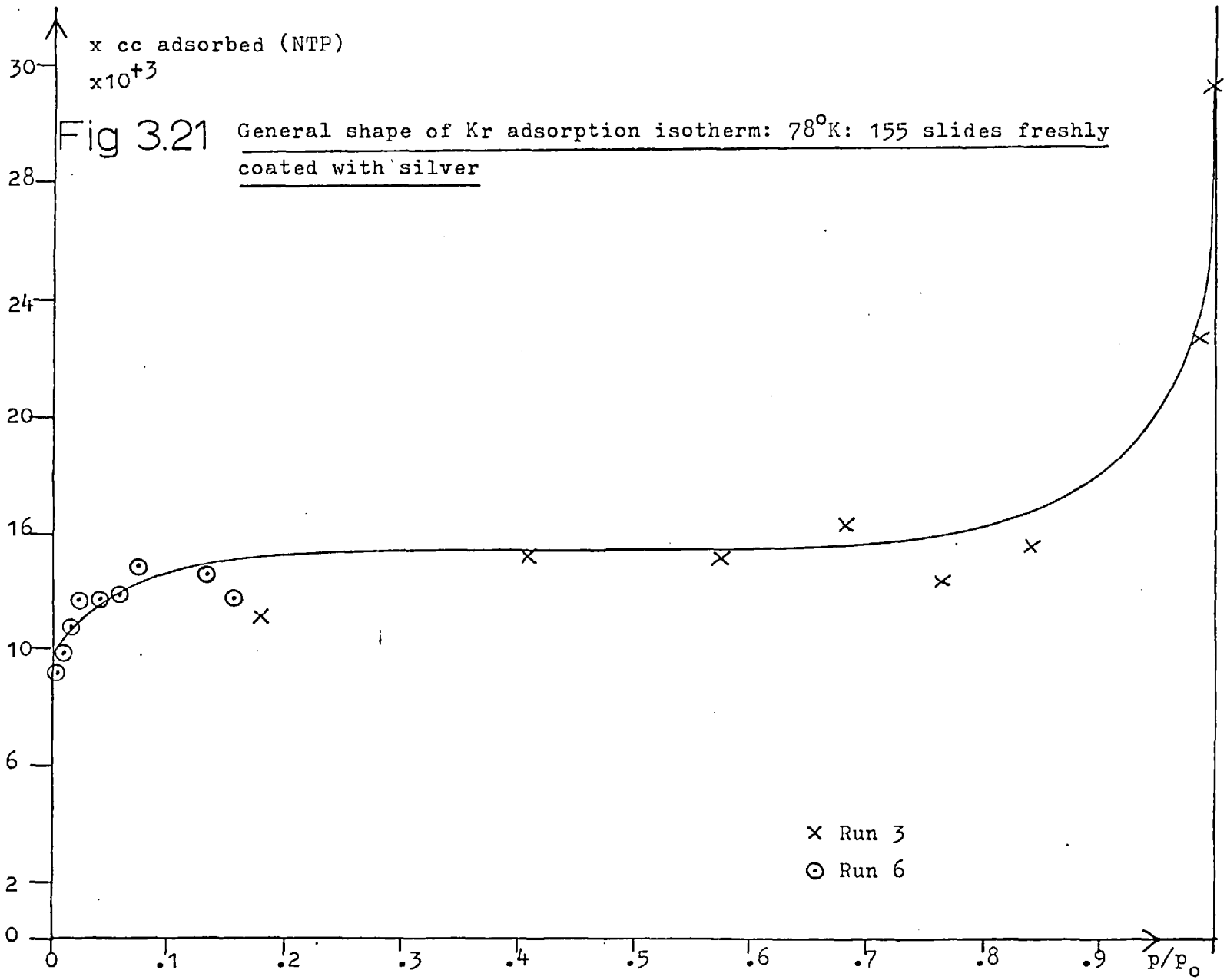
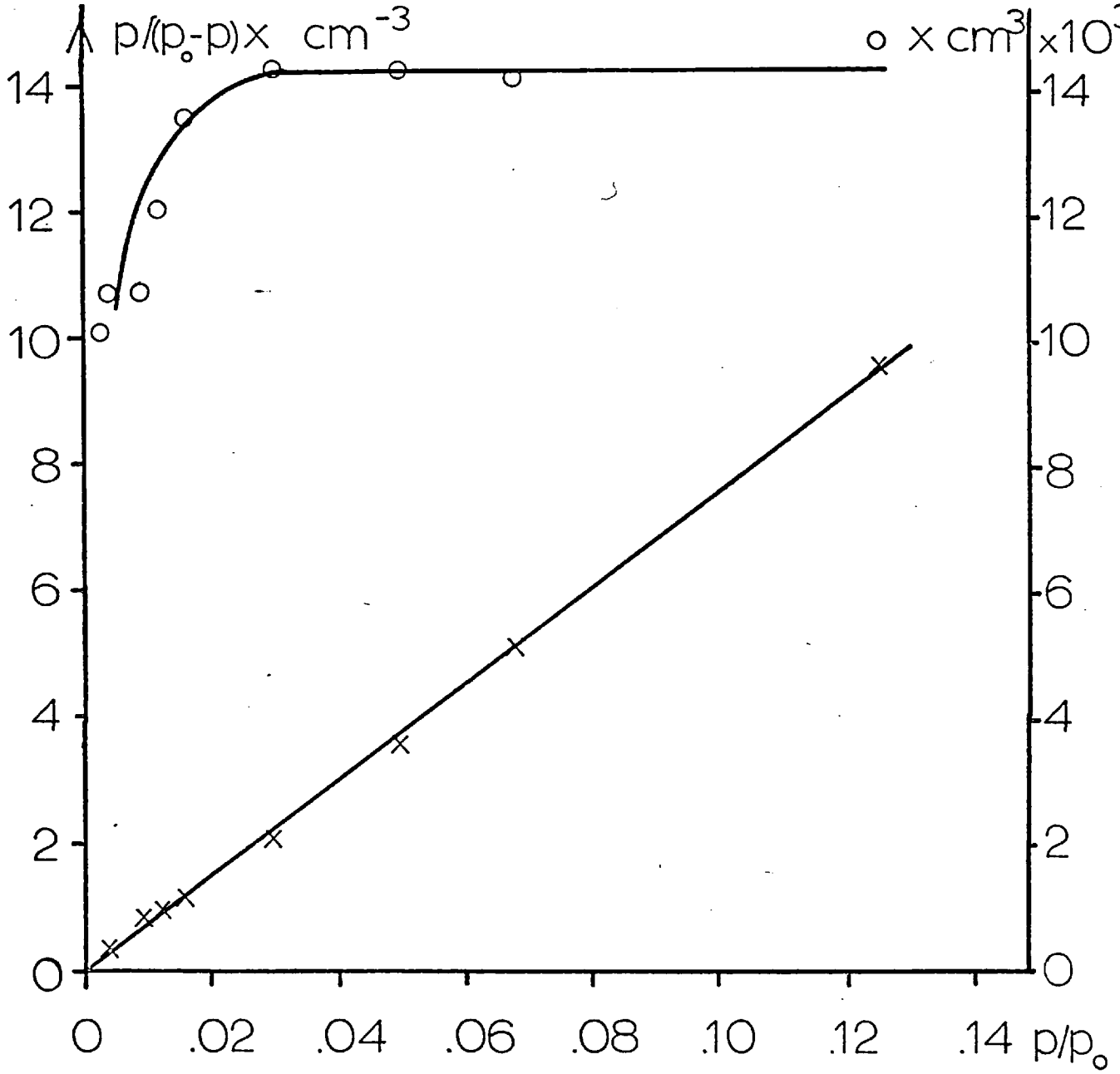


Fig 3.21 General shape of Kr adsorption isotherm: 78°K: 155 slides freshly coated with silver

Fig 3.22 Adsorption isotherm and B.E.T. plot: 155 slides freshly coated with silver, 380 Å



SURFACE AREA CHANGE

adsorption specimens



Fig 3.23

380 Å 6' 266°

x 8,100

adsorption area 1.27 x original



adsorption area 1.36 x original

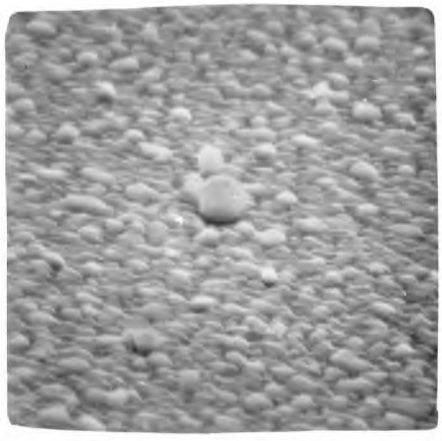
60' 266°

x 7,600

GRID SHADOWED CATALYST: channel centre after 1hr H_2 228°



x 16,800





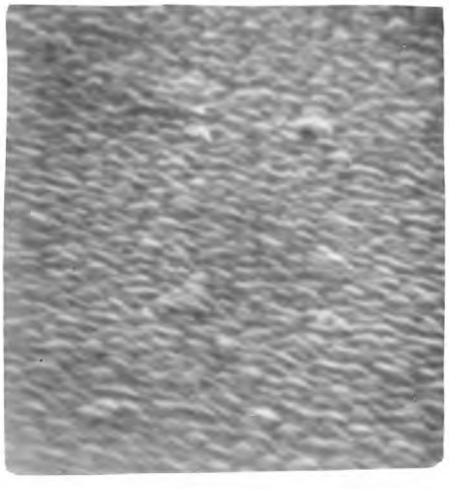
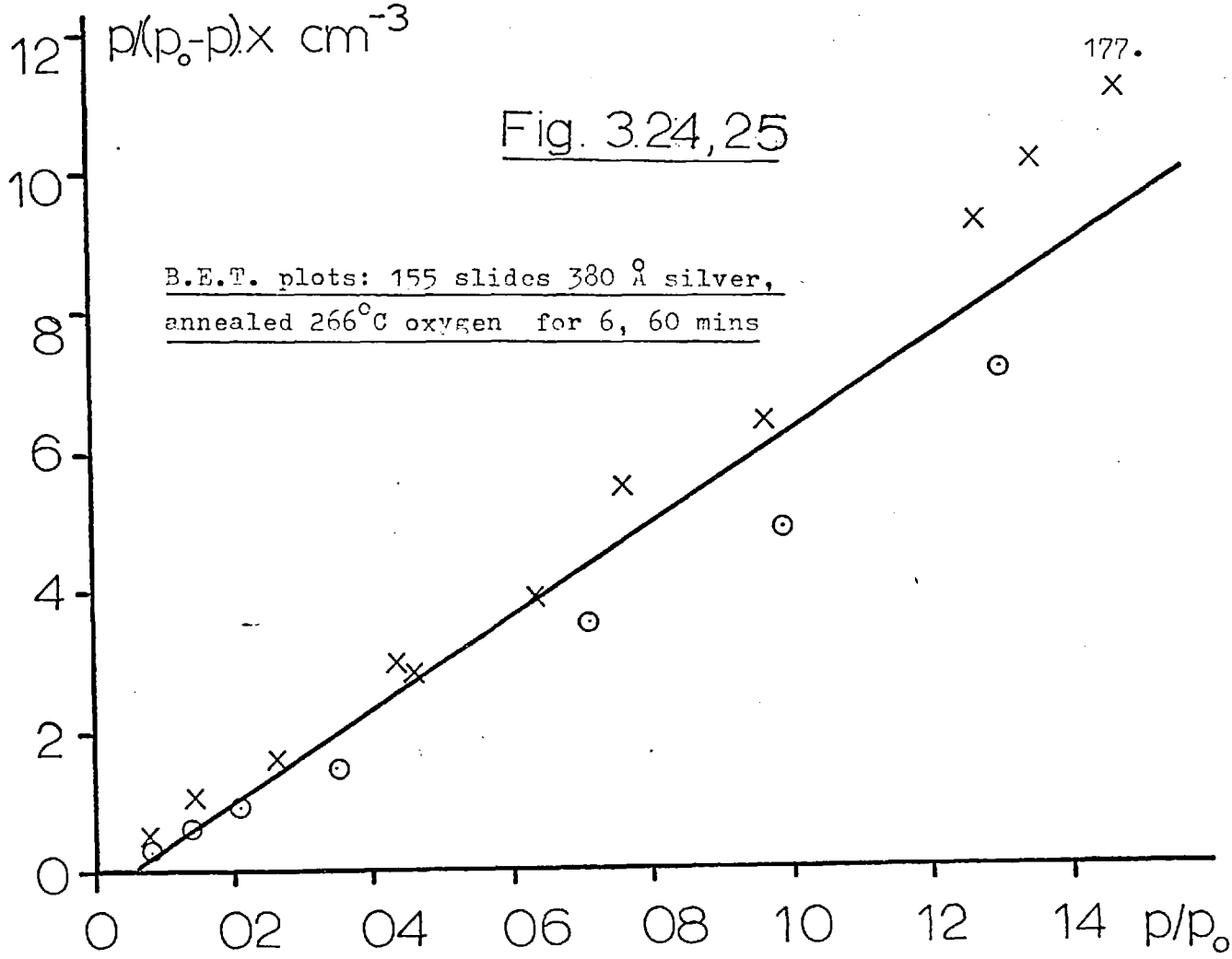
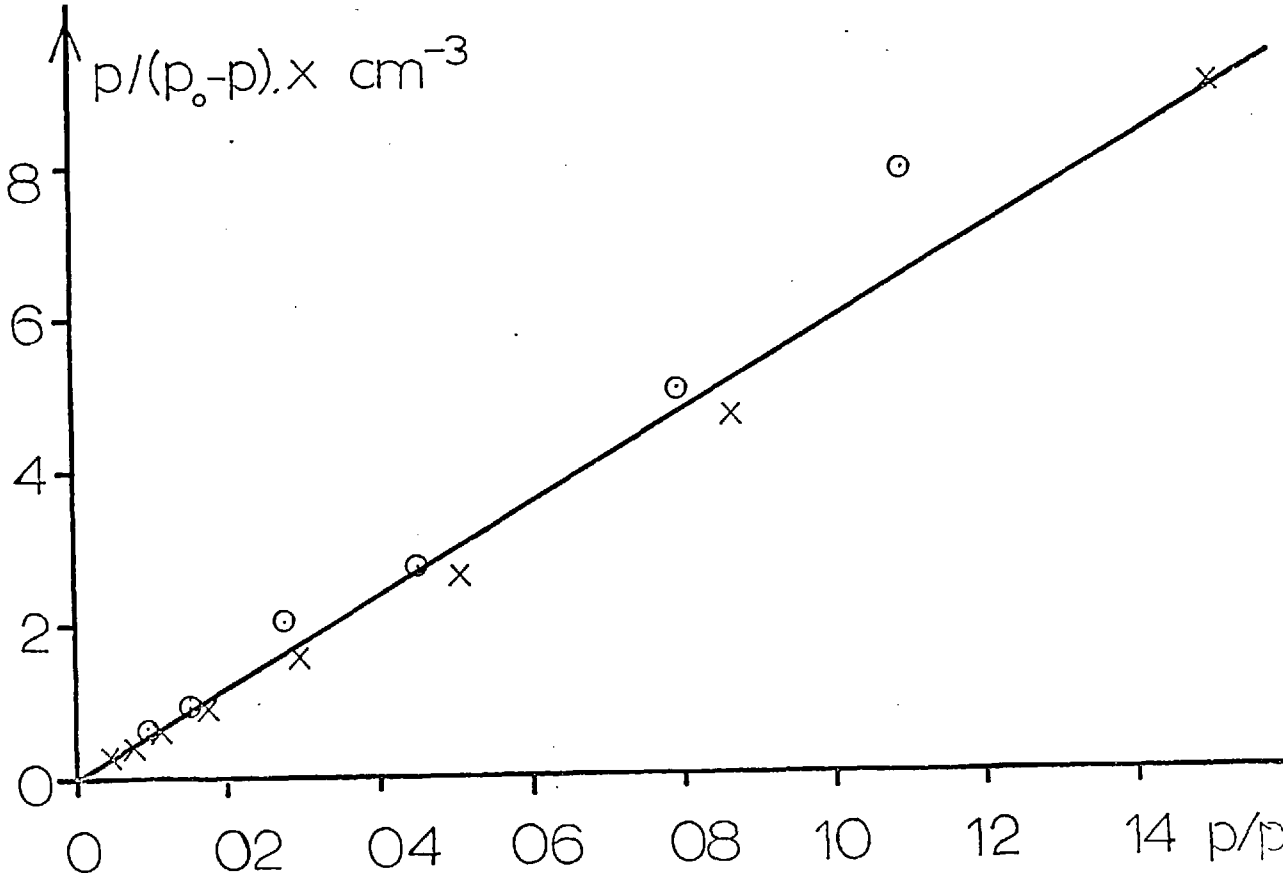


Fig. 3.24,25

B.E.T. plots: 155 slides 380 Å silver, annealed 266°C oxygen for 6, 60 mins





Calculation of the surface areas of the specimens followed from the krypton monolayer volume calculated from the B.E.T. equation. The area occupied by one krypton atom was taken as 19.5 $Å^2$ (section 1.2.2.3). The results are shown in Table 3.5, both uncorrected and after applying the calibration factor (section 2.5.2.3). The metal-substrate interfacial areas are also recorded for each specimen.

Table 3.5.

Adsorption surface area of freshly deposited and oxygen annealed films.

380 Å silver film on 155 pyrex 19 mm circles, geometric area 878 cm^2.

Annealing time 266°C, mins.	Area cm^2	Corrected area cm^2	% substrate covered by silver.
0	690	805	92
6	878	1020	88
60	940	1090	31
do, 125 circles	722	838	do
155 fresh pyrex circles	580	640	-
113 fresh gauze shadowed circles	666	776	-

3.4. Changes in Catalytic Activity of Films in Relation to Microstructural Changes.

3.4.1. Ethylene oxidation.

3.4.1.1. Continuous film catalyst.

The catalytic activity for ethylene oxidation was in all cases measured from the exit concentration of ethylene oxide, using a 2:1 (oxygen:ethylene) flow at 228°C. The total flow rate was 45 ml/min., giving a residence time in the 8.9 ml reactor of ca. 5 secs assuming complete mixing. The homogeneous reaction under these conditions was found to be negligible.

The activity of the continuous films was measured, and found to be substantially constant over a five hour period. The catalyst film after use was found to have agglomerated slightly on the upper surface, but no island formation had occurred (as expected for this temperature and film thickness). A fresh continuous film was then annealed for several hours in oxygen at 410°C to produce an island structure, and then used as a catalyst: the activity was again measured, and found to be constant. The reactivity for both catalysts is shown in fig. 3.27. By t.e.m. the final metal-support area was found to be ca. 31% of the original.

3.4.1.2. "Shadowed" catalysts.

Catalyst films were prepared with the substrate supported on a copper gauze (2.2.2), originally as a convenient way of supporting the circular slides above the evaporant. Only in the course of investigating the reasons for the rapid loss of activity in these films was the particular method of their production considered as a contributory factor, and non-shadowed films used (3.4.1.1).

Catalyst films prepared in this way were found to have a very much higher initial activity than continuous films, and the activity was found to fall off markedly with time. The product concentrations of CO_2, H_2O and C_2H_4O were followed by repeated sampling; fig. 3.26 shows the variation of product concentration with time, and fig. 3.27 shows the variation of activity from total product concentrations, compared with the activity of continuous film and island structures (3.5.1.1).

The activity of this catalyst was found to be little affected by cooling in oxygen, or by reduction in hydrogen: figs. 3.28 and 3.29. The initial activity was found to be unaffected by previous annealing in ethylene: fig. 3.30 and fig. 3.31 show the activity patterns after ca. 50 mins pre-annealing at 228°C. The initial activity was also unaffected by pre-annealing in hydrogen: the activity patterns shown in figs. 3.28 and 3.29 were obtained

Activity pattern for ethylene oxidation

Fig 3.26

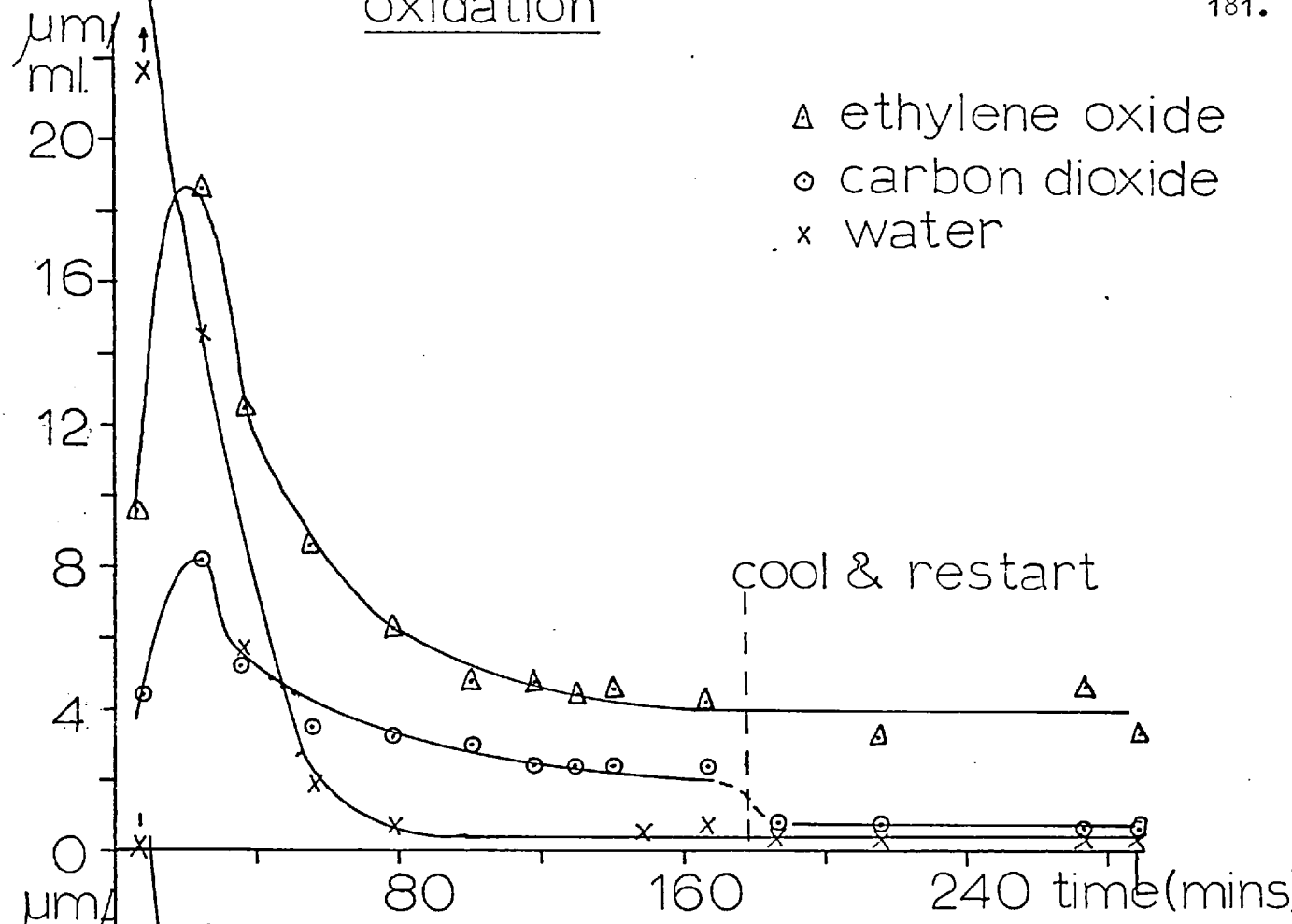


Fig 3.27

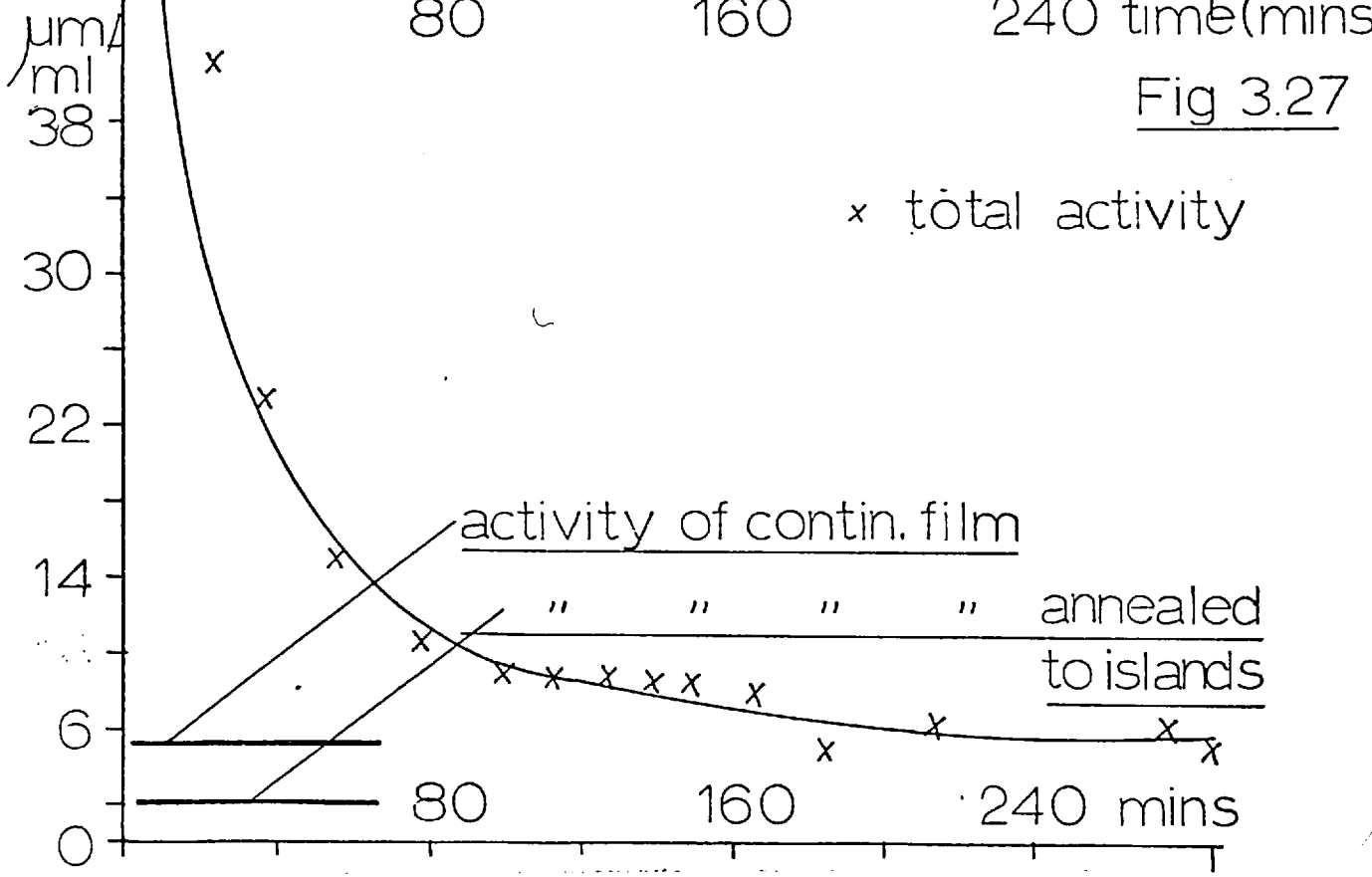


Fig 3.28

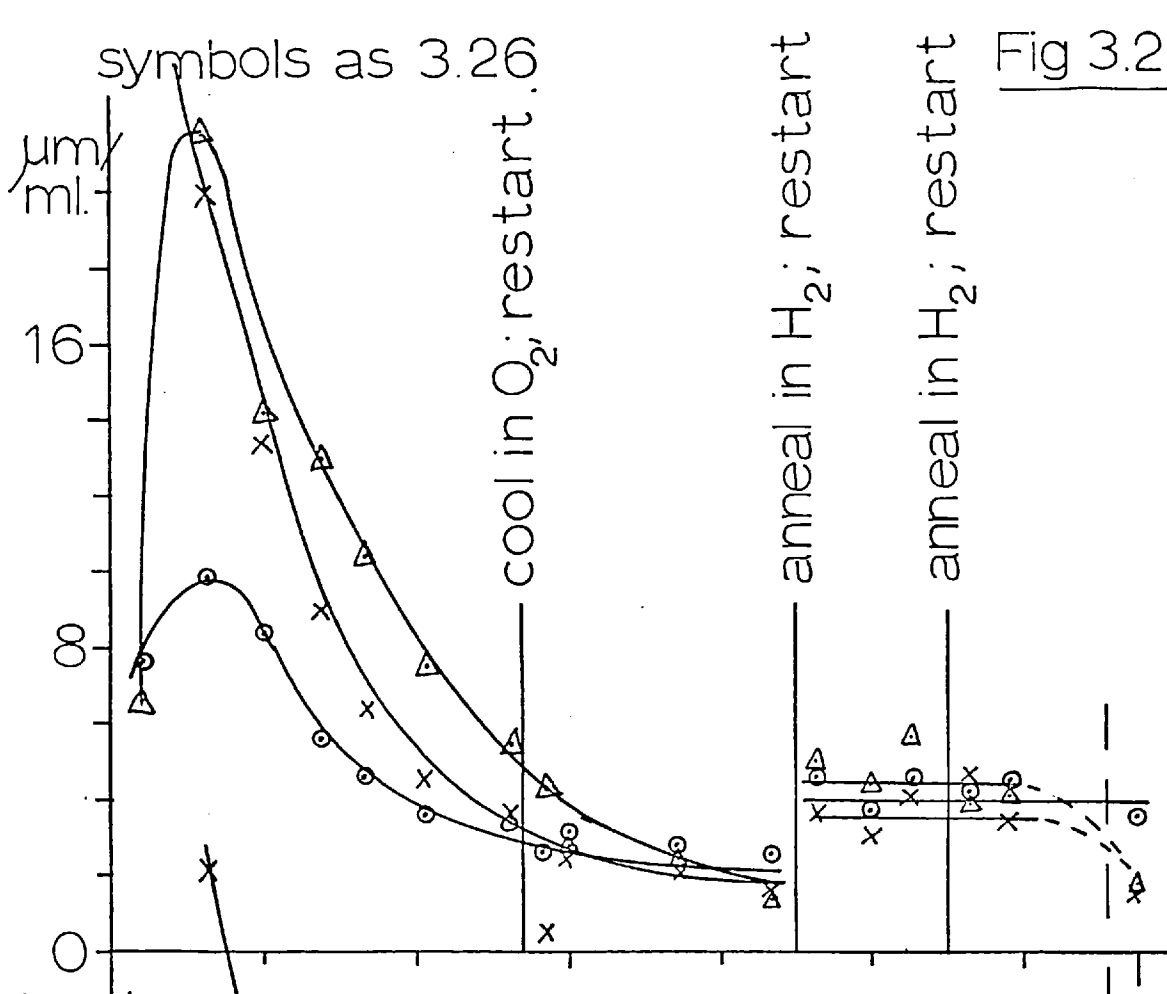


Fig 3.29

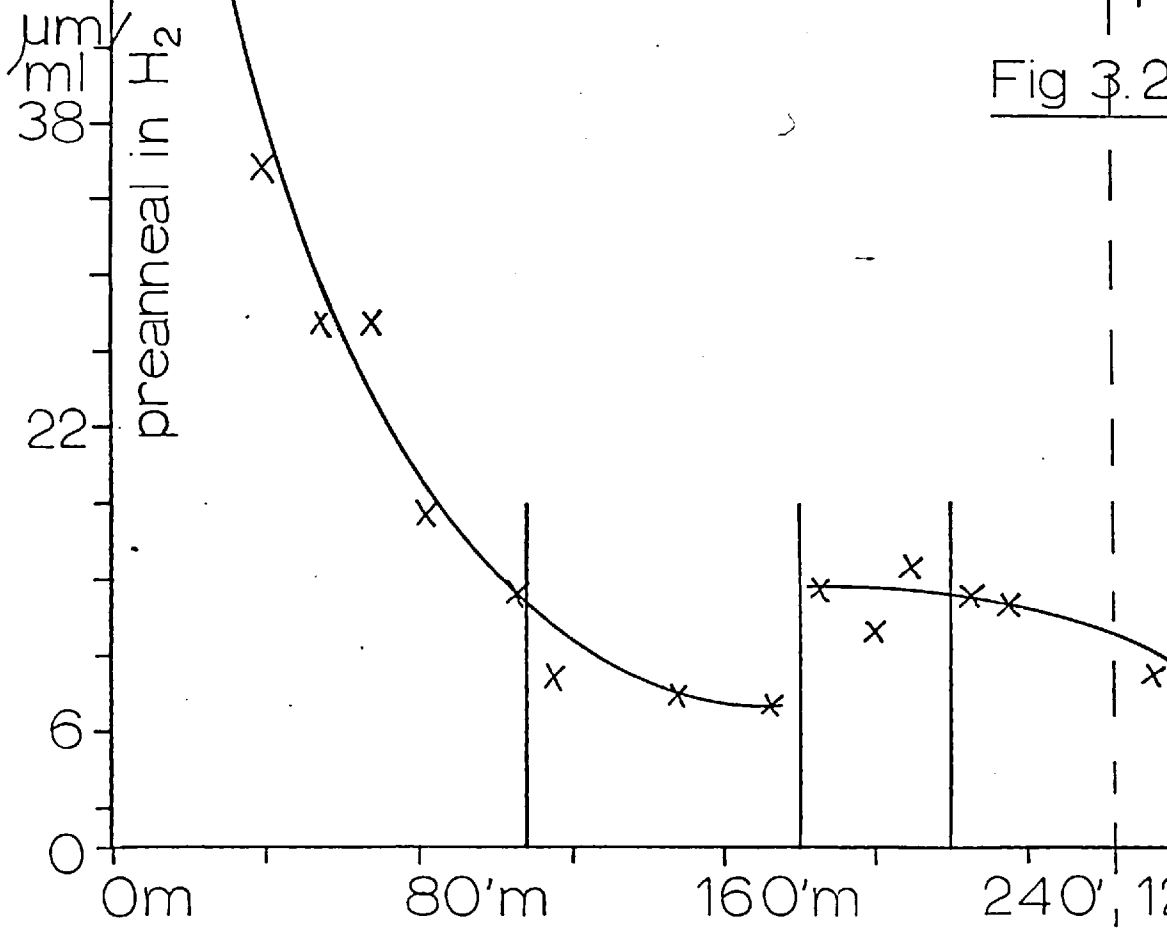


Fig 3.30

symbols as 3.26

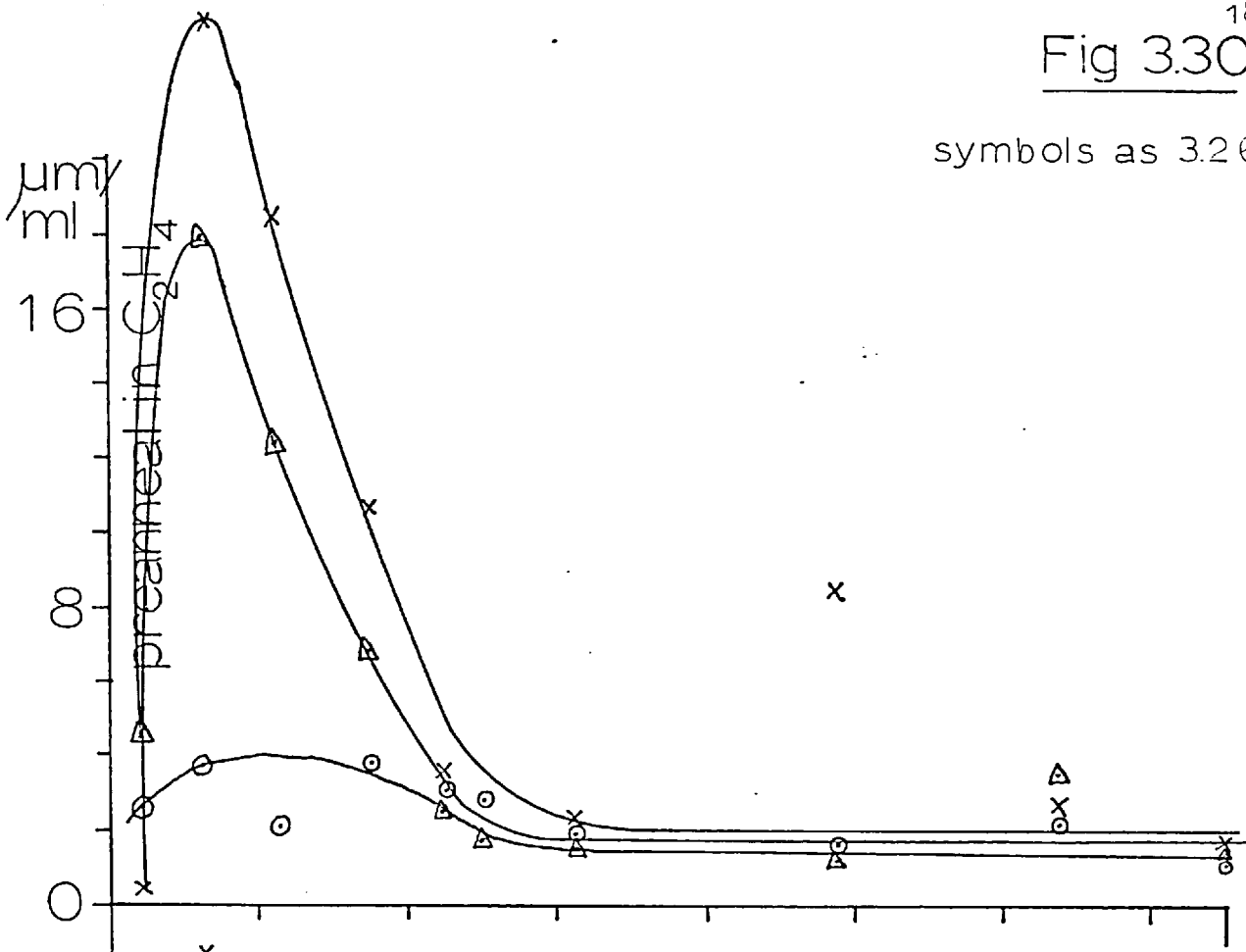
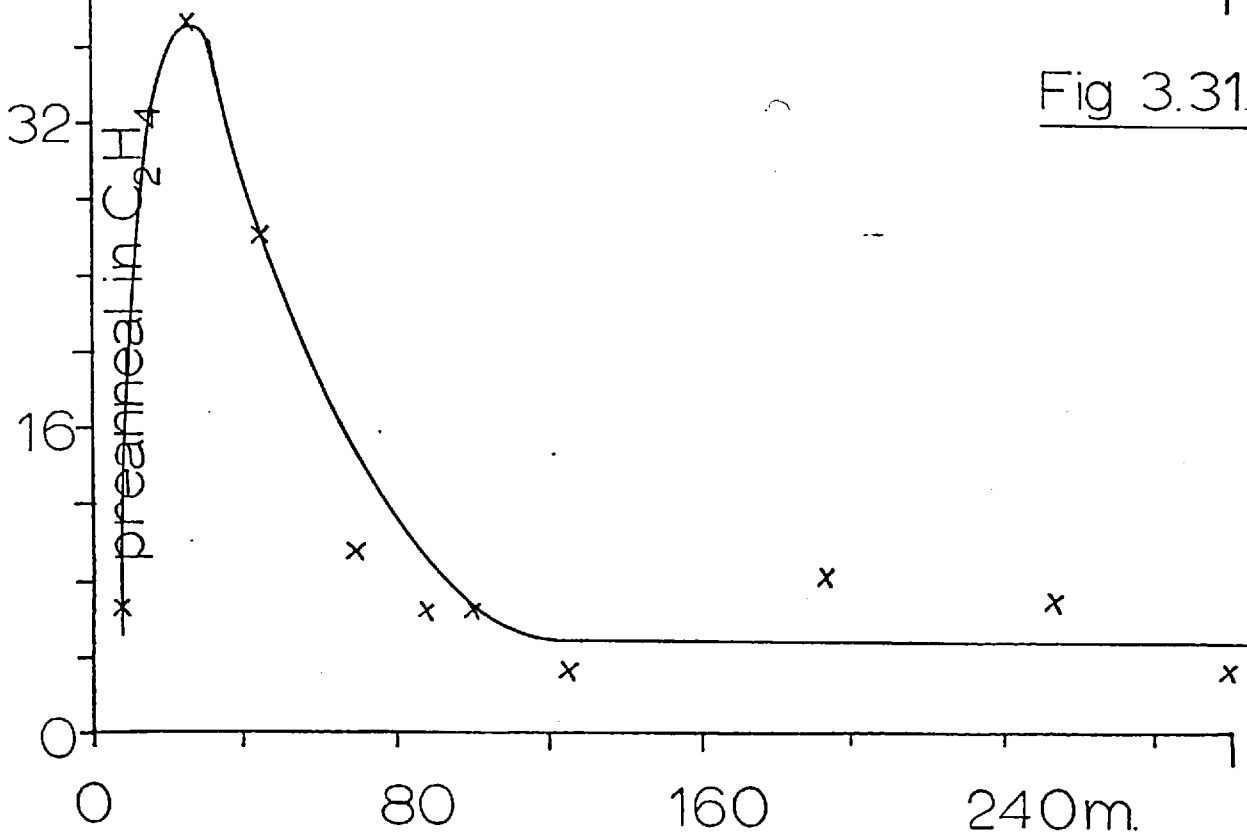


Fig 3.31



after 1 hour annealing in hydrogen at 228°C. followed by cooling in hydrogen.

The activity changes were found to correspond closely to those produced by pre-annealing the catalyst in oxygen alone at 228°C. Table 3.6 shows the initial activities obtained after four different annealing times.

Table 3.6.

Effect of oxygen pre-annealing (228°C) on "shadowed" catalyst activity.

Annealing time mins.	Total activity
35	32.2
60	11.8
120	10.5
180	7.0

Electron micrographs taken of the fresh catalyst and the catalyst after various reaction times showed:

i) Between the squares of continuous film, appreciable amounts of silver had migrated into the "shadow" channel. T.e.m. showed that particles of 2000 down to 100 Å diameter were present at the channel centre. S.e.m. showed the general distribution of material into the shadowed zone, decreasing in amount towards the channel centre, as illustrated in fig. 3.32.

ii) This structure was very little changed after annealing in hydrogen: fig. 3.23c).

"SHADOWED" CATALYST 332

as deposited

transition region

'channel'



x 27

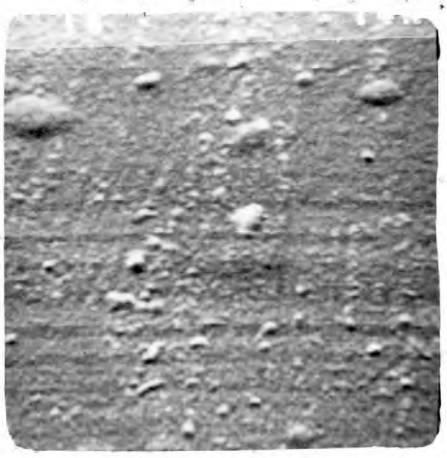


channel centre x11,000



transition region x11,000







iii) After about 30 min use in reaction, large changes had occurred in the island structure in the channels, although the continuous areas were very little changed. Island growth is illustrated in fig. 3.33 for comparison with the fresh film. S.e.m. observations suggested complete loss of islands below about 500 Å at the channel centre, and t.e.m. observations confirmed this, although here there were difficulties of locating the area viewed in relation to the overall "grid" structure.

iv) No further large changes were observed in specimens from longer reaction times.

3.4.2. Hydrogen oxidation.

3.4.2.1. Continuous film catalysts.

A hydrogen:oxygen mixture of 2:1 volume ratio was used at a total flow rate of 67.5 ml/minute, giving a residence time in the reactor of 7.5 secs, assuming complete mixing. A continuous film catalyst was used, prepared as before. The activity was measured both for a fresh silver film, and for an island structure. The results are shown in fig. 3.34. They are similar to those for ethylene oxidation, showing a constant activity for the fresh and annealed catalyst. Transmission micrographs of the annealed catalyst showed a final metal-substrate area of ca. 36%.

"SHADOWED" CATALYST 3.33

After 30 mins. reaction 228°C



'transition' region

×1200



'transition' region

×3050

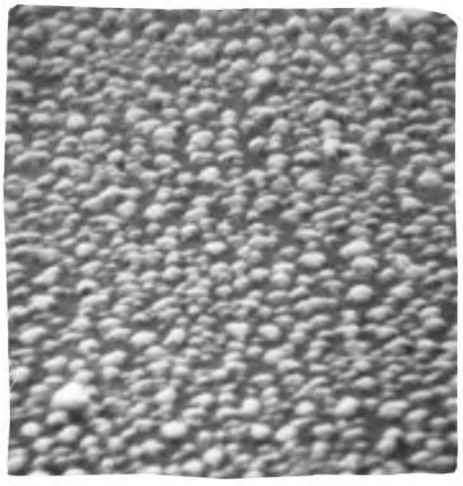


'channel' centre

×11,000



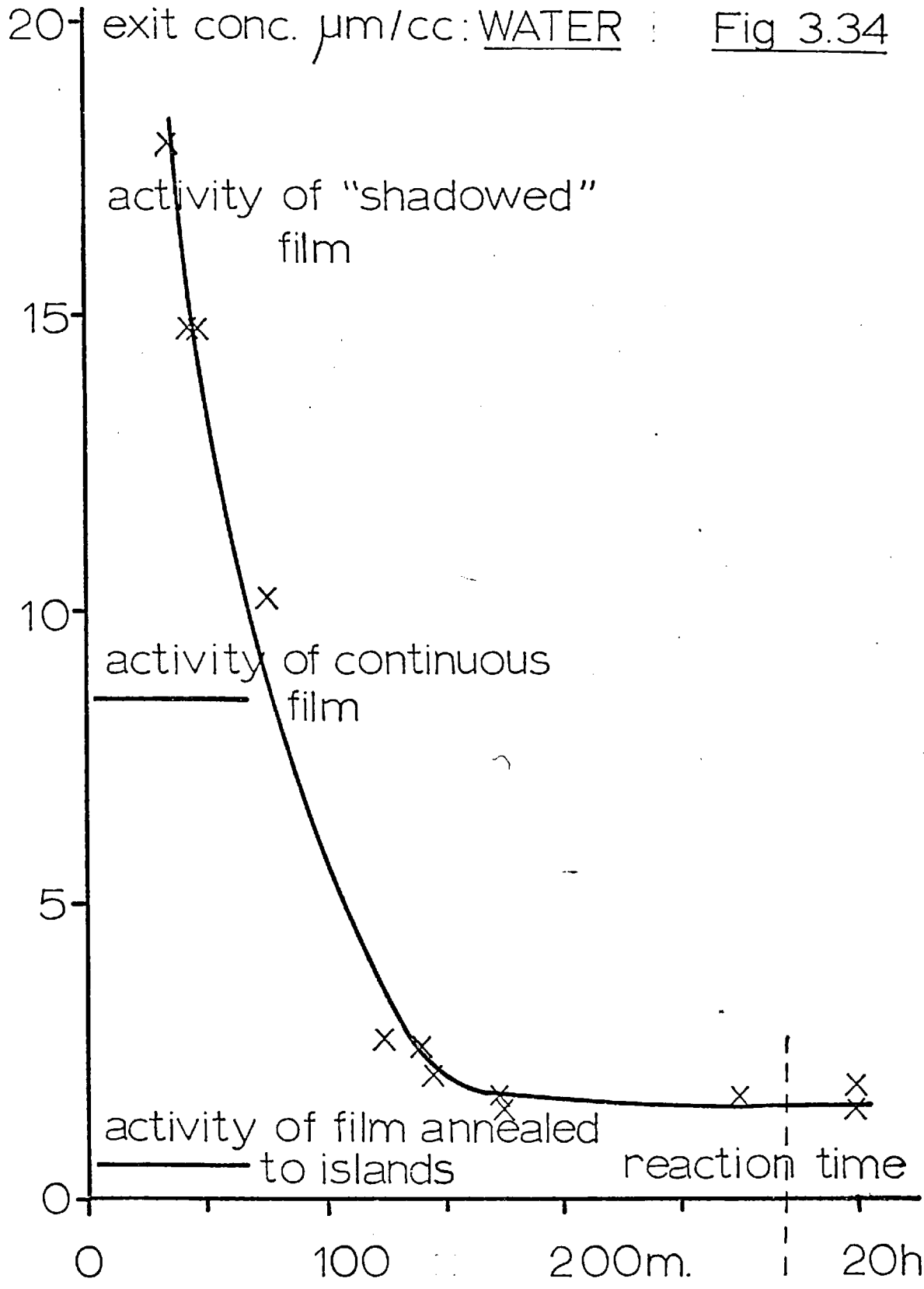




3.4.2.2. "Grid-shadowed" catalysts.

The activity of a full catalyst charge of 62 'shadowed' circles was found to saturate the hydrogen-oxygen stream with water vapour. After checking that the activity of plain pyrex circles was negligible, the catalyst was used with each circle separated from the next by 4 plain pyrex circles, thus reducing the product concentration and removing the need to heat the exit lines to maintain the water produced as vapour.

The activity-time pattern was found to be very similar to that for ethylene oxidation, the water produced fell off rapidly to a low final value after ca. 60 mins. (fig. 3.34). S.e.m. examination of the used catalyst showed that the smallest islands were lost in the same way as was observed in ethylene.


20
exit conc. μm/cc: WATER
Fig 3.34
activity of "shadowed" film
15
10
activity of continuous film
5
activity of film annealed to islands
reaction time
0
0
100
200m.
20h.

CHAPTER 4.

DISCUSSION.

4.1. General. 193

4.2. Microstructural changes on annealing continuous catalyst films.

4.2.1. Outline. 194

4.2.2. Relationship of island structure to original film. 195

4.2.2.1. Origin and size of catchment area. 195

4.2.2.2. Catchment area in relation to film growth. 197

4.2.2.3. Critical hole size. 201

4.2.3. Rate controlling process in island formation. 204

4.2.4. Driving force and diffusivity in island formation. 206

4.2.4.1. Surface energy and reactive atmosphere effects. 206

4.2.4.2. Film stress effects. 210

4.2.5. Kinetics of agglomeration. 214

4.2.5.1. Induction period. 214

4.2.5.2. Hole growth period and island equilibration. 218

4.2.6. Surface diffusion processes in oxygen atmospheres. 225

4.2.6.1. Effect of oxygen pressure. 225

4.2.6.2. Mechanism. 226

4.2.7. Structure of final islands. 228

4.2.7.1. Crystallinity. 228

4.2.7.2. Shape. 231

4.3. Microstructural changes on annealing "shadowed" films.

4.3.1. Original structure. 231

4.3.2. Island growth process. 232

4.4. Surface area of catalyst films.

4.4.1. Adsorption isotherms. 233

4.4.2. Area of fresh film. 233

4.4.3. Area variation in island formation. 234

4.5. Catalytic activity of silver films.

4.5.1. Continuous films. 235

4.5.1.1. Freshly deposited films. 235

4.5.1.2. Freshly annealed films. 236

4.5.2. "Shadowed" films. 237

4.6. Conclusions. 239

4.1. General.

The technique developed in this work for quantitative observations of the agglomeration of continuous silver films, has made it possible to record a range of kinetic and geometrical information. The aim of the first part of this discussion (section 4.2) is to evolve a model of island formation from these observations, in terms of fundamental energetics and mass transfer processes, and so to fulfil the main intention of this work of investigating the physical processes underlying the reorganization of supported catalysts. The intrinsic interest of the model for the understanding of thin film surface structure and of surface diffusion is also explored. The significance of the particle growth effects observed in 'shadowed' films is also discussed (section 4.3).

Microstructural observations are then related to factors relevant to catalysis, in a discussion of surface area changes measured by adsorption (section 4.4). Finally, the relation of catalytic activity changes to microstructure is investigated (section 4.5).

4.2. Microstructural changes on annealing continuous catalyst films.

4.2.1. Outline.

The geometrical relationship of the island structure (formed after annealing films in oxygen at atmospheric pressure) to the original film, is first considered alone (section 4.2.2). The kinetics of the induction period in particular are then discussed (section 4.2.3), and a probable mass transfer mechanism is inferred. Attention is given in the next section (section 4.2.4) to possible driving forces for the early stages of agglomeration and here the marked effects of reducing and oxidizing atmospheres are considered. In section 4.2.5, the kinetics of the various stages are considered; a quantitative model of surface tension driven surface diffusion transport in the hole growth period is compared with results. In section 4.2.6, the implications of the effects of oxygen on surface diffusion, for the atomic mechanism of transport under these conditions, are briefly discussed. The result of the discussion is an account of most features of agglomeration in terms of fundamental energetics and mass transfer processes. Finally, in section 4.2.7, results on the final equilibrium state of the islands are discussed.

4.2.2. Relationship of island structure to original film.

4.2.2.1. Origin and size of catchment area.

On comparing observed island densities I with features of the structure of the original film, it is immediately seen that the final island density (0.1 - 1.0/micron^2) is far smaller than the initial grain density of the film (ca. 100 $\mathring{A}^2 \equiv 10^4$/micron^2). The grain boundary structure of the film cannot therefore be assigned a governing role in delimiting island catchment areas.

The order of magnitude agreement between I and the densities of residual holes n in the original film (fig. 4.1), suggests a comparison between n and I for the same film. Additional points were obtained by an obvious graphical construction from figs. 3.1 and 3.16, and the relationship between n and I is shown in fig. 4.1. A linear relation is seen to hold for all but the thinnest films, as follows:

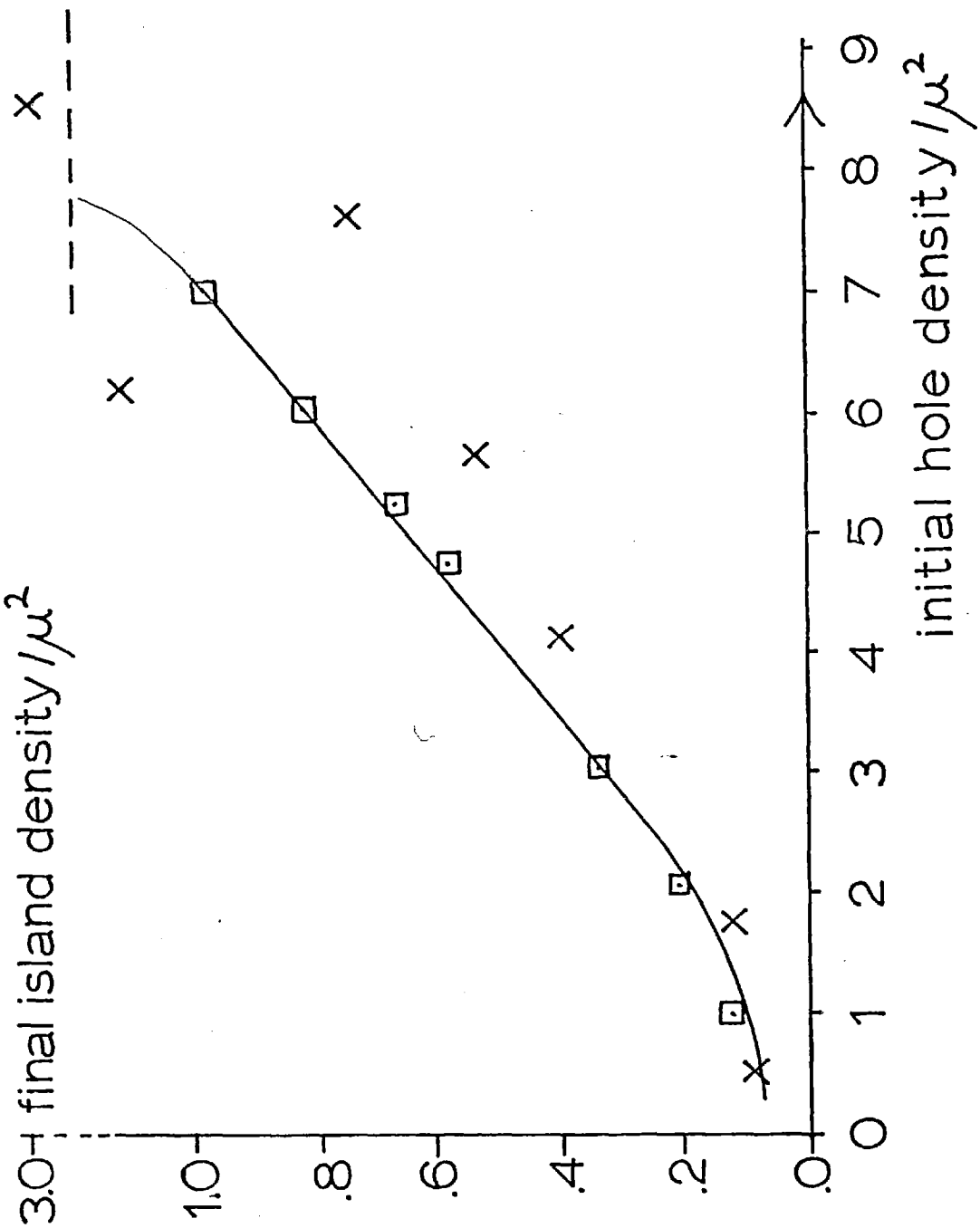
$$I = cn - f \qquad (4.1)$$

where c = 0.17 islands/initial hole, f = 0.1 islands/microns^2. This suggests that the network of residual holes present in the initial film after nucleation and growth has a governing effect on the density of islands formed on agglomeration. Thus the area of film from which a final island draws its material, the catchment area A_c, depends inversely on n.

The catchment areas form a network of adjacent

Dependence of final island density I (μ^{-2}) on initial hole density n' (μ^{-2}): 266°C, oxygen 760 torr

Fig. 4.1



polygons with varying numbers of sides. With little error, their dimensions can conveniently be represented as the radii of tangent circles. If we define a mean catchment radius r_c, then

$$r_c = \sqrt{\frac{A_c}{\pi}} \qquad (4.2)$$

From (4.2) and (3.5), the observed relation between A_c and the thickness of the film l,

$$A_c = 4.57 \times 10^{-6}\, l^2 \qquad (3.5)$$

we expect r_c to be proportional to l. On replotting the data, we find a closely linear relation (fig. 4.2) expressed by

$$r_c = d\, l \qquad (4.3)$$

where d = 12.8. This relation shows that there is a constant 'aspect ratio' (i.e. thickness:radius) of 1:12.8 for all but the thinnest films.

4.2.2.2. Catchment area in relation to film growth.

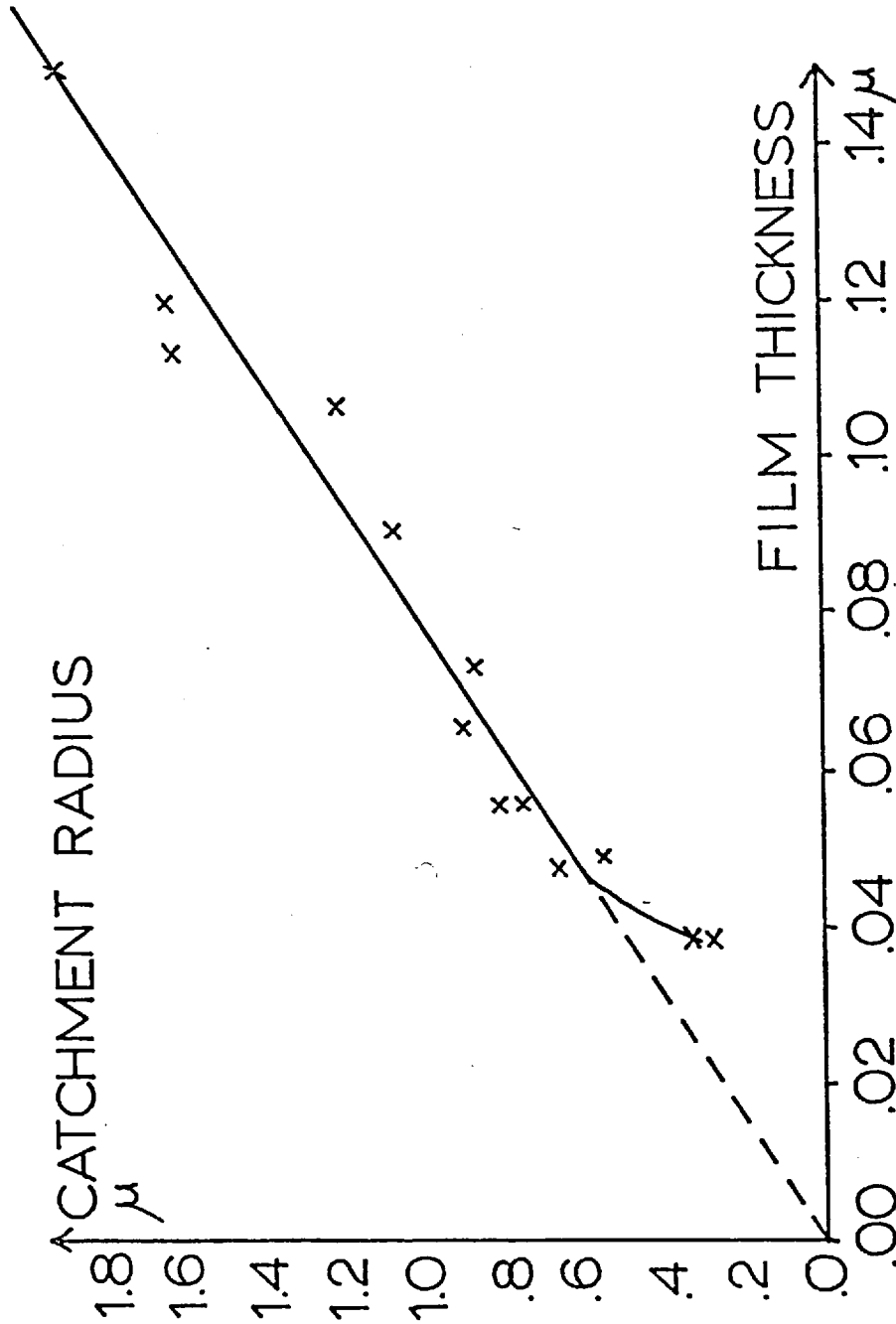
The relation found between island formation and the initial network of holes may now be explored in relation to film growth and structure.

If we neglect the small intercept value f in (4.1), then another way of expressing the proportionality between I and n is to say that I and n vary in the same way with film thickness. From equation (3.5), we deduce that I varies with l according to

$$I = 2.2 \times 10^{5}\, l^{-2} \qquad (4.4)$$

Relation between catchment radius R_c (μ) and film thickness l (μ)

Fig 4.2



n is therefore expected to vary similarly with l^{-2}. The data is plotted according to this relation in fig.4.3. The relation is confirmed by the linear plot obtained for points from all but the thinnest films, expressed by the relation,

$$n = 1.5 \times 10^6 \, l^{-2} \qquad (4.5)$$

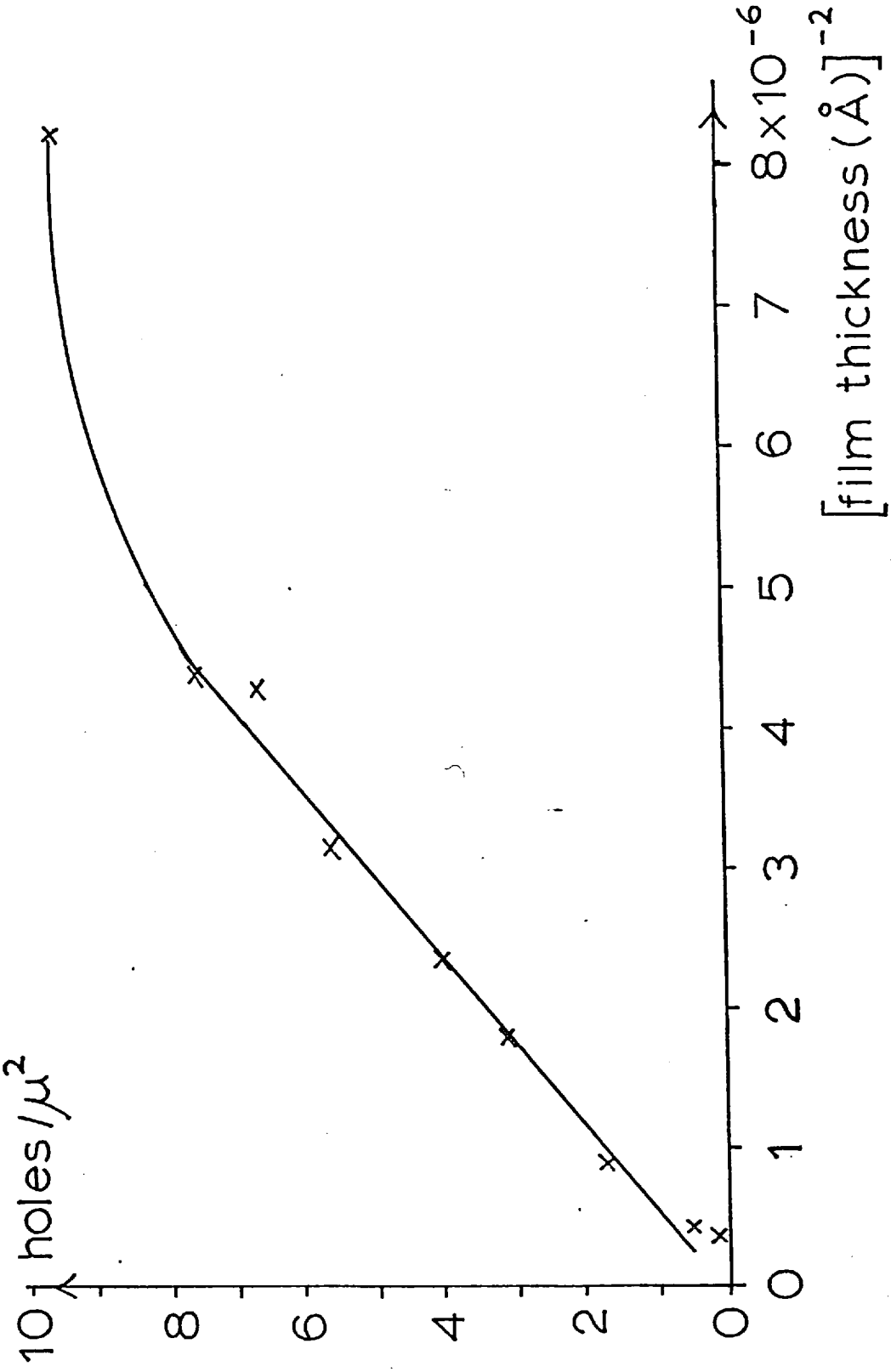
Comparison of equations (4.5) and (4.4) gives equation (4.1) within the limits of the approximation made.

Equation (4.5) gives a relation between the thickness of a growing film, and the density of residual holes, thus expressing quantitatively what has long been recognized for film growth, i.e. the gradual filling in of holes with increasing thickness. Despite the extent of work on thin film growth, it appears that no studies exist of hole size distributions at different film thicknesses. If these distributions were known, they could be used in conjunction with the observed variation of n with l, to give information on the rate of filling of holes of different sizes, and this would shed light on surface transport in thin film growth processes.

An overall picture of catchment area in relation to film structure can now be presented. In fig. 4.4a, film nucleation, growth and formation of initial holes between touching nuclei, are presented diagrammatically, as if all nucleation took place on points of a square

Relation between initial hole density n' (μ^{-2}) and (film thickness l Å)$^{-2}$

Fig 4.3



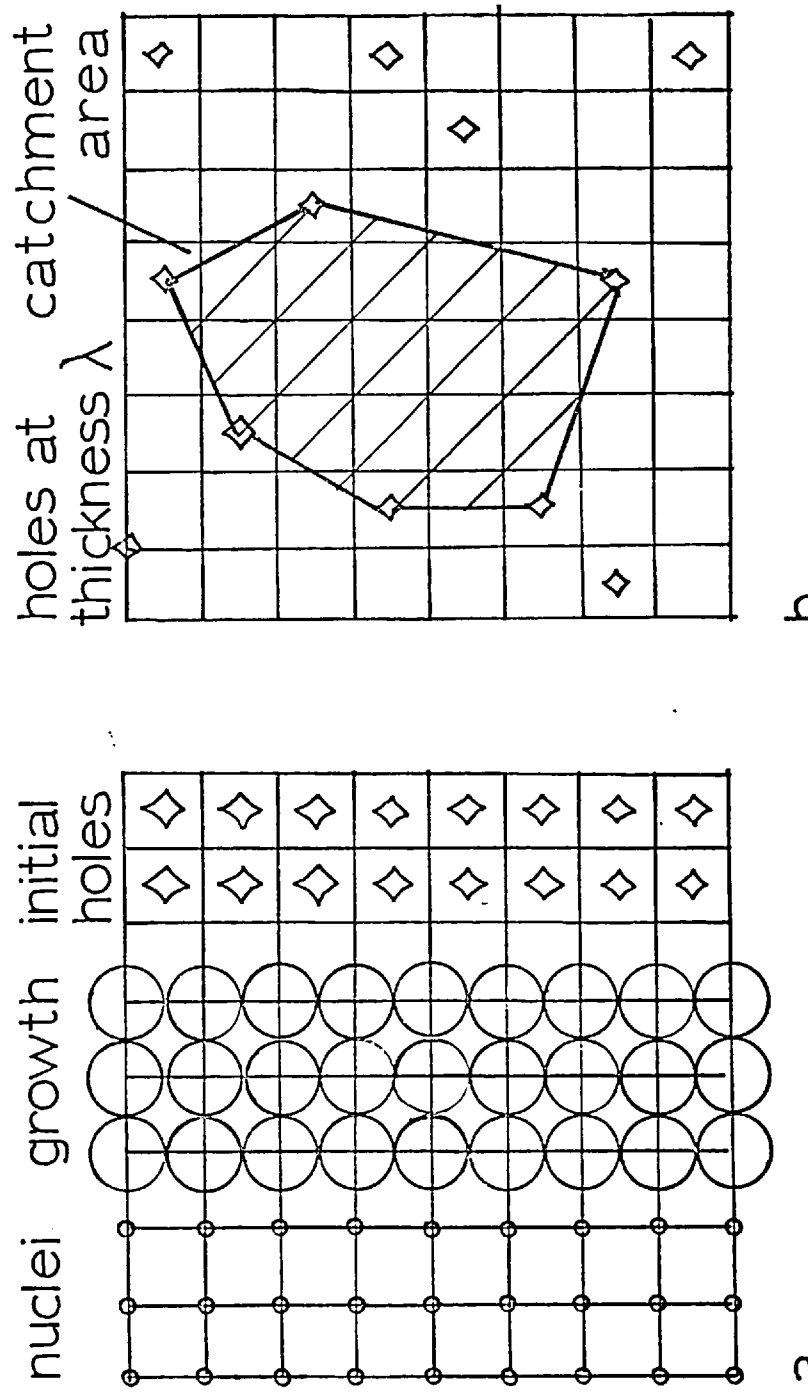
lattice. In fig. 4.4b, the random array of residual holes at a greater film thickness l is shown, and the delineation of catchment area by a network joined between holes, is indicated. The present results show that during annealing, the holes effectively join up, cutting off those areas of deposit which form the final islands.

The lines joining the holes cover the deposit in an irregular network. In the case both of a regular and of an irregular lattice, the number of catchment areas so defined approaches the number of holes n as n approaches infinity. We therefore deduce that from the original hole lattice, only one hole becomes the origin of each catchment area. It was observed experimentally, however, that $1/c$ = ca. 6 holes were associated with each island formed (in oxygen at atmospheric pressure). Of these, one must be the actual origin point for the catchment area of the island, and five others must be ineffective under these conditions.

4.2.2.3. Critical hole size.

We now consider the factors limiting (to ca. 1/6) the effectiveness of the residual holes in the catchment area network. It was observed that decreasing oxygen pressure gave rise to an increased catchment area (section 3.2.5.4). During the variation of p_{O_2}, both the surface energy γ and the surface diffusivity D_s are known

Fig 4.4


holes at thickness λ
catchment area
b
nuclei growth
initial holes
a

to vary (sections 1.3.2 and 1.3.3); either or both of these factors may affect A_c.

In order to find the effect of changing D_s alone on A_c, we consider the comparison of A_c and temperature made in section 3.2.5.3. Over the temperature range used, D_s is expected to vary by a factor of ca. 15x, but A_c remained substantially constant. In addition, the observations made on the mean number of holes present during the induction period, gave the same result of independence of temperature (section 3.2.3.3). D_s has therefore no effect on catchment area.

This independence of D_s suggests that the variation of A_c with log p_{O_2} may be due to variation in γ. This was suggested initially by the fairly linear variation of A_c with γ that follows from the experimental relation (section 3.2.5.4)

$$A_c = 0.67 - 0.16 \log_{10} p_{O_2} \qquad (4.6)$$

If A_c depends on γ, this may be because at lower oxygen pressures, the number of holes that participate in delineating the catchment area decreases: i.e. c decreases. This could arise if there is a critical hole size at a given value of γ, below which size the hole will not grow. If the critical hole size increased as γ increased (log p_{O_2} decreases), then an increase in A_c would follow. (see further section 4.2.4.2), below.

4.2.3. Rate controlling process in island formation.

The apparent activation energy (14.9 kcal/mole) governing the length of the induction period, was measured in order to gain information on the processes governing the rate of microstructural changes. Several possibilities were considered for fundamental processes giving rise to this activation energy.

(i) diffusion of oxygen through the film. If withdrawal of metal from the substrate occurred when the metal-substrate energy γ_{M-S} was reduced through the arrival of diffused oxygen, then the activation energy of the induction period would be that for oxygen diffusion in silver, and the time related to that required for diffusion.

The diffusion coefficient for dissociated oxygen in silver is quoted by Eichenauer and Muller (1962) as

$$D = 2.72 \times 10^{-2} \exp(-11{,}000/RT) \text{ cm}^2/\text{sec}$$

so that at a median temperature of 550°K, $D \approx 10^{-8}$ cm^2/sec. Standard treatments of non-steady state diffusion into an infinite slab of thickness 2L (e.g. Darken and Gurry, 1953, p.446) show that the time t required for one side of a slab to reach by diffusion the same concentration of the diffusing species as the other, exposed side, is of the order of L^2/D. In this case, $2L \approx 10^{-5}$ cm, and hence $t \approx 2.10^{-3}$ secs. In other words, oxygen diffusion through a 1000 Å film is extremely rapid, and is completed far

faster than the processes governing the induction period.

(ii) volume self-diffusion. The self diffusion coefficient D_v for volume diffusion in silver is given by

$$D_v = 0.40 \exp [-44,090/RT] \text{ cm}^2/\text{sec}$$

(Tomizuka and Sonder, 1956). The activation energy is so high that volume diffusion cannot be considered as the mass transfer process operating in the induction period.

(iii) surface self-diffusion. At the temperatures used in this work, ($<= 0.44\ T_m$) the surface self diffusion coefficient D_s for clean (hydrogen or good vacuum) silver surfaces is given by

$$D_s = 1.4 \times 10^{-2} \exp [-13\ T_m/RT]$$

(section 1.3.3.1). $T_m = 1234^{\circ}K$, so

$$D_s = 1.4 \times 10^{-2} \exp [-16,040/RT]$$

In section 1.3.3.2, work was reviewed in which low temperature mass transfer on silver, in oxygen containing atmospheres, was observed, and in which the kinetics of shape changes agreed with extensions of Mullin's analysis for surface mass transport. In this work, values of Q_s obtained in the presence of oxygen were consistent (within experimental limits) with the value of ca. 16 kcals/mole reported for both clean and oxygen covered surfaces (section 1.3.3). The activation energy for the induction period can therefore provisionally be interpreted as arising from surface diffusion control of the microstructural

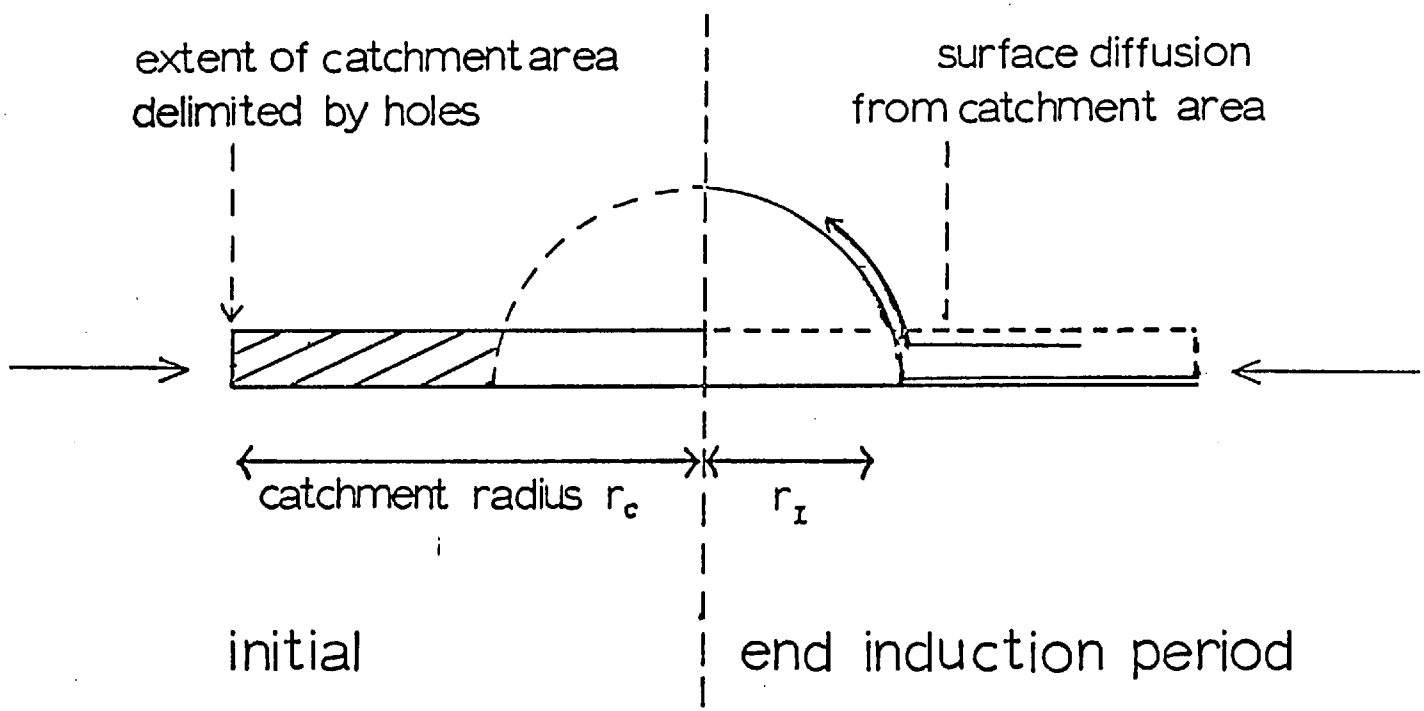
changes.

In later sections (4.2.4), the hypothesis of surface self-diffusion transport is used to develop a kinetic model of the induction and hole growth periods, and further comparison then becomes possible between observed and predicted surface diffusion behaviour. A diagram of surface diffusion transport during the induction period is shown in fig. 4.5, illustrating the progressive thinning of 'lands'.

4.2.4. Driving force and diffusivity in island formation.

4.2.4.1. Surface energy and reactive atmosphere effects.

Solid thin films at temperatures too low to allow diffusion causing shape changes, are necessarily metastable with regard to surface energy since they have such a high specific area. One purpose of the measurements made of the adsorption surface area of newly deposited films (section 3.4.2) was to determine their specific area. If it had proved that considerable internal surface existed due to the presence of micropores, then an account of the energetics of shape changes in the film would have had to take account of surface energy changes as this internal surface collapsed during agglomeration. The observation that the films are non-porous (see further section 4.5) removed this possibility, and showed that loss of internal



Hillock growth from single catchment area

Fig 4.5

surface effects do not contribute to the driving force for agglomeration.

The overall island formation process clearly results in a reduction of the total interfacial energy of the film. Assuming complete contact in the initial film between metal and substrate, then the metal-substrate area decreases to about 0.35 of its original value for island formation from a 1000 Å film, and there is a comparable decrease in metal-gas area. Considered overall, we can certainly say that nett surface energy loss by the metal deposit is a driving force for island formation. The application of this to different observed stages of agglomeration, will now be considered.

The observed hole growth and island withdrawal phenomena can be understood quite satisfactorily in surface energy-driving force terms. The profile of the withdrawing "lands", and of the recently separated islands, (figs. 3.9, 3.14) differs considerably from the final equilibrium shape, which is approximately hemispherical. Mass transport towards this shape results in a continuous reduction in total surface energy for the particle. Changes in the surface energy of the substrate can be ignored to a first approximation, since $\gamma_{SP} \simeq \gamma_{SV} \simeq 1000$ ergs/cm^2 (Winterbottom, 1967; Pilliar and Nutting, 1967). The metal particle can therefore be considered as a separate system,

for which the shape changes give a net free energy reduction.

At the microscopic level, the energetics can be considered in terms of minimizing the surface curvature of the particle; diffusion away from highly curved surfaces occurs due to the increased chemical potential of surface atoms at these points (see further section 4.2.4.2).

However, surface energy arguments alone do not give a satisfactory treatment of the early stages of agglomeration, nor of the overall effects of oxygen versus hydrogen atmospheres. During the induction period, hillocks are observed to grow on the film surface only when annealed in oxygen-containing atmospheres (fig. 3.4), resulting in a progressive thinning of the surrounding areas. For constant γ_{PV}, this process increases $\{\gamma_{PV}.A_{PV}\}$ It may be argued that, since hillock formation is a necessary preliminary in island formation, the concurrent surface area increase by hillock growth is stablized by the reduction in oxygen atmospheres, of γ_{PV}. This by itself is at best a 'permissive' argument, and does not show why hillock formation should occur in the first place.

A similar argument is that hillock formation occurs in oxygen atmospheres alone, because the energy reduction at the metal-gas interface γ_{PV} in some way causes a surface energy imbalance between the upper and lower interfaces of the film, which is relieved by hillock

formation. On this view, the dependence of induction time on oxygen pressure,

$$t_i = 11.3 - 3.8 \log_{p_{O_2}} \text{(torr)} \qquad (3.2)$$

arises from the log dependence of γ_{PV} on p_{O_2}

$$\gamma_{PV} = 228 - 188 \log_{10} p_{O_2} \text{ (atm.)} \qquad (1.3)$$

This tentative argument is unsatisfactory because, in view of the rapid diffusion of oxygen through the film, there seems to be no good reason why γ_{SP} should not be affected by oxygen in the same way as γ_{PV}, producing a balanced effect at the two metal interfaces.

Further, if surface energy reduction is the driving force during hillock formation, we would expect this to proceed <u>slowest</u> in the environment (oxygen) in which γ is least. Hillock formation occurring in the induction period does not therefore seem to be adequately explained by surface energy considerations.

4.2.4.2. <u>Film stress effects</u>.

So far, the interaction of metal and substrate has only been considered in terms of the surface energy of their interfaces. However, when the film is annealed, it cannot be considered in isolation from its substrate: in particular, thermal expansion of both film and substrate will occur, and will change the stress σ in the film. This effect will now be considered.

The change in stress $\Delta\sigma$, due to a temperature change ΔT can be calculated from the expression of d'Heurle (1966)

$$\Delta\sigma = (\alpha_{Ag} - \alpha_{SiO_2}) \cdot \Delta T \left(\frac{E}{1-\nu} \right) \qquad (4.7)$$

where α = thermal expansion coefficient:

$\alpha_{Ag} = 19.1 \times 10^{-6}/^{o}C$ (Smithells, 1967) (S)

$\alpha\, SiO_2 = 0.5 \times 10^{-6}/^{o}C$ (Chemical Rubber Co. Handbook)

E = Young's modulus of film

$E_{Ag} = 8.27 \times 10^{11}$ dynes/cm^2 (S)

ν = Poisson's ratio of film

$\nu_{Ag} = 0.367$ (S)

For a 300^{o}C temperature rise, $\Delta\sigma = + 12.5 \times 10^{9}$ dynes/cm^2 (compressive). The initial stress of silver films deposited on glass substrates at room temperature is tensile; values reported are ca. -0.3×10^{9} dynes/cm^2 (Klockholm and Berry, 1968; Campbell, 1966). The heating of the silver film, in any atmosphere, to ca. 325^{o}C, therefore changes the stress from -0.3×10^{9} (tensile) to $+12.2 \times 10^{9}$ dynes/cm^2 (compressive). This large compressive stress caused on heating is the most likely cause of the hillock growth observed on first annealing.

Growth of hillocks to relieve film stress has been observed before by Pennebaker (1968) (1.4.3.1). In

his experiments, growth of hillocks to a maximum size of ca. 3 microns did not cause denuding of the surrounding substrate, as the film was several thousand Ångstroms thick. The theory used to interpret the results saw stress relief as caused by recrystallization: the activation energy for the implicit grain boundary motion was taken to be that for grain boundary diffusion. (Values quoted for Q_{gb} are ca. 19-22 kcal/mole for silver (Smithells, 1967). Kinetic results from the present work are not in sufficiently close agreement with that activation energy for grain boundary motion to be considered as the rate controlling step for the induction period. (It is not clear how Pennebaker's treatment of grain boundary velocities can account for the transport of mass to the hillocks).

Hillock growth of the type observed will relieve stress in the film by transferring material above the plane of the film remaining bound to the substrate, whatever the mechanism. Compressive stresses therefore provide a plausible driving force for initial hillock growth.

A compressive driving force will operate, whatever atmosphere the film is annealed in, providing that film-substrate bonding is not affected. The very marked effect of oxygen on the rate of film break-up has still therefore to be accounted for in any complete theory. Acceleration of film break-up can of course take place by oxygen promotion

of surface diffusion. The increase in D_s between good vacuum and oxygen (760 torr) probably does not exceed 100 x, however (1.3.3.2). When silver films were annealed in hydrogen, times and temperatures were such that, if agglomeration depended solely on surface diffusion values, it would have been observed even if D_s were less by 1000 x in hydrogen; no large-scale hillock formation was in fact observed.

Oxygen atmospheres must therefore have a further effect in promoting hillock growth, and this is sought in the known effect on surface energy. If such an effect were important, the stability of gold films even in oxygen at high temperatures would be explained, since γ_{PV} for gold is known to be unaffected by oxygen (Hondros and Gladman, 1968). If we consider the initial development of hillocks as a nucleation step towards the development of an unstable surface configuration, the importance of surface energy in the context of the stability of the initial nuclei, and their rate of growth, is suggested. Analogies may be made with similar effects in solid and liquid particle nucleation from fluids. In the following section, such a treatment is carried out for the kinetics of the induction period; the hypotheses of compressive stress driving force, and of surface energy effects on hillock nucleation, are shown to lead to a result in quantitative agreement with the observed kinetics.

4.2.5. Kinetics of agglomeration.

4.2.5.1. Induction period.

The film thickness (l) dependence of t_i was originally investigated to check whether grooving of some of the grain boundaries to the surface was rate controlling - neglecting the effect of compressive stresses. Mullin's grooving theory shows that constant surface diffusion would cause the time required for a groove to penetrate to the substrate to vary as l^4. Although the scatter in the experimental dependence was large (fig. 3.7), the thickness dependence did not approach a l^4 relation, but could be expressed by

$$t_i = 3.8 \times 10^{-9} l^3 \text{ mins.} \qquad (3.1)$$

The kinetics of the induction period cannot therefore be ascribed to grain boundary grooving, and indeed no evidence for such grooving was seen in the s.e.m.

Following the arguments advanced in the previous section for the importance of compressive stress effects in hillock growth energetics, an analogy was then suggested between stress relief by hillock growth on the surface of a compressed material, and stress relief by grain boundary void growth inside a material in tension. A quantitative theory already exists for the growth of grain boundary voids (Hull and Rimmer, 1959), in which the time for failure of a specimen is calculated from the time for voids to grow to a

size equal to the mean spacing of their nuclei. In the following treatment, this theory is adapted to calculate the induction time, from the time required for hillocks to grow to a size which incorporates virtually all (excepting the thin lands) the material in the catchment area (compare fig. 4.5).

We assume that atoms reaching the hillock over the surface do so within a ring around each hillock which lies in the surface layer effective for surface diffusion of thickness δ .

The rate of hillock growth is determined by the chemical potential gradient $\nabla\mu$ in the surface, since the diffusion flux j is given by (Herring, 1950)

$$j = \frac{D_s \nabla\mu}{kT\ \Omega} \qquad (4.8)$$

where Ω is the atomic volume.

In the surface, well away from the hillock, we have the potential (Herring, 1950)

$$\mu_s = + \sigma_n \Omega \qquad (4.9)$$

where σ_n is the normal tension acting across the surface. On the surface of a hillock,

$$\mu_h = + \frac{2\ \gamma\ \Omega}{r} \qquad (4.10)$$

where γ is γ_{PV} and r is the hillock radius.

Hence as a rough approximation we may take

$$\nabla\mu = \frac{\Omega}{2r_c} \{\sigma - \frac{2\ \gamma}{r}\} \qquad (4.11)$$

since $2 r_c$ is the inter-hillock spacing

giving

$$j \approx \frac{D_s}{kT\, r_c} \{ \sigma - \frac{2\gamma}{r} \} \qquad (4.12)$$

This shows that the possibility of hillock growth is governed by the balance between σ and $\frac{2\gamma}{r_o}$, where r_o is the size of initial surface irregularities acting as nucleating sites. For hillock growth to occur, the condition is

$$\gamma < \frac{\sigma r_o}{2} \qquad (4.13)$$

In void growth, the applied tensile stress must be sufficient to overcome the increase in surface energy caused by creating a void. Similarly, in hillock growth, the applied stress is only sufficient to create a hillock, if the surface energy is low enough, to be outbalanced by the stress. The effect of oxygen in allowing hillock growth is immediately explained by its effect in reducing γ.

The area of hillock "surface" into which diffusion takes place is $2\pi r \delta$, so that the rate of increase of hillock volume is given by

$$\frac{dV}{dt} = \frac{(D_s \delta).\ \sigma\ .\ 2\pi r \Omega}{kT\, r_c} \qquad (4.14)$$

(if we assume that when the nuclei grow, the largest ones determine the induction time, i.e. $\frac{r\sigma}{2} >> \gamma$).

If the hillock maintains hemispherical shape by

surface diffusion (as observed), we have

$$\frac{dr}{dt} = \frac{D_s \delta \sigma \Omega}{kTr_c.r} \qquad (4.15)$$

To obtain the induction time t_i, this expression is integrated between $r = 0$ and $r = 6\,l$, being the radius for a hillock to contain virtually all the material in a catchment area radius $13\,l$. Hence

$$t_i \simeq \frac{k\,T\,r_c\,(6\,l)^2}{2(D_s \delta)\,\sigma\,\Omega} = \frac{234\,k\,T}{(D_s \delta)\,\sigma\Omega}\,l^3 \qquad (4.16)$$

To compare this relation with experiment, we note that the l^3 thickness dependence relation predicted is exactly that observed experimentally (3.1). Assuming approximate values for $\delta = 2 \times 10^{-8}$ cm, $\Omega = 2 \times 10^{-24}$ cm^3 and $D_s = 10^{-7}$ cm^2/sec (Brandon and Bradshaw), $\sigma = 10^{10}$ dynes/cm^2 at T = 540°C, then the predicted dependence is

$$t_i \simeq 6.\ 10^{-10}\ l^3 \text{ mins} \qquad (4.17)$$

comparing quite reasonably with the experimental observation,

$$t_i = 3.8 \times 10^{-9}\ l^3 \text{ mins.} \qquad (3.1)$$

in view of the approximation made. Indeed, measurements of the induction time can now be regarded as an approximate method for determining D_s.

The significant features of this adaptation of void growth theory are

(i) t_i is infinite unless γ is low enough for $\frac{r_g}{2} > \gamma$

Surface energy reduction in the presence of oxygen is

essential for hillock formation.

(ii) t_i depends on l^3, and varies inversely with D_s. Thus the compressive stress relief model explains the observed thickness dependence and temperature variation. Confirmation comes from quite close quantitative agreement between theory and observation. The effect of variations in γ is discussed below (section 4.2.6).

4.2.5.2. Hole growth period and island equilibration.

a) conditions for withdrawal from substrate.

The transfer of material to hillocks above the surface of the film proceeds until, at the end of the induction period, hole growth begins by metal withdrawing from the substrate. For this to occur, the positive radius of curvature at the hole edge must decrease to a sufficiently small value. As in section 1.4.2.c), the chemical potential of atoms at the (assumed uniformly) curved edge of the hole μ_L, differs from that on a plane μ_∞ by

$$\mu_L - \mu_\infty = -\left(\frac{1}{l} - \frac{1}{r}\right).\Omega.\gamma_{PV} \qquad (4.18)$$

For hole growth to occur, $\mu_L >= \mu_\infty$, and hence $l <= r$. This suggests that hole growth begins when the "lands" thickness approaches that of the largest holes, which then grow rapidly. Certainly s.e.m. reveals selective growth of a proportion of holes to large dimensions (fig. 3.9).

Growth of these holes of critical size finally delimits the catchment area, and effectively confines into one area all the material that finally forms an island.

The observed effect of p_{O_2} on catchment area was suggested earlier (4.2.1.3) to indicate variation of the critical hole size r_o with oxygen pressure, by altering the surface energy. In thesimple theory so far outlined, γ_{PV} variations would not affect r_o. However, if diffusion from the hole were actually from the metal-substrate perimeter, we could postulate another, invariant, line energy $\dagger_{SP}$ governing the reduction in chemical potential by the hole radius of curvature r.

Then $$\mu_L - \mu_\infty = -\left\{ \frac{\gamma_{PV}}{l} - \frac{\dagger_{SP}}{r} \right\} \Omega \qquad (4.19)$$

Hole growth would then occur when $\frac{l}{\gamma_{PV}} < \frac{r}{\dagger_{SP}}$, and would be affected by γ_{PV} variations.

b) Extension of hole growth theory of Brandon and Bradshaw (1966).

A treatment of the kinetics of metal withdrawal from the substrate has been developed with reference to surface energy driving forces alone, by extension of the treatment of hole growth in single crystal films given by Brandon and Bradshaw (1966). This model is then compared with the observed kinetics.

Hole growth: The radius (r)-time(t) dependence for a hole in a film of thickness d was given by Brandon and Bradshaw

as
$$r^{5/2} = \frac{5\pi^{1/2} Bt}{2d^{3/2}} \qquad (1.15)$$

and verified experimentally. If the hole area is A, then
$$r^{5/2} = (A/\pi)^{5/4} \qquad (4.20)$$

Hence
$$A^{5/4} = \frac{5\pi^{5/4} Bt}{2d^{3/2}} \qquad (4.21)$$

For constant B_o (constant T, D_s) and the same film thickness d_o,
$$A^{5/4} = f.t \quad \text{where } f = \frac{5\pi^{5/4} B}{2d^{3/2}} \qquad (4.21a)$$

giving a relation between hole area and annealing time.

Island equilibration: In the theory of hole growth, we have
$$\mu_L - \mu_\infty = - \Omega \gamma \left(\frac{1}{x} - \frac{1}{r} \right) \qquad (1.9)$$

For $r >> x$, we have $(\mu_L - \mu_\infty) = - \frac{\Omega \gamma}{x}$ (1.9)

For hole growth, x is small (x_h) and of the order of the thickness of the withdrawing lands (ca. 100-300 Å), giving a large driving force - $\Omega \gamma_s / x_h$. For island withdrawal, however, x_i is the radius of curvature of the whole island (ca. 0.1 - 1 μ), and the driving force $(\mu_L - \mu_\infty)_i$ is correspondingly greatly reduced to $\Omega \gamma_s / x_i$. A sharp reduction in the rate of withdrawal of material from the substrate is therefore to be expected when island withdrawal takes over from hole growth.

c) Comparison of observed hole growth kinetics with theory. The kinetics of hole growth observed in the present work,

were average measurements of the area of a large number of holes. Before a growth law predicted for single holes can be applied to an array, two assumptions must be justified: (i) the number of growing holes n must remain constant; (ii) the relative size distribution of the holes must remain the same. In practice, n' decreases slowly (fig. 3.11), and th the size distribution changes somewhat (fig. 3.12). Since several other assumptions are made in the Brandon and Bradshaw theory, it was decided to ignore corrections for these deviations, and to plot the uncorrected average % hole area A' as a function of time.

Fig. 4.6 shows a plot of $(A')^{5/4}$ vs. time for the 305°C data. The remaining data at other temperatures is shown in fig. 4.7. The general shape of the plot confirms the predictions of the extended Brandon and Bradshaw theory. The initial straight line portion confirms the relation

$$A^{5/4} = f \cdot t \qquad (4.21a)$$

The change in slope at the end of the hole growth stage shows the decreased withdrawal rate predicted from the increase in radius of curvature.

For the hole growth stage, an Arrhenius plot was made of the rate constant f: see fig. 4.8. A linear relation was obtained, giving an activation energy of 16.5 kcal/mole, in quite good agreement both with the 14.9 kcal value observed for the induction period, and the expected

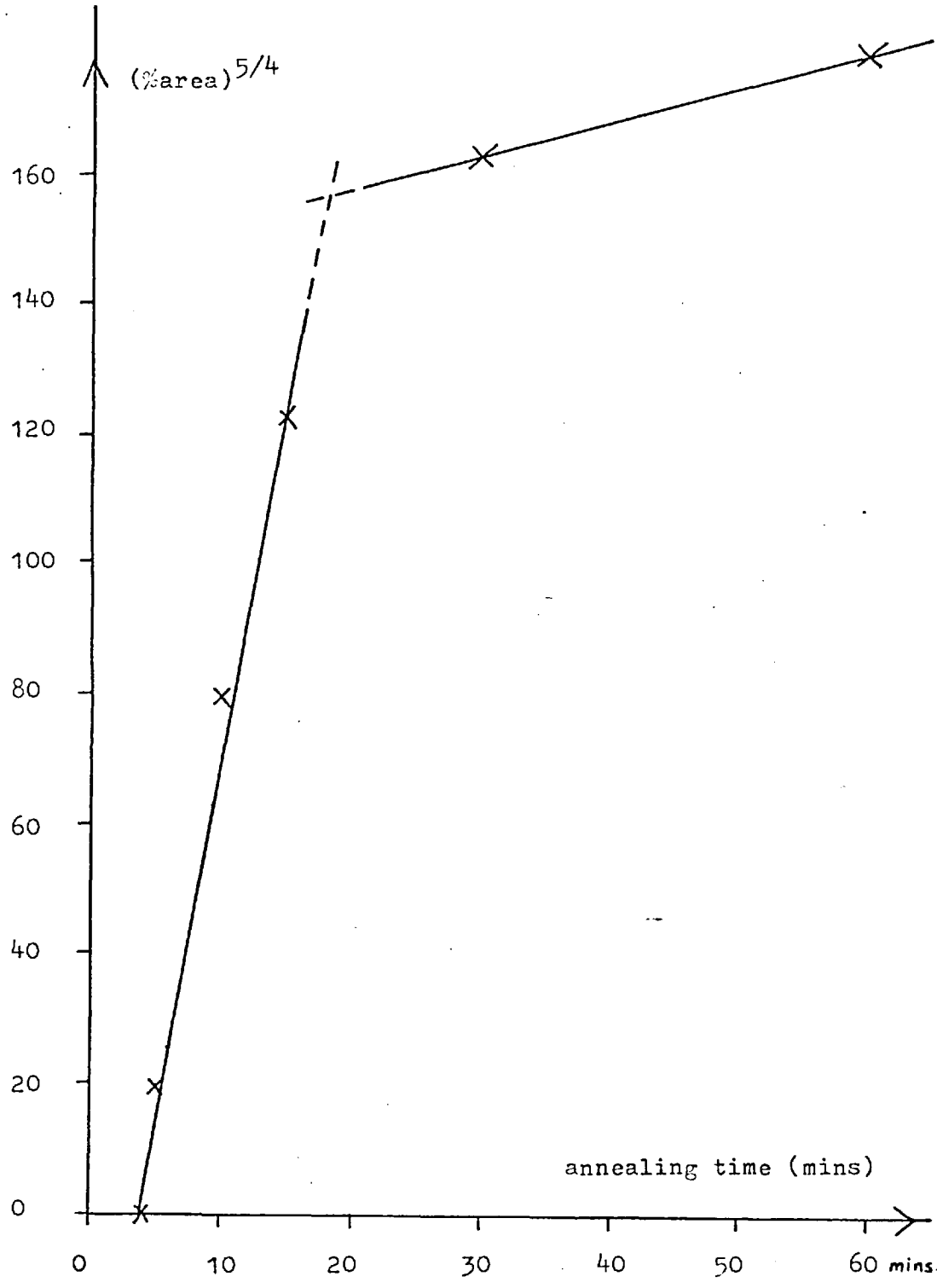
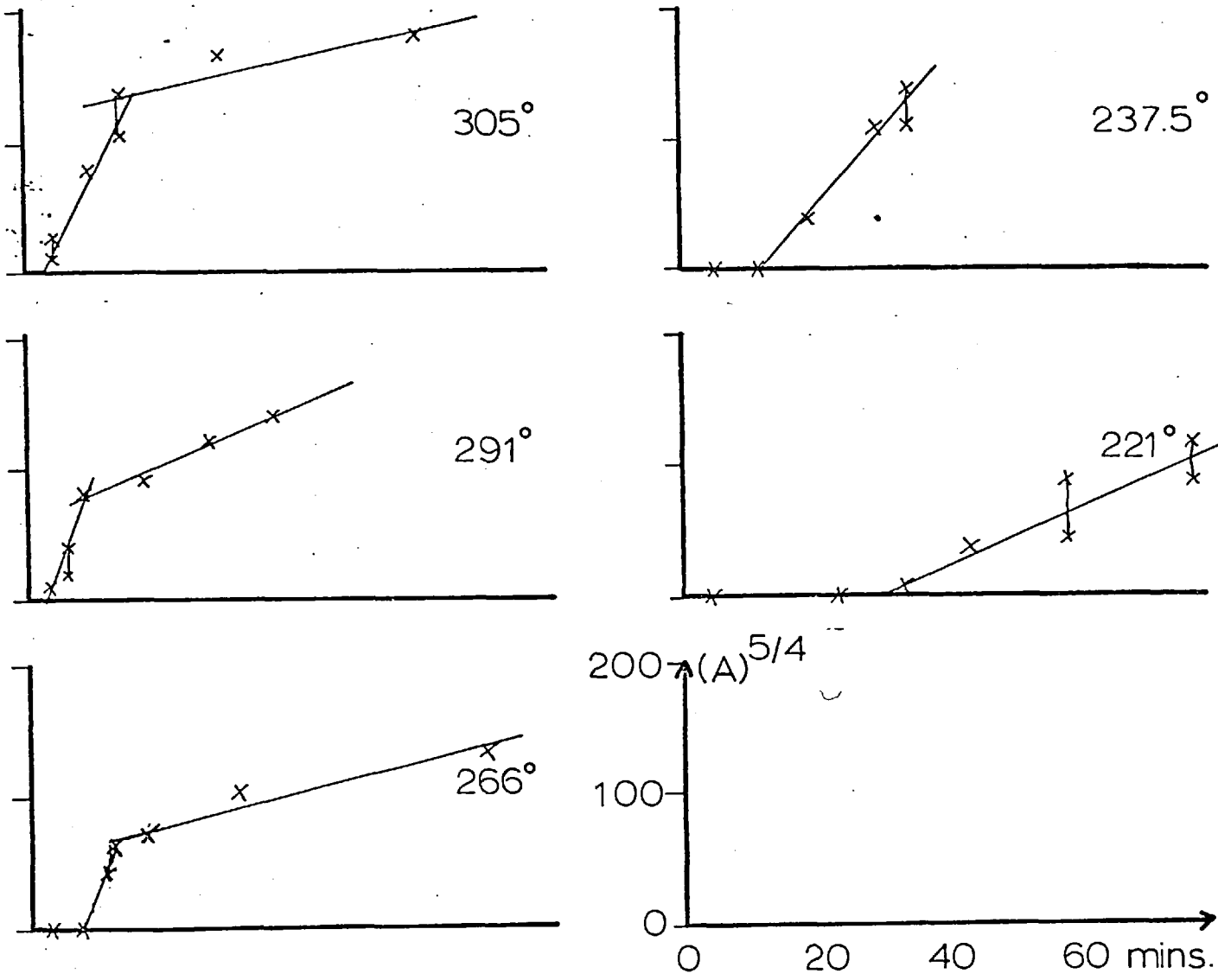


Fig 4.6 Plot of (%hole area)$^{5/4}$ vs annealing time 305°C 1180 Å 760 torr

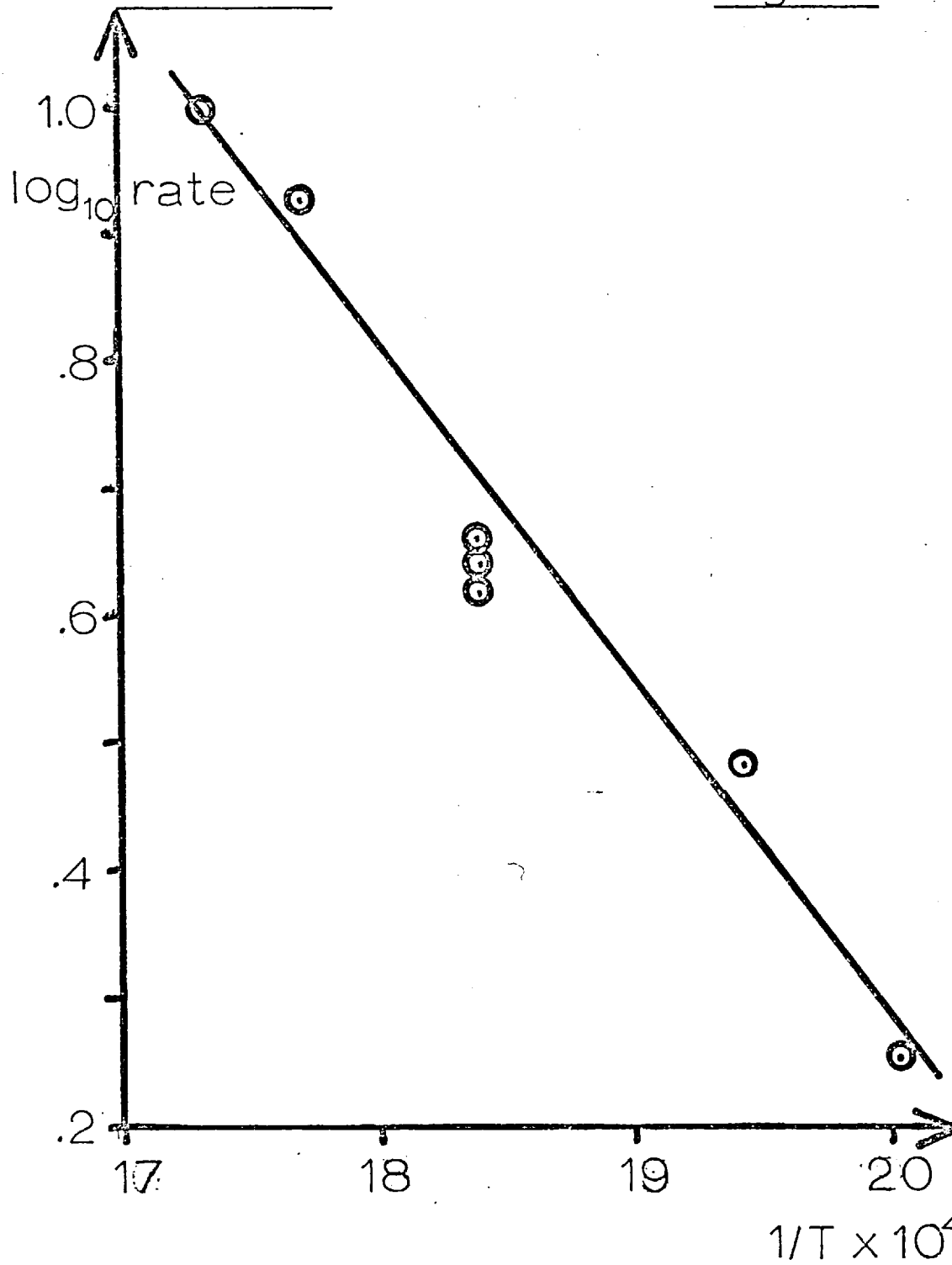
Hole growth rate relation: variation with temperature

Fig 4.7



Hole growth rate: temperature variation

Fig 4.8



value of 16.0 kcal for silver self-diffusion on clean and oxygen-carrying surfaces.

The accuracy of data for the small area changes in the island withdrawal period suffered from the 5% error inherent in A' measurement (section 2.5.1.2) and comparison of theory with experiment was not attempted at this stage.

The hole growth stage can therefore be accounted for quantitatively in terms of surface-tension driven surface diffusion, resulting in withdrawal from the substrate. It is probable that this mechanism also accounts for the final equilibration of islands.

4.2.6. Surface diffusion processes in oxygen atmospheres.

4.2.6.1. Effect of oxygen pressure.

The observed effect of p_{O_2} on t_i,

$$t_i = 1.5 - 3.8 \log p_{O_2} \qquad (3.2)$$

originally suggested that t_i was governed by $\gamma_{,PV}$ alone, but the drawbacks of this view were outlined in section 4.2.4.1. In the quantitative theory then developed for the kinetics of the induction period, three possibilities exist for an effect of lowered oxygen pressure in retarding hillock growth: (i) the increased catchment area, resulting in a smaller potential gradient between surface and hillock; (ii) the possibility that in an exact treatment, the increased value of $\frac{2\gamma}{r}$ should not be neglected in relation

to σ, and (iii) the possibility that D_s decreases with p_{O_2}. Hence the difficulty is to separate surface energy effects (i, ii) from surface diffusivity effects (iii). A tentative approach only is made here, neglecting (ii).

Over the range 760 - 10^{-4} torr, r_c changes by about 2 x, and thus r by about $\sqrt{2}$ x. This would have the effect of increasing t_i (proportional to $r_c.r^2$) by about 4 x over the range. This is not sufficient to account for the observed increase in t_i of about 25 x over this pressure range. We conclude tentatively that estimated surface energy effects, if operative, do not account for the whole of the increased induction time at lower pressures and that reduction in surface diffusivity is also important. Relation (3.2) is not completely explained, however. Further, if D_s changes by only about (25/4) x over this pressure range, the difference is an order of magnitude smaller than that observed by other workers (section 1.3.3.2).

4.2.6.2. Mechanism.

The hillock and hole growth kinetics observed in this work and in that of Brandon and Bradshaw agree well with the prediction of a surface diffusion model for material transport. In each case, the work was carried out under conditions where oxygen chemisorption is strong (Brandon and Bradshaw show that even at 800°C $\theta > \approx \frac{1}{2}$ at $> \approx 10^{-4.7}$ torr). The fact that the "macroscopic" kinetics obey surface

transport predictions, does not give any information about the atomic mechanism of transport on an oxygen covered surface. The only data in the present work which throws light on this, are the measured activation energies for the induction and hole growth periods of 14.9 and 16.5 kcals/mole The agreement between these values and Q_s expected on a clean silver surface, (ca. 16 kcal/mole) is striking, and accords with the observations of other workers (fig. 1.6). It suggests that the atomic mechanism is the same in both cases.

For an adatom diffusion mechanism this would certainly be a surprising result, as we would expect Q_s to be affected by the energy required to promote metal atoms from level 2 or level 3 (fig.1.5). Present indications (1.3.3.2) are that a vacancy or divacancy mechanism may operate at the lower temperatures used in this work. Prediction of the effect of chemisorption on vacancy formation energies is not simple. Changes in nearest neighbour coordination would probably be accompanied by changes in the relaxation energies for bonds around the vacancy. The necessary experimental and theoretical treatment for these and other effects of adsorption on surface diffusion mechanisms do not yet exist (Gjostein, 1967). At present, the observed agreement between activation energies can only be taken as evidence of possibly similar atomic mechanisms for surface diffusion with or without

chemisorption. Diffusion inhibition experiments with traces of 3+ or 4+ metal ions present might throw light on whether e.g. charged Ag^+ species were important in the migration process (compare Furuoya et al, 1969a, b) (section 1.1.4.2).

The probable increase in D_o of up to 25 x between 10^{-4} and 760 torr O_2 parallels the increase in D_s observed at high pressures by Rhead (1965). In his case, an adatom mechanism was postulated, and the increase could be explained by suggesting that as the pressure rose, the number of vacant adsorption sites between which adatoms could move, decreased, giving longer jump distances and so larger D_o values - though very large (ca. 10^4 x) increases in jump distances had to be postulated. In the present case, where a vacancy mechanism is probably appropriate (1.3.3.1), it seems more likely that adsorption increases D_o by affecting the vacancy concentration. Possibly the recent combination of LEED surface observations with quantitative D_s measurements may shed light on these problems of surface structure in relation to diffusion mechanisms (Bonzel and Gjostein, 1968).

4.2.7. Structure of final islands.

4.2.7.1. Crystallinity.

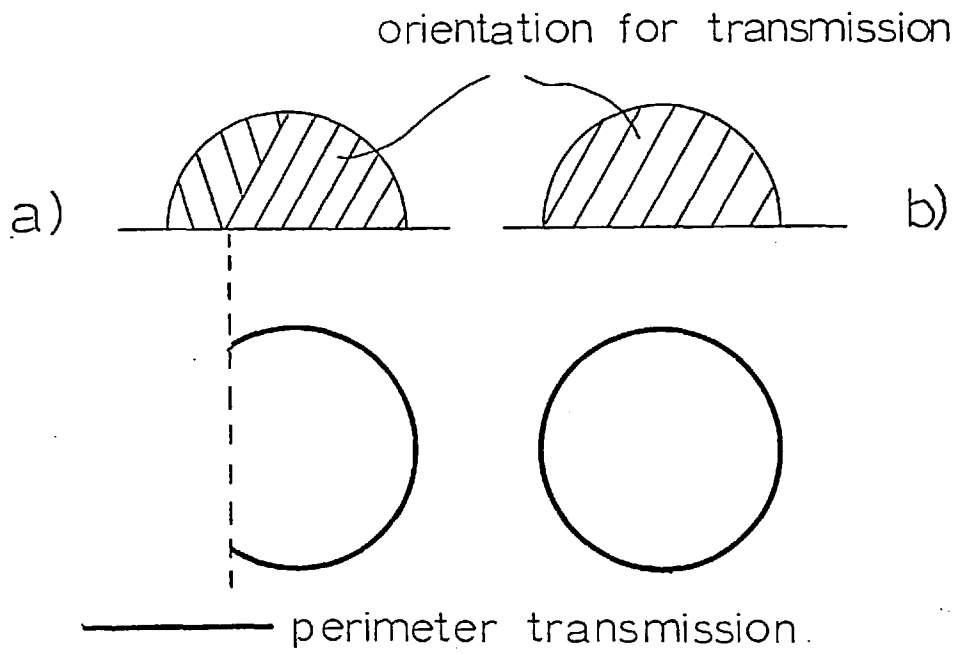
The purpose of the dark field e.m. observations made on well annealed islands (section 3.2.5.5) was to investigate their crystallinity. Two cases are illustrated in fig. 4.9: a) an island crossed by a grain

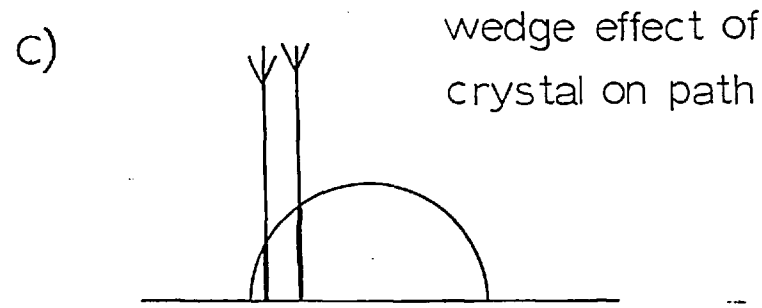
boundary, viewed in dark field. In this case, only one of the grains is oriented to diffract the incident beam into the objective aperture. As shown, transmission (around the perimeter) would be seen from this grain only. b) a single crystal island. Here the whole island is correctly oriented for transmission, and the complete perimeter will appear bright.

The experimental observation that transmission occurs around the complete perimeter of islands up to ca. 2,500 Å diameter, shows that after long annealing, these islands become single crystals. This shows that the theory of the equilibrium shapes of small crystals can be applied to their shapes.

The intensity profiles (fig. 3.20) show that the width of the transmitting perimeter is not greater than ca. 100 Å. This means that line broadening crystallite size measurements on an array of islands such as this would give quite misleading results; effectively, the longest diffracting dimension is ca. 100 Å only, even though the true crystallite size equals that of the whole island.

The reason for this narrow transmission perimeter is the extinction by increasing thickness of electrons passing nearer to the centre of the hemispherical islands (fig. 4.9c). The second order transmission peak observed for islands of intermediate diameter is probably due to the periodic relation between diffracted intensity and crystal





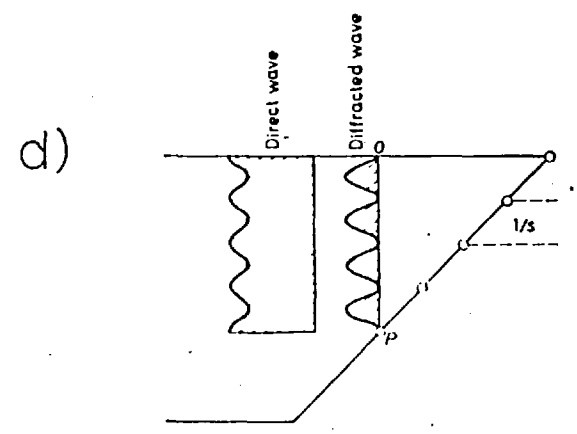


Figure 7.5a. Oscillations of diffracted and transmitted wave in crystal, showing how thickness fringes are produced in a wedge crystal. On this approximation the intensity of the transmitted wave at the points marked o is the same as that at the top surface

from Hirsch et al (1965)

Fig 4.9

thickness t (intensity $\propto \sin^2 t$) observed in e.g. wedge fringes from specimens of varying thickness (fig.4.9d) (Hirsch et al, 1965, p.158).

4.2.7.2. Shape.

The profile of well annealed islands viewed by s.e.m. (fig. 3.14) shows a "contact angle" of near to 90°, indicating that $\gamma_{SV} \approx 1000$ ergs/cm^2 $\approx \gamma_{SP}$. This value for the interfacial energy is similar to that obtained for silver - oxide substrate energies, by Pilliar and Nutting (1967) and by Winterbottom (1968), for deposits made in vacua of ca. 10^{-5} torr in an oil pumped system.

The effect of varying the initial metal-substrate energy could well provide further information on the role that the energy of the surface plays in the island formation process. For example, Winterbottom's work on the final equilibrium shapes of particles of metal originally deposited in U.H.V, could be extended to a study of the kinetics of island formation from such a film.

4.3. Microstructural changes on annealing "shadowed" films.

In this section, the results obtained in the brief study made of "shadowed" films are reviewed and suggestions made for their extension.

4.3.1. Original structure.

S.e.m. and t.e.m. rapidly showed that even in the

substrate areas shielded from the source by the copper grid, deposit islands had nevertheless formed small areas, with sizes decreasing further into the "shadow". These islands must have formed by migration of the silver over the substrate during deposition, before energy transfer between evaporant atoms and the substrate reduced their mobility.

4.3.2. Island growth process.

Growth of islands, with loss of the smallest size range, was observed after the "shadowed" catalyst had been annealed in oxygen. Two possible mechanisms exist: atomic diffusion over the substrate from small, highly curved stationary islands, to add material to larger ones: and gross mobility and coalescence of separate islands resulting in growth. Of these, the coalescence mechanism seems most likely in view of the observations of Skofronick and Phillips (section 1.4.3.2) of just such gross mobility with annihilation of small islands. However, transport from the continuous film edge cannot be ruled out. This mechanism could only be checked conclusively by looking for island mobility in a controlled atmosphere cell with hot stage, designed for use with an electron microscope.

The stability of the island distribution on annealing in hydrogen is striking confirmation of the observations of Thomas and Walker (1964) (1.4.3.2) that the annealing atmosphere can have a profound effect on the

mobility of islands. The influence of oxygen observed here in promoting mobility is parallel to the similar observations reported then of the mobility of cobalt in oxygen.

4.4. Surface area of catalyst films.

4.4.1. Adsorption isotherms.

Results from the adapted method of Aylmore and Jepson (1961) indicate its ability to measure low areas with an internal accuracy of about 5% (Table 3.5). Using a krypton specific area of 19.5 $\mathring{A}^2$, reasonable agreement was obtained between calculated surface areas, and both the geometric area of the glass sample (assumed plane) and the area of an independently known specimen. The adsorption behaviour of specimens used was in line with that observed elsewhere. The "plateau" isotherms observed in silver are similar to those observed by Klemperer and Stone; Roberts, and Anderson (1.2.2.3) for krypton on transition metal films. The isotherm curvature, and the very small intercept on the B.E.T. plot, indicate a high "c" value i.e. a large heat of adsorption of the gas on silver. The knee point at ca. 0.05 was in line with the normal values observed by Klemperer, Roberts. On pyrex, a low c-value of about 12 was obtained, in agreement with other observations (Gregg and Sing, 1967, p.89).

4.4.2. Area of fresh films.

The observation that the corrected surface area of

freshly evaporated film (805 cm^2) was close to that expected from the geometric area of the substrate, together with the absence of hysteresis effects, removed the possibility that the film had an internal pore structure accessible to krypton (atomic radius 1.97 Å). This observation was not unexpected in that except at very low temperatures, higher ambient gas pressures, very high source temperatures, or for highly reactive metals, metal films deposited by evaporation are non-porous (section 1.2.2.2). The importance of this observation is (i) surface energy changes due to loss of internal area do not have to be considered in the energetics of island formation from films (4.2.3.1); (ii) when measuring the specific activity of evaporated films, the reacting area can be taken as approximately equal to the geometric area of the film.

4.4.3. Area variation in island formation.

The approximate total surface area change expected after island formation can be calculated from the final island density (ca. 3.6/$micron^2$ for 380 Å film) and the approximate size (0.2 micron) on the assumption that final islands are hemispheres. For an initial plane surface A, a final area (islands plus exposed substrate) of ca. 1.11 A is calculated: hence the final metal area exposed is ca. 0.22 of the original area. Experimentally, the final area after island formation was found to be rather higher at

1.36 A, possibly because of the smallest island population increasing the area disproportionately. The area at the end of the induction period was very similar (1.27 A); this agrees with the s.e.m. observation, that most of the additional area caused by hillock growth above the surface was formed by the end of the induction period.

With the reasonable agreement found between electron microscopic and adsorption methods of metal area determination, the reliablity of e.m. methods of estimating reactive surface area is established for the present system.

4.5. Catalytic activity of metal films.

The conclusion, that changes in metal-gas area available for reaction followed quite closely the areas revealed by e.m. methods, simplified the approach to catalytic activity observations on the films before and after microstructural changes. These measurements were undertaken in order to follow the activity alone at fixed conditions, and so no discussion of the kinetics is possible. The simpler results for the continuous films will be considered first.

4.5.1. "Continuous" films.

4.5.1.1. Freshly deposited films.

The constant activity observed for fresh "continuous" films when used for several hours in ethylene or

hydrogen oxidation agrees with the stability of the surface under the conditions used. Films had been chosen of sufficient thickness to give only slow agglomeration at 228°C; in the event, only a little hillock growth was observed to occur on the surface at this low temperature. That activity decreases were not seen, shows that the reactant stream was free of significant poisons, and shows that any annealing out of defects does not affect the reactivity of the surface for either reaction.

4.5.1.2. Fully annealed films.

The island structure produced by full annealing is expected (4.4.3) to have a metal area of ca. 0.22 x the original surface area (380 Å film). The activity decrease observed for the ethylene oxidation reaction was to ca. 0.25 x, comparable with the expected area decrease. Had selective poisoning, loss of preferred orientation/ reaction sites occurred as well, greater decrease could have been expected. It is concluded that the activity is in fact governed by the surface area decrease alone in this case.

The film activity in the case of hydrogen oxidation fell to about 0.06 x the original on annealing to islands, a greater fall than can be accounted for in the reduction in surface area. The stability of the original film activity under conditions where selective poisoning, loss of defects or of preferred orientations, were possible,

makes these factors unlikely to be responsible for the unexpectedly large activity decrease after island formation. Possibly, changes in the oxidation state of the surface silver-oxygen layer occurred during island formation, affecting the energetics of chemisorption on the surface.

4.5.2. "Shadowed" films.

Results on "shadowed" films were obtained near the conclusion of the present study, by an accident of catalyst preparation. They are discussed within the limits of the experiments undertaken, and points of interest for further work are noted.

The main characteristic of these catalysts was their very high initial activity in comparison with continuous films. This was probably responsible for the low ethylene oxide concentration noted in samples taken after short reaction times (e.g. fig. 3.26) - over-oxidation of this product to carbon dioxide occurred. (That this result was not a spurious effect due to any condensation of ethylene oxide in the sampling system, is shown by there being no parallel initial peak in water concentration, a much less volatile product).

That the rapid initial loss of activity was not due to poisoning by any minor constituent in the ethylene, was shown by the unchanged activity after pre-annealing in ethylene or hydrogen. However, the activity loss was found

to follow quite closely that produced by pre-annealing in oxygen alone. Marked microstructural changes occurred after annealing, and were nearly complete after ca. 30 mins, the time over which most of the activity change took place. The microstructural changes detected were almost entirely in the "shadowed" area, where marked island growth was detected after annealing.

The "shadowed" film structure differs from that of continuous catalysts only in this area of small islands. It seems reasonable to propose that the high initial activity is associated with these islands, and that the subsequent activity losses are in some way related to their growth on annealing. Possibilities for such an effect of the island population on activity are now considered.

1. The high initial activity cannot be ascribed to increased surface area in the island area: the adsorption area measurements show a 'roughness factor' of only 1.31 x compared with an equivalent freshly deposited continuous film (Table 3.5).

2. Island growth on annealing results in a large reduction in the total perimeter of the island population. If catalysis of the reaction is affected by substrate-silver interactions at this exposed interface, then reduction in the perimeter might be important. However, substrate-metal interactions would be more plausible in a semi-conductor support, where diffusion of metal into the support could

affect the surface electronic properties in the region.

3. The temperature of annealing allows diffusion of oxygen into the surface and equilibration of non-stoichiometric silver-oxygen compounds with greatly reduced catalytic activity. Further exploration of this possibility is clearly necessary by extending the experiments. It is not clear why such an effect should operate only with the "shadowed" films of small island populations. Their high initial activity can perhaps be ascribed to high activity of small crystallites (though such effects are normally observed in hydrocarbon isomerisation/hydrogenolysis reactions).

Conclusions.

1. The kinetics of changes in the morphology of supported metal catalysts under reactive conditions can be followed by the use of electron microscopy to examine a model catalyst-support system.

2. Island formation on annealing thin silver catalyst films on silica, has been shown to occur in the presence of oxygen bearing atmospheres, whose effect depends on the changes produced in the surface energy and diffusivity of the silver.

3. Surface hillock growth in the early stages of agglomeration occurs to relieve compressive stresses in the catalyst film set up by differential thermal expansion

between catalyst and support. Hillock growth is only possible in oxygen-bearing atmospheres, which reduce the interfacial energy. A quantitative description can be given accounting for the observed kinetics of hillock growth in terms of stress-driven surface self-diffusion.

4. Progressive withdrawal of catalyst metal from the support occurs, minimizing the interfacial energy of the metal. The kinetics of the growth of holes in the film at this stage can be accounted for in terms of surface energy driven surface self-diffusion.

5. The original hole structure of the catalyst film as deposited from the vapour, has a governing role in determining the area from which islands formed during agglomeration draw the material that composes them.

6. The changes in the area of catalyst available for reaction are quite closely related both to the observed changes in catalytic activity for ethylene and hydrogen oxidation, and to the area as observed by microscopy.

7. Abnormally high catalytic activities have been observed from populations of very small discrete silver islands in the "shadowed" regions produced by partial masking during evaporation.

REFERENCES.

Adams, C.R., (1962) J.Catalysis, 1, 336.

Allen, J.A., Evans, C.C., Mitchell, J.W., (1959) in Strucure and Properties of Thin Films, ed. Neugebauer et al, Wiley, p.46.

Allen, J.A., Mitchell, J.W., (1950) Disc.Faraday Soc., 8, 309.

Allpress, J.G., Sanders, J.V., (1964a), J.Catalysis, 3, 528; (1964b), Phil.Mag, 3, 1042.

Anderson, J.R., Baker, B.G., (1962) J.Phys.Chem., 66, 482.

Aylmore, D.W., Jepson, W.B., (1961) J.Sci.Instruments, 38, 156.

Bachmann, L., Sawyer, D.L., Siegel, B.M., (1965) J.Appl. Phys., 36, 304.

Bagg, J., Jaeger, H., Sanders, J.V., (1963) J.Catalysis, 2, 449.

Baker, B.G., Fox, P.G., (1965) Trans.Faraday Soc., 61, 2001.

Balandin, A.A., (1929) Z.Phys. Chem., 132, 289; (1958) Adv. Catalysis, 10, 96.

Bassett, G., (1958) Phil. Mag., 3, 1042; (1961) Proc. European Regional Conference on Electron Microscopy, Delft, 1960, 1,270.

Beeck, O., Wheeler, A., Smith, A.E., (1940) Proc. Roy. Soc., A172, 62.

Beeck, O., (1950) Disc. Faraday Soc., 8, 118.

Beeck, O., Ritchie, A.W., (1950) Disc.Faraday Soc., 8, 159.

Bethge, H., (1969) J.Vac.Sci.Tech., 6, 460.

Bhakhta, M.A., Taylor, H.A., (1966) J.Chem.Phys., 44, 1264.

Birchenall, C.E., (1959) Physical Metallurgy, McGraw-Hill.

Birchenall, C.E., Williams, J.M., (1966) in Bonis et al, 1966.

Blakeley, J.M., (1963) Progress in Materials Science, 10 "Surface Diffusion".

Blakeley, J.M., Olson, D.M., (1968) J.Appl.Phys., 39, 3476.

Blois, M.S., Rieser, L.M., (1954) J.Appl.Phys., 25, 338.

Bond, G.C., (1962) Catalysis by Metals, Academic Press.

Bond, G.C., (1966) Disc. Faraday Soc., 41, 200.

Bonis, L.J., De Bruyn, P.L., Duga, J.J., (1966) Fundamental Phenomena in the Materials Sciences, Vol.3, Plenum Press, N.Y.

Bonzel, H.P., Gjostein, N.A. (1968) J.Appl.Phys., 39, 3480; (1969) in "Molecular Processes on Solid Surfaces, ed. E.Drauglis et al, McGraw-Hill.

Borel, J-P., (1955) Memoires de la Societe Vaudoise des Sciences Naturelles, 11, 2.

Boudart, M., (1949) J.Am.Chem.Soc., 72, 1040.

Boudart, M., Aldag, A.W., Ptak, L.D., Benson, J.E., (1968) J.Catalysis, 11, 35.

Bowden, H.G., Baluffi, R.W., (1969) Phil.Mag., 19, 1001.

Bowden, F.P., Singer, K.E., (1969) Nature, 222, 977.

Brandon, R.H., Bradshaw, F.J., Wheeler, R.C., (1964) Acta Met., 12, 1057.

Brandon, R.H., Bradshaw, F.J., (1966) Royal Aircraft Establishment, Farnborough Report No.66095.

Brennan, D., Graham, M.J., Hayes, F.H., (1963) Nature, 199, 1152.

Brooks, C.S., Christopher, G.L.M., (1968) J.Catalysis, 10, 211.

Brownlie, S.C., Fryer, J.R., Webb, G., (1969) J.Catalysis, 14, 3.

Burton, W.K., Cabrera, N., Frank, F.C., (1951) Proc.Roy.Soc., A243, 40, 299.

Buttner, F.H., Funk, E.R., Udin, H., (1952) J.Phys.Chem., 56, 657.

Campbell, D.S., (1966) in ed. Niedermayer and Meyer, 1966.

Campbell, K.C., Duthie, D.T., (1965) Trans.Faraday Soc., 61, 558.

Carter, D.L., Cusumano, J.A., Sinfelt, J.H., (1966) J.Phys.Chem., 70, 2257.

Caswell, H.L., Priest, J.R., Budo, Y., (1963) J.Appl. Phys., 34, 3261.

Caswell, H.L., Budo, Y., (1964) J.Appl.Phys., 35, 644.

Chaudhari, P., (1969) I.B.M.Journal of Research and Development, March 1969, 197.

Collins, H.E., Showmon, P.G., (1966) Trans.Met.Soc. A.I.M.E., 236, 1354.

Cormack, D., Moss, R.L., (1969) J.Catalysis, 13, 1.

Cosslett, V.E., (1950) Introduction to Electron Optics, OUP.

Crocker, A.J., Robertson, A.J.B., (1958) Trans.Faraday Soc., 54, 931.

Cyrot-Lackmann, F., (1969) Surface Science, 15, 535.

d'Heurle, F., Berenbaum, L., Rosenberg, R., (1968) Trans.Met.Soc. A.I.M.E., 242, 502.

d'Heurle, F.M., (1966) Trans.Met.Soc.A.I.M.E., 236, 321.

Darken, L.S., Gurry, R.W., (1953) Physical Chemistry of Metals, McGraw-Hill.

Dinghas, A., (1944) Z.fur Kristallog., 105, 304.

Dorling, T.A., Moss, R.L., (1966) J.Catalysis, 5, 111;
(1967) J.Catalysis, 7, 378.

Dorling, T.A., Eastlake, M.J., Moss, R.L., (1969)
J.Catalysis, 14, 23.

Dowden, D.A., McKenzie, N., Trapnell, B.M.W., (1956)
Proc. Roy. Soc., A237, 245.

Dowden, D.A., Wells, D., (1961) Actes 2^{e} Congr.Int.Catal.,
p.1499.

Dowden, D.A., (1967) Chem.Eng.Progress Symp. Series No.73,
63, 90.

Dunning, W.J., (1967) in "The Solid-Gas Interface"
ed. E.Alison Flood, Arnold.

Echigoya, E., Furuoya, I., Morikawa, K., (1968)
Bull.Chem.Soc., Japan, 71, 1768.

Eckell, J., (1933) Z.Electrochem., 39, 433.

Edgecumbe, J., (1966) J.Vac.Sci.Tech., 3, 28.

Ehrlich, G., Hudda, F., (1959) J.Chem.Phys., 30, 493.

Eichenauer, W., Muller, G., (1962) Z.Metallkunde, 53, 321.

Farkas, A., Melville, H.W., (1939) Experimental Methods in
Gas Reactions, Macmillan, p.201.

Firth, J.G., (1966) Trans.Faraday Soc., 62, 2566.

Fisher, C.F., Cole, M., (1968) The Microscope, 16 The Metals
Research Image Analysing Computer.

Furuoya, I., Shirashaki, T., et al., (1969)
(a) Bull.Soc.Chem. Japan, 72, 1223;
(b) Bull.Soc.Chem. Japan, 72, 1431.

Gabbay, D.S., (1969) Ph.D. Thesis, London University.

Geguzin, Y., (1964) Soviet Physics (solid state) 5, 2627.

Gibbs, J.W., (1928) "On the Equilibrium of Heterogeneous Substances" Collected Works, p.328.

Gimpl, M.L., McMaster, A.D., Fuschillo, N., (1964) J.Appl. Phys., 35, 3572.

Gjostein, N.A., Rhines, (1959) Acta Met., 7, 224.

Gjostein, N.A. (1963a) in "Metal Surfaces", American Society for Metals, Cleveland, Ohio.
(1963b) Acta Met., 11, 957.
(1963c) Acta Met., 11, 969.

Gjostein, N.A. (1967) in "Surfaces and Interfaces" ed. Burke, T.T., Reed, N.L., Weiss, V. Syracuse U.P.

Gjostein, N.A., Winterbottom, W.L., (1967) in Fundamentals of Gas-Surface Interactions, ed. Saltsburg, H., Smith, J.N.Jr., Academic Press.

Gregg, S.J., Sing, K.S.W., (1967) Adsorption, Surface Area and Porosity, Academic Press.

Hall, C.E., (1953) Introduction to Electron Microscopy, McGraw-Hill.

Hartmann, T.C., (1965) J.Vac.Sci.Tech., 2, 239.

Harvey, J., Matthews, H.I., Wilman, H., (1960) Disc. Faraday Soc., 30, 113.

Hayward, D.O., Trapnell, B.M.W., (1964) Chemisorption, Butterworths.

Henning, F., Stock, A., (1921) Z.Physik, 4, 227.

Herring, C., (1950) J.Appl. Phys., 21, 437.

Herring, C., (1953) in "Structure and Properties of Solid Surfaces" ed. Gomer, R., Smith, C.S. Chicago U.P.

d'Heurle, F., (1966) Trans. A.I.M.E., 236, 321.

Hirsch, P.B., Howie, A., Nicholson, R.B., Whelan, M.J. Pashley, D.W., (1965) Electron Microscopy of Thin Crystals, Butterworths.

Hirth, J.P., (1965) in "Energetics in Metallurgical Phenomena" ed W.M.Mueller, Gordon and Breach.

Hirth, J.P., Pound, G.M., (1963) Condensation and Evaporation, Pergamon.

Holcomb, D.F., Norberg, R.E., (1955) Phys.Rev., 98, 1074.

Holland, L., (1956) Vacuum Deposition of Thin Films, Chapmen and Hall, London.

Hondros, E.D., (1968) Surface Science, 16, 1377.

Hull, D., Rimmer, D.E. (1959) Phil. Mag., 4, 673.

Jaeger, H., (1967) J.Catalysis, 9, 237.

Johnson, D.L., (1969) J.Appl. Phys., 40, 192.

Jorgenson, G.V., Wehner, G.K., (1963) Trans. 10th National Vacuum Symposium (Amer. Vacuum Society

Kane, W.M., Spratt, J.P., Herschinger, L.W., (1966) J.Appl. Phys., 37, 2085.

Keesom, W.H., Mazur, J., Meihuizen, J.J., (1935) Physica, 2, 669.

Kimoto, K., Kamiya, Y., Nomoyama, M., Uyeda, R., (1963) J.Appl. Phys. (Japan), 2, 702.

Kishimoto, S., (1963) J.Phys.Chem., 67, 1161.

Klemperer, D.F., Stone, F.S., (1957) Proc.Roy.Soc., A243,375.

Klockholm, E., Berry, B.S., (1968) I.B.M.Research Report, RC-1969.

Kossel, W., (1927) Nach.Ges.Wiss., Gottingen.

Lawson, A., (1968a) J.Catalysis, 11, 283;
(1968b) J.Catalysis, 11, 295.

Lewis, B., Campbell, D.S., (1967) J.Vac.Sci.Tech., 4, 209.

Liang, S.C., (1953) J.Phys.Chem., 57, 910;
(1955) Canad. J.Chem., 33, 279.

Lovell, S., Rollinson, E., (1968) Nature, 218, 1179.

McLean, M., Mykura, H., (1964) Acta Met., 12, 326.

McLean, M., Hirth, J.P., (1968) Surface Science, 12, 177.

McLean, M., Gale, B., (1969) Phil.Mag., 20, 1033.

Meelheim, R.Y., Cunningham, R.E., Lawless, K.R., (1960)
Proc. 2^{e} Congr. Int. Catal., 2, 2005.

Melmed, A.J., (1967) J.Appl. Phys., 36, 1885.

Mills, B., Douglas, P., Leak, G.M. (1969)
Trans. Met. Soc., A.I.M., 245, 1291.

Moore, A.J.W., (1963) in "Metal Surfaces", Amer Society for Metals, Cleveland, Ohio.

Moss, R.L., Thomas, D.H., (1967) J.Catalysis, 8, 151.

Moss, R.L., Duell, M.J., Thomas, D.H., (1963)
Trans. Faraday Soc., 59, 216.

Mullins, W.W., (1957) J.Appl. Phys., 28, 335;
(1959) J.Appl. Phys., 30, 77;
(1960) Trans.Met.Soc. A.I.M.E., 218, 354;
(1961) Phil.Mag., 6, 1313.
(1963) in "Metal Surfaces", Amer.Soc. for Metals, Cleveland, Ohio.

Mullins, W.W., Shewmon, P.G., (1959) Acta Met., 7, 163.

Mykura, H., (1961) Acta Met., 9, 570.

Neugebauer, C.A., Newkirk, J.B., Vermilyea, D.A., (1959) Structure and Properties of Thin Films, Wiley, N.Y.

Newman, R.C., Pashley, D.W., (1955) Phil.Mag., 46, 917.

Niedermayer, R., Mayer, H., (1966) Basic Problems in Thin Film Physics, Gottingen.

Nielsen, N.A., Keating, K.B., Miller, W.R., (1967) Surface Science, 8, 307.

Nichols, F.A., (1967) Acta Met., 15, 365.

Nowick, A.S., Dienes, G.J., (1967) Phys.Stat.Solidi, 24,461.

Orgel, L.E., (1966) An Introduction to Transition Metal Chemistry, Methuen, London.

Pashley, D.W., Stowell, M.J., Jacobs, M.H., Law, T.J., (1964) Phil. Mag., 10, 127.

Pask, J.A., Fulrath, R.M., (1962) J.Am.Ceram.Soc., 45, 592.

Pauling, L., (1949) Proc. Roy. Soc., A196, 343.

Pennebaker, W.B., (1968) I.B.M.Research Report RC-2105, May

Perdereau, J., Rhead, G.E., (1965) Surface Science, 7, 175.

Perrin, J., Faure, R., (1966) C.R.Acad.Sci.(Paris) 262,B-433

Phillips, W.B., Desloge, E.A., Skofronick, J.G., (1968) J.Appl.Phys., 39, 3210.

Pilliar, R.M., Nutting, J., (1967) Phil.Mag., 16, 181.

Pinsker, Z.G., (1953) Electron Diffraction, Butterworths.

Porter, A.S., Tompkins, F.C., (1953) Proc.Roy.Soc., A217, 544.

Rhead, G.E., (1965) Acta Met., 13, 223.

Rhead, G.E., (1969) Surface Science, 15, 353.

Rhodin, T.N., Walton, D., (1963) Single Crystal Films, ed. M.H.Francombe and H.Sato, Pergamon.

Romanowski, W., (1969) Surface Science, 18, 373.

Roberts, M.W., (1960) Trans.Faraday Soc., 56, 128.

Robertson, W.M., Shewmon, P.G., (1963) in "Metal Surfaces" Amer. Soc. for Metals, Cleveland, p.63.

Rosenberg, A.J., (1956) J.Am.Chem.Soc., 78, 2929.

Sanders, J.V., (1964) J.Austral. Inst. Metals, 9, 63.

Schwoebel, R.L., (1967) J.Appl.Phys., 38, 3154.

Sears, G.W., Hudson, J.B., (1963) J.Chem.Phys., 39, 2380.

Seeger, A., Schottky, G., Schumaker, D., (1965). Phys. Stat. Solidi, 11, 363.

Selwood, P.W., Adler, S., Phillips, T.R., (1955) J.Am.Chem.Soc., 77, 1462.

Shewmon, P.G., (1966) in Bonis et al., 1966.

Sinfelt, J.H., (1967) Chem.Eng.Progress Symposium, Series 73, 63, 16.

Skapski, A.S., (1956) Acta Met., 4, 576.

Skofronick, J.G., Phillips, W.B., (1966) in Niedermayer and Mayer, 1966; (1967) J.Appl.Phys., 38, 4791.

Slin'ko, M.G., Chesalova, V.S., (1956) Zh.Fiz.Khim., 30, 2560.

Smith, B.A., Nutting, J., (1956) Brit.J.Appl.Phys., 7, 214.

Smithells, C.J., (1967) Metals Reference Book, Butterworths.

Sosnovsky, H.M.C., (1955) J.Chem.Phys., 23, 1486. (1959) J.Phys.Chem.Solids, 10, 304.

Sundquist, B.E., (1964a) Acta Met., 12, 67; (1964b) Acta met., 12, 585.

Swank, T.F., Lawless, K.R., (1965) J.Appl.Phys., 36, 2089.

Szabo, Z.G., Solymosi, F., (1960) Proc.2^{e} Congr. Int. Catal., Paris, 1627.

Taylor, D., (1951) The Measurement of Radio Isotopes, Methuen.

Taylor, W.F. n.d. Factors Affecting the Activity of Supported Metal Catalysts, Esso Research Linden, N.J. 07036.

Taylor, W.F., Yates, D.C.J., Sinfelt, J.H., (1964) J.Phys.Chem., 68, 2962; (1965) J.Phys.Chem., 69, 3857.

Taylor, W.F., Staffin, H.K., (1967) Trans.Faraday Soc., 63, 2309.

Thomas, J.M., Walker, P.L.Jr., (1964) J.Chem.Phys., 41,587.

Thomas, J.M., Thomas, W.J., (1967) Introduction to the Principles of Heterogeneous Catalysis, Academic Press.

Thornton, P.R., (1968) Scanning Eelectron Microscopy, Chapman and Hall.

Tolansky, S., (1948) Multiple Beam Interferometry, O.U.P.

Tomizuka, C.T., Sonder, E., (1956) Phys.Rev., 103, 1182.

Trapnell, B.M.W., (1953) Proc.Roy.Soc., A218, 566.

Twigg, G.H., (1945) Proc.Roy.Soc., A166, 92.

Volmer, M., Weber, A., (1925) Z.Phys.Chem., 119, 277.

Wainfain, N., Scott, N.J., Parratt, L.G., (1959) J.Appl.Phys., 30, 1604.

Warner, H.E., (1967) Ph.D. Thesis, Carnegie-Mellon Univ., Pittsburgh.

Waterbeem, J.van der., Oosterhout, G.W. van., (1967) Philips Research Report, 22, 375.

Weinstein, A.M., D'Antonio, C.D., Mukherjee, K., (1968) Nature, 220, 778.

Wolter, A.R., (1965) J.Appl.Phys., 36, 2377.

Winterbottom, W.L., (1966) Proc. 13th Sagamore Army Materials Conference, Raquette Lake, New York.

Winterbottom, W.L., Gjostein, N.A., (1966) Acta Met., 14, 1041.

Winterbottom, W.L., (1967) Acta Met., 15, 303.

Wulff, G., (1901) Z.fur Kristallog., 34, 449.

Wynblatt, P., (1969) J.Phys.Chem. Solids, 30, 2201.

Yates, D.C.J., Taylor, W.F., Sinfelt, J.H. (1964) J.Am.Chem.Soc., 86, 2296;
(1965) Trans.Faraday Soc., 61, 2044.

Zinsmeister, G. (1966a) Vacuum, 16, 529;
(1966b) in Niedermayer and Mayer, 1966;
(1968) Thin Solid Films, 2, 497.